

**NUMERICAL AND EXPERIMENTAL  
INVESTIGATIONS ON DAMAGE  
DETECTION IN JOINTS BASED ON  
STATISTICAL ENERGY ANALYSIS LIKE  
APPROACH**

Thesis

Submitted in partial fulfillment of the requirements for the degree of

**DOCTOR OF PHILOSOPHY**

by

**ACHUTHAN. C. PANKAJ**



DEPARTMENT OF MECHANICAL ENGINEERING  
NATIONAL INSTITUTE OF TECHNOLOGY KARNATAKA,  
SURATHKAL, MANGALORE – 575025

JANUARY, 2019



## DECLARATION

I hereby *declare* that the Research Thesis entitled “**NUMERICAL AND EXPERIMENTAL INVESTIGATIONS ON DAMAGE DETECTION IN JOINTS BASED ON STATISTICAL ENERGY ANALYSIS LIKE APPROACH**” which is being submitted to the **National Institute of Technology Karnataka, Surathkal** in partial fulfillment of the requirements for the award of the Degree of **Doctor of Philosophy** in **Department of Mechanical Engineering** is a *bonafide report of the research work carried out by me*. The material contained in this Research Thesis has not been submitted to any University or Institution for the award of any degree.

Register Number : **121184ME12P01**

Name of the Research Scholar : **ACHUTHAN. C. PANKAJ**

Signature of the Research Scholar :

Department of Mechanical Engineering

Place : **NITK-Surathkal**

Date :

## **CERTIFICATE**

This is to *certify* that the Research Thesis entitled “**NUMERICAL AND EXPERIMENTAL INVESTIGATIONS ON DAMAGE DETECTION IN JOINTS BASED ON STATISTICAL ENERGY ANALYSIS LIKE APPROACH**” submitted by **Mr. ACHUTHAN. C. PANKAJ** (Register Number: **121184ME12P01**) as the record of the research work carried out by him, is *accepted as the Research Thesis submission* in partial fulfillment of the requirements for the award of degree of **Doctor of Philosophy**.

### **Research Guide**

**Dr. S.M. MURIGENDRAPPA**  
Professor  
Department of Mechanical Engineering  
NITK, Surathkal

Chairman-DRPC  
Date:

## ACKNOWLEDGEMENTS

With a deep sense of gratitude, I wish to express my sincere thanks to my supervisor **Prof. S.M. Murigendrappa**, Professor, Department of Mechanical Engineering, National Institute of Technology Karnataka (NITK), Surathkal, for his timely and excellent guidance throughout the work. I received very useful, encouraging and excellent academic feedback from him, which has stood in good stead while writing this thesis. His constant encouragement, help and review of the entire work during the course of the investigation were invaluable. I owe my deepest gratitude to the RPAC members **Dr. H. Ramesh**, Associate Professor, Department of Applied Mechanics and Hydraulics and **Dr. P. Jeyraj**, Associate Professor, Department of Mechanical Engineering for their constant guidance.

I acknowledge my thanks to the **Head** of the Department of Mechanical Engineering and Chairman, DRPC for his constant encouragement and providing the necessary facilities. I express my heartfelt thanks to the **Director**, NITK, Surathkal.

I gratefully acknowledge the help received from Mr. M.V. Shiva Prasad, senior scientist, NAL, Bangalore for helping me out in carrying out the experimental work. I also acknowledge help rendered by Mr. Mahesh (Senior Technical Assistant), NAL, Bangalore. I owe my deepest gratitude to Dr. S. Raja, Group Head, Dynamics and adaptive structures group and Dr. S. Chandra, Head, Structural Technologies Division, NAL, Bangalore, for permitting me to carry out the experimental work. I wish to express my sincere gratitude to the Director, NAL, Bangalore and Dr. M. Manjuprasad, Chief Scientist, Structural Technologies Division, NAL, Bangalore.

I am indebted to all the faculty members and research scholars of the Department of Mechanical Engineering, N.I.T.K Surathkal for their help, encouragement and support all through this research work. Finally, I am grateful to my family for their constant encouragement and trust throughout my life.

*(Achuthan.C.Pankaj.)*

## ABSTRACT

Engineering structures have to be regularly monitored to avert catastrophic failure and for maintenance, etc. The extent of damage has frequently been used for low-frequency vibration based health monitoring problems. However, there are incipient damage effects on connections of structures with spot welds or bolted joints, etc., which affects mainly on highest modes, rather than on lowest. Energy based approaches like statistical energy analysis (SEA) is one of the widely used methods in such conditions. The present study focuses on the numerical and experimental investigation on damage detection in plates with lap joint configurations viz. spot welded, bolted and adhesive bonded joints using statistical energy analysis like (SEAL) approach. Two materials mild steel and acrylic have been used in the investigation. In the first phase, studies have been carried out to investigate the effects of internal loss factor on the estimation of coupling factors of mild steel plates and the finite element models for spot welds, bolted joints and adhesive bonds. In the second phase, forced harmonic analysis is performed experimentally and numerically using commercially available finite element tool (ANSYS V13) to obtain the velocity responses, total energies and coupling factors of the assembly of two plates with lap joint for the healthy and damaged configurations. Further, the velocity and acceleration responses have been simulated by FEA and predicted by the SEAL approach for an assembly of three plates with lap joint configurations and compared with experiments for healthy and damaged configurations.

Results have revealed that at low damping, the coupling factors computed by the analytical approach are overestimated and the coupling factors computed by finite element analysis and the experimental SEA is observed to be more accurate. Responses predicted at low frequencies are found to be not accurate due to the reduction in modal density, modal overlap and violation of assumptions in SEA like approach. A database of the simulated velocity responses and total energies for the possible damaged configurations based on SEAL approach has been developed. The percentage deviation in the acceleration responses on each plate for different damage scenarios in comparison to the healthy configuration has been used as one of the damage indicator. The novelty of this work lies in the demonstration of the utilization of SEAL approach in damage detection of joints.

**Keywords:** *Apparent coupling factor, Adhesive joints, Bolted joints, Damping loss factor, FEM, Modal density, Spot-welded joints, Statistical energy analysis.*

# CONTENTS

**Declaration**

**Certificate**

**Acknowledgements**

**Abstract**

**Contents**.....i

**List of figures**.....v

**List of tables**.....xii

**Abbreviations**.....xvi

**Nomenclature**.....xviii

## **1. INTRODUCTION**

1.1 Overview..... 01

1.2 Vibration based diagnostics..... 02

*1.2.1 Signal monitoring*..... 03

*1.2.2 Signal processing*..... 03

*1.2.3 Data interpretation and discrimination*..... 04

1.3 Statistical energy analysis..... 05

*1.3.1 Steady state power balance*..... 06

*1.3.2 Loss factors*..... 08

*1.3.3 Power balance* ..... 09

1.4 Spot welded joints..... 09

1.5 Bolted joints..... 10

1.6 Adhesive joints..... 11

1.7 SEAL approach..... 12

1.8 Organization of the thesis..... 12

## **2. LITERATURE REVIEW**

2.1 Introduction..... 15

2.2 Statistical energy analysis..... 15

2.3 Analysis of spot welded joints..... 17

2.4	Analysis of bolted joints.....	17
2.5	Analysis of adhesive bonded joints.....	18
2.6	Vibration-based health monitoring.....	19
2.7	Pattern recognition approaches.....	22
2.8	Motivation.....	23
2.9	Objectives of the research work.....	24
2.10	Scope of the research work.....	25
2.11	Summary.....	26
<b>3.</b>	<b>EFFECTS OF INTERNAL DAMPING FOR COUPLING LOSS FACTOR ESTIMATION</b>	
3.1	Introduction.....	27
3.2	Analysis and Procedure.....	28
3.2.1	<i>Analytical wave approach for plates</i> .....	28
3.2.2	<i>Analytical wave approach for beams</i> .....	30
3.2.3	<i>Finite element analysis</i> .....	31
3.3	Results and Discussion.....	34
3.4	Summary.....	41
<b>4.</b>	<b>FINITE ELEMENT MODELS FOR SPOT WELDED AND ADHESIVE BONDED PLATES TO DETERMINE COUPLING LOSS FACTORS USING FINITE ELEMENT ANALYSIS</b>	
4.1	Introduction.....	42
4.2	Spot welded plates (Case 1).....	43
4.2.1	<i>Material Properties and Geometric Dimensions</i> .....	43
4.2.2	<i>Finite Element Analysis</i> .....	44
4.3	Adhesive bonded plates (Case 2).....	48
4.3.1	<i>Material Properties and Geometric Dimensions</i> .....	49
4.3.2	<i>Finite Element Analysis</i> .....	50
4.4	Results and Discussion.....	51
4.5	Summary.....	61



<b>5. DAMAGE DETECTION OF SPOT WELDED PLATES USING STATISTICAL ENERGY ANALYSIS LIKE APPROACH</b>	
5.1 Introduction.....	62
5.2 Test specimens.....	62
5.3 Statistical energy analysis like approach.....	64
5.4 Experimental set – up.....	65
5.5 Experimental procedure.....	70
5.6 Power injection method.....	74
5.7 Finite element analysis.....	75
5.8 Results and Discussion.....	78
5.8.1 <i>Joint damage detection</i> .....	87
5.9 Summary.....	94
<b>6. DAMAGE DETECTION OF BOLTED PLATES USING STATISTICAL ENERGY ANALYSIS LIKE APPROACH</b>	
6.1 Introduction.....	95
6.2 Test specimens.....	95
6.3 Experimental set – up.....	99
6.4 Finite element analysis.....	103
6.5 Results and Discussion.....	109
6.5.1 <i>Joint damage detection</i> .....	116
6.6 Summary.....	122
<b>7. DAMAGE DETECTION OF ADHESIVE BONDED PLATES USING STATISTICAL ENERGY ANALYSIS LIKE APPROACH</b>	
7.1 Introduction.....	123
7.2 Test specimens.....	123
7.3 Experimental set – up.....	125
7.4 Finite element analysis.....	129
7.5 Results and Discussion.....	134
7.5.1 <i>Joint damage detection</i> .....	144
7.6 Summary.....	150

<b>8. CONCLUSIONS</b>	
8.1 Summary.....	151
8.2 Key contributions.....	154
8.3 Limitations.....	155
8.4 Future scope.....	155
REFERENCES.....	156
LIST OF PUBLICATIONS.....	167
BIO-DATA	

## LIST OF FIGURES

<b>Figure No.</b>	<b>Description</b>	<b>Page No.</b>
Figure 1.1	Schematic of two substructures with power input to substructure-1	6
Figure 2.1	Broad classification of vibration signal processing-based VHM techniques	20
Figure 3.1	Two plates coupled at right angles	27
Figure 3.2	(a) Finite element L shaped plate model	33
Figure 3.2	(b) Finite element L shaped beam model	33
Figure 3.3	Variation of coupling loss factor <i>vs.</i> excitation frequencies for plate	35
Figure 3.4	Variation of coupling loss factor <i>vs.</i> excitation frequencies for beam	35
Figure 3.5	Variation of coupling loss factor with internal loss factor for plate	37
Figure 3.6	Variation of coupling loss factor with internal loss factor for beam	37
Figure 3.7	Variation of coupling factor with width for plate	38
Figure 3.8	Variation of coupling factor with width for beam	38
Figure 3.9	Velocity responses <i>vs.</i> excitation frequency for the horizontal beam	39
Figure 3.10	Velocity responses <i>vs.</i> excitation frequency for the horizontal plate	40
Figure 3.11	Variation of velocity responses for horizontal plate with width	40
Figure 4.1	Geometric dimensions of plates with spot- welds.	44

Figure 4.2	ACM2 Spot weld model	45
Figure 4.3	Finite element model (spot welded plates)	46
Figure 4.4	Overlapping region (spot welded plates)	47
Figure 4.5	Region near a spot weld	47
Figure 4.6	Geometric dimensions (in mm) of the adhesive bonded plates with lap joint	49
Figure 4.7	(a) Finite element model of adhesive bonded plates with lap joint	50
Figure 4.7	(b) Section of adhesive joint	51
Figure 4.8	Variation of the coupling loss factors <i>vs.</i> excited frequencies of plates with spot-welded joint	52
Figure 4.9	Velocity responses <i>vs.</i> excited frequencies for the excited plate with spot-welded lap joint	53
Figure 4.10	Velocity responses <i>vs.</i> excited frequencies for the receiver plate with spot-welded lap joint	53
Figure 4.11	Displacement response of plate with spot welded joint excited at frequency of 2000 Hz obtained using FE-ACM2 model	54
Figure 4.12	Displacement response of plate with spot welded lap joint excited at frequency of 2000 Hz obtained using FE-Monolithic model	55
Figure 4.13	Displacement response of plate with spot welded lap joint excited at frequency of 8000 Hz obtained using FE-ACM2 model	55
Figure 4.14	Displacement response of plate with spot welded lap joint excited at frequency of 8000 Hz obtained using FE-Monolithic model	56
Figure 4.15	Variation of coupling loss factors <i>vs.</i> excited frequencies of	57

	plates with adhesive bonded lap joint	
Figure 4.16	Velocity responses <i>vs.</i> excited frequencies for the excited plate with adhesive bonded lap joint	57
Figure 4.17	Velocity responses <i>vs.</i> excited frequencies for the receiver plate with adhesive bonded lap joint	58
Figure 4.18	Displacement response of plate at an excitation frequency of 2000 Hz. (actual FE adhesive modelled joint)	59
Figure 4.19	Displacement response of plate at an excitation frequency of 2000 Hz (FE-monolithic model for adhesive bond)	59
Figure 4.20	Displacement response of plate at an excitation frequency 8000 Hz. (actual FE-adhesive modelled lap joint)	60
Figure 4.21	Displacement response of plate at an excitation frequency 8000 Hz (FE-monolithic model for adhesive bonded lap joint)	60
Figure 5.1	Geometric dimensions of plates with spot- welds (Case-1)	63
Figure 5.2	Geometric dimensions of plates with spot- welds (Case-2)	63
Figure 5.3	Geometric dimensions of plates with spot- welds (Case-3)	64
Figure 5.4	Geometric dimensions of plates with spot- welds (Case-4)	64
Figure 5.5	Experimental set-up	66
Figure 5.6	Shaker for excitation	62
Figure 5.7	Shaker-stinger-force transducer attachment	67
Figure 5.8	LMS Data acquisition system	68
Figure 5.9	LMS test lab front panel to represent the acquired data	69
Figure 5.10	Force transducer	69
Figure 5.11	Geometry created in Test. Lab	71
Figure 5.12	Schematic of two plates with locations of 18 accelerometers	72
Figure 5.13	Experimental set up for two spot welded plates (Case-1)	73

Figure 5.14	Excitation location near the edge of LH-plate	74
Figure 5.15	Finite element model of two spot welded plates (Case-1)	76
Figure 5.16	Power injection method for a single plate	77
Figure 5.17	Comparison of mode shape for a single plate (Mode. No-2 )	80
Figure 5.18	Experimental sum-FRF (Case-1 )	80
Figure 5.19	Comparison of mode shape for case-1 (Mode. No-1 )	81
Figure 5.20	Comparison of mode shape for case-1 (Mode. No-4)	81
Figure 5.21	Velocity responses of Case -1 for spot-welded plates	84
Figure 5.22	Velocity responses of Case -2 for spot-welded plates	85
Figure 5.23	Velocity responses of Case -3 for spot-welded plates	85
Figure 5.24	Velocity responses of Case -4 for spot-welded plates	85
Figure 5.25	Three plates with spot-welded lap joints (healthy configuration: combination -1)	88
Figure 5.26	Three spot-welded plates with absence of spot-weld S <sub>22</sub> (damaged configuration: combination -2)	89
Figure 5.27	Velocity responses for spot-welded lap joints of healthy configuration	89
Figure 5.28	Velocity responses for spot-welded lap joints of damaged configuration	90
Figure 5.29	Flow chart for possible damage detection in joints	93
Figure 6.1	Bitumen based damping sheet glued on one side of the mild steel plate	96
Figure 6.2	Geometric dimensions of plates with bolted lap joint (Case-1)	97
Figure 6.3	Geometric dimensions of plates with bolted lap joint (Case-2)	97
Figure 6.4	Geometric dimensions of plates with bolted lap joint (Case-3)	98

Figure 6.5	Geometric dimensions of plates with bolted lap joint (Case-4)	98
Figure 6.6	Experimental set-up	99
Figure 6.7	Accelerometer for measuring the vibration	100
Figure 6.8	Geometry created in Test. Lab	101
Figure 6.9	Experimental setup for two bolted plates of Case-3	101
Figure 6.10	Two substructures with a non-conservative coupling joint	102
Figure 6.11	Finite element model of two plates	104
Figure 6.12	Finite element model of three plates	104
Figure 6.13	Coupled bolt finite element model	105
Figure 6.14	Bolt, nut and washers used for joining the plates	106
Figure 6.15	Experimental power injection method showing single-plate	108
Figure 6.16	Comparison of FEA and experimental mode shape (Mode. No-3)	110
Figure 6.17	Comparison of mode shape of Case-1 with initial strain (Mode. No-4)	111
Figure 6.18	Velocity responses of bolted joints for Case -1	114
Figure 6.19	Velocity responses of bolted joints for Case -2	114
Figure 6.20	Velocity responses of bolted joints for Case -3	114
Figure 6.21	Velocity responses of bolted joints for Case -4	115
Figure 6.22	Three plates with bolted lap joints (healthy configuration: combination -1)	117
Figure 6.23	Three bolted plates with absence of bolt B <sub>22</sub> (damaged configuration: combination -2)	118
Figure 6.24	Velocity responses for bolted lap joints of healthy configuration	118
Figure 6.25	Velocity responses for bolted lap joints of damaged	119

configuration

Figure 7.1	Geometric dimensions of plates with adhesive lap joint (Case-1)	124
Figure 7.2	Geometric dimensions of plates with adhesive lap joint (Case-2)	124
Figure 7.3	Geometric dimensions of plates with adhesive lap joint (Case-3)	125
Figure 7.4	Geometric dimensions of plates with adhesive lap joint (Case-4)	125
Figure 7.5	Experimental set-up	126
Figure 7.6	Accelerometer for measuring the vibration	126
Figure 7.7	Geometry created in Test. Lab	128
Figure 7.8	Experimentation for two adhesive bonded lap joint plates (Case-1)	129
Figure 7.9	Finite element model of an adhesive bonded lap joint (Case-1)	130
Figure 7.10	Densitometer for measuring density of acrylic plate	131
Figure 7.11	Experimental set-up for measuring elastic modulus of acrylic	132
Figure 7.12	Power injection method for a single acrylic plate	133
Figure 7.13	Comparison of mode shape (Mode. No-3)	135
Figure 7.14	Comparison of mode shape (Mode. No-5)	136
Figure 7.15	Comparison of mode shape for Case-1 ( Mode No-1)	137
Figure 7.16	Comparison of mode shape for Case-1 (Mode. No-4)	137
Figure 7.17	Velocity responses of Case-1 for adhesive bonded plates	141
Figure 7.18	Velocity responses of Case-2 for adhesive bonded plates	141
Figure 7.19	Velocity responses of Case-3 for adhesive bonded plates	141
Figure 7.20	Velocity responses of Case-4 for adhesive bonded plates	142
Figure 7.21	Variation of velocity responses with adhesive patch length	143
Figure 7.22	Three plates with adhesive bonded lap joints (healthy configuration)	145



Figure 7.23	Three adhesive bonded plates with absence of adhesive segment $A_{22}$ (damaged configuration)	146
Figure 7.24	Velocity responses for adhesive bonded lap joints of healthy configuration.	146
Figure 7.25	Velocity responses for adhesive bonded lap joints of damaged configuration	147

## LIST OF TABLES

<b>Table No.</b>	<b>Description</b>	<b>Page No.</b>
Table 3.1	Material and geometrical specifications	28
Table 3.2	Variation of coupling loss factor vs. excitation frequencies for the plate	34
Table 3.3	Variation of coupling loss factor vs. excitation frequencies for the beam	36
Table 4.1	Material and geometrical specifications	44
Table 4.2	Material and geometrical specifications	49
Table 5.1	Specification of the accelerometer	67
Table 5.2	Specification of the shaker	68
Table 5.3	Specification of the force transducer	70
Table 5.4	Material and Geometrical specifications	76
Table 5.5	Internal loss factor for the excited frequencies	77
Table 5.6	Comparison of resonance frequencies for elastic modes of a single mild steel plate	79
Table 5.7	Comparison of resonance frequencies for elastic modes (Case -1)	79
Table 5.8	Acceleration responses of spot-welded lap joint plate for Case-1	82
Table 5.9	Acceleration responses of spot-welded lap joint plate for Case-1 under unit force.	82
Table 5.10	Apparent coupling factor obtained experimentally for spot-welded plates	83
Table 5.11	Apparent coupling factor obtained numerically for spot-welded plates	83
Table 5.12	Power input (N-m/s) measured experimentally for spot-welded	84

plates

Table 5.13	Power input (N-m/s) obtained numerically for spot-welded plates	84
Table 5.14	Ratio of velocity responses obtained for spot-welded joints of LH-plate and RH-plate for excitation frequency, 3000 Hz	86
Table 5.15	List of possible combinations for three plates with spot-welded lap joints	87
Table 5.16	Comparison of acceleration responses for spot-welded joints, excitation frequency of 3000 Hz	91
Table 5.17	Percentage deviation of acceleration responses of the other possible combination in comparison to the healthy configuration (Combination 1), excitation frequency of 3000 Hz	92
Table 6.1	Specification of the accelerometer (bolted case)	100
Table 6.2	Material and Geometrical specifications of the Bolt M8 grade 4.6	107
Table 6.3	Internal loss factor at excited frequencies	108
Table 6.4	Comparison of resonance frequencies of a single plate for elastic modes	109
Table 6.5	Comparison of resonance frequencies for two and three bolted plates (FEA)	110
Table 6.6	Acceleration responses of bolted lap joint plate for Case-1	111
Table 6.7	Acceleration responses of bolted lap joint plate for Case-1 under unit force	111
Table 6.8	Apparent Coupling factors obtained experimentally for bolted plates	112
Table 6.9	Apparent Coupling factors obtained numerically for bolted plates	112
Table 6.10	Power input (N-m/s) measured experimentally for bolted plates	113
Table 6.11	Power input (N-m/s) obtained numerically for bolted plates	113
Table 6.12	Comparison of resonance frequencies (Hz) for two bolted plates	113

(FEA)

Table 6.13	Ratio of velocity responses obtained for bolted joints of LH-plate and RH-plate for excitation frequency, 3000 Hz	115
Table 6.14	List of possible combinations for three plates with bolted lap joints	116
Table 6.15	Comparison of acceleration responses for bolted joints, excitation frequency of 3000 Hz	120
Table 6.16	Percentage deviation of acceleration responses of the other possible in comparison to the healthy configuration (Combination 1) at an excitation frequency of 3000 Hz	121
Table 7.1	Specification of the accelerometer	127
Table 7.2	Elastic modulus of acrylic obtained from natural frequencies	132
Table 7.3	Material and geometrical specifications	132
Table 7.4	Internal loss factor at excited frequencies	134
Table 7.5	Comparison of resonance frequencies for elastic modes (single-plate)	135
Table 7.6	Comparison of resonance frequencies for elastic modes (Case -1)	136
Table 7.7	Acceleration responses of adhesive lap joint plate for Case-1	138
Table 7.8	Acceleration responses of adhesive lap joint plate for Case-1 under unit force excitation	138
Table 7.9	Apparent coupling factor obtained experimentally for adhesive bonded plates	139
Table 7.10	Apparent coupling factor obtained numerically for adhesive bonded plates	139
Table 7.11	Power input (N-m/s) measured experimentally for adhesive bonded plates	140
Table 7.12	Power input (N-m/s) obtained numerically for adhesive bonded	140

plates

Table 7.13	Ratio of velocity responses obtained for adhesive bonded joints of LH-plate and RH-plate for frequency, 3000 Hz	142
Table 7.14	Coupling factor for edge loading (3000 Hz)	143
Table 7.15	List of Possible Combinations for three adhesive lap bonded plates	144
Table 7.16	Comparison of acceleration responses for adhesive bonded joints, excitation frequency of 3000 Hz	148
Table 7.17	Percentage deviation of acceleration responses of the other possible combinations in comparison to the healthy configuration (Combination 1), at an excitation frequency of 3000 Hz	149

## ABBREVIATIONS

ACLF	: Apparent coupling factor
ACM	: Area contact model
ADC	: Analog to digital converter
ANSYS	: Analysis of systems
APDL	: Ansys Parametric Design language
CLF	: Coupling Loss Factor
CWELD	: Contact weld model
CWT	: Continuous wavelet transform
DAQ	: Data acquisition system
DOF	: Degree of freedom
DSP	: Digital signal processing
DI	: Damage index
EFC	: Energy flow coefficient
EIC	: Energy influence coefficient
EXP	: Experimental
ESEA	: Experimental statistical energy analysis
FE	: Finite element
FEA	: Finite element analysis
FEM	: Finite element method
FFT	: Fast Fourier transform
FRF	: Frequency response function
ICP	: Integrated circuit piezoelectric

MATLAB	: Matrix laboratory
LH	: Left hand
LMS	: Leuven measurement systems
RH	: Right hand
PIM	: Power injection method
RBE	: Rigid body element
RMS	: Root mean square
ROTX	: Rotation degree of freedom in 'X' direction
ROTY	: Rotation degree of freedom in 'Y' direction
ROTZ	: Rotation degree of freedom in 'Z' direction
SEA	: Statistical energy analysis
SEAL	: Statistical energy analysis like
SHM	: Structural health monitoring
STFT	: Short-time Fourier transforms
UX	: Translation degree of freedom in 'X' direction
UY	: Translation degree of freedom in 'Y' direction
UZ	: Translation degree of freedom in 'Z' direction
VHM	: Vibration based health monitoring
WT	: Wavelet transform

## NOMENCLATURE

$A$	: Area
$C_B$	: Bending wave speed
$C_L$	: Longitudinal wave speed
$d$	: Diameter
$E$	: Modulus of elasticity
$E_i$	: Energy in system $i$
$F$	: Force
$f$	: frequency
$I_i$	: Second moment of area
$M$	: Mass of system
$n(f)$	: Modal density per Hz
$P$	: Power input
$p$	: Pitch
$S_{af}(\omega)$	: Cross spectrum
$T$	: Preload torque
$t$	: Thickness
$V_i$	: Velocity in system $i$
$V^*$	: Complex conjugate velocity
$w$	: Width
$X$	: Ratio of plate thicknesses
$\eta$	: Internal loss factor
$\eta_{ij}$	: Coupling factor between system $i$ and $j$
$\rho$	: Density of the material
$\tau_{12}$	: Wave transmission coefficient
$\omega$	: Angular forcing frequency (rad/sec)
$\sigma$	: Proof stress
$\varepsilon$	: Initial strain
$\nu$	: Poissons ratio



# CHAPTER 1

## INTRODUCTION

### 1.1 OVERVIEW

A large number of engineering components used in automobile, aeronautical, marine and nuclear industries, are to be regularly monitored and maintained in order to avoid any catastrophic failures. Damage detection is a challenging area of structural dynamics research involving identification and quantification of damage at an early stage, moreover, it can cause serious problems and is relevant to take proper decisions regarding repair, part replacement, maintenance, etc. Enormous efforts have been directed towards the development of structural health monitoring (SHM) and condition monitoring techniques by X-ray, electric impedance technique, eddy current technique, local ultrasonic method, vibration method, etc., to predict the presence of damages or flaws, estimation of remaining useful life, improving reliability and safety of engineering structures and machine systems. The use of expensive systems and components can be optimized by adopting these techniques for identification of damages, leading to cost savings between 10 to 40 % due to reduced maintenance and the extended lifetime beyond the original design prediction (Doebling et al., 1997). Damage identification can be classified into the following levels (Rytter, 1991; Park et al., 2001).

Level 1: Determination that damage is present in the structure,

Level 2: Including Level 1, geometric localization of the damage,

Level 3: Including Level 2, quantification of the damage severity,

Level 4: Including Level 3, prediction of the remaining structure service life  
and

Level 5: Self-healing structures.

SHM is aimed at determination of the existence and type of damage, and its location and size, for detection and diagnostics. It involves (1) Operational evaluation, (2) Data acquisition, cleaning, and fusion (3) Feature extraction and (4) Statistical model development for feature discrimination.

## 1.2 VIBRATION BASED DIAGNOSTICS

Non-destructive testing methods like visual inspection, acoustic, ultrasonic, magnetic field, eddy-current, thermal field or radiography methods that have been widely used for structural damage detection are very time consuming and laborious, but are also localized to a single component or segment of a much larger structure. These methods require close proximity to the damaged location and easy accessibility for application. One emerging potential candidate for the detection is vibration based health monitoring, using modal parameters which are functions of the physical properties of the structure. Any changes in the properties like mass, stiffness, damping due to damage or internal defects can cause variations in modal parameters of the structure like natural frequencies, mode shapes, mode shape curvatures, strain energy distributions, etc. Changes in the natural frequencies requires the presence of a large damage and cannot determine the damages if the measurements acquired is not accurate (Doebbling et al., 1996). It also calls for the requirement of a single excitation point and a roving exciter for the vibration measurement (Castellini et al., 2006) to minimize the drawbacks of mode shape parameters. Changes in the mode shape curvatures have been found to be more suitable than mode shape variations for locating damage (Carden et al., 2004). These methods correlate the observed signatures of the damaged structure with analytical or computational models to detect the damage. Various models such as autoregressive and moving average (ARMA) model, hidden Markov model (HMM), artificial neural network (ANN) including the use of finite element models, etc. fall in this category.

Piezoelectric sensing agents have contributed to the recent strides in guide wave based damage detection like the use of acousto-ultrasonics, lamb waves, etc. due to the method's non-destructive nature (Purekar, 2006; Mahapatra et al., 2004). The basic objective of guide wave technique is to detect small incidences of damage over a wide area using transducers attached to the structure. SHM is also categorized into local and global methods (Fritzen et al., 2006), wherein the classification is based on the relation of the wavelength of the experimented signals with respect to the defect size and the whole structure dimensions. Another is the feature-based method of damage detection involving feature extraction from signals. Various features that can be used,

include (a) Time-domain features (such as mean, standard deviation, range, root mean squares, skewness, kurtosis, crest factor, etc.), (b) Frequency-domain features (such as frequencies, damping ratios, energy in different frequency bands, etc.), (c) Spatial domain features and (d) Time-frequency domain features (i.e. time-frequency distribution). The SHM based on the vibration approach consists of three steps, i.e., signal monitoring, signal processing and data interpretation. These are of present research interest and is discussed in the following sections.

### **1.2.1 Signal monitoring**

Vibration measurement is an effective, reliable and nonintrusive technique to monitor the condition of a structure or machine (Scheffer et al., 2004). Vibration sensors are the heart of modern SHM systems that detects the vibration parameters from a vibrating element and converts it into equivalent electrical signals. These signals are analyzed by signal processing techniques to extract features of interest like amplitude, frequency, displacement, velocity, acceleration, phase and period. Typical vibration transducers either contact or noncontact used are displacement transducers (vibrometer or proximity probes), velocity transducers, accelerometers or laser doppler vibrometers.

### **1.2.2 Signal processing**

Some of the commonly used signal processing methods are statistical time series models, probability distribution and density function, Fast Fourier transform (FFT), short-time Fourier transform, Cohen's class, wavelet transform (WT), cepstrum analysis, Hilbert–Huang transform, power spectral density (PSD). Modal domain based signal processing methods are interpreted easily in terms of natural frequencies, mode shapes and damping factors than features extracted from the time domain (e.g., residuals of the autoregressive model) and frequency domain (e.g., the distortion identification functions) (Carden et al., 2004). Various feature extraction techniques like statistical domain, frequency domain, time domain and time-frequency domain are used for obtaining diagnostic information. Measured raw data from the structure by the vibration transducers *viz.* accelerometer, is usually in the time domain. The

frequencies present in the response of the structure can be obtained by using Fast Fourier Transform (FFT), a real-time analysis to perform quick transformations of functions from the time domain to frequency domain or vice versa. After that, the modal domain data is obtained from the frequency domain data or using modern techniques that directly convert the time domain data to modal domain data (Maeck et al., 2000).

### **1.2.3 Data interpretation and discrimination**

Practical applications require geometric localization discriminator with damage quantification for maintenance related repair, prognosis, and the remaining useful life. Many discrimination techniques are application-specific and rule-based, depending on feature selection. Damage indices have been developed and applied to engineering structures (Stubbs, et al., 1996). Fisher discrimination techniques (Sierra, 2001) can be used to statistically validate an expert-based system. Euclidean distance classifier is a simple way to discriminate between damaged and undamaged scenarios. Machine learning techniques train models with the help of training dataset, based on which, it creates some threshold values for classification. The trained model is then used for analyzing and classify the testing dataset using these threshold values. Feature extraction, selection and classification are the most important phases in machine learning techniques. Data interpretation includes artificial neural networks, fuzzy logic, support vector machine, bayesian classifiers and hybrid classifiers.

Vibration-based health monitoring has been used for low-frequency problems (e.g., Doebling et al., 1998). However, there are situations and issues, wherein the incipient damage affects mainly on highest modes, rather than on lowest in cases of connections of structures with cleats, spot welds, etc. found in the automobile, aerospace, nuclear and marine applications (Lopez-Diez et al., 2005). High-frequency structural analysis so far has been a major issue in dynamic analysis. There are conventional and traditional modal analyses used to analyze the low-order modes (Hopkins, 2007). Statistical energy analysis (SEA) is one of the widely used methods in this regime with advantages in the analysis of high frequency, high modal density,

and complex dynamic systems, well-suited to periodic structures consisting of an assembly of identical elements or substructures.

The present work focuses on the numerical and experimental investigations on damage detection in plates with lap joints based on statistical energy analysis like approach. Detection based on apparent coupling factors have been used to predict velocity and acceleration responses for possible detection of damages in the spot-welded, bolted and adhesive bonded plates.

### **1.3 STATISTICAL ENERGY ANALYSIS**

Statistical energy analysis (SEA) was developed by Lyon and Smith in 1959, based on their work on power and response of linearly coupled resonators. SEA concerns mainly on two basic principles. Firstly, long-term averages of vibrational energy levels are considered as the primary variables used to describe problems. These time-invariant energy flows along with the known forcing functions, system parameters, and dissipative flows are computed to set up energy balance equations that can be solved further to predict the long-term average vibrational energy levels in all parts of the system. It allows the designer in knowing the distribution of vibrational energy around a system. The second principle is based on the random parameters in which responses are computed as averages across ensembles of similar systems. SEA uses substructures that store modal energy to represent structures and enclosed acoustic volumes within a system. These substructure responses describe the ensemble average response of a set of similar systems. Substructures are structural or acoustical entities that have modes which are similar in nature. In many applications, geometrical structural elements are substructures, sometimes different wave types, e.g., bending or longitudinal waves, form substructures. SEA approach is most applicable to structures made of parts containing a significant number of resonant modes and has a high degree of modal overlap, although it is difficult to produce definitive guidelines. Large and lightweight structures acted upon by high frequency broad-band loads can analyzed using SEA Approach. Examples are the spacecraft or aircraft fuselage panels excited by aerodynamic turbulence, car panels, offshore and ship structures under structural or airborne excitation.

### 1.3.1 Steady-state power balance

Lyon (1975) had used a thermal analogy to describe the distribution of modal energy in the SEA system for each substructure. Heat flows from substructures with a high temperature to those with a low temperature. Similarly, energy flows from high modal energy substructures to low modal energy substructures. The principle of SEA is demonstrated with a two-substructure model as shown in Figure 1.1. The power dissipated by each substructure is shown with power flows from substructure 1 to 2 as  $P_{12}$ , and from substructure 2 to 1 as  $P_{21}$ , via internal losses due to dissipations,  $P_{diss,1}$  and  $P_{diss,2}$  in substructures 1 and 2, respectively. The power input into substructure-1 assumed to be a higher modal density than substructure-2. In general, the power flow from substructure  $i$  to substructure  $j$ , is described by (Norton, 1989)

$$P_{ij} = \omega \eta_{ij} E_i \quad (1.1)$$

$$\frac{dE_i}{dt} = 0 \quad (1.2)$$

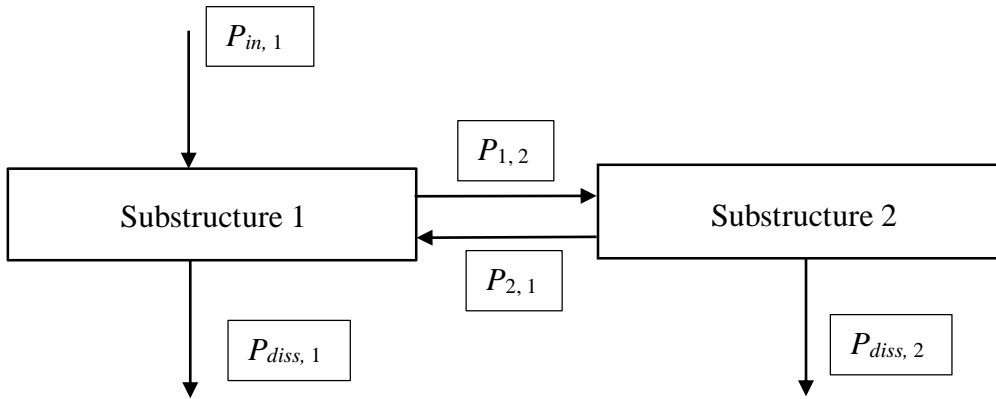


Figure 1.1 Schematic of two substructures with power input to substructure-1

where,  $P_{ij}$  is the power flow,  $E_i$  is the vibrational energy in substructure  $i$ ,  $\omega$  is the angular frequency, and  $\eta_{ij}$  is the coupling loss factor from substructure  $i$  to substructure  $j$ . Steady-state SEA assumes that the energy within a substructure does not change over time, whereas the time-averaged total vibrational energy in a substructure is defined by (Norton, 1989)

Therefore, the power gained by one substructure is equal to the power lost by another substructure. The power balance equations for the two-substructure model with power

input to substructure 1 can be expressed through following Equations (1.3) and (1.4) for substructures 1 and 2, respectively.

$$P_{in,1} + \omega\eta_{21}E_2 = \omega\eta_{11}E_1 + \omega\eta_{12}E_1 \quad (1.3)$$

$$\omega\eta_{12}E_1 = \omega\eta_{22}E_2 + \omega\eta_{21}E_2 \quad (1.4)$$

Equations (1.3) and (1.4) are solved for determining two unknown vibrational energies in substructures,  $E_1$  and  $E_2$ . Additionally, the following few assumptions need to be satisfied to study sets of substructures using SEA (Hopkins, 2007):

1. Statistically autonomous excitation forces.
2. Equal possibilities of modes happening in a certain frequency range.
3. Power flow between substructures is proportional to the differences in modal energies of the coupled substructures.
4. Power input or power transmitted to a substructure is either dissipated in the substructure or transmitted to adjacent substructures via junctions of structures or interfaces between structures and acoustic spaces. Thus, the entire power is accounted.
5. Equal partition of modal energy in a substructure and incoherent modal response among nodes in the coupled substructures.
6. Light or weak coupling among substructures.

The first criterion is of particular interest in the present study. The statistically autonomous forces of excitation can be realized by employing rain-on-the-roof excitation. This can be approximated by averaging the response from point excitations at a number of random positions for measurement and numerical simulation. There are several assumptions that are generally made in the development of SEA models and following few of them are considered in the present study.

- a) The input power spectrum is broadband, i.e. there are no strong, pure tones in the input power spectra.
- b) Energy is not created in the couplings between substructures. Energy may be dissipated in junctions between substructures, such as in isolation

mounts, but generally, this effect is added to substructure damping loss factors.

- c) The damping loss factor is equal for all modes within a substructure and analysis band.
- d) Modes within a substructure do not interact except to share an equal partition of energy. The coherent effects between modes are ignored to facilitate the application of power sums.

### 1.3.2 Loss factors

The three loss factors, namely, coupling, internal and total loss are described in energy loss per radian cycle in a given frequency band, which is usually an octave-band or one-third octave-band. The coupling loss factor (CLF) describes the fraction of energy transferred from one substructure to another per radian cycle. There is a consistency relationship between two substructures and relates two CLFs using substructures' modal densities (Norton, 1989) as

$$\frac{\eta_{ij}}{n_j} = \frac{\eta_{ji}}{n_i} \quad (1.5)$$

where  $\eta_{ij}$  is the CLF from substructure  $i$  to substructure  $j$ , and  $n_i$  and  $n_j$  are the modal densities of substructures  $i$  and  $j$ , respectively. The internal loss factor describes the fraction of energy transferred due to dissipative processes contained within a substructure. The total loss factor for a substructure describes the damping for that substructure due to all processes and equals the sum of the internal loss factor and CLFs. That is,

$$\eta_i = \eta_{ii} + \sum_{i \neq j} \eta_{ij} \quad (1.6)$$

where  $\eta_i$  is the total loss factor for substructure  $i$ , and  $\eta_{ii}$  is the internal loss factor for substructure  $i$ .



### 1.3.3 Power balance

A complex structure is divided into several substructures, and its vibration response is predicted through SEA (Lyon, 1975). The power balance relation for  $N$  structures is given by

$$\omega \begin{bmatrix} \left( \eta_1 + \sum_{i \neq 1}^N \eta_{1i} \right) n_1 & -\eta_{12} n_1 & \cdots & -\eta_{1N} n_1 \\ -\eta_{21} n_2 & \left( \eta_2 + \sum_{i \neq 2}^N \eta_{2i} \right) n_2 & \cdots & -\eta_{2N} n_2 \\ \vdots & \vdots & \ddots & \vdots \\ -\eta_{N1} n_N & \cdots & \cdots & \left( \eta_N + \sum_{i \neq N}^{N-1} \eta_{Ni} \right) n_N \end{bmatrix} \times \begin{bmatrix} \frac{\langle \bar{E}_1 \rangle}{n_1} \\ \frac{\langle \bar{E}_2 \rangle}{n_2} \\ \vdots \\ \frac{\langle \bar{E}_N \rangle}{n_N} \end{bmatrix} = \begin{bmatrix} \bar{P}_{i,1} \\ \bar{P}_{i,2} \\ \vdots \\ \bar{P}_{i,N} \end{bmatrix} \quad (1.7)$$

where,  $P_{i,n}$  is the power injected in substructure  $i$ ,  $\langle E \rangle$  is the frequency averaged energy in substructure  $i$ . The bar above symbol indicates frequency averaging,  $\langle \rangle$  indicates spatial averaging,  $\eta_i$  is the internal damping loss factor in substructure  $i$ ,  $\eta_{ij}$  is the coupling loss factor from substructure  $i$  to substructure  $j$ , where  $n$  is the modal density.

General matrix solution solves  $N$  simultaneous equations to determine the energy in each of the  $N$  substructures via inversion of the loss factor matrix. The energies of the substructures can be computed if the internal loss and coupling factors are known for corresponding power inputs. Similarly, the loss factors can be computed once the energies in the substructures are known for the corresponding power inputs. The advantages, limitations, and applications of spot-welded, bolted and adhesive joints, which are considered for the analysis in the present study and discussed in the following sections.

## 1.4 SPOT WELDED JOINTS

Resistive spot welding is a process in which contacting metal surfaces, typically sheets in the 0.5 to 3 mm thickness range are joined by the heat obtained from resistance to electric current. The process uses two shaped copper alloy electrodes to concentrate welding current into a small "spot" to simultaneously clamp the sheets

together. Connecting surfaces should be free of contaminants such as scale, oil, and dirt, to ensure quality welds. However, the resistance welding depends on three factors, namely, time of current flow ( $T$ ), the resistance of the conductor ( $R$ ) and amperage ( $I$ ).

The main advantages are adaptability for automation in the high-rate production of sheet metal assemblies, dimensional accuracy and economical. The limitations are the difficulty for maintenance or repair, adds weight and material cost to the product compared with a butt joint, generally have a higher cost than most arc welding equipment, produces unfavorable line power demands, low tensile and fatigue strength. The full strength of the sheet cannot prevail across a spot welded joint. Thicker stock is more difficult to spot weld because the heat flows into the surrounding metal more easily.

## **1.5 BOLTED JOINTS**

Structural system design involves connections of parts or components through bolts, rivets, and pins. The advantages of bolted joints are ease of assembly and disassembly and do not require specialized personnel in comparison to the welding process. Their limitations are that they require holes, which introduces stress concentrations and failure modes and can become loose over time as the nut backs off. They usually require access to both sides of the joint and damage to a threaded hole is tough to replace. A bolted joint adds to the part count and corrosion between a bolt, and the parent material should be considered, and bolted joints require a gasket to seal a joint, whereas, a weld is usually leak-proof. A joint consisting of un-tightened bolts will frequently fail within a few cycles. If the preload provided by the bolt is insufficient, joint separation and movement can occur resulting in possible bolt fatigue and self-loosening issues.

## 1.6 ADHESIVE JOINTS

Adhesive bonding has gained importance in structural bonding in the aircraft industry as an alternative method of joining materials together over the more conventional joining methods. It is gaining interest due to the increasing demand for joining similar or dissimilar structural components, mostly within the framework of designing light weight structures. It offers the possibility to join dissimilar materials, tending to have good sealing, noise, and vibration damping properties. It is often a convenient and cost-effective technique. The limitations are that surface pre-treatment of the substrates to be joined, and environmental conditions have a major effect on the strength of the joint. It has a limited service temperature range. The strength and toughness of adhesives are typically relatively low compared to metals, and therefore their use is limited to only joining thin sheet metals. Commercial techniques for non-destructive testing of adhesively-bonded joints are relatively limited compared to those used with other fastening methods. Adhesive joints are inherently weak in peel, and vehicle designs need to take account of this, particularly with regard to crashworthiness.

The application of energy approaches based on SEA like approach and parameters like apparent coupling loss factor or energy influence coefficients between substructures can be used to detect and localize the damage. Energy based approaches for high-frequency analyses are well-suited to periodic structures consisting of an assembly of identical elements or substructures that are connected in some identical manner, e.g., skin-stringer panels found in airplane fuselages and truss beams that form the support structure of a space station.

The present work is oriented towards the damage detection of joints based on statistical energy analysis like principles using the vibration signals obtained from finite element analysis and experiments. Detection based on parameters like apparent coupling factors have been used to predict velocity and acceleration responses to detect damages in the spot-welded, bolted and adhesive bonded plates.

## **1.7 SEAL APPROACH**

The power balance equation (1.7) of SEA relates the ensemble average powers and energies, whereas the predictions from finite element analysis based on a single frequency depends on the specific input data chosen for the FEA. Thus the individual case is different from the mean in an ensemble of cases. The term SEA like (SEAL) is adopted to distinguish between SEA and the use of the energy flow balance in SEA as applied in the energy flow model for the individual case (Fredo, 1997). The coupling loss factor estimated is also referred to as an apparent coupling loss-factor (ACLF) or energy flow coefficient (EFC) for such specific cases, dependent on the system properties, boundary conditions, and excitation to distinguish it from ensemble-based estimates. The variation of the ACLF or EFC's decreases with the increase in modal overlap and modal density and tends towards the CLF at high frequencies. SEAL approach is thus a method for applying the conventional SEA for the individual case.

## **1.8 ORGANISATION OF THE THESIS**

The thesis comprises of eight chapters. A brief discussion on each chapter is highlighted below:

Chapter 1 introduces the importance of damage detection, vibration-based health monitoring, significance of high-frequency based damage detection and the use of statistical energy analysis in the high-frequency domain. This chapter also brings out the brief outline of the theory of SEA and a brief description regarding spot-welded, adhesive and bolted joints used in the present study.

A detailed literature review on statistical energy analysis (SEA) techniques specifically using experimental and finite element based SEA, numerical modeling of spot-welded, adhesive and bonded joints, vibration-based health monitoring and pattern recognition approaches have been reported in Chapter 2. The chapter also describes the motivation of the present study, objectives, and scope of the research work.

Chapter 3 discusses the effects of internal loss factor of the material on the determination of coupling loss factors of two mild steel plates coupled in an 'L'

configuration. The detailed procedure of determination of coupling loss factors (CLF) and velocity responses using finite element analysis and its comparison with the analytical wave-based approach are discussed in this chapter.

Finite element models used in the finite element analysis of spot-welded and adhesive joints are given in Chapter 4. Two lap joined plates by spot-welds, and adhesive bond are considered for the studies. The velocity responses and coupling loss factors obtained by the finite element analysis has been compared with the analytical wave-based approach and monolithic finite element model assumption based analysis.

Chapter 5 describes the damage detection studies carried out for plates with spot-welded lap joints. It also covers the details about the experimental setup, sensors used, data acquisition system, experimental procedures, finite element analysis, determination of velocity responses and coupling factors for two plates lap joined by spot welds for four cases. Moreover the results and discussion about the joint damage detection using the statistical energy analysis like (SEAL) approach for three plates lap joined by spot-welds for the healthy and damaged configuration and its comparison with the finite element analysis and experiments is also studied in detail.

Damage detection studies are carried out for plates with bolted lap joints and reported in Chapter 6. The chapter also highlights the experimental setup, experimental procedures, finite element analysis, determination of velocity responses and coupling factors for two plates lap joined by bolts for four cases. It also describes the results and discussion about the joint damage detection using the statistical energy analysis like (SEAL) approach for three plates lap joined by bolted joints for the healthy and damaged configuration and comparative studies with the finite element analysis and experiments are made.

Chapter 7 describes the damage detection studies carried out for plates with adhesive bonded lap joints. It also mentions the details about the experimental setup, sensors used, data acquisition system, experimental procedures, finite element analysis, determination of velocity responses and coupling factors for two plates lap joined by an adhesive patch for four cases. It also highlights the results and discussion about the

joint damage detection using the statistical energy analysis like (SEAL) approach for three plates lap joined by adhesive bond for the healthy and damaged configuration and its comparison with the finite element analysis and experiments.

Finally, Chapter 8 concludes the findings from the research work, presents the future scope of this study and provides the key contributions from the study. This chapter is followed by the references and list of publications.

## **CHAPTER 2**

### **LITERATURE REVIEW**

#### **2.1 INTRODUCTION**

In this chapter, the most important and significant contributions of the present state-of-art related to statistical energy analysis, finite element modelling of spot welded, bolted joints and adhesive bonded, vibration based health monitoring, SEA based damage detection, and pattern recognition approaches are discussed in detail.

#### **2.2 STATISTICAL ENERGY ANALYSIS**

Lyon (1975) predicted the coupling loss factors (CLFs) during the initial stage of the development of statistical energy analysis (SEA) by using finite element analysis (FEA). Input and dissipated powers, frequency averaged substructure energies, yielding time and energy flow models are formed by the post-processing of the outcomes of a system' FEA through the description of computationally efficient methods (Mace et al., 2000). CLFs (Hopkins, 2002) are used in SEA and are determined by using Monte Carlo methods, experimental statistical energy analysis (ESEA) and finite element methods. The intention was to facilitate the use of SEA with plate substructures that have low modal overlap and low modal density by using the concept of an ESEA ensemble. Systems are modeled as a combination of SEA substructures and finite element (FE) components with parametric uncertainty, which has been dealt by Monte Carlo simulations, first order reliability method and Laplace's method. Langley (2014) developed efficient algorithms for propagating parametric uncertainty within the context of the hybrid FEA or SEA method to the analysis of composite vibro-acoustic systems

Nack et al. (2000) extended SEA to the middle-frequency region by using impedance matrices that can be found by FEA software like NASTRAN and the results have been post processed to determine CLFs. Although it is often hard to realize an ensemble in real applications, the power balance equations for SEA are assessed

purely in terms of ensemble averages. Instead, a term similar to CLF may be received for a specific realization and the power balance equations hold for a single realization. According to Park et al. (2004), this is denoted as the effective CLF. Therefore, instead of the precise CLFs based on an average of several realizations, the apparent or effective CLFs are obtained. In order to deduce the power transmission between two thin plates, the FE technique is combined with a statistical energy analysis-like (SEAL) energy flow balance (Fredo, 1997). The major difference is that SEAL covers individual case, whereas SEA is applied to ensembles.

The power injection method (PIM) has become widely accepted as a valuable technique to predict the SEA parameters of a structure in situ. PIM requires the measurement of the power input into every single substructure and the measurement of the energy level of every substructure. By inverting the appropriate measured energy matrix, the SEA parameters can be obtained. (Bies et al., 1980). Conventional PIM suggests using a more or less predefined number of excitation and response locations. Most often, three excitation and five response locations are taken (Lalor, 1990). Due to the spatial variation of the energy density in a substructure, there will always be a substantial variability associated with the space-averaged energy of vibration and hence associated with the SEA parameters. An accurate SEA model requires accurately measured space averaged energies of vibration and power input levels (Langhe et al., 1996).

Cereceda et al. (2015) has employed a hierarchical cluster analysis based on the problem eigen modes to divide the system into cells and group them into substructures. They have proposed an automatic technique of identifying SEA substructures within a vibro-acoustic system. Àngels Aragonès et al. (2015) have defined stochastic biparametric SEA graphs for addressing the contributions of transmission paths in SEA models for detecting and rectifying vibro-acoustic problems. The mean and variance values are assigned to the edges of the SEA graphs. Rapid classification deterministic algorithms have been applied in the conversion of the stochastic SEA graph into an extended deterministic SEA graph for devising an efficient ranking of paths. Lopez-Diez et al. (2005) have applied SEA on a stiffened panel in the detection of initial damages in a distinctive structure of spacecraft. The



impact on the system features has been studied to determine the damage on the attachment element. The damage is detected and localized by using the CLFs between sub-elements and instead of being on the lowest modes, the effects of initial damages are primarily on the highest modes. Park et al. (2017) has applied SEA to two different floor systems: a concrete double tee floor and a concrete floor supported by concrete beams and columns to assess impact noise horizontally.

### **2.3 ANALYSIS OF SPOT WELDED JOINTS**

The most widely used spot weld models are CWELD and Area Contact Model 2 (ACM2). Palmonella et al. (2004) has given the guidelines for optimally implementing the CWELD and ACM2 models, which are examined and improved by updating models in structural dynamics. The veracity of the most common coarse models of spot welds is improved by reviewing the available literature and by model update done by evaluating the vibration features (Palmonella et al., 2004). ACM2 is a simplified spot weld model appropriate for vibration analysis. Kurtani et al. (2011) modelled three spot welds as ACM2 model to join the dynamic features of two steel plates. Appropriate mesh size in the spot weld area and the effect of the mesh pattern (surrounding a spot weld) on the model properties (mode shape and natural frequency) of a spot welded structure have been suggested for the ACM2 model. The outcomes depict that the model properties are significantly impacted by the size and configuration of the patch (group of shell elements in the ACM2 model). The variation in the natural frequency is small when the patch is composed of shell elements, which are either smaller than or similar to the solid element size, defined by the spot weld diameter.

### **2.4 ANALYSIS OF BOLTED JOINTS**

Yoshimura (1977) suggested a simple analytical joint model for describing bolted and welded joints. The model was comprised of a parallel dashpot and a spring that connected all co-ordinate directions of the two substructures. The damping coefficients of the dampers and the stiffness of the springs used in the model were found to be equal to the joints' damping coefficients and stiffness. In order to

represent bolted joints, Wang and Liou (1991) formulated a direct identification technique by using the same model as a group of dashpots and parallel stiffness. A least-squares technique, with the input of frequency response functions (FRFs) of the substructures and their assemblies, was used to identify the parameters of damping coefficients and stiffness.

Bickford (1991) proposed an equation on the basis of FEA for gauging the effective area of the bolted joint. A standard cone angle of  $30^\circ$  is proposed by Shigley and Mischke (2006) that proves to be a simple technique and the best value of joint material stiffness. Wileman et al. (1991) suggested an exponential expression for member stiffness after carrying out an axi-symmetric FEA. In order to assess the member stiffness on the basis of the structure's elastic energy, a contact FEA was conducted by Pedersen (2008).

In order to identify the dynamic equivalent features of bolted joints, Tol et al. (2015) used various approaches, such as measuring the coupled structure and FRFs of substructures and employing the FRF decoupling technique. Likewise, a damper was used to simulate the damping effects of the joint and a combination of linear and non-linear springs was used to model the joint interface.

Hamid and Jalali (2007) have proposed a method of minimization of the difference between the experimentally measured data and the model predictions to identify the damper coefficient and the spring constants of the bolt model. These two parameters are the functions of normal and tangential stresses at the interface of the joint. In order to consider the contact behavior and the pre-tension effect between the flanges to be joined, Kim et al. (2007) have proposed four types of FE models, namely, solid bolt model, coupled bolt model, spider bolt model and no-bolt model.

## **2.5 ANALYSIS OF ADHESIVE BONDED JOINTS**

The effects of adhesive layer thickness, mechanical properties and its loss factor on the dynamic response of lap joint have been studied by Vaziri et al. (2004) where accelerometer and a noncontact laser vibrometer were used on aluminum adherents joined by Hysol EA 9689 adhesive films. FEA is employed for examining the effects

of several features on the joints that are subjected to dynamic forces and bonded by adhesives. It was noticed that the resonance amplitudes were extraordinarily reduced by damping (Kaya et al., 2004) and the torsional frequencies increased according to the rise in Young's adhesive modulus. This observation was possible by studying the effects caused by variations in the material properties of the structural adhesives. Various deformations in the jointed section of the odd and even modes were demonstrated by the mode shapes (He et al., 2010).

Structural health monitoring technology has been applied for the detection of debonding in composite bonded patches through changes in the frequency response (White et al., 2009). Pandurangan et. al. (2006) have identified the changes in modal damping ratios and its co-relation to the damage in metal-to-metal adhesive joints through vibration-based non-destructive evaluation.

Whittingam et al. (2006) have used the acoustic and structural responses received from adhesive bonded GFRP composite beam specimens to identify the presence, location and size of a delamination. These specimens are with artificial delamination of various locations and sizes embedded in the bond-line and are excited by using piezoelectric actuators that are bonded to the surface.

## **2.6 VIBRATION-BASED HEALTH MONITORING**

The structural vibration response is altered by a change in the physical properties caused by the changes in a structure (including damage). Such changes can be controlled through global non-destructive testing methods, known as vibration-based health monitoring (VHM) methods. They can be broadly classified into two classes, namely, modal analysis and frequency response analysis. Modal analysis techniques analyze modal parameters obtained from acquiring vibration responses, while frequency response techniques analyze various frequency components acquired from the vibration responses. Frequency response techniques can be further classified into low-frequency and high-frequency response techniques, as visualized in Figure 2.1.

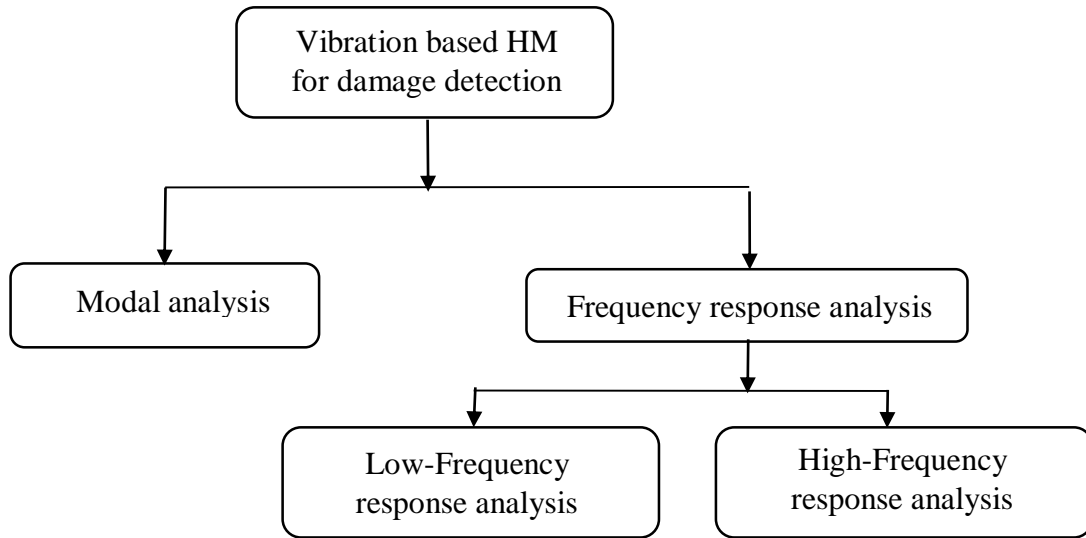


Figure 2.1 Broad classification of vibration signal processing-based VHM techniques

A study involving the experimental usage of mode shape curvatures to detect damages in beam structures was presented by Hamey et al. (2004). Wahab and De Roeck (1999) has compared the absolute difference of four techniques of curvature mode shape, curvature damage factor, damage index (Stubbs et al., 1995) and FRF curvatures. Rather than using the general approximations to the second order derivatives of displacements, the utilization of direct measurements of mode shape curvatures from piezoelectric materials was suggested. The time domain responses were measured from a set of measurement points by Choi and Stubbs (2004) for developing a method of locating and determining the size of damage. The mean strain energy was computed for each element of the structure over a period of time and was used for devising a DI that represented the ratio of the parameters of stiffness of pre-damaged and post-damaged structures. In order to locate the damages and their severities in the structure, they used this DI and employed a statistical classification algorithm called hypothesis testing. They used a beam structure to validate their methodology.

The easily experiment able and measurable modal features of the structure and the lower resonant frequencies are utilized for applying VHM in most of the applications. These frequencies have unfortunately turned out to be insensitive to damage, particularly to the lower levels, as reported in several case studies. Substantial

inaccuracies may result from the estimate of mode shapes, which are difficult to measure and which present an alternative for damage evaluation. Updating techniques are another option that depend on a particular model of the structure (mostly linear) and thereby result in inaccuracies. This is found to be particularly true in cases where non-linear effects are present and/or when the structure is more complex (Doebbling et al., 1998). Farrar et al. (1997) has shown that the resonant frequencies of a structure are statistically resistant to random error sources as compared to other modal parameters. Further, it requires predetermined types and quantities of damage. Since modal parameter methods do not provide high sensitivity from high frequency ranges, it is necessary to explore other means for damage detection. In the present research, excitation frequency ranges outside the limitations of current modal parameter analysis methods.

Frequency response-based techniques involve measurement of responses from active vibrations in the structure and their analysis for damage detection. In this approach, a structure is excited first with some load, transient impact or sinusoidal vibration, and the traveling vibrations are measured at some distance by sensors. The signal responses are picked up instead of modal parameters and are analyzed through signal processing or some other techniques for assessing the severity and/or location of the damage in the structure. The advantages of the FRF curvature method were relatively studied with those of other methods in frequency response-based damage detection by Sampaio et al. (1999). They ascertained that the FRF curvature method works well with only measured response data and does not need to refer to any modal parameter for damage identification. Apart from the modal frequencies, it encompasses the frequencies in the measurement range too. Madhavan et al. (2014) have utilized the vibration responses of bladed disk rotor on an operational turbine as an effective rotor condition monitoring tool and the damage to blade has been detected in situ from observed vibration abnormalities. Capozucca (2014) has analyzed the vibration of damaged and undamaged carbon fiber reinforced polymer beam elements. The single positions of the accelerometer are considered for the experimental extraction of frequencies at each damage level and the experimental outcomes are discussed and compared with the definition of the theoretical data Lakhdaret et al. (2013) have

detected damage by vibration analysis and exploitation of the dynamic response of a composite structure. The obtained results have been compared with the predicted numerical models to ascertain the effectiveness of the approach.

Vibration-based damage detection at high frequencies in kHz range based on piezoelectric sensing have been developed and employed (Doebbling et al., 1999). Acousto ultrasonics is one such popular NDT method in the structural health monitoring. Mahapatra et al. (2004) have detected delamination in composites experimentally and by finite element analysis. The limitations of the method is the sensitivity exchange between detection of small damages and the ability to globally interrogate a structure. Lamb wave analysis has been used with an active smart sensing system on a variety of experimental specimens to assess its success as a damage detection method (Purekar, 2006). Lamb wave features measured from spatially limited target points are prone to piling up other lamb wave signals reflected from other lamb wave signals in complex structural boundaries, making it difficult for identification in real life complex structures. Wavelet transformation and analysis has been utilized in a variety of applications for damage diagnostics. Yen and Lin (1999) have used wavelet packet transforms for damage detection from vibration signals recorded from the aft main power transmission of a U.S. Navy CH-46R helicopter. Wang et al. (1996) have investigated the bearing failure of laminated composite double-lap metal, composite, metal and bolted joints.

## **2.7 PATTERN RECOGNITION APPROACHES**

There is a need for a damage discrimination method for successful damage prediction that can prove to be useful to determine the need for repair. Expert discrimination systems are rule-based, application-oriented and, depending on feature selection. As such, the discrimination between two or more categories of signal are suggested by the pattern recognition problems for vibration-based damage detection, quantification and localization. Tan et al. (1995) have developed damage indices and applied to aerospace engineering structures. A number of statistical methods like the Fisher discrimination techniques provide a means to validate a specific expert system (Ma et al., 2004). The categories of signal may be those from an intact structure and a

damaged structure or those from a structure with various damage levels or locations (Sohn et al., 2001; Manson et al., 2003; Trendafilova and Heylen, 2003). Several studies have suggested the application of principal component analysis (PCA) for VHM and structural vibration (Trendafilova and Imbabi, 2004; Ni, et al., 2006; Zang and Imregun, 2001). Data compression becomes necessary as the experimental data becomes large and the identification of key features for damage detection is very important.

## **2.8 MOTIVATION**

Traditional damage detection methods are consisting of visual inspection and localized non-destructive evaluation techniques that are based on foreseen damage locations (Doebbling et al., 1998). The research work draws an attention to overcome these disadvantages like vibration based health monitoring deals at low frequencies. An issue with these methods is the general level of sensitivity that modal parameters have to small flaws and the ability to discriminate changes resulting from small damage, changing environmental and test conditions.

The finite element method requires highly refined meshes with large number of degrees-of-freedom of a structure, to capture the shorter wavelengths. The densely packed modes in the high frequency analyses, increases the computational power, time and cost. Additionally, higher order modes of a structure are sensitive to boundary conditions, small perturbations, material and geometrical properties. Thus, the traditional finite element based modal analyses are unsuitable for high frequency analyses. SEA is widely used in this domain for vibro-acoustic analysis in the initial stages to obtain the responses and vibrational energy flow in structures to aid in noise and vibration reduction. Literature review reveals that bulk of the papers on the subject deals with the computation of coupling loss factors for various structural configurations and regarding the statistics, effects of modal overlap, damping, coupling effects and assumptions made in SEA.

There are situations and problems, wherein the incipient damage affects mainly on the highest modes, rather than on lowest, like point connections of structures with spot-welds, cleats, rivets and bolts. As reported in the references (Doebbling et al., 1998),

the lower modes may not detect a local damage in contrast to the higher modes, which is significant in locating the damage in discrete joints like the spot-welded or riveted structures. The damage initiated in such cases does not significantly affect the main or first few modes. Mode shape modification and shift of frequency are also too small to be significant.

In general, plates with joints in power plants, chemical plants, automobile, aeronautical, marine, nuclear, oil and natural gas industries, are subjected to substantial static and dynamic loads. In the case of such conditions, there is a possibility of damage developing at the joints due to stress-corrosion. These problems have significant importance in industries. Usually, the field components, are taken to the laboratory for the vibration-based damage detection. To help attain an in-situ testing capability they should be tested in the laboratory under conditions similar to the operating conditions. The literature review has revealed that research work related to the application of energy approach like SEA for damage detection in structures is minimal. There is a need to examine the possibility of adoption of the Statistical Energy Analysis like (SEAL) approach to detect damage of joints in plates, with spot-welded, bolted and adhesive joints.

Based on the above facts, it is required to carry out investigations with the main goal of this research study to utilize the Statistical Energy Analysis like Approach to detect damage in spot- welded, bolted and adhesive joints. The objectives set out to achieve this main goal were:

## **2.9 OBJECTIVES OF THE RESEARCH WORK**

1. To arrive at the selection of the finite element or analytical approach for the actual damage detection studies using Statistical Energy Analysis like approach. The task of investigation of the effects of the internal loss factor of the parent materials to be joined on the computed coupling factors by the finite element and analytical approach forms the basis for this selection.
2. To arrive at the approach of finite element modelling of plates with three type of joints, i.e., spot welded, adhesive bonded and bolted joints.



3. The sub tasks to achieve the main goal of damage detection studies of plates with lap joints viz. spot welded, adhesively bonded and bolted configurations are:
  - a) Experimental measurement of loss factors of mild steel and acrylic plates with joints.
  - b) Computation of the velocity responses, total vibrational energies and the coupling factors for two plates with various joint conditions (healthy and damaged) experimentally and numerically.
  - c) To utilize the coupling factors computed in the above Step (b) to predict velocity and acceleration responses of three plates with lap joints using the SEAL approach and compare the results numerically and experimentally to detect the healthy and damaged status.
  - d) To develop a database based on percentage deviation in the acceleration responses for all possible damage configurations of three plates with lap joints considered here based on statistical energy analysis like approach in comparison to the healthy configuration. The percentage deviations can be used as one of the damage indicators.

## **2.10 SCOPE OF THE RESEARCH WORK**

The scope of the current research work is drawn as follows;

This thesis is focused on the methodology to use SEAL approach for damage detection in joints. The motivation is derived from the fact that the use of SEA for damage detection in structures, wherein the damage affects mainly the highest modes, is minimal. The studies are limited to the use of lap joined spot-welded, bolted and adhesive bonded plates. For the proposed damage detection method, a linear finite element model of the structure is modelled in commercially available finite element tool (ANSYS). The internal loss factors of the material are updated in the finite element model by experimentation. The experimentation is carried out using LMS test Lab based set up limited to excitation frequency of 3500 Hz. The measured FRF data

from the LMS test Lab software are post processed for further computations using MATLAB. However, the effects of noise radiation and uncertainties have not been considered in the present investigation.

## **2.11 SUMMARY**

This chapter reported a comprehensive review on vibration based health monitoring techniques. Literature was basically categorized based on statistical energy analysis, finite element models used for spot-welds, bolted joints and adhesive bonds. In addition, an overview of application of SEA and pattern recognition approaches are also presented citing various researchers who have successfully implemented these techniques for their applications of interest. Also the objectives and scope of the present research work are discussed in this chapter. The methodology adopted and experimental approach are described in Chapters 3 to 8.

## CHAPTER 3

### EFFECTS OF INTERNAL DAMPING ON COUPLING LOSS FACTOR ESTIMATION

#### 3.1 INTRODUCTION

This chapter discusses the investigations on effects of internal loss factors on the coupling loss factors computed for two plates joined in an ‘ $L$ ’ junction configuration. The results are compared using finite element analysis and analytical wave based approach. Mild steel plates have low values of internal loss factor and is used for spot-welded and bolted joints in the present research work.

#### 3.2 ANALYSIS AND PROCEDURE

The coupling loss factors and velocity responses for two typical configurations of  $L$ -shaped plate and beam have been investigated by using analytical wave approach and finite element analysis. Figure 3.1 illustrates the schematic of  $L$ -shaped plate. Material properties and geometrical parameters considered in the study are presented in Table 3.1.

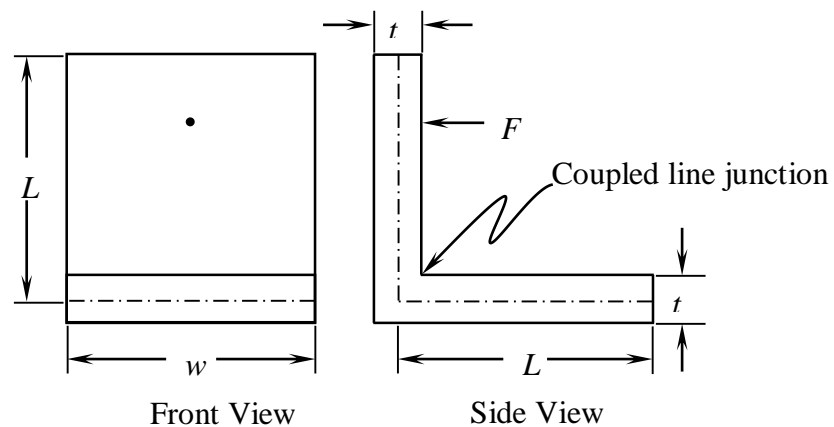


Figure 3.1 Two plates coupled at right angles

Table 3.1 Material and geometrical specifications

Parameter	Values
Internal Damping( $\eta$ )	0.00001 to 0.04
Width( $w$ )	0.01 to 0.9 m (Plate) 0.0025 m to 0.1 m (Beam)
Length( $L$ )	1.0 m
Thickness( $t$ )	2 mm
Density( $\rho$ )	7800 kg/m <sup>3</sup>
Poisson's ratio( $\mu$ )	0.3
Young's Modulus( $E$ )	200 GPa
Force( $F$ )	1 N
Frequency( $f$ )	1000 to 8000 Hz

Pinned boundary conditions have been assumed near the 'L' junction. The analyses have been carried out to study the effect of internal loss factor on the CLF for the configurations by varying the internal loss factor in the range of 0.00001 to 0.04 with a width of 0.9 m for the plate, and for a width of 0.01 m for beam configurations. Also studies have also been carried out to estimate the coupling loss factors and velocity responses for different widths, varying from 0.01 m to 0.9 m for the *L*-shaped plate and 0.0025 m to 0.1m for the *L*-shaped beam with a constant value of internal loss factor of 0.04.

### 3.2.1 Analytical wave approach for plates

The substructure in consideration has been analyzed for flexural waves, which plays an important role for vibrations at high frequencies and sound radiation. The CLF,  $\eta_{12}$  between two plates for a line junction is given by (Park, 2005)

$$\eta_{12} = \frac{2C_B L \tau_{12}}{\pi \omega A} \quad (3.1)$$

where  $\omega$  is the angular forcing frequency,  $A$  is the surface area,  $L$  is the length of the junction of the two plates, and  $C_B$  is the bending wave speed of the first plate for two connected plates as the function of center frequency,  $f$  given by (Norton, 1989).

$$C_B = \sqrt{1.8C_L t f} \quad (3.2)$$

The wave transmission coefficient ( $\tau_{12}$ ) is defined as the ratio of transmitted power to the incident power. The wave transmission coefficient for random incidence vibrational energy of two coupled plates at right angles to each other can be calculated by the approximate relation (Bies et al., 1980).

$$\tau_{12} = \tau_{12}(0) \frac{2.754X}{1 + 3.24X} \quad (3.3)$$

where  $X$  is the ratio of plate thicknesses. The normal transmission coefficient  $\tau_{12}(0)$  may be calculated as (Bies et al., 1980).

$$\tau_{12}(0) = 2 \left( \psi^{1/2} + \psi^{-1/2} \right)^{-2} \quad (3.4)$$

$$\psi = \frac{\rho_1 C_{L1}^{3/2} t_1^{5/2}}{\rho_2 C_{L2}^{3/2} t_2^{5/2}} \quad (3.5)$$

The modal density per Hz of flat plate in flexural vibration is given by (Cremer et al., 1973)

$$n(f) = \frac{A\sqrt{3}}{tC_L} \quad (3.6)$$

where longitudinal wave speed is given by (Bies et al., 1980).

$$C_L = \sqrt{\frac{E}{\rho(1 - \nu^2)}} \quad (3.7)$$

$E$  is Young's modulus,  $\nu$  is the Poisson's ratio,  $A$  is the surface area and  $t$  the thickness of the plate under consideration. The time-averaged power input for a unit force  $F$  is given by

$$P_{in} = \frac{1}{2} |\tilde{F}|^2 \text{Re}\{\tilde{Z}_m^{-1}\} \quad (3.8)$$

The real part of the drive-point mechanical impedance of an infinite plate of thickness  $t$  and mass per unit area  $\rho_a$  in flexural vibration is given by:

$$\text{Re}\{\tilde{Z}_m^{-1}\} = 8 \sqrt{\frac{Et^3 \rho_a}{12(1-\nu^2)}} \quad (3.9)$$

The forcing frequencies are in the range of 0-8000 Hz. The total energies in each substructure are computed from Equation (1.7) after computation of power input and coupling loss factor. The maximum velocity response  $V_i$  of each substructure is derived from the obtained energy  $E_i$  under a particular power input by Equation (3.10).

$$V_i = \sqrt{\frac{2E_i}{M}} \quad (3.10)$$

### 3.2.2 Analytical wave approach for beams

The CLF for two beams joined at right angles to each other in terms of transmission coefficient ( $\tau_{ij}$ ) is given by (Shankar, 1997)

$$\eta_{ij} = \frac{C_{Bi} \tau_{ij}}{\omega L_i} \quad (3.11)$$

where the bending wave speed is given by

$$C_{Bi} = \sqrt{\frac{\omega^4 E_i I_i}{\rho_i A_i}} \quad (3.12)$$

where  $L_i$  is the length of the beam  $i$  under consideration,  $\omega$  is the angular forcing frequency and  $C_{Bi}$  is the sound speed of flexural waves,  $E_i$  is the Young's Modulus,  $I_i$  is the second moment of area,  $\rho_i$  is the density and  $A_i$  is the cross-sectional area. The transmission coefficient across the joint relating the incident waves in substructure  $i$  to be transmitted in substructure  $j$  for the flexural wave may be computed as

$$\tau_{ij} = \frac{1 + 2\beta^2}{9\beta^2 + 6\beta + 2} \quad (3.13)$$

$$\beta = \frac{C_{Li}}{C_{Bi}} \quad (3.14)$$

Longitudinal wave speed for the beam is given by

$$C_L = \sqrt{\frac{E}{\rho}} \quad (3.15)$$

The real part of drive-point mechanical impedance of an infinite beam of thickness ( $t$ ), cross-sectional area ( $A$ ) and density ( $\rho$ ) in flexural vibration for an end loading and central loading, respectively are given by (Norton, 1989)

$$Re\{\tilde{Z}_m^{-1}\} = 2.67\rho A\sqrt{C_L t f} \quad (3.16)$$

$$Re\{\tilde{Z}_m^{-1}\} = 0.67\rho A\sqrt{C_L t f} \quad (3.17)$$

The forcing frequencies are in the range of 0-8000 Hz. The total energies in each substructure have been computed from Equation (1.7) after computation of power inputs and coupling loss factor for two plates. The maximum velocity response  $V_i$  of each substructure has been computed from the total vibrational energy  $E_i$  under a particular power input by Equation (3.10). The coupling loss factors and velocity amplitudes have been computed by in-house programs built using the equations discussed above, in MATLAB software.

### 3.2.3 Finite element analysis

The finite element analysis using the modal approach has been carried out using Ansys V13 software. In numerical methods, the behavior of SEA parameters with change in inputs (geometry, boundary conditions, and damping) for the given structure can be modeled easily and is less time consuming as compared to the experimentation of the real structure. The other advantages of the numerical method include cost efficiency and flexibility. The finite element size is related to the wavelength, and this number of elements per wavelength varies between six and ten, that meets certain technical requirements (Marburg et al., 2003). The  $L$ -shaped plate

has been modeled using eighteen thousand shell 63 elements as shown in Figure 3.2 (a) with pinned boundary conditions. Shell63 has both bending and membrane capabilities. Both in-plane and normal loads are permitted. The element has six degrees of freedom at each node: translations in the nodal  $x$ ,  $y$ , and  $z$  directions and rotations about the nodal  $x$ -,  $y$ - and  $z$ -axes. A harmonic force with unit load intensity has been applied in the range of frequencies of 1000-8000 Hz. The load has been applied on one plate, and the velocity responses on both the plates were computed. In case of beam elements, the configuration under consideration has been modeled using more than two hundred Beam3 elements (Figure 3.2 b). Beam3 is uniaxial element with tension, compression, and bending capabilities. The element has three degrees-of-freedom at each node, translations in the nodal  $x$ - and  $y$ -directions and rotation about the nodal  $z$ -axis.

In-house programs and macros have been developed in Ansys Parametric Design language (APDL) for automating the computation of vibrational energy of each substructure  $E_i$  with mass  $M_i$  and maximum substructure velocity  $V_i$  according to Equation (3.18). The spatial average has been obtained by loading each substructure at 25%, 50%, 75% and 100% of its length.

$$E_i = \frac{M_i V_i^2}{2}, \quad (3.18)$$

The coupling loss factors are computed by the Equation (1.7) after computation of power inputs and corresponding energies in all the substructures. The maximum velocity response  $V_i$  of each substructure can be obtained directly from the post-processing of the output results.



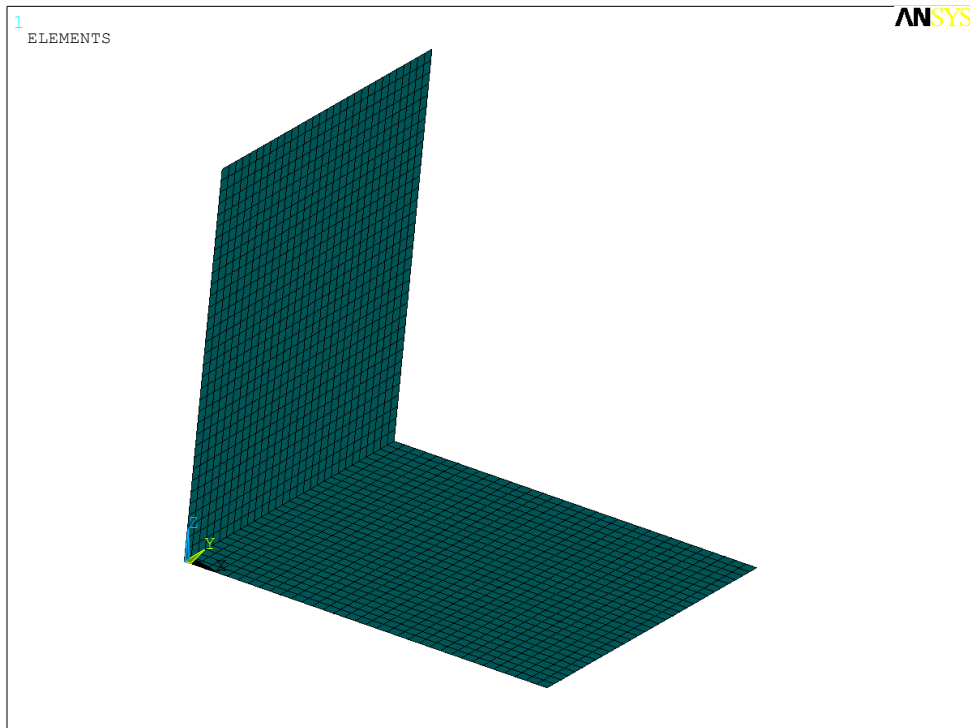


Figure 3.2 (a) Finite Element *L*-shaped plate model

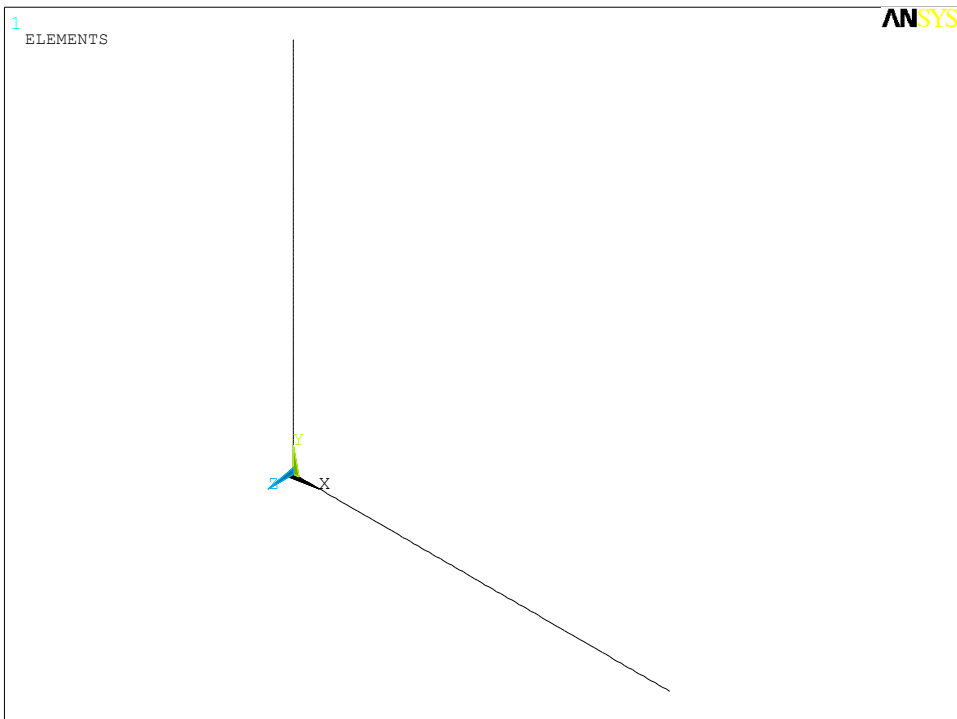


Figure 3.2 (b) Finite Element *L*-shaped beam model

### 3.3 RESULTS AND DISCUSSION

Table 3.2 and Figure. 3.3 presents the variation of CLF with excitation frequencies, for the plate formulation with a width of 0.9 m and internal loss factor of 0.04. Similarly, Table 3.3 and Figure 3.4 presents the variation of CLF with frequencies, for the beam formulation with a width of 0.01m and internal loss factor of 0.04. The frequency averaged coupling loss factor computed using finite element method is lower by 5.64% as compared to the factor obtain by analytical approach. The percentage variation between the frequency averaged coupling factor obtained by FEA for the beams is 8% lower than the analytically obtained values for beams (Table 3.3).

Table 3.2 Variation of coupling loss factor vs. excitation frequencies for the plate.

<b>Excitation Frequency (Hz)</b>	<b>Coupling Loss Factor</b>	
	<b>Analytical</b>	<b>FEM</b>
1000	0.0046	0.006268
2000	0.0032	0.005084
3000	0.0026	0.001899
4000	0.0023	0.001878
5000	0.0020	0.001196
6000	0.0019	0.000986
7000	0.0017	0.000804
8000	0.0016	0.000746
<b>Average</b>	0.0025	0.002359

The plates have a modal density of 0.1468 modes / Hz. The coupling factors are obtained by spatial and frequency averaging of the response and excitation points called as rain on the roof excitation. A strict rain-on-the-roof field corresponds to an infinite number of uncorrelated excitation points owing to the conditions intrinsic in their definition: e.g., that they relate to systems of infinite size or that they apply for ensembles (Fredo, 1997). The energy equipartition is a direct consequence of rain-on-

the-roof excitation (Lafont et al., 2014). Thus the assumptions of equal partition of modal energy in a substructure and statistically autonomous excitation forces are approximated by the rain on the roof excitation in the FE analyses by uncorrelated forces acting at a limited number of locations on the excited plate. These findings are in accordance with similar studies in the literature (Grushtesky, 2005; Hwang et.al, 2004; Ma et.al, 2002; Park et.al, 2004).

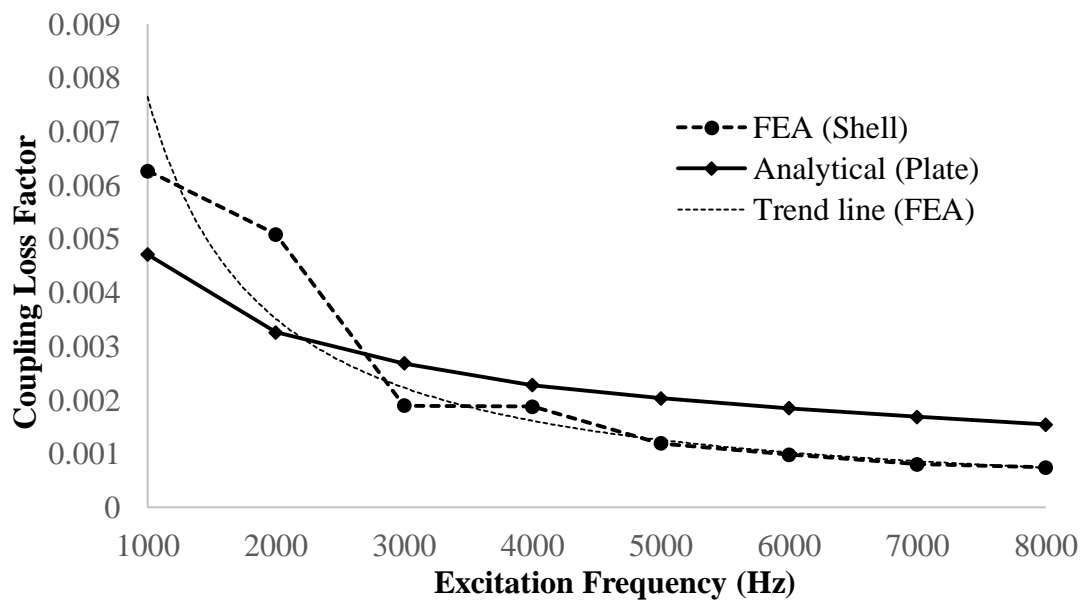


Figure 3.3 Variation of coupling loss factor vs. excitation frequencies for plate

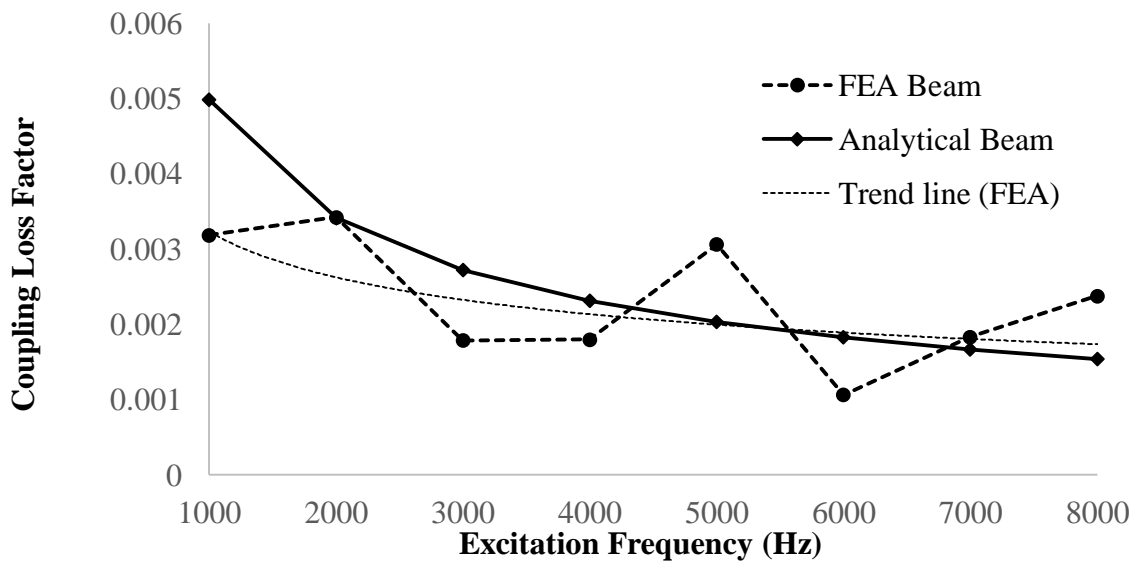


Figure 3.4 Variation of coupling loss factor vs. excitation frequencies for beam

A mean fitted curve (trend line) from the FEA results has been plotted for better comparison. In the present thesis, the focus is on application of the energy flow balance with FE computed data for the individual case, which may typically differ from the mean value of the SEA ensemble and are dependent on the system properties, boundary conditions and excitation

Table 3.3 Variation of coupling loss factor vs. excitation frequencies for the beam.

<b>Excitation Frequency (Hz)</b>	<b>Coupling Loss Factor</b>	
	<b>Analytical</b>	<b>FEM</b>
1000	0.0050	0.0032
2000	0.0034	0.0034
3000	0.0027	0.0018
4000	0.0023	0.0018
5000	0.0020	0.0031
6000	0.0018	0.0011
7000	0.0017	0.0018
8000	0.0015	0.0024
<b>Average</b>	0.0025	0.0023

In the classical SEA, coupling loss factors are determined by the nature of the coupling between subsystems independent of subsystem damping as the wave estimates do not take damping effects into account. When the damping is high the CLFs are quite insensitive to changes in the damping. The studies have revealed that the CLF computed using finite element analysis increases linearly as the internal loss factor varies from a zero value, followed by a transition region and converges to the values obtained by the analytical wave approach and remains insensitive to changes at higher values of damping (Fig 3.5 and 3.6). The observed results are in agreement with similar studies carried out by Yap et al. (1996) for simply supported coupled plates. At low values of damping, the coupling factors computed by the analytical wave approach would thus be overestimated as compared to ESEA or FEA.

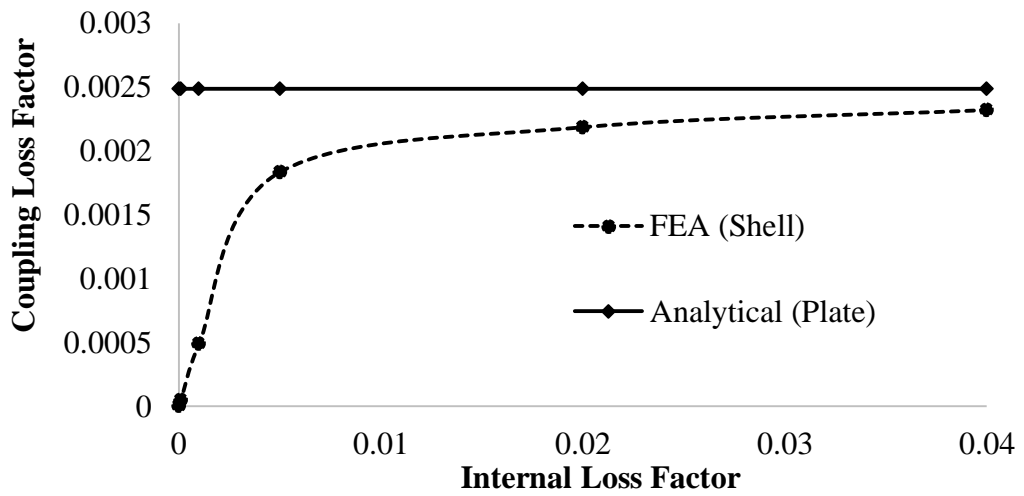


Figure 3.5 Variation of coupling loss factor with internal loss factor for plate

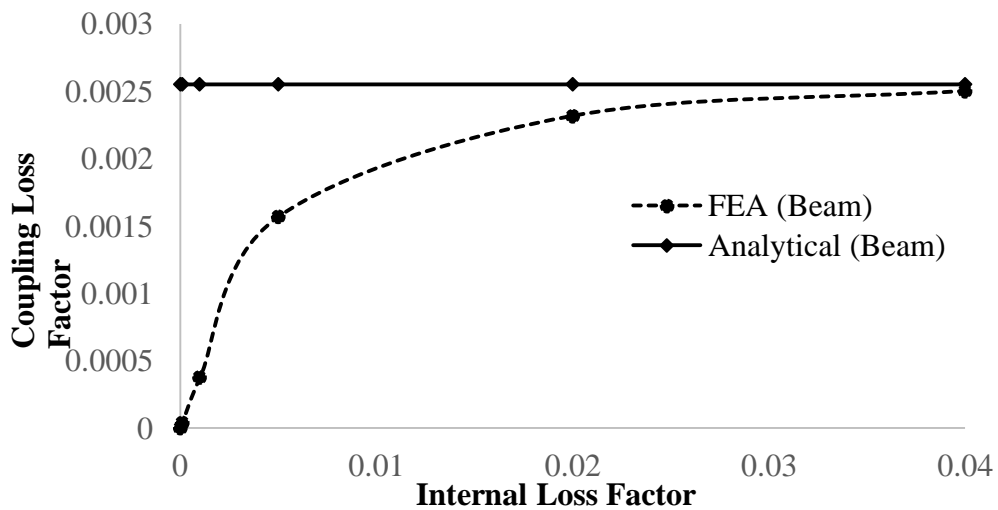


Figure 3.6 Variation of coupling loss factor with internal loss factor for beam

In infinite free wave system, the energy variables focus on the energy density that describes the energy of vibration system per unit length, area or volume. It can be observed from equation 3.1, for the analytical case, the coupling factors for the rectangular plates considered in the present study, are insensitive to width. However, for plates wherein area may vary due to varying width but have the same coupled junction length or vice-versa, the coupling factor will also vary as per equation 3.1. In case of FEA, the coupling factor is derived by spatial and frequency averaging of the energies obtained by excitation on the plate. The velocity response amplitudes and the

corresponding energies generated vary based on the frequency and location of excitation, which determine the FEA obtained values of coupling factor. The variation of CLF with variation in width for the plate and beam have been plotted in Figure 3.7 and Figure 3.8.

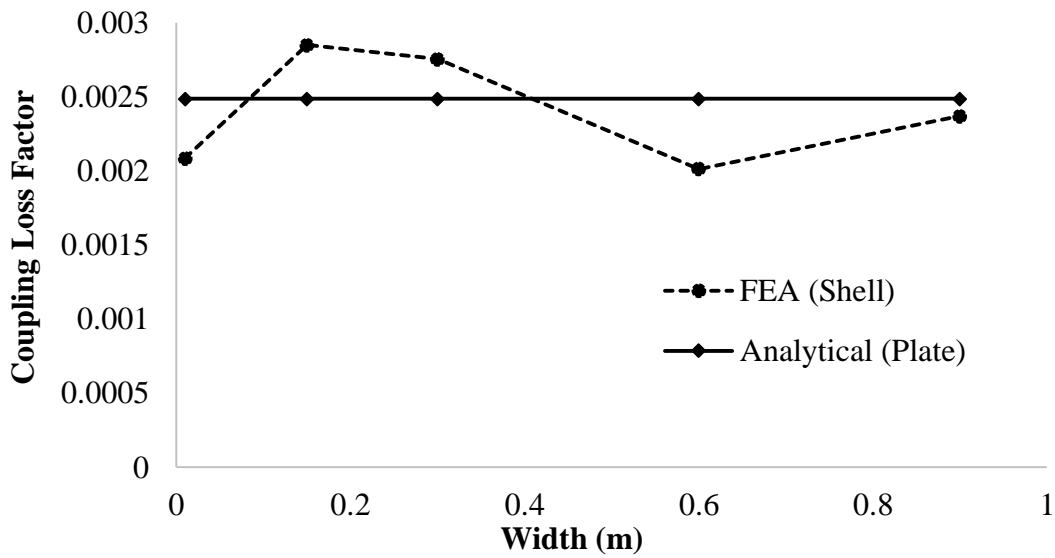


Fig. 3.7 Variation of coupling factor with width for plate

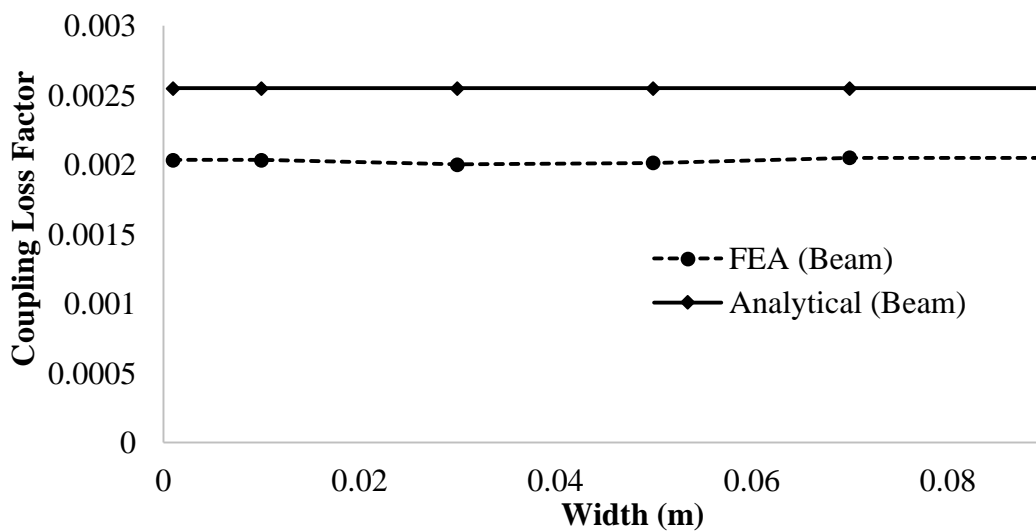


Figure 3.8 Variation of coupling factor with width for beam

The results for velocity responses obtained for horizontal plate with unit force loading against the variation in excitation frequencies for a plate width of 0.9 m and internal loss factor of 0.04 has been plotted in Figure 3.9. The percentage variation between the velocity responses obtained from FEA varied from 14% at the lowest excitation frequency of 1000 Hz to 0.4% at a higher excitation frequency of 8000 Hz (Fig. 3.9) in comparison to the analytically obtained velocity responses for the plates. At higher frequencies, the modal overlap increases and the frequency response is smoothed down, as the statistical energy analysis principles are satisfied and the variance in the velocity responses due to the variation in the location of excitation reduces. Thus the deviation in the velocity responses computed by both the approaches reduces with increase in the excitation frequencies.

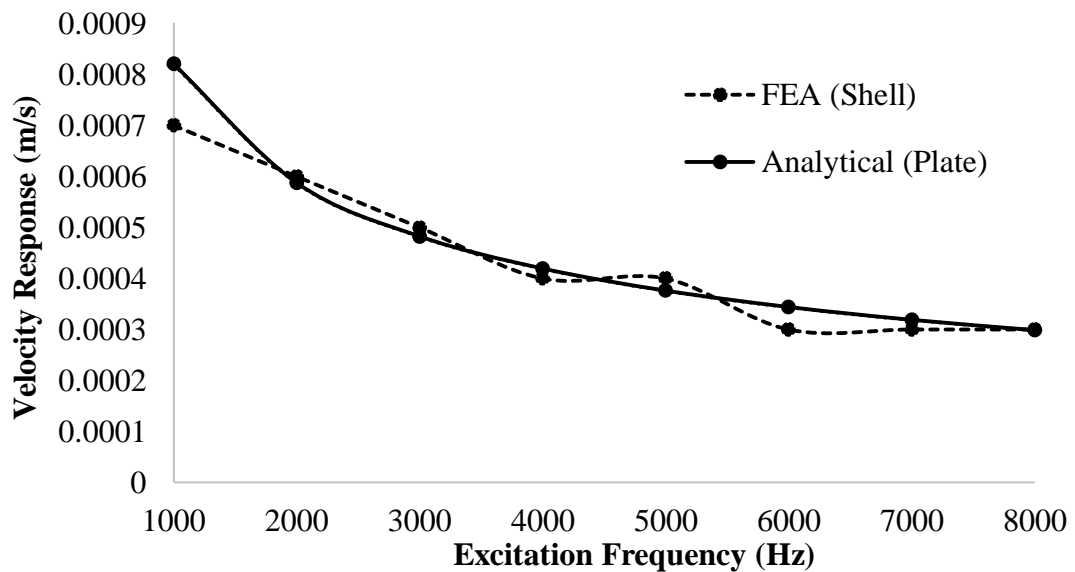


Figure. 3.9. Velocity responses vs. excitation frequency for the horizontal plate

Similarly, Figure 3.10 presents the variation of velocity responses with excitation frequencies for the horizontal beam with unit force loading having a width of 0.01m and internal loss factor of 0.04.

Finally, the results for velocity responses obtained for horizontal plate with variation in widths has been plotted in Figure 3.11. Unit force acts on the plate for the value of internal loss factor of 0.04 and a frequency of 8000 Hz. The deviation in the velocity responses computed using the finite element analysis is 66.6% higher than the

analytically obtained values at a width of 0.01m and reduces to a value of 0.3% at a width of 0.9 m.

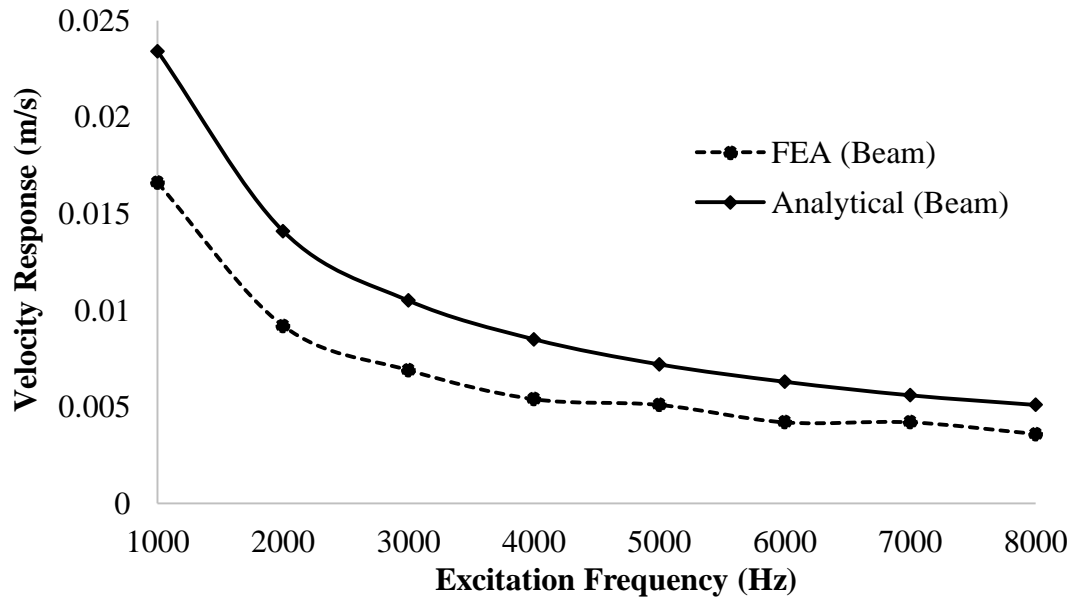


Figure 3.10 Velocity responses vs. excitation frequency for the horizontal beam

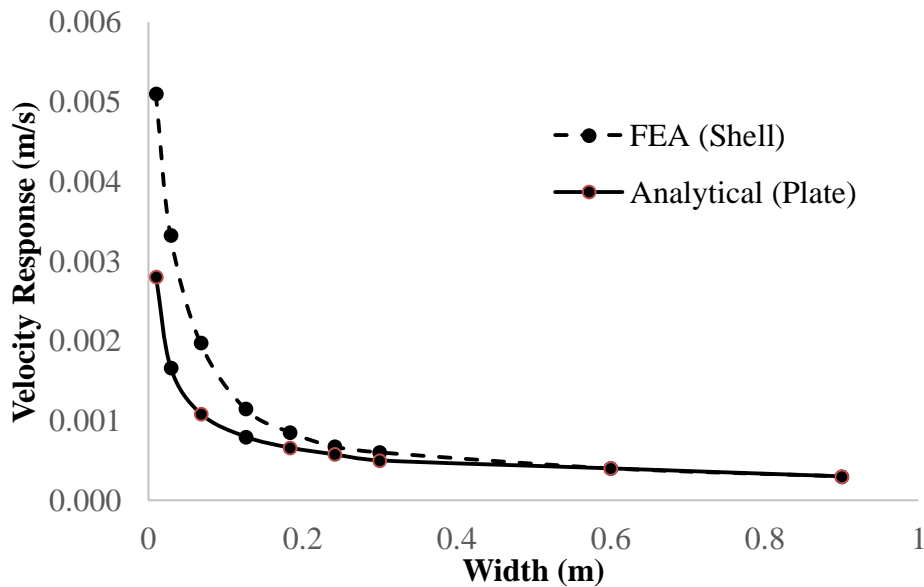


Figure 3.11 Variation of velocity responses for horizontal plate with width



### **3.4 SUMMARY**

The FE computed coupling factors and velocity amplitudes for an L shaped plate was compared with results from the analytical approach. It can be concluded that the FE computed CLFs are case specific with the forcing excitation limited to a few locations, as opposed to SEA and may typically differ from the mean value of the SEA ensemble, depending on the system properties, boundary conditions and excitation.

In the present research work on damage detection of spot welded plates, mild steel is the feasible material for the plates. As mild steel has low values of internal loss factor, it was necessary to study the effects of the internal loss factor on the computed coupling factors. At low values of damping, the coupling factors computed by the analytical wave approach is overestimated as compared to ESEA or FEA. The selection of using FEA and ESEA for the computation of coupling factors for the further damage detection studies has been based on these results.

## CHAPTER 4

### **FINITE ELEMENT MODELS FOR SPOT WELDED AND ADHESIVE BONDED PLATES TO DETERMINE COUPLING LOSS FACTORS USING FINITE ELEMENT ANALYSIS**

#### **4.1 INTRODUCTION**

The preceding chapter dealt with the effects of the internal loss factor on the derived coupling factors. It was observed for most of the materials such as mild steel plates, the coupling factors computed by the analytical wave approach would be overestimated compared to ESEA or FEA at low damping. The present chapter discusses the details of the finite element models for modelling the discrete spot welded and adhesive bonded joint to compute the coupling loss factors. The chapter also discusses the comparison of the analytically (wave approach) obtained coupling loss factors of two coupled plates (assuming a line junction at the joint) with the computed coupling loss factors and velocity responses for the cases, Case-1- two lap joined spot welded and Case-2- two lap joined adhesive bonded plates using finite element analysis. In both the cases, the material of the plates is assumed to have a high internal loss factor to avoid the effects of internal loss factor on the computed coupling loss factors, when comparing with the analytical wave-based approach. An additional FE model with Solid 185 elements having properties of the parent plates i.e. mild steel, at the coupled junction has been modeled as a monolithic model to compare the results obtained by FEA with the analytical approach by assuming a line junction at the joint. In case of adhesive bonded plates, the additional FE model is created with Solid 186 elements having properties of the adherend plates i.e., acrylic at the coupled junction to compare the results with the analytical wave-based approach.

## **4.2 SPOT WELDED PLATES (CASE 1)**

Spot welds have found wide applications in the automotive and aerospace industry to join thin sheet metals. A typical structure used in these industries may contain thousands of spot welds, and it is impractical to have a detailed FE model due to the requirement of a large amount of effort in modeling and computational time. Reasonable results of the dynamic characteristics of welded structures can be obtained with a small number of degrees-of-freedom. The modeling is such that, it must be easy to connect congruent as well as non-congruent meshes and locate spot welds anywhere in the meshes. For this purpose, area contact model 2 (ACM2) and CWELD model are the widely used finite element models (Kurtani et al., 2011). An additional FE model with Solid 185 elements at the coupled junction are used as a monolithic model to compare the results with the analytical approach.

In this present study, a finite element model of a structure as shown in Figure 4.1, consisting of two steel plates joined by three spot welds has been modeled using ANSYS V13 software. The spot welds have been modeled as ACM2 model. Comparisons have been made for the computed coupling loss factors and velocity responses for the spot welded plates using finite element analysis, the monolithic FE model analysis, and analytical wave approach.

### **4.2.1 Material properties and geometric dimensions**

The coupling loss factor and velocity responses for two thin steel plates joined by spot-welds (Figure 4.1) have been analyzed by using analytical wave approach and finite element analysis. Two steel plates with dimensions of length, 500 mm, width, 500 mm and thickness, 1.6 mm are lap joined by three spot welds. The overlap length of the two plates is 50 mm. Three spot welds are lined up on the center of the overlap. One of the three spot welds is centrally located, and the others are located 20 mm away from the edge of the plate. The diameters of weld nuggets are approximately 6 mm.

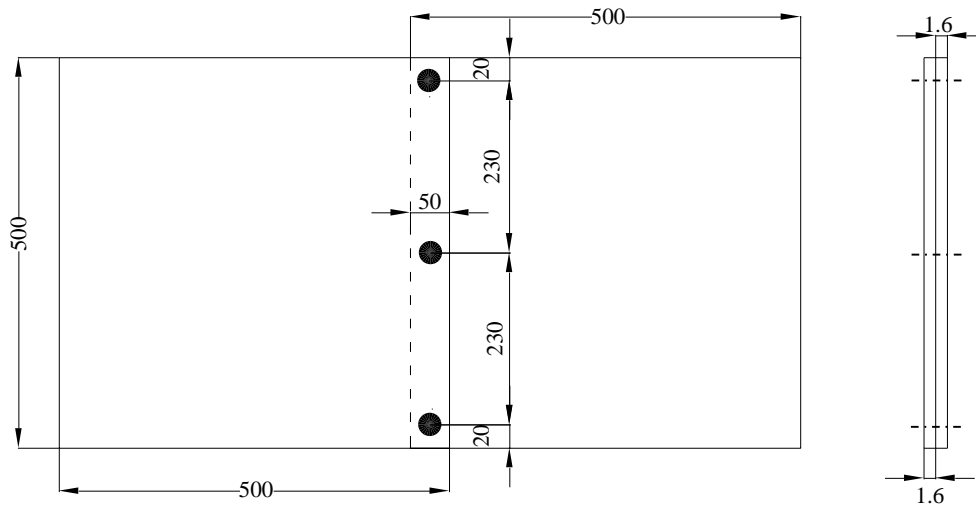


Figure 4.1 Geometric dimensions of plates with spot- welds

Table 4.1 Material and geometrical specifications.

Parameter	Values
Internal loss factor( $\eta$ )	0.05
Width( $w$ )	0.5 m
Length( $L$ )	0.5 m
Thickness( $t$ )	1.6 mm
Density( $\rho$ )	7850 kg/m <sup>3</sup>
Poisson's ratio( $\mu$ )	0.3
Young's Modulus( $E$ )	210 GPa
Force( $F$ )	1 N
Excitation Frequency( $f$ )	1000 to 8000 Hz

The material properties considered for the configurations are given in Table 4.1. The equations for the analytical computations using SEA are the same as discussed in Section 3.2.1.

#### 4.2.2 Finite element analysis

Stress analyses may require a detailed model of the spot welded joint near the spot weld. However, this is not necessary for vibration analysis as the model is required to only represent the stiffness characteristics of spot welds. Simplistic models have been used to model the spot-welds using a single beam or a solid element, and the joined

plates are modeled using shell elements. The most commonly used finite element models are the ACM2 and CWELD the models. These models have the advantage of connecting sheets with non-congruent meshes and locating the welds anywhere in the meshes. The ACM2 consists of a single solid element that connects the upper and lower shell elements with constraint elements as shown in Figure 4.2. Each node of the solid element is connected to four nodes of one shell element using constraint equation elements. This group of shell elements forms a patch consisting of four shell elements for each of the two sheets. The RBE3 element is an interpolation element and automatically generates internal multi-point constraint (MPC) equations in FE analysis. RBE3 creates constraint equations such that the motion of the master is the average of the slaves. For the rotations, a least-squares approach is used to define the average rotation at the master from the translations of the slaves. RBE3 is a rigid body element used to distribute force or moment from the master node to slave nodes proportional to the weighting factors. It distributes the force or moment applied at the master node to a set of slave nodes, taking into account the geometry of the slave nodes as well as weighting factors. The node at which the force or moment to be distributed will be applied must be associated with an element for the master node to be included in the master node degrees of freedom solution to be used in constraint equations. The force is distributed to the slave nodes proportional to the weighting factors. The moment is distributed as forces to the slaves; these forces are proportional to the distance from the center of gravity of the slave nodes times the weighting factors. Only the translational degrees of freedom of the slave nodes are used for constructing the constraint equations. Constraint equations are converted to distributed forces or moments on the slave nodes during solution. The finite element analysis has been carried out using ANSYS V13 software.

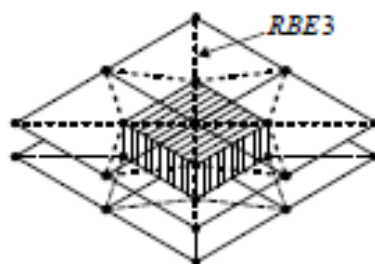
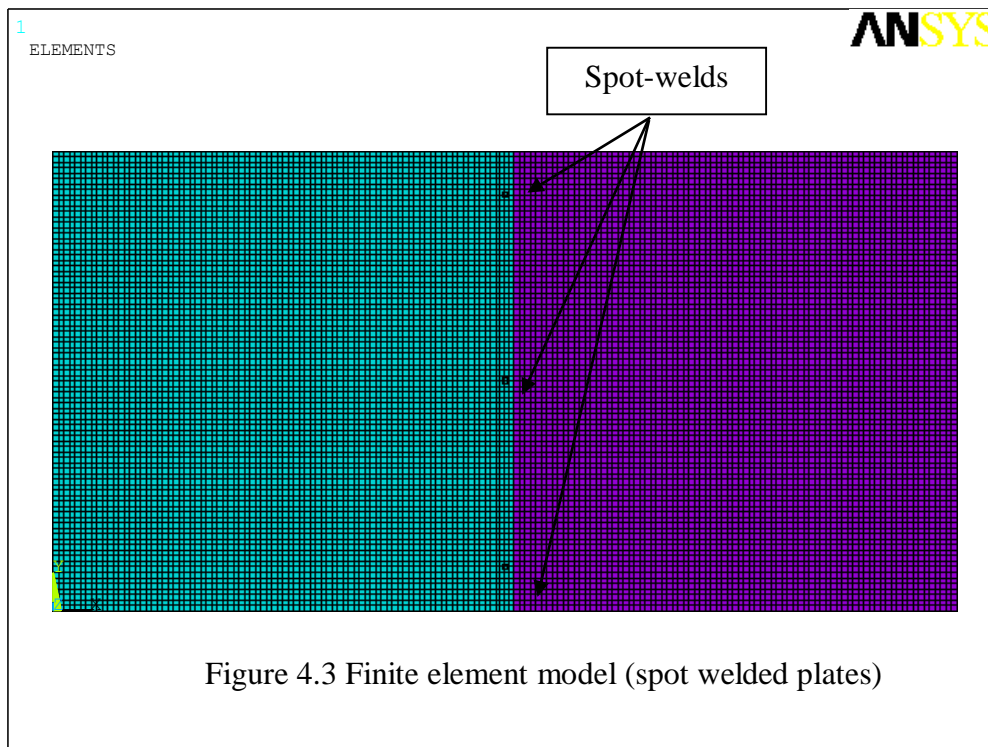
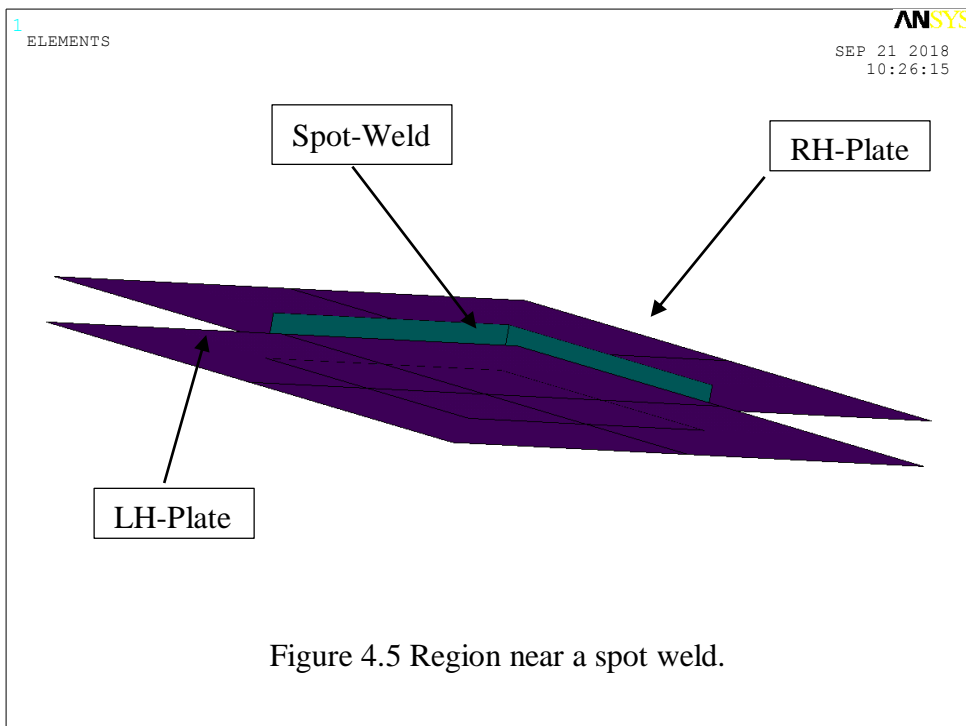
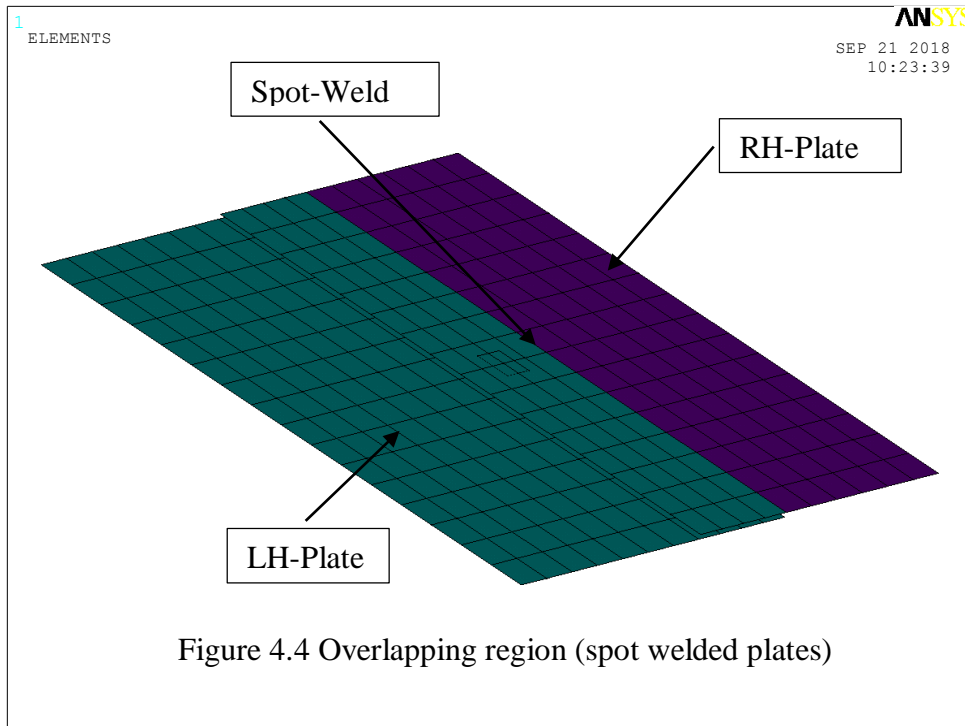


Figure 4.2 ACM2 Spot weld model

Figure 4.3 depicts the FE model of the structure. The plates are modeled using SHELL63 elements. Shell63 has both bending and membrane capabilities. Both in-plane and normal loads are permitted. The element has six degrees-of-freedom at each node: translations in the nodal  $x$ ,  $y$  and  $z$ -directions and rotations about the nodal  $x$ ,  $y$  and  $z$ -axes.



The spot welds have been modeled using a single solid element, SOLID185 with 6 mm square and 1.6 mm high, i.e., ACM2 model. The finite element size is related to the wavelength, and this number of elements per wavelength varies between six and ten (Marburg et al., 2003). The plates have been meshed with a mean mesh size of 6 mm. The patches are meshed with 6 mm square shell elements, while areas along the edges are meshed with less than 6 mm non-square elements. Also, for the ACM2 model, the center of the patch area is coincident with the center of solid element. The overlapping region near a spot weld is shown in Figures 4.4 and 4.5.



Present studies have also been carried out to estimate the coupling factors and velocity responses for frequencies from 1000 to 8000 Hz in steps of 1000 Hz. A harmonic force with unit load intensity is applied in the range of frequencies of 1000-

8000 Hz. The load is applied on one plate, and the velocity responses on both the plates are computed. The velocity responses at all the nodes of the plates including the power input location are determined. In-house programs developed in Ansys Parametric Design language (APDL) for computation of vibrational energy ( $E_i$ ) of each substructure with mass ( $M_i$ ) and the maximum substructure velocity ( $V_i$ ) using relation,

$$E_i = \frac{M_i V_i^2}{2} \quad (4.1)$$

The coupling factors are computed by Equation (1.7) after computation of power inputs and corresponding energies in all the substructures. The maximum velocity response ( $V_i$ ) of each substructure is obtain directly from the post-processing of the output results.

The time-averaged power input into the structural substructure is given by (De Langhe, 1996)

$$P = \frac{1}{\omega} \text{Im} (S_{af}(\omega)) \quad (4.2)$$

where,  $S_{af}$ . is the imaginary part of the cross-spectrum of force and acceleration. Alternatively, it can also be given in terms of

$$P = \frac{1}{2} \text{Re}(FV^*) \quad (4.3)$$

where  $V^*$  is the complex conjugate velocity and  $F$  is the force at the driving point.

### 4.3 ADHESIVE BONDED PLATES (CASE 2)

In the present study, a finite element model of a structure, consisting of two acrylic plates lap joined by an adhesive has been modeled using ANSYS V13 software. Comparisons have been made for the computed coupling loss factors and velocity



responses using finite element analysis and analytical wave approach. An additional FE model with Solid 186 elements having properties of the adherend plates (i.e. acrylic) at the coupled junction is utilized to compare the results with the analytical wave-based approach.

#### 4.3.1 Material properties and geometric parameters

The coupling factor and velocity responses for two acrylic plates joined by a double sided adhesive tape (Figure 4.6) have been analyzed by using analytical wave approach and finite element analysis.

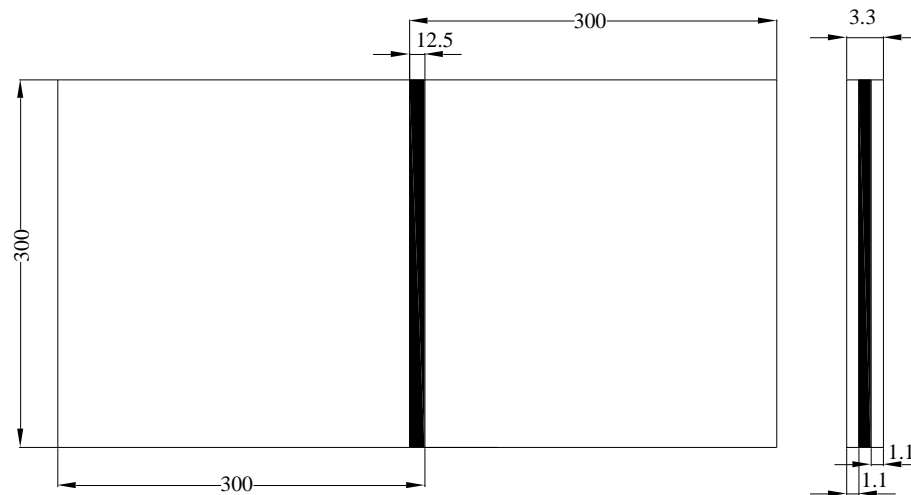


Figure 4.6 Geometric dimensions (in mm) of the adhesive bonded plates with lap joint

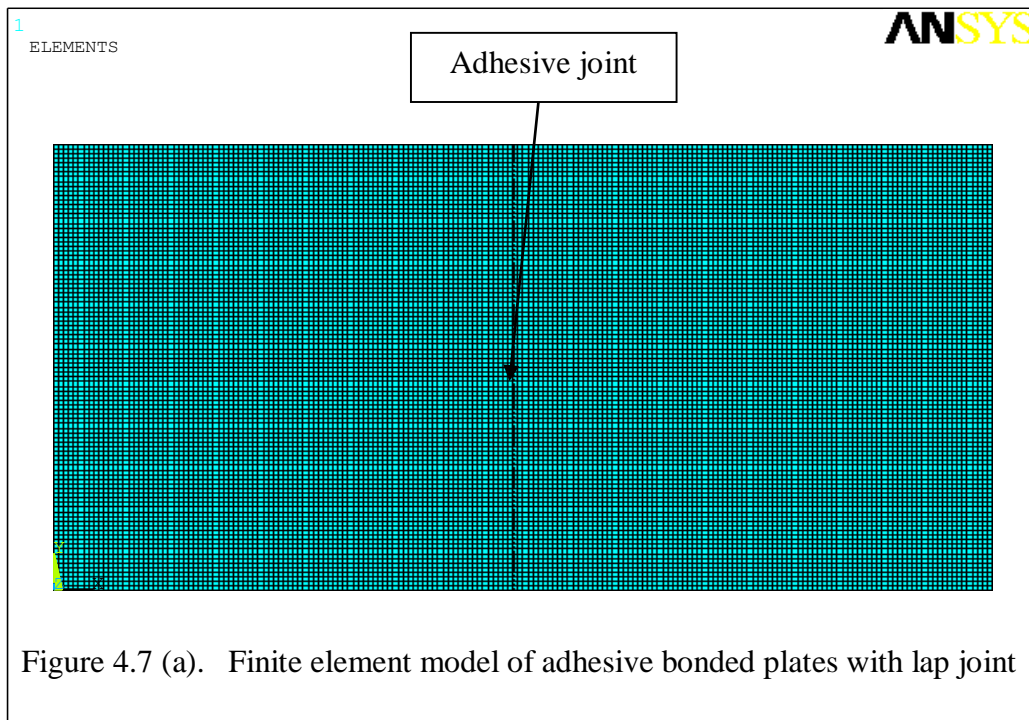
Table 4.2 Material and geometrical specifications

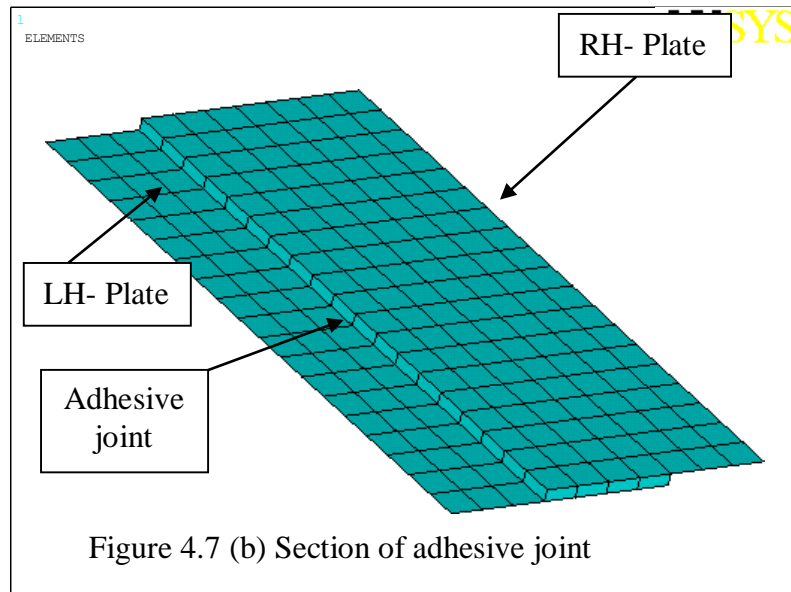
Parameter	Values
Internal loss factor ( $\eta$ )	0.02
Width( $w$ )	0.3 m
Length( $L$ )	0.3 m
Thickness( $t$ )	1.1 mm
Density( $\rho$ )	1140 kg/m <sup>3</sup>
Poisson's ratio( $\mu$ )	0.37
Young's Modulus( $E$ )	3.18 GPa
Excitation Frequency( $f$ )	1000 to 8000 Hz

The structure consists of two acrylic plates with the dimensions of length, 300 mm, width, 300 mm and thickness 1.1 mm, joined together by a double-sided adhesive tape. The overlap length of the two sheets is 12.5 mm. The adhesive modulus of elasticity of 0.2 MPa and internal loss factor of 0.02 has been considered for the studies. Table 4.2 presents' material properties of the acrylic plates considered and internal loss factor of the plates have a value of 0.02. Coupling factors and velocity responses are determined for frequencies from 1000 to 8000 Hz in steps of 1000 Hz. The analytical equations for computations by SEA of plates are as explained in section 3.2.1.

### 4.3.2 Finite element analysis

A FE model of the structure is as shown in Figure 4.7. The plates are modeled using SHELL 281 elements. SHELL 281 is suitable for analyzing thin to moderately-thick plate structures. The element has eight nodes with six degrees-of-freedom at each node. The adhesive joint patch of 12.5 mm has been modeled using solid elements, SOLID 186 with size 3.125 mm and 1.1 mm high.





The element is defined by 20 nodes with three degrees-of-freedom per node. The plates have been meshed with a mean mesh size of 3.1 mm. The minimum finite element size in the relation of a number of elements per wavelength of six is maintained. A harmonic force with unit load intensity is applied in the range of frequencies of 1000-8000 Hz. The load is applied on one plate, and the velocity responses on both the plates are computed. The velocity responses at all the nodes of the plates including the power input location are determined. In-house APDL codes are used for the computation of vibrational energy ( $E_i$ ) of each substructure using Equation (4.1). The coupling factors are computed by the Equation (1.7) after computation of power inputs and corresponding energies in all the substructures. The maximum average velocity amplitude ( $V_i$ ) of each substructure can be obtained directly from the post-processing of the output results.

#### 4.4 RESULTS AND DISCUSSION

Figure 4.8 presents the variation of the coupling loss factors with excitation frequencies obtained for the analytical, FE-monolithic model and FE-ACM2 model. It is observed that the coupling factor obtained by FE-ACM2 model is lower by 82.3% at 1000 Hz to 86.7 % at 8000 Hz in comparison to the FE-monolithic model (Figure

4.8). Similarly, the coupling factor obtained by FE-ACM2 model is lower by 77.9 % at 1000 Hz to 88.37 % at 8000 Hz than the analytically obtained values (Figure 4.8).

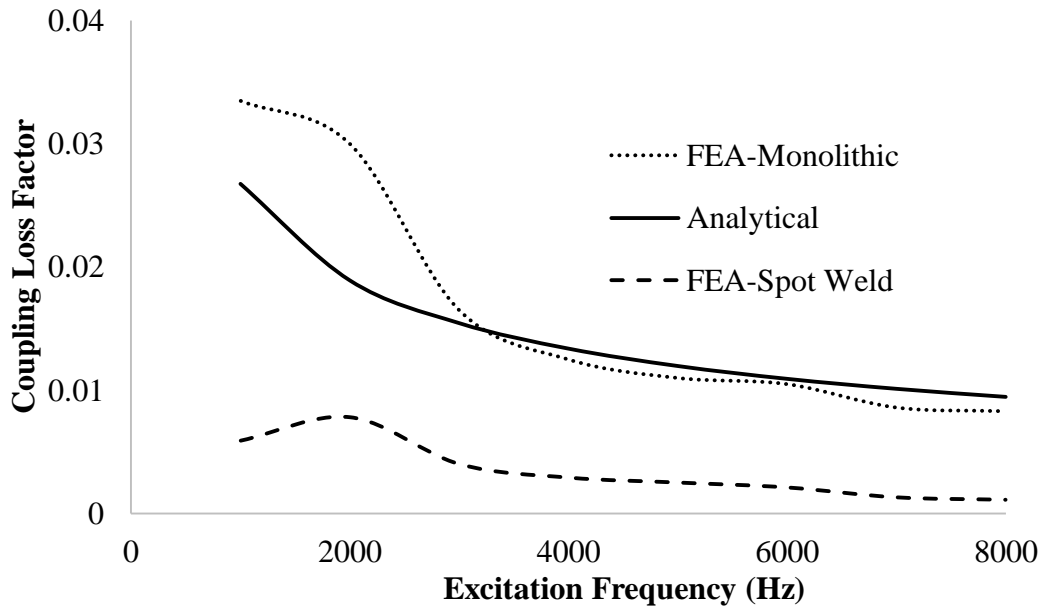


Figure 4.8 Variation of the coupling loss factors vs. excited frequencies of plates with spot-welded joint

Figure 4.9 depicts the variation of velocity amplitudes with excited frequencies on the excited plate with spot-weld joints. All the points in the plots have been joined by smooth lines. In case of the spot welds modelled using FEA, the percentage variation in the velocity responses varies from 20% at the lower frequencies to 2% at higher frequencies in comparison to the analytically obtained velocity amplitudes for the excited plate (Figure 4.9). The average percentage of variation in the velocity responses is in the range of 40 % more in comparison to the analytically obtained velocity amplitudes for the receiver plate (Figure 4.10).

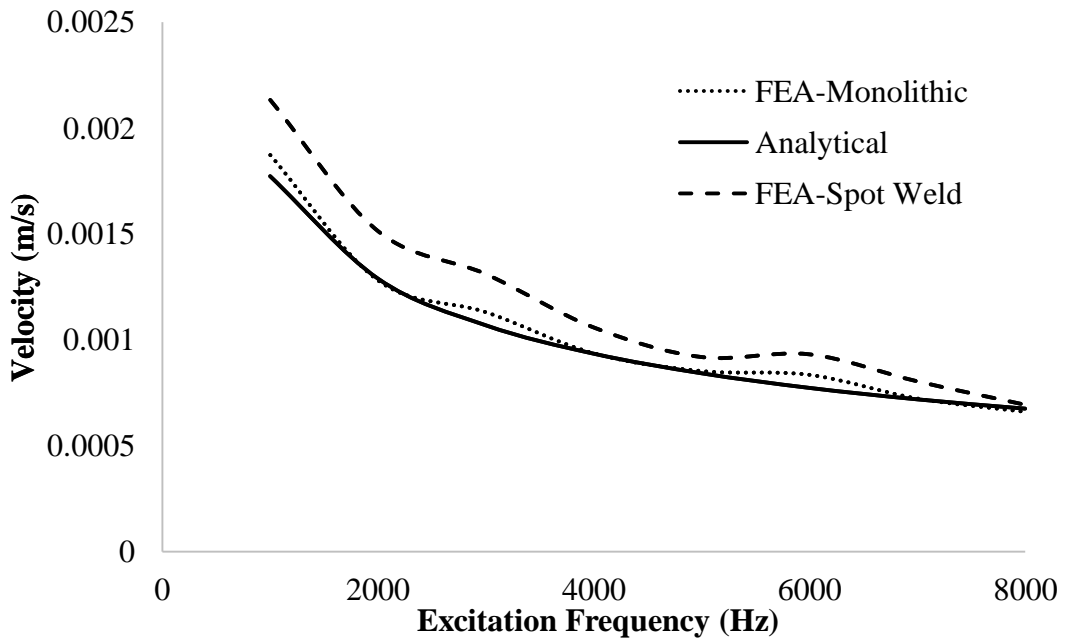


Figure 4.9 Velocity amplitudes vs. excited frequencies for the excited plate with spot-welded lap joint

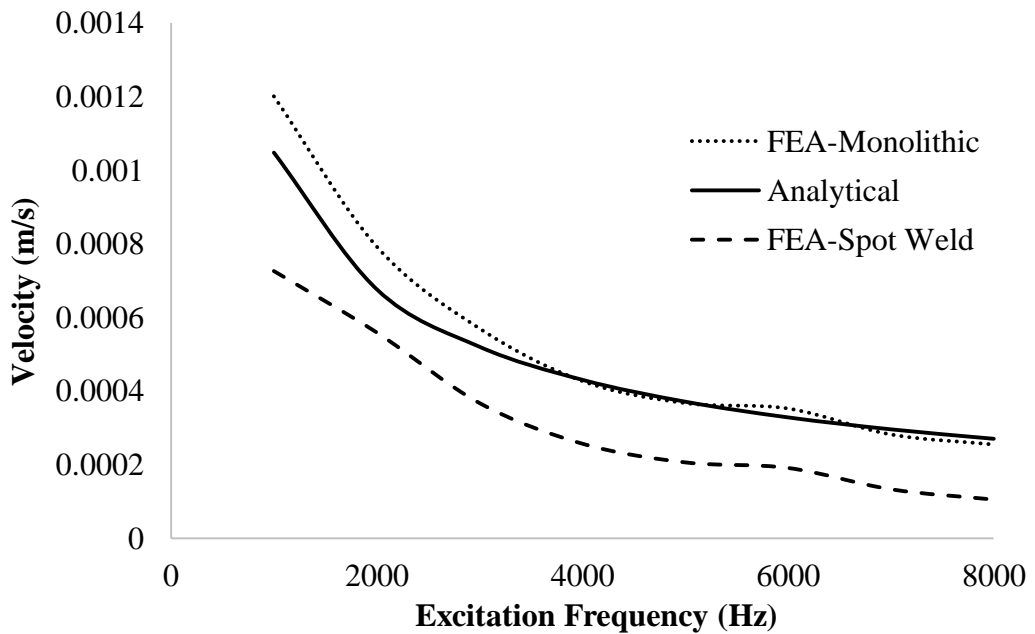


Figure 4.10 Velocity amplitudes vs. excitation frequency for the receiver plate with spot-welded lap joint

Figures 4.11 and 4.13 presents displacement plot of plates with spot-welded joint excited at frequencies 2000 and 8000 Hz, respectively, obtained using FE-ACM2 model, an indicator of the energy propagations. Whereas, Figures 4.12 and 4.14 presents the displacements plots obtained by FE- monolithic model for excitation frequencies 2000 and 8000 Hz, respectively. The location of excitation is at the centre of the left hand plate as shown in Figures 4.11 to 4.14, wherein, the maximum displacement amplitude response is observed. The results obtained from these models indicates significant influence on modeling of discrete joints like spot-welded joints in computation of the coupling loss factors and its further use in computation of total energies and velocity responses using statistical energy approach as compared to the analytical wave-based approach or FE-monolithic model assuming a continuous line junction.

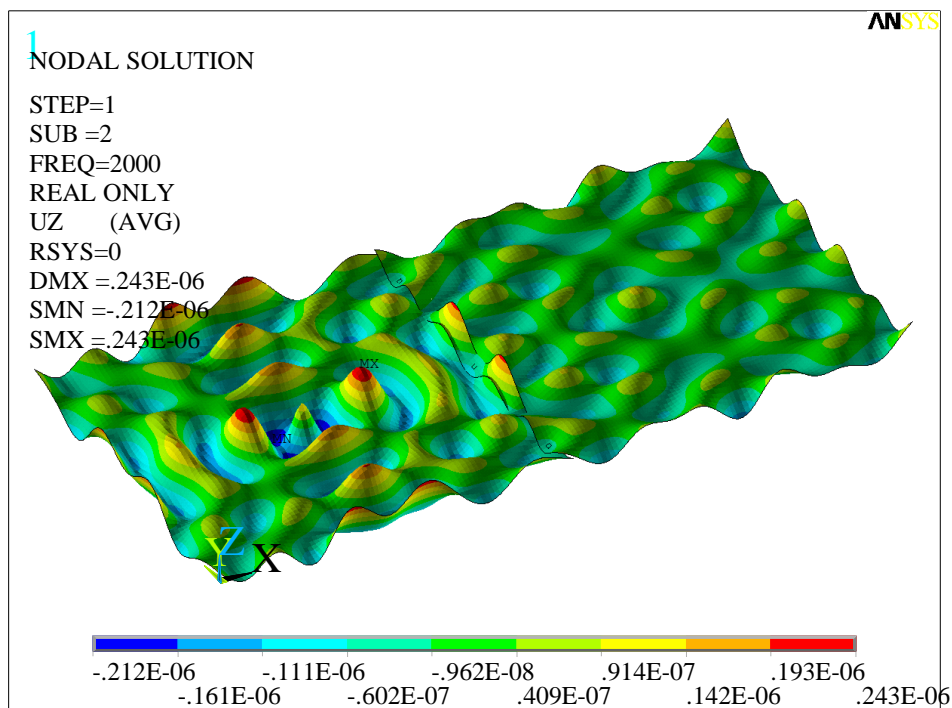


Figure 4.11 Displacement response of plate with spot-welded joint excited at frequency of 2000 Hz obtained using FE-ACM2 model

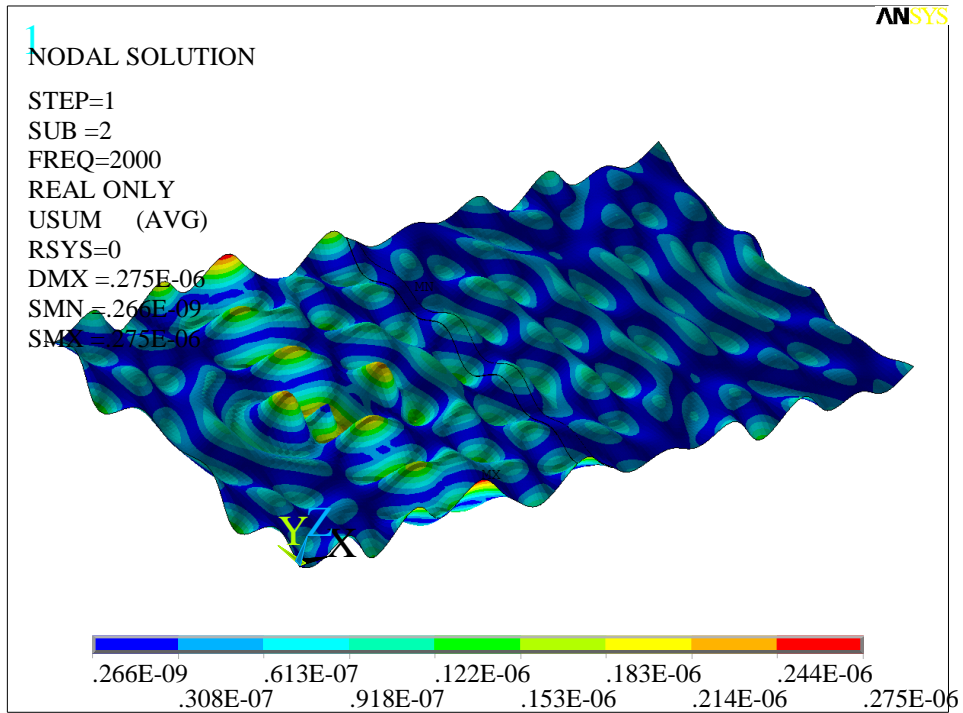


Figure 4.12 Displacement response of plate with spot-welded lap joint excited at frequency of 2000 Hz obtained using FE-Monolithic model

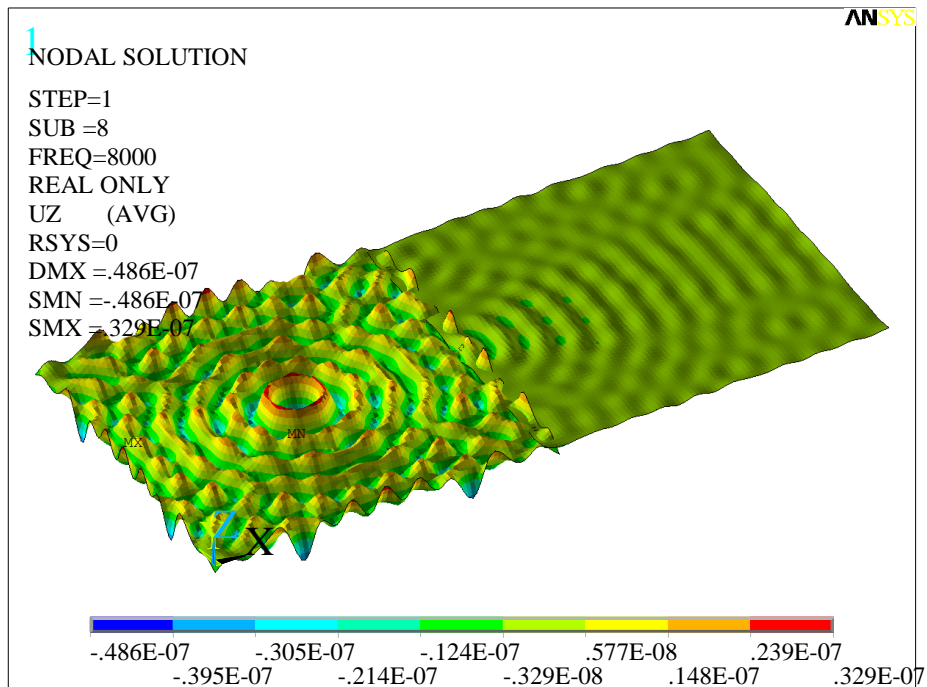


Figure 4.13 Displacement response of plate with spot-welded lap joint excited at frequency of 8000 Hz obtained using FE-ACM2 model

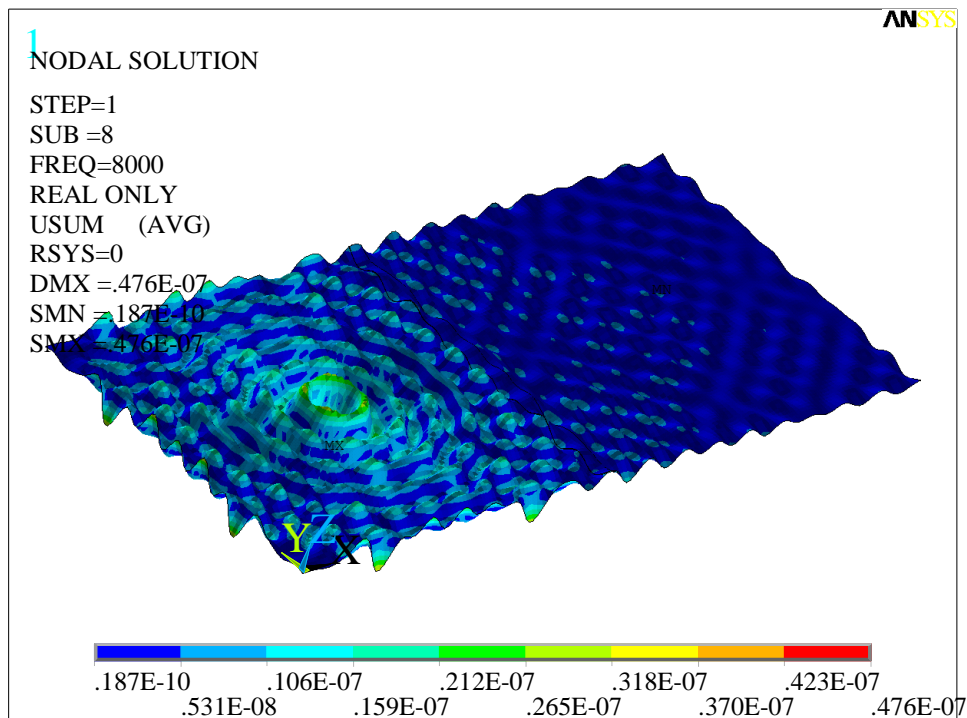


Figure 4.14 Displacement response of plate with spot-welded lap joint excited at frequency of 8000 Hz obtained using FE-monolithic model

Figure 4.15 depicts the variation between the coupling loss factors and excited frequencies computed by analytical, FE-monolithic model and modeling of actual adhesive patch for the adhesive bonded plates. It is observed that the coupling loss factor for the actual adhesive bonded joint is higher by 20.72 % at 1000 Hz and reduces to 1.6 % lower than the values of monolithic model for the same (Figure. 4.15). Similarly, the coupling loss factor for the actual adhesive bonded joint is higher by 59.26% at 1000 Hz and reduces to 17.8 % lower than the values of analytical line junction assumption (Figure.4.15). This reduction of coupling strength in the actual adhesive bonded joint is due to the reduced elastic modulus of the adhesive in comparison to the FE-monolithic and analytical model of the adhesive bonded joint. However, the deviation is far lower as the adhesive joint is along the junction length in comparison to the spot-welded (point junction) case which is in the average range of 80% (Figure. 4.8).



In case of the adhesive joint modelled using FEA, the percentage variation in the velocity responses varies from 12% at 1000 Hz to 3% at 8000 Hz in comparison to the analytically obtained velocity responses for the excited plate (Figure. 4.16).

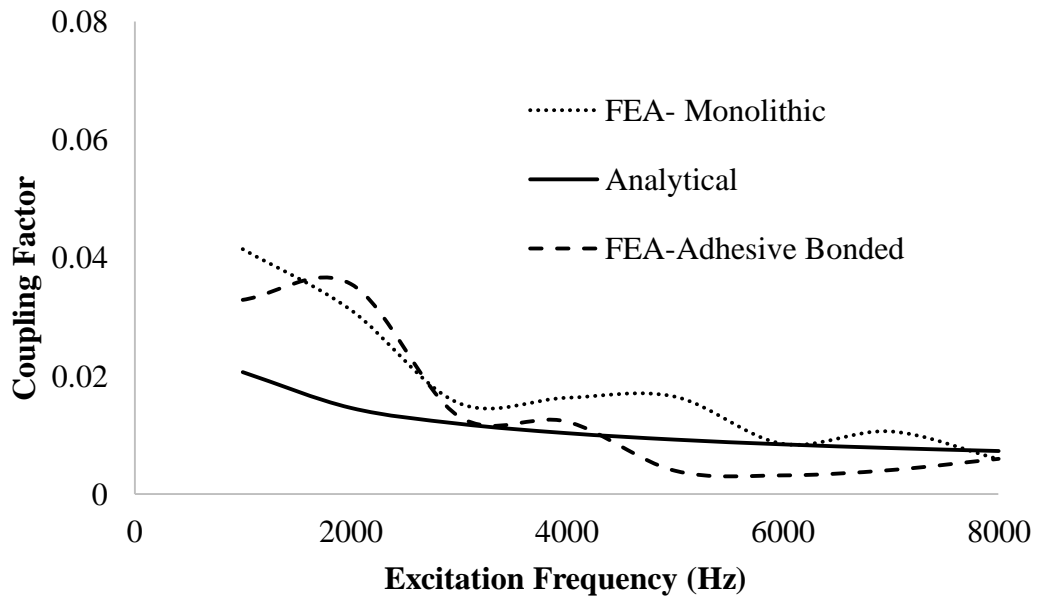


Figure 4.15 Variation of coupling loss factors vs. excited frequencies of plates with adhesive bonded lap joint

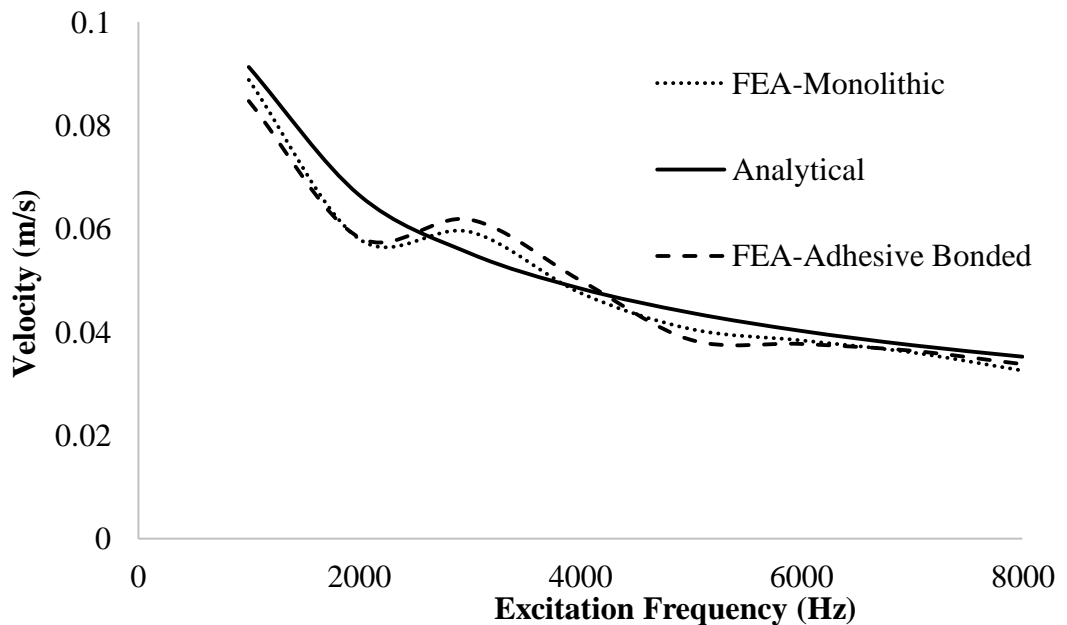


Figure 4.16 Velocity amplitudes vs. excited frequencies for the excited plate with adhesive bonded lap joint

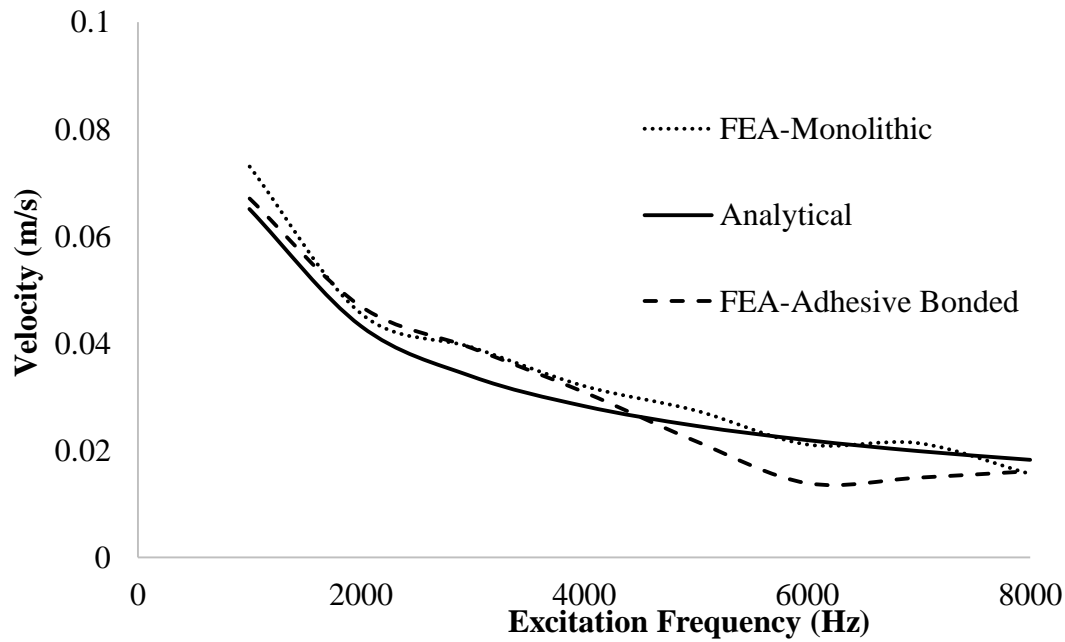


Figure 4.17 Velocity amplitudes *vs.* excited frequencies for the receiver plate with adhesive bonded lap joint

The energy propagation effects can also be observed in the displacement response plots for the FE model with the actual adhesive joint (Figures 4.18 and 4.20). The displacement response plots for the FE-monolithic model is shown in Figures 4.19 and 4.21. It is observed that due to the presence of continuous adhesive patch along the junction, the mode shapes are similar, with higher coupling effects, when compared with the spot-welded joints which are point junctions having lesser coupling effects.

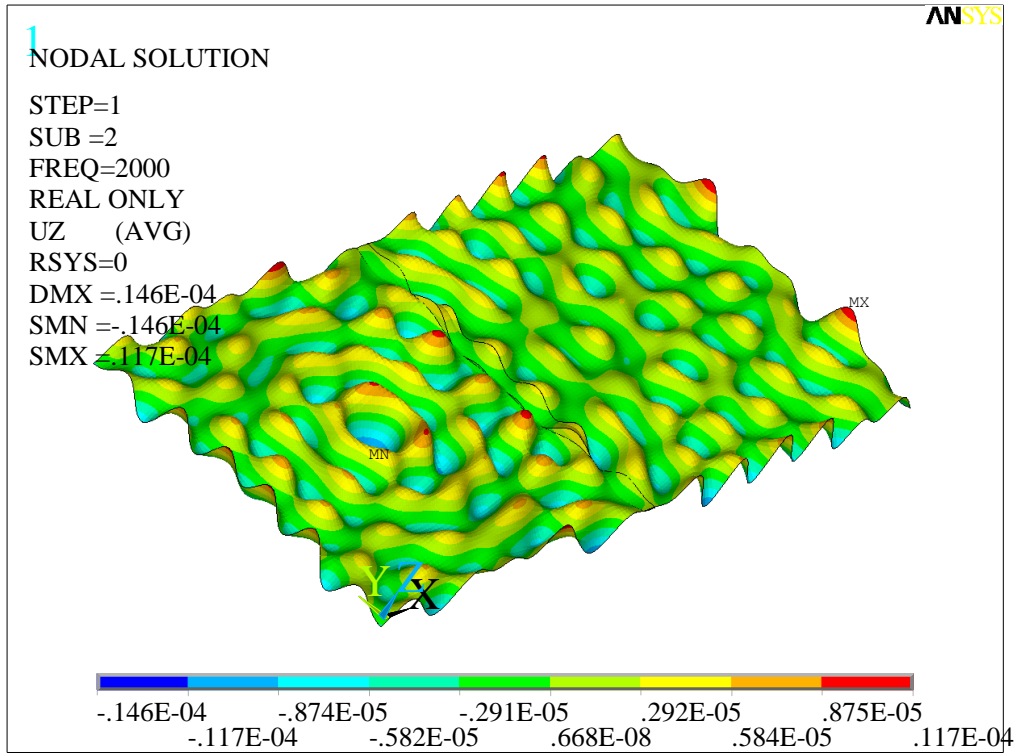


Figure 4.18 Displacement response of plate at an excitation frequency of 2000 Hz (actual FE-adhesive modelled lap joint)

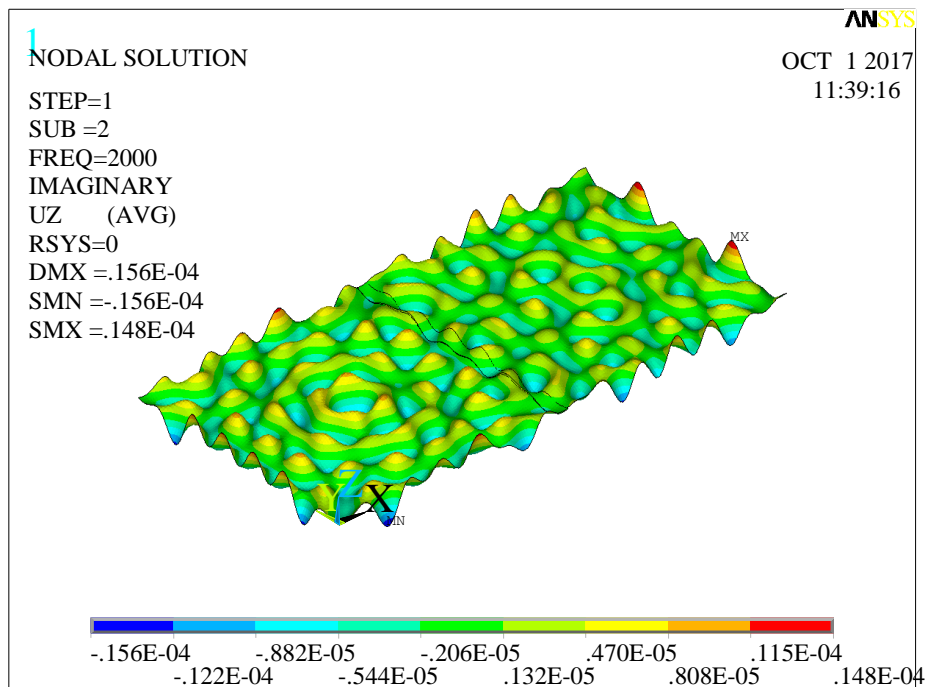


Figure 4.19 Displacement response of plate at an excitation frequency 2000 Hz (FE-monolithic model for adhesive bond)

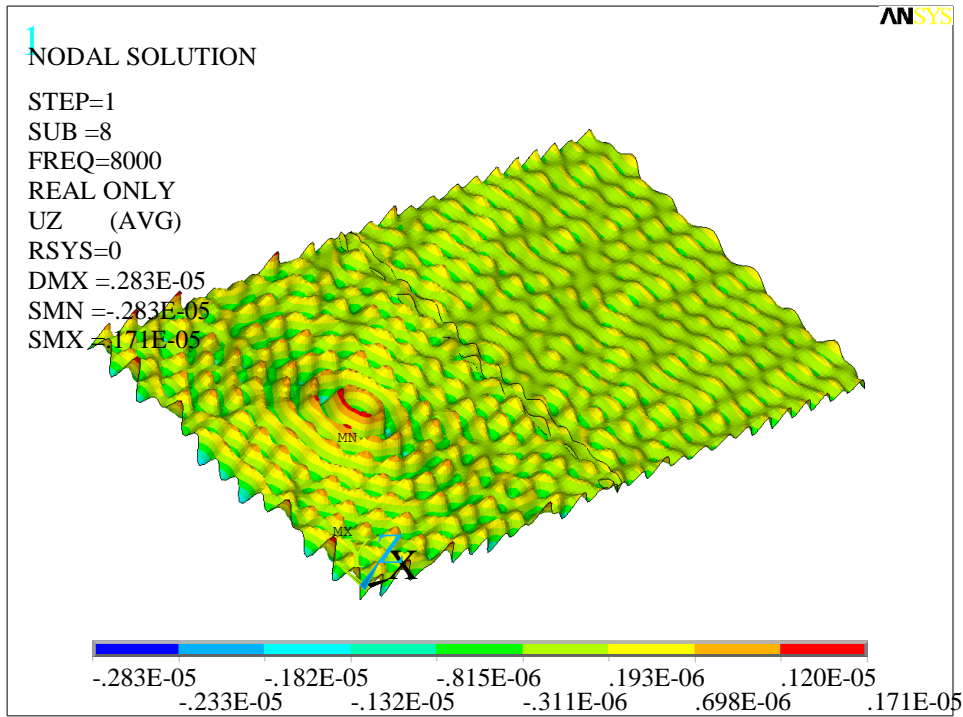


Figure 4.20 Displacement response of plate at an excitation frequency 8000 Hz. (actual FE-adhesive modelled lap joint)

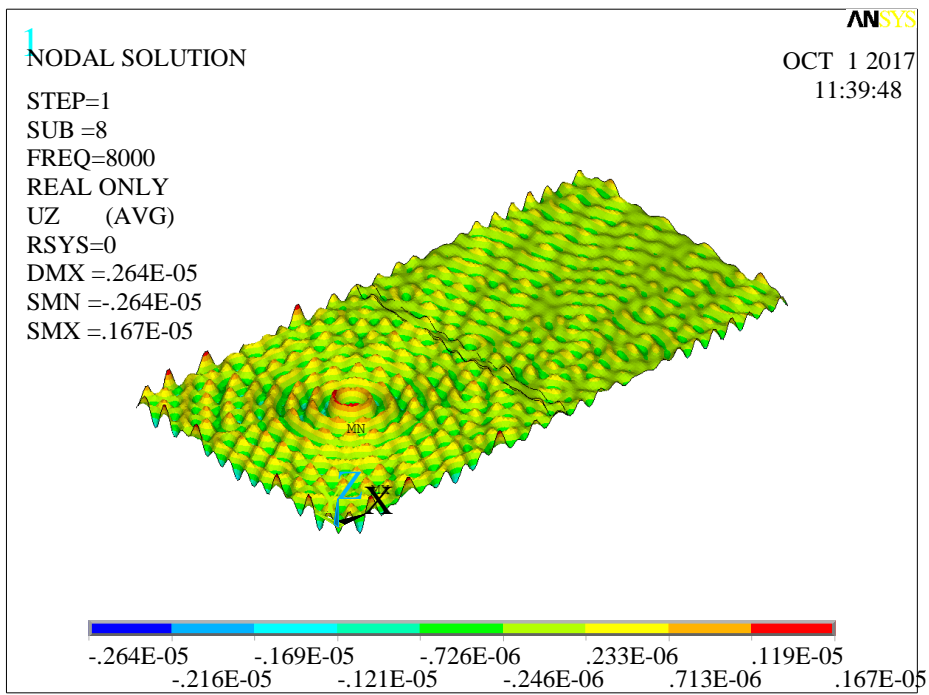


Figure 4.21 Displacement response of plate at an excitation frequency 8000 Hz (FE-monolithic model for adhesive bonded lap joint)

#### **4.5 SUMMARY**

The CLFs of two lap joined plates have been computed through FEA using the area contact model (ACM2) approach and SOLID 186 elements for the spot welded and adhesive joint, respectively. The effects of these coupling factors computed using FEA has been compared with the analytical wave-based approach and FE-monolithic model with continuous line junction assumption. These FE modelling approaches are used for the further work on damage detection studies. The results obtained from the studies in this chapter signifies the importance of FE modelling of joints, discrete joints in particular like the spot welded joints in computation of the coupling factors for its use in the SEAL predictions explained in the successive chapters.

In case of bolted joints, the finite element model requires experimentation to be carried out for tuning the FE details of the bolts using frequency response identification techniques etc. High fidelity FE models for the joint interface can be developed from experimentation (Ahmadian, et al., 2007; Iranzad, et al., 2012). In the present studies, a simplified coupled bolt model has been used with the viscous damping of the bolt beam element tuned to 0.1 to get a close match with the experimental results. The details are reported in Chapter 6.

## CHAPTER 5

### DAMAGE DETECTION OF SPOT WELDED PLATES USING STATISTICAL ENERGY ANALYSIS LIKE APPROACH

#### 5.1 INTRODUCTION

This chapter discusses the damage detection investigations on spot welded plates, wherein, apparent coupling factors have been derived for four cases of two mild steel plates lap joined by spot welds. The derived apparent coupling factors are further used to predict the velocity and acceleration responses using SEAL approach for an assembly of three plates lap joined by spot welds. The results obtained have been discussed and compared by experiments and finite element simulation for a healthy and damaged configuration of the same.

#### 5.2 TEST SPECIMENS

The dimensions of each mild steel plate considered in the studies are of length, 500 mm, width, 500 mm and thickness of 1.21 mm. The plates are joined by spot welds with an overlap length between two sheets of 50 mm. The diameters of the spot weld nuggets are approximately 6 mm. The following cases of two plates joined by spot-welds have been considered to obtain the apparent coupling factors using statistical energy analysis like (SEAL) approach.

**Case-1:** Two plates with lap joint having three spot welds,  $S_1$ ,  $S_2$  and  $S_3$  (Healthy Configuration; Figure 5.1)

**Case-2:** Two plates with lap joint having two spot welds,  $S_1$  and  $S_3$  (Centre weld,  $S_2$  assumed to be damaged; Figure 5.2)

**Case-3:** Two plates with lap joint having two spot welds,  $S_1$  and  $S_2$  (Bottom most weld,  $S_3$  assumed to be damaged; Figure 5.3)

**Case-4:** Two plates with lap joint having one spot weld,  $S_2$  at the Centre (Two extreme spot welds,  $S_1$  and  $S_3$  assumed to be damaged; Figure 5.4).

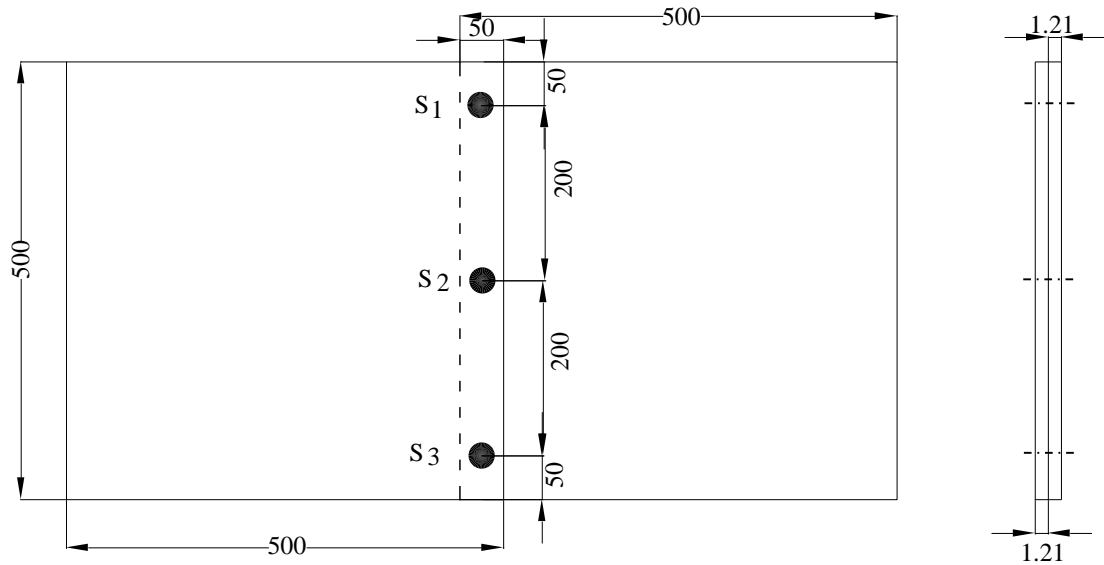


Figure 5.1 Geometric dimensions of plates with spot- welds (Case-1)

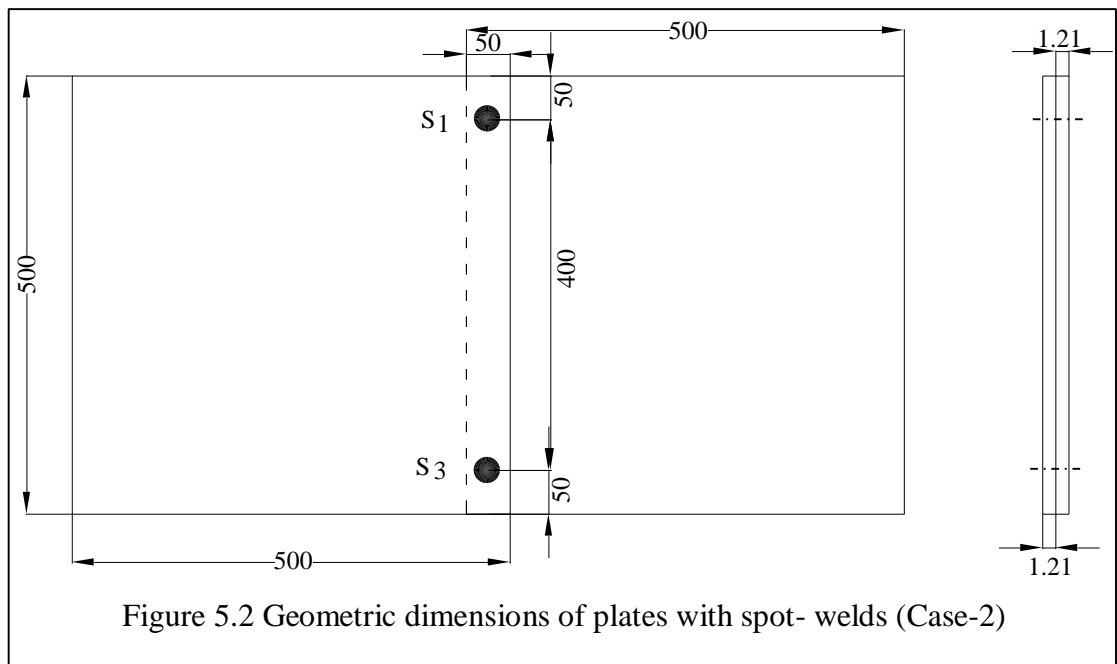


Figure 5.2 Geometric dimensions of plates with spot- welds (Case-2)

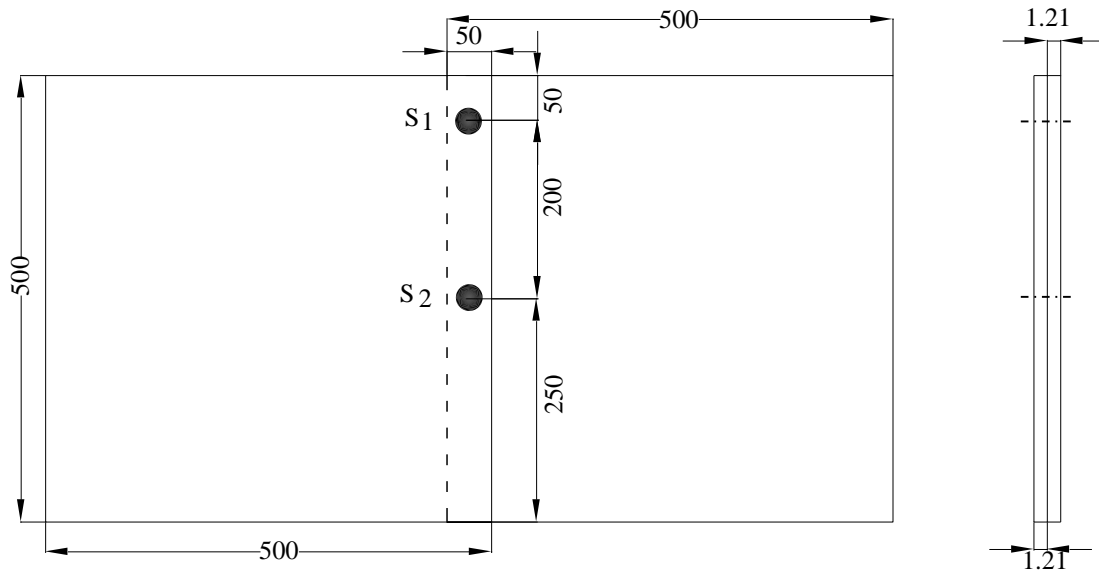


Figure 5.3 Geometric dimensions of plates with spot- welds (Case-3)

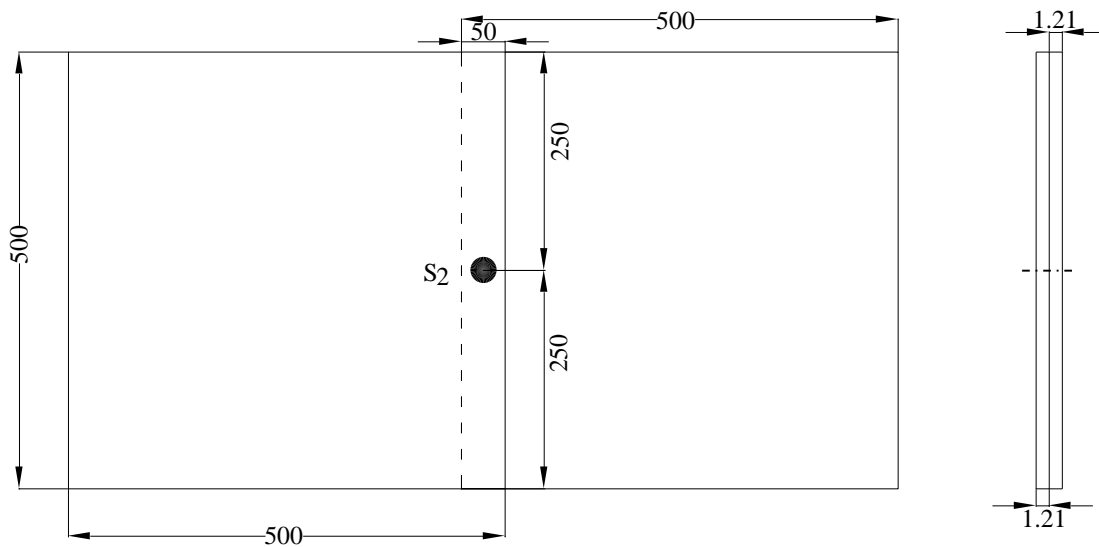


Figure 5.4 Geometric dimensions of plates with spot- welds (Case-4)

### 5.3 STATISTICAL ENERGY ANALYSIS LIKE APPROACH (SEAL)

The apparent coupling factors obtained from experiments and finite element simulations could be used to predict the total energies and velocities of sub-structures connected to each other. Numerical estimates of the CLFs can be obtained from finite element analysis (FEA) of a system and the process is essentially a numerical analog



of the power injection method (PIM) which is often used to develop an experimental SEA model of a structure. The basic power balance Equation (1.7) of SEA relates the ensemble average powers and energies, whereas the predictions from finite element analysis are based on a single estimate of frequency average quantities and depend on the specific input data chosen for the FEA.

The focus in the present study is the use of an energy flow balance for the individual case exploiting the principles in SEA rather than applying its underlying assumptions and rules in the process of analysis. Thus the individual case is different from the mean in an ensemble of cases. Accordingly, the coupling loss factor estimated from an individual case is referred to as an apparent coupling loss-factor (ACLF) or energy influence coefficient (EIC) in the literature, to distinguish it from ensemble-based estimates. The term SEA like is adopted to distinguish between SEA and the use of the energy flow balance in SEA as applied in the energy flow model (Fredo, 1997). ACLF or EICs in contrast to the CLFs in SEA are case specific and dependent on the system properties, boundary conditions, and excitation. In cases, when the non-resonant transmission from the source through the excited substructure is substantial, negative EFCs can exist. The variation of the ACLF or EICs decreases with the increase in modal overlap and modal density.

The advantages of this approach have been the ease in its application for complicated substructures, joints, and sources with excitation frequency spectra containing non-resonant transmission mechanisms. SEAL approach is thus a method for applying the conventional SEA for the individual case.

#### **5.4 EXPERIMENTAL SET - UP**

The experimental setup consists of spot-welded plates to be tested, data acquisition hardware, sensors, shakers and computer with modal analysis software as shown in the Figure 5.5.

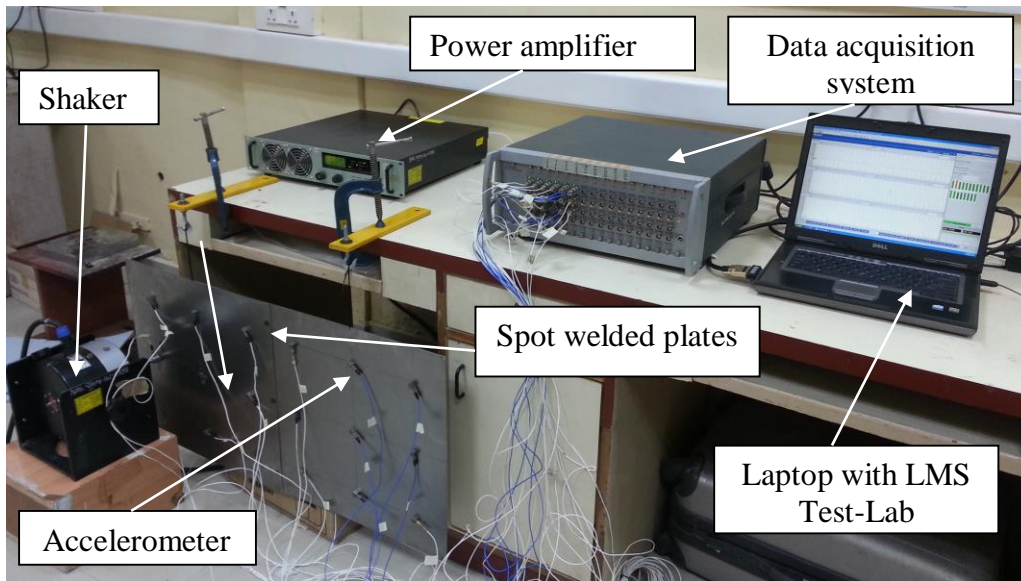


Figure 5.5 Experimental set-up

For acquiring the vibration signals, a uniaxial piezoelectric accelerometer was used. The specifications of the accelerometer are as shown in Table 5.1. Electrodynamics shakers of Bruel and Kjaer with a force rating of 200 N sine (Type 4825) and a compatible power amplifier has been used to excite the plate. For excitation, a shaker was used. Figures 5.6 and 5.7 shows the shaker and the specifications of the shaker are as shown in Table 5.2.

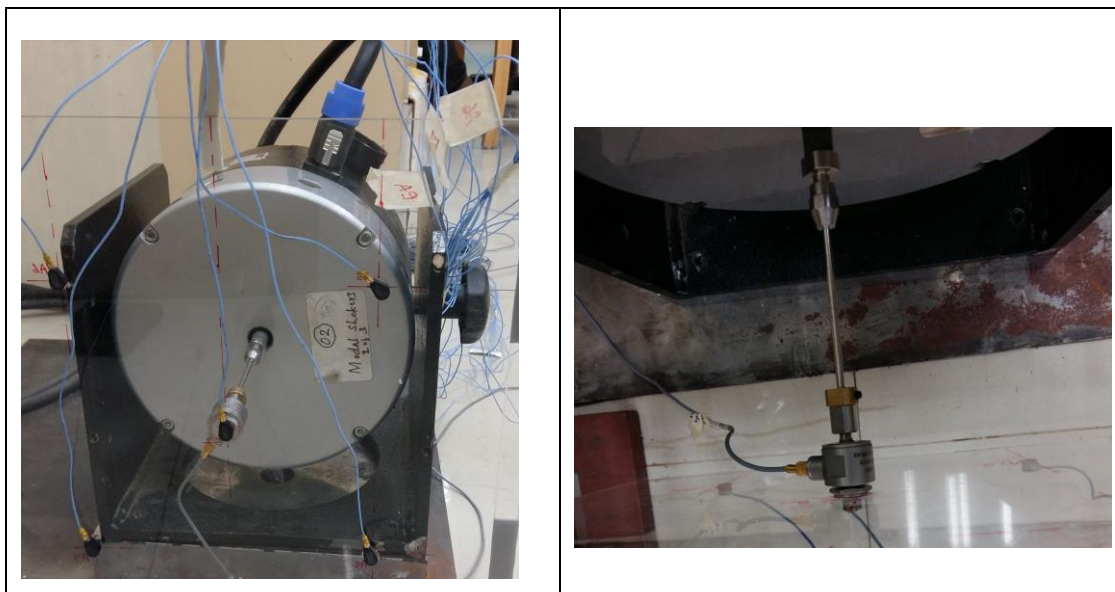


Figure 5.6 Shaker for excitation

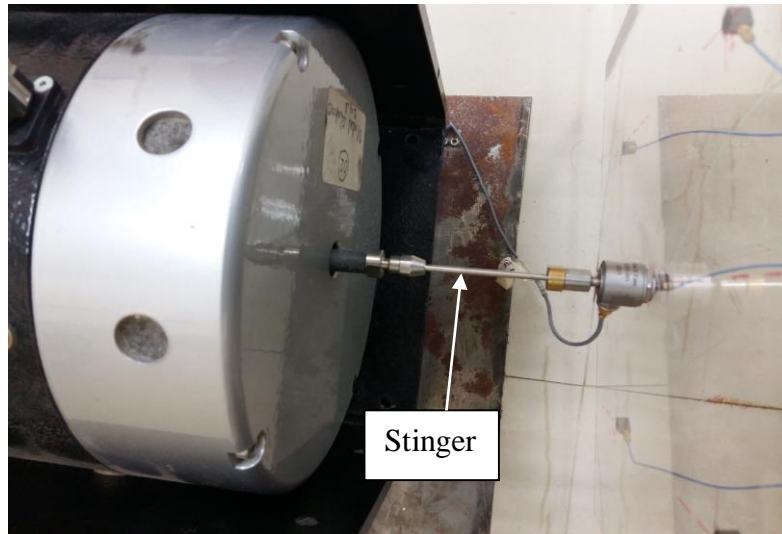


Figure 5.7 Shaker-stinger-force transducer attachment

Table 5.1 Specification of the accelerometer

Make (PCB piezotronics)	Integrated circuit piezoelectric
Model	333B30
Sensitivity	100 mV/g
Frequency range ( $\pm 5\%$ )	0.5 to 3000 Hz
Resonant frequency	>40 kHz
Measuring range	$\pm 50$ g
Weight	4 to 5 gm
Temperature range	-18 to 66 <sup>0</sup> C
Size	10.2 mm x 16.0 mm x 10.2 mm

Table 5.2 Specification of the shaker

Model (Bruel & Kjaer)	4825
Rated Force	200 N sine
Frequency range	2 to 5000 Hz
Max. rated travel	25.4 mm
Max. Velocity	1.5 m/s
Max. Acceleration	88 g
Weight with trunnion	21 kg
Resonance frequency	>6000 Hz
Size	306 mm x 220 mm x 241 mm

SCADAS III is a multichannel 24 bit data acquisition system with inbuilt ADC and signal conditioners for ICP type of accelerometers (Figure 5.8). Communication between data acquisition hardware and the computer system is established through SCASI card, and a Laptop (Figure 5.9) with advanced modal analysis software LMS test lab is used for data acquisition, analysis and extracting the modal parameters.

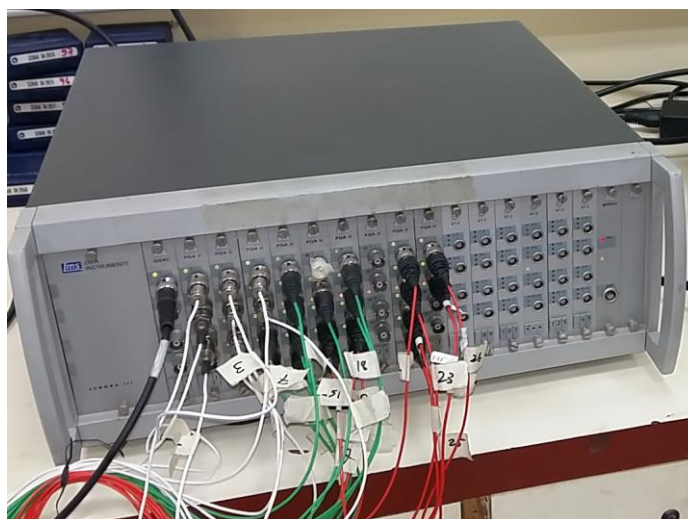


Figure 5.8 LMS Data acquisition system

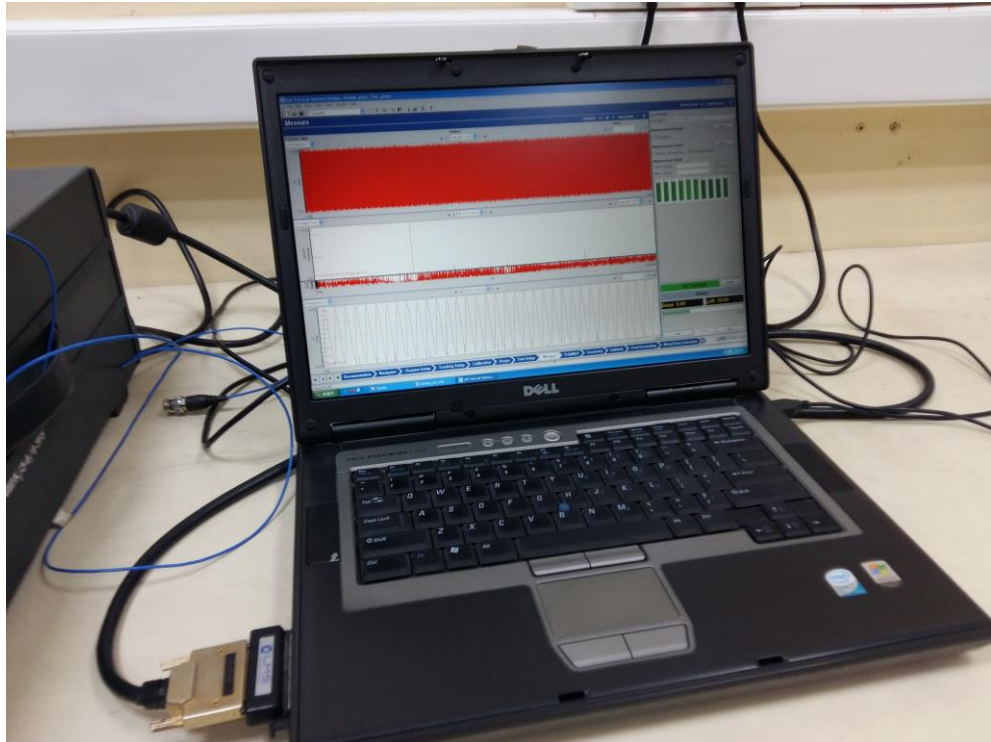


Figure 5.9 LMS test lab front panel to represent the acquired data

The excitation force is measured using force transducer as shown in Figure 5.10. The specifications of the force transducer are listed out in Table 5.3.

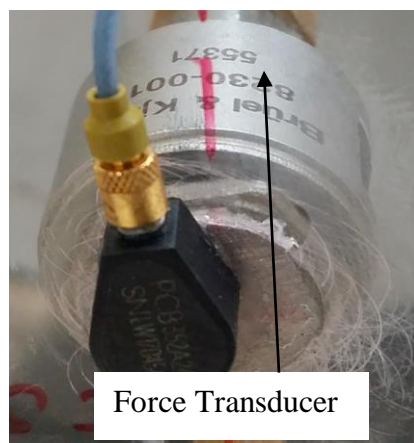


Figure 5.10 Force transducer

Table 5.3 Specification of the force transducer

Make (Bruel & Kjaer)	Voltage output type
Model	8230-001
Sensitivity	22 mV/N
Force range (compression)	220 N
Force range (tensile)	220 N
Max. Compression	4.5 kN
Resonant frequency	75 kHz
Weight (mass above piezo element)	9.5 to 10 gms
Temperature range	-73 to 121 <sup>0</sup> C
Size	19.05 mm x 29.46 mm x 15.9 mm

## 5.5 EXPERIMENTAL PROCEDURE

The following methodology is adopted during the experimentation process. The repeatability of the experiments is also taken care.

1. A small portion of wax is applied to the underside of the accelerometer and pressed on the location on the plate, wherein the response is to be measured.
2. Low noise, Teflon jacketed cable is connected to the accelerometers mating socket by inserting the cable's connector pin. Then the connector is threaded into place by turning the cable connector's outer shell onto the accelerometer's electrical connector.
3. Constant current signal conditioners are used for constant current excitation of sensors. Calibration is done by verifying the performance of each accelerometer with a handheld shaker for a quick check of its sensitivity.

4. A small portion of adhesive is applied on the underside of the force transducer and pressed on the location of shaker excitation on the plate and connected to the shaker by a cable.
5. The maximum range for the accelerometer used for the experimentation of spot welded plates is 3000 Hz. Accordingly the excitation frequency for the experiments was limited between 1000 to 3000 Hz. The spot welded plates have been hung by soft cords to simulate a free-free boundary condition.
6. Using LMS test lab new project is created. The first step after creating new project is to generate the geometry as per the test points were chosen for measurements. Each plate is divided equally into nine regions, and the responses were obtained using nine accelerometers, placed centrally for each of the regions. The nodes, i.e., the accelerometer positions and wire frame geometry created is as shown in the Figure 5.11. Channels setup is carried out with the setting type of sensor, excitation voltage, units, reference point, measurement point identifications and gain settings. Figure 5.11 shows the geometry created in test lab for two spot welded plates.

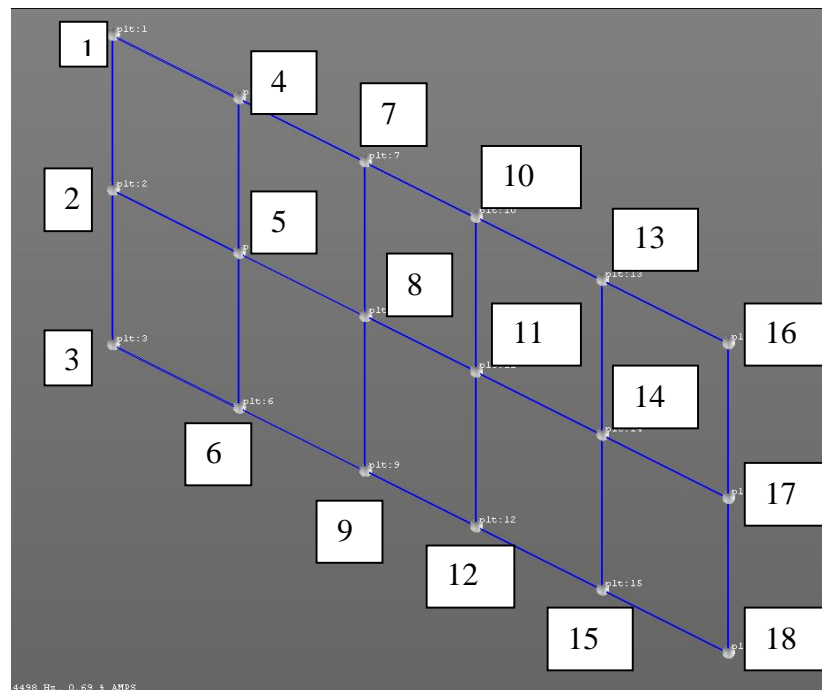


Figure 5.11 Geometry created in Test. Lab

Figure 5.11 has been presented in an isometric position of the plate with locations of accelerometers. Figure 5.11 has been modified with more details as shown in Figure 5.12. The following figure shows the nine locations of accelerometers numbered with 1 to 9 for the LH-Plate. Similarly, accelerometers 10 to 18 have been placed centrally in the regions of the RH-Plate.

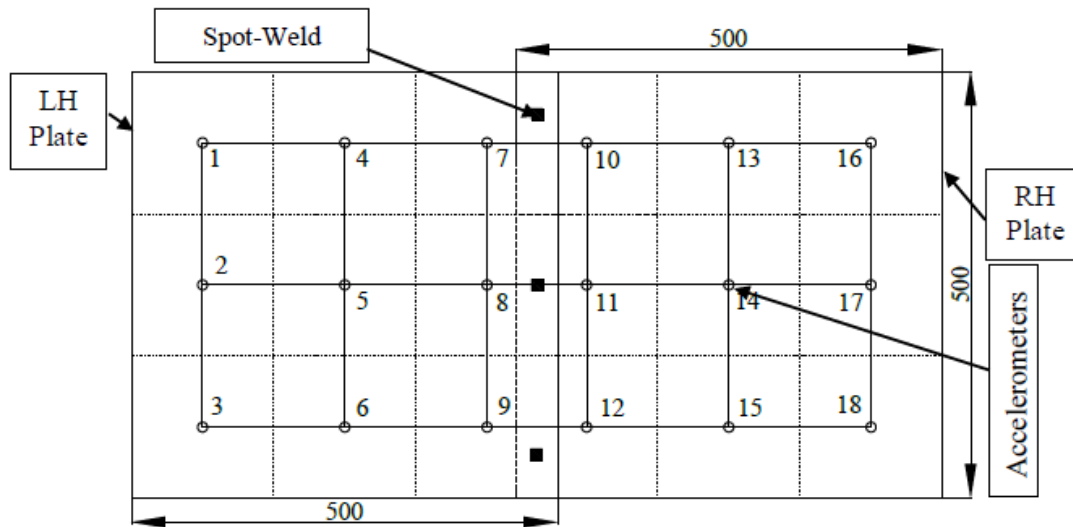


Figure 5.12 Schematic of two plates with locations of 18 accelerometers.

7. To measure the natural frequencies, scope settings with maximum frequency is set to 512 Hz and spectral lines of 2622 Hz, which gives a frequency resolution of 0.19 Hz. Uniform windows are chosen for both excitation and response signals. 50% burst random signal is used for exciting the plate. Same scope settings are imported to test setup and required functions such as time domain data, cross power spectrums, peak spectra, FRF, and auto power spectra, etc. are selected to store into the computer database.
8. In case of harmonic sinusoidal excitation and acceleration response measurement, 32768 Hz sampling frequency and a maximum bandwidth of 10000 Hz is set. The experimental set up for one case (Case-1) for two spot welded plates is shown in Figure 5.13. The plate is hung by soft cords to simulate the free-free boundary conditions.



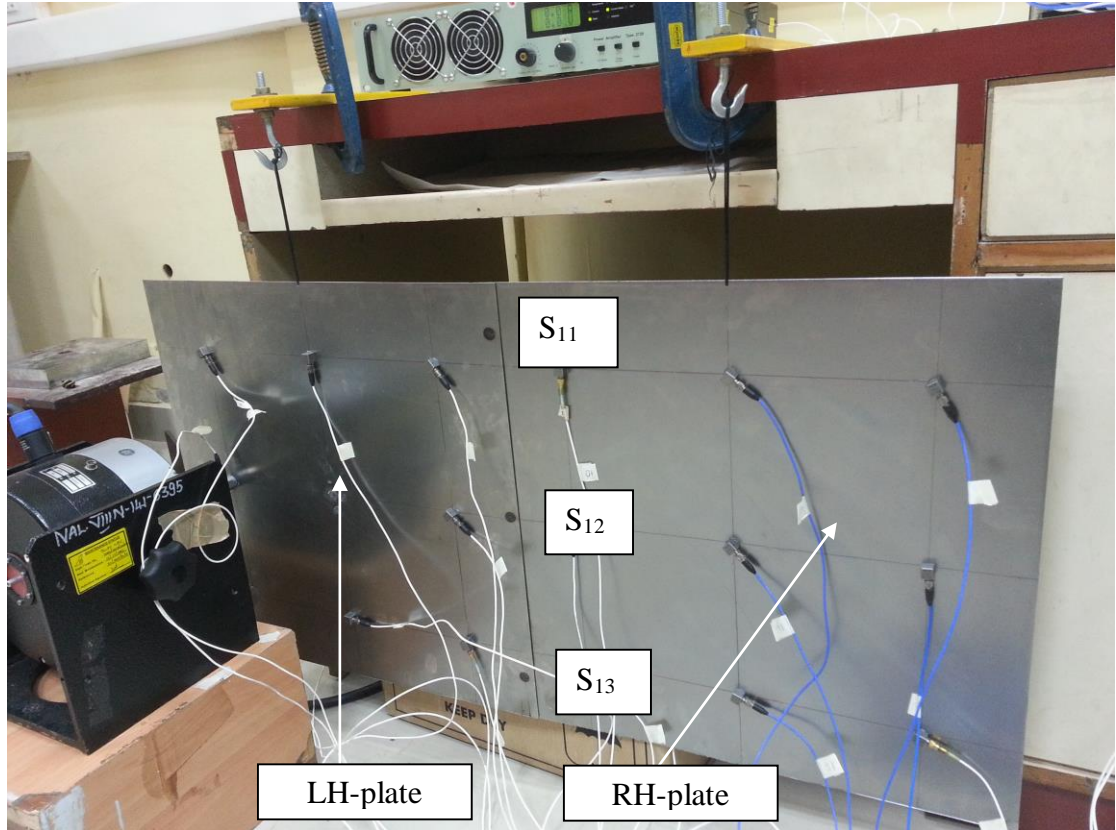


Figure 5.13 Experimental set up for two spot welded plates (Case-1)

9. The time-averaged power input into the structural substructure is given by (De Langhe, 1996)

$$P = \frac{1}{\omega} \text{Im} (S_{af}(\omega)) \quad (5.1)$$

10. Power input measurements ( $P$ ) require the evaluation of the imaginary part of the cross-spectrum  $S_{af}$ . Hence, unlike the energy measurements for which phase information is not essential, an accurate knowledge of the phase between force and acceleration at the excitation point is vital in the case of power input measurements. In the present case, excitation is carried out at discrete frequencies of 1000 to 3000 Hz in steps of 500 Hz.
11. The input excitation force is applied to the center (0.25 m, 0.25 m) of one plate (Pt-5, Figure 5.14). The plate is excited for flexural vibratory modes. Additionally, while repeating the trials, excitation force location is varied near the central location and the average coupling factor is obtained.

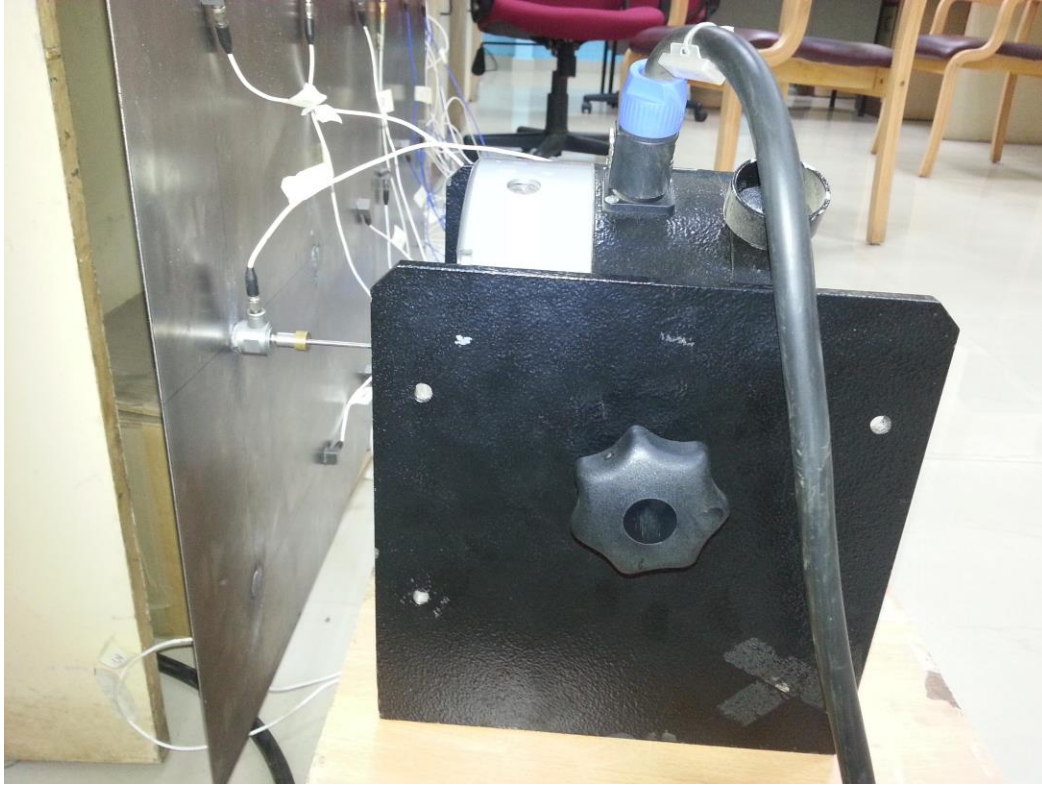


Figure 5.14 Excitation location near the edge of LH-plate

## 5.6 POWER INJECTION METHOD

The power injection method (PIM) is based on the comparison of the dissipated energy of a system to the total vibrational energy ( $E_{Total}$ ) of the system under steady-state vibration. PIM is theoretically unbiased as it is based on the definition of the loss factor ( $\eta$ ) and is applicable at all frequencies. At higher frequencies, with higher modal overlap, the PIM is used to calculate loss factors over broad frequency ranges. These band averaged loss factors are used in models based on finite element analysis (FEA) and statistical energy analysis (SEA) (Bloss and Rao, 2002). Under steady state conditions as the power input ( $P$ ) into a single system is dissipated by the system, the dissipated power can be replaced with the power input to obtain the internal loss factor (Equation 5.2)

$$\eta = \frac{P}{\omega E_{Total}} \quad (5.2)$$

In case of coupled sub-structures, PIM requires the measurement of the power input into every single substructure and the measurement of the total vibrational energy level of every substructure. By inverting the appropriate measured total vibrational energy matrix, the SEA parameters of internal loss factor and coupling loss factor in Equation 5.3 can be obtained. (Bies. et.al. 1980)

$$\omega \begin{bmatrix} \left( \eta_1 + \sum_{i \neq 1}^N \eta_{1i} \right) n_1 & -\eta_{12} n_1 & \cdots & -\eta_{1N} n_1 \\ -\eta_{21} n_2 & \left( \eta_2 + \sum_{i \neq 2}^N \eta_{2i} \right) n_2 & \cdots & -\eta_{2N} n_2 \\ \vdots & \vdots & \ddots & \vdots \\ -\eta_{N1} n_N & \cdots & \cdots & \left( \eta_N + \sum_{i \neq N}^{N-1} \eta_{Ni} \right) n_N \end{bmatrix} \times \begin{bmatrix} \frac{\langle \bar{E}_1 \rangle}{n_1} \\ \frac{\langle \bar{E}_2 \rangle}{n_2} \\ \vdots \\ \frac{\langle \bar{E}_N \rangle}{n_N} \end{bmatrix} = \begin{bmatrix} \bar{P}_{i,1} \\ \bar{P}_{i,2} \\ \vdots \\ \bar{P}_{i,N} \end{bmatrix} \quad (5.3)$$

## 5.7 FINITE ELEMENT ANALYSIS

The procedure for the creation of finite element mesh model of the plates with spot-weld (Figure 5.15) is as discussed in section 4.2.2 of Chapter 4. The plates are modeled using SHELL63 elements with both bending and membrane capabilities. Both in-plane and normal loads are permitted. The element has six degrees of freedom at each node: translations in the nodal x, y, and z directions and rotations about the nodal x, y, and z-axes. The spot weld nuggets have been modeled using a single solid element (SOLID185 with 6 mm square and 1.21 mm high), that is the ACM2 model.

The plates have been meshed with a mean mesh size of 6 mm. The FEA calculations were carried out using element dimensions smaller than one-sixth of the minimum bending wavelength in the excitation frequency range considered. The patches are meshed with 6 mm square shell elements, while areas along the edges are meshed with less than 6 mm non-square elements. Also, for the ACM2 model, the center of the patch area is coincident with the center of the solid element. Table 5.4 lists out the material properties of the plates.

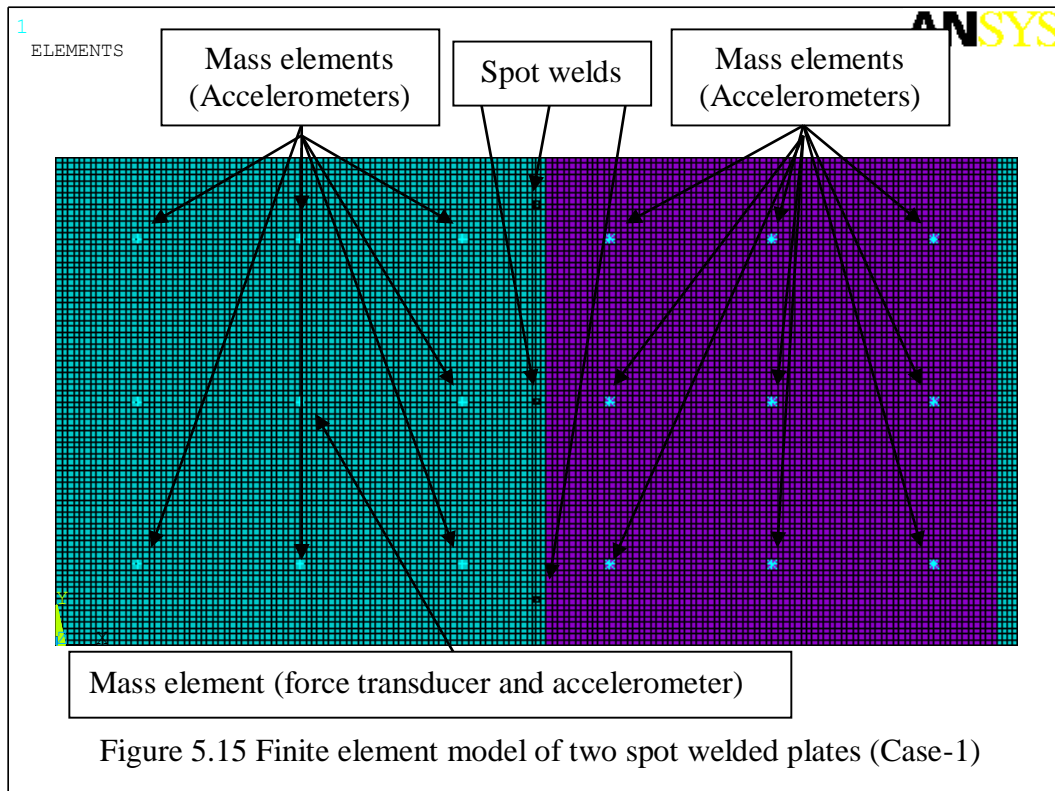


Table 5.4 Material and Geometrical specifications

Parameter	Values
Width( $w$ )	0.5 m
Length( $L$ )	0.5 m
Thickness( $t$ )	1.214 mm
Density( $\rho$ )	7850 kg/m <sup>3</sup>
Poisson's ratio( $\mu$ )	0.3
Young's Modulus( $E$ )	210 GPa
Force( $F$ )	1 N
Frequency( $f$ )	1000 to 3000 Hz

The damaged spot welds have not been modeled representing the stiffness loss for a spot welded joint at that particular location. Dynamic analysis of the FE model of the spot-welded plates is carried out for a free-free condition, and then dynamic frequency spectrum obtained by invoking the lanczos method in ANSYS, with unit mass criteria for normalizing mode shapes. The full method available in ANSYS has been used for the harmonic analysis. The advantages of the full method are that it is

easy to use and uses full matrices, so is more accurate as no mass matrix approximation is involved and allows asymmetric matrices. A harmonic force with unit load intensity is applied in the range of frequencies of 1000-3000 Hz at steps of 500 Hz. Unit force of 1 N is applied to the first plate, and the velocity responses on both the plates have been computed. The internal loss factors estimated by the experimental power injection method on a single plate (Figure 5.16) for different frequencies as listed out in Table 5.5 have been used for the finite element analysis at the respective frequencies. The internal loss factors obtained have been found to be consistent with the ones obtained during the experiments for the coupled spot-welded plates for all the cases.

Table 5.5 Internal loss factors for the excited frequencies

Excitation frequency(Hz)	1000	1500	2000	2500	3000
Loss factor( $\eta$ )	0.0017	0.0042	0.0052	0.0059	0.0072

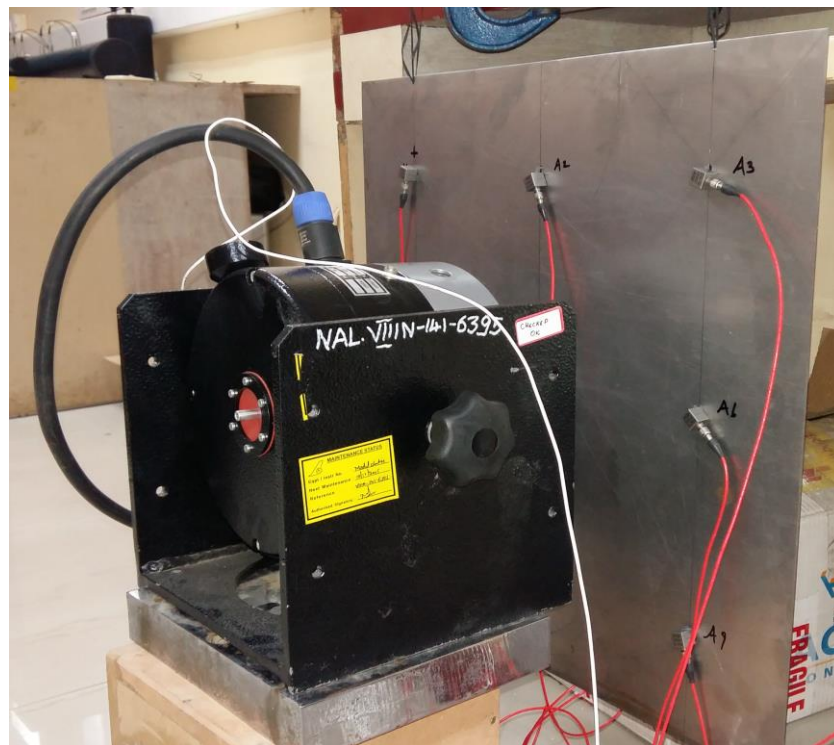


Figure 5.16 Power injection method for a single plate

The mass of the accelerometers is modeled as a concentrated mass element (mass 21) at the locations wherein the accelerometers have been placed during the experiments. The additional mass of the force transducer has also been included in the concentrated mass element (mass 21) element at the point of excitation force. The velocity responses at the nodes of the plates are measured and the power input locations are computed from FEA. Finally, the total vibrational energy ( $E_i$ ) of each region of the plate is computed using Equation (5.4),

$$E_i = \frac{M_i V_i^2}{2} \quad (5.4)$$

where ( $M_i$ ) is the mass of one of the nine regions on each plate and the representative substructure velocity ( $V_i$ ) corresponding to that region.

The total vibrational energy of each plate is computed by the summation of the energies obtained from individual regions of that plate ( $E = E_1 + E_2 \dots E_9$ ). The apparent coupling factors are computed by the Equation (5.3) after computation of power inputs and corresponding energies of each plate. The maximum velocity response of each plate is obtained directly from the post-processing of the output results. Inhouse codes and programs have been developed in Ansys Parametric Design language (APDL) and MATLAB for post-processing and computation of total energies, velocity responses and power inputs.

## 5.8 RESULTS AND DISCUSSION

Table.5.6. presents the comparison of the resonance frequencies obtained from finite element analysis and experiments for the elastic modes for a single mild steel plate. It is observed that the maximum error of the FEA obtained resonance frequencies, when compared with the experimentally obtained values is within an acceptable range of 5 %. Figure 5.17 compares a mode shape obtained from the finite element analysis and experiments. Fig.5.18 shows the sum-FRF obtained for the same case from experiments.

Table.5.7. presents the comparison of the resonance frequencies obtained from finite element analysis and experiments for the elastic modes of Case-1. Figures 5.19 and

5.20 show the mode shapes for two typical modes obtained for Case-1 from the finite element analysis and experiments. The plates have been hung by soft cords to simulate the free-free boundary conditions.

Table 5.6 Comparison of resonance frequencies for elastic modes of a single mild steel plate

Mode No.	Resonance frequencies (Hz)		% Difference
	FEA	Experimental	
1	16.13	16.82	-4.10
2	23.54	24.59	-4.26
3	29.84	29.13	2.44
4	41.91	40.93	2.39
5	74.51	71.39	4.37
6	76.83	74.61	2.97
7	83.42	80.66	3.43
8	94.12	92.83	1.39
9	127.5	125.97	1.21
10	142.42	142.73	-0.22
11	149.75	150.36	-0.40

Table 5.7 Comparison of resonance frequencies for elastic modes (Case -1)

Mode No.	Resonance frequencies (Hz)		% Difference
	FEA (Hz)	Experimental (Hz)	
1	6.11	5.98	2.17
2	8.19	8.01	2.25
3	17.40	16.8	3.57
4	18.74	18.5	1.30
5	27.47	28.9	-4.95
6	31.45	31.25	0.64
7	31.86	31.5	1.14
8	35.07	36.7	-4.44
9	44.54	45.5	-2.11
10	47.51	49.02	-3.08
11	60.62	59.5	1.88
12	62.62	62.5	0.19

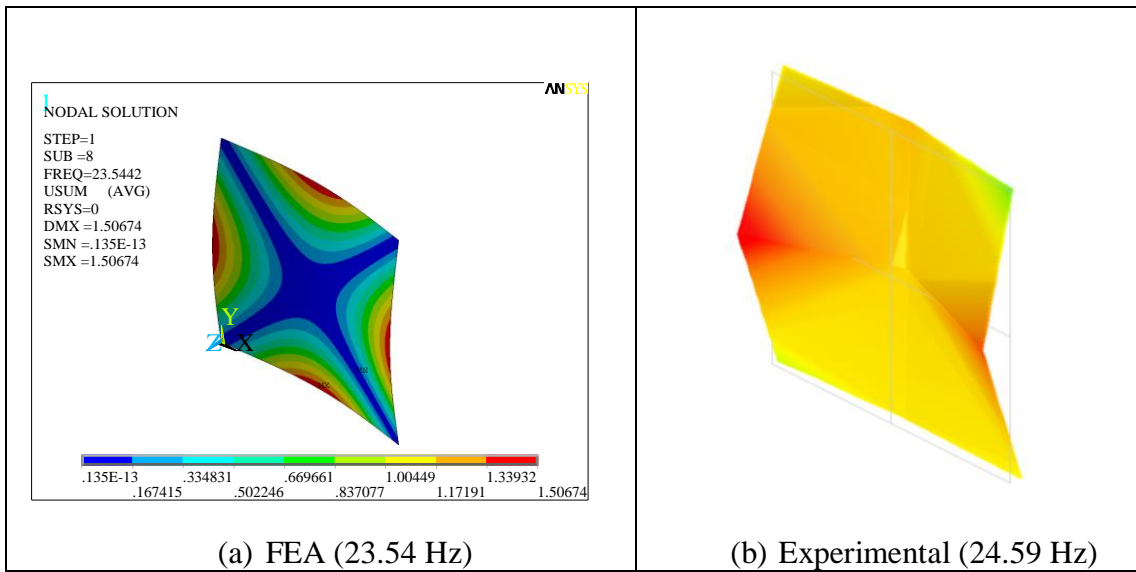


Figure 5.17 Comparison of mode shape for a single plate (Mode No-2)

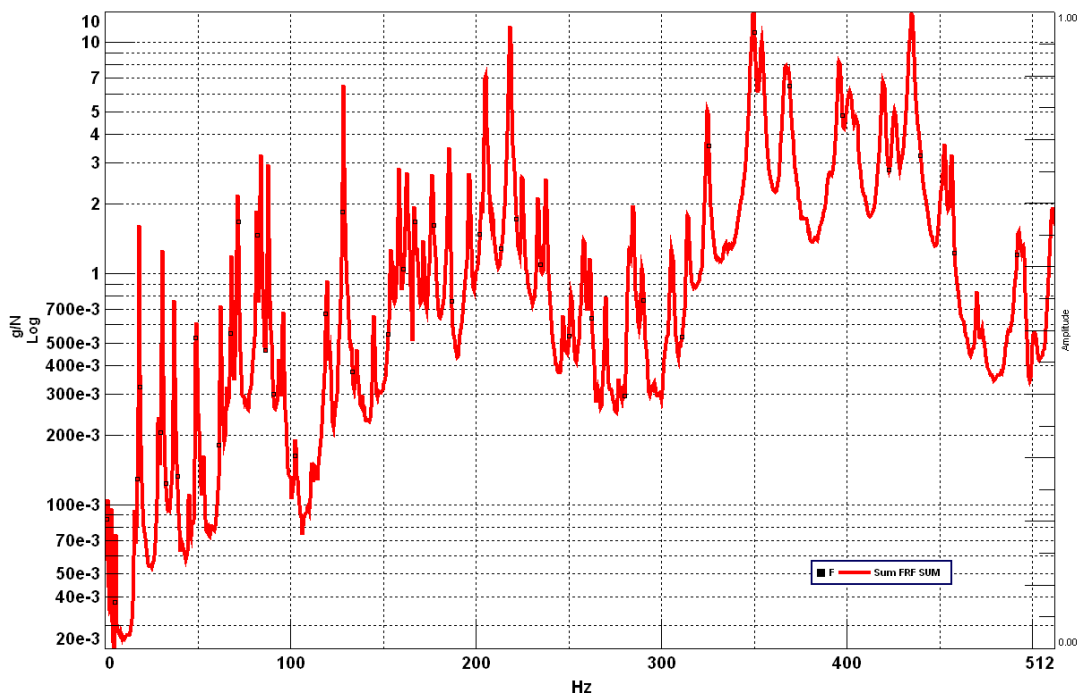


Figure 5.18 Experimental sum-FRF (Case -1)



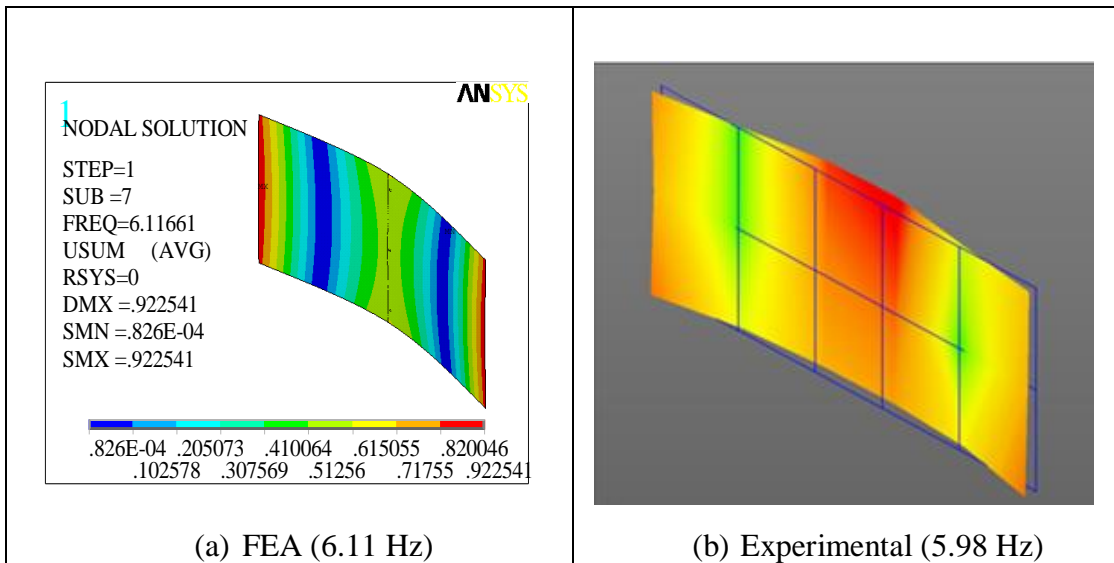


Figure 5.19 Comparison of mode shape for Case-1 (Mode No-1)

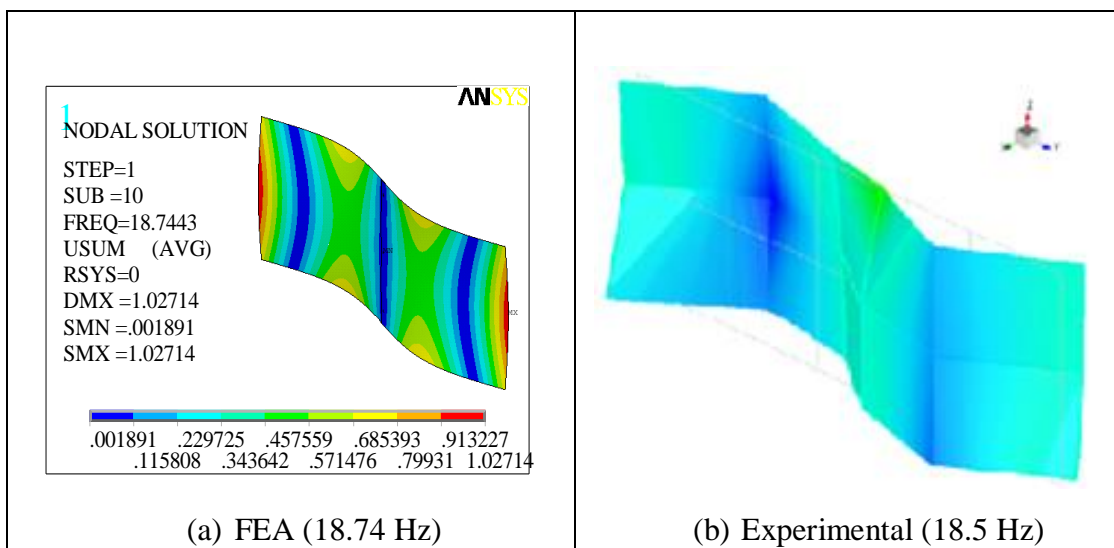


Figure 5.20 Comparison of mode shape for Case-1 (Mode No-4)

In case of the experimental harmonic response analysis, the measured acceleration and force responses are sinusoidal in nature. The maximum amplitude for the acceleration and force values are obtained. Subsequently, these accelerations for unit excitation force is obtained. This step has been carried out to compare the experimental results with the FEA results, wherein the excitation force applied is 1 N.

The acceleration responses have been obtained from the defined locations by experimentation on the plates (Table 5.8). Some sample values at nodes 1, 2 and 18 for representative times has been shown in Table 5.8. The last column of table 5.8 shows the sinusoidal force excitation at the excitation point on the plate. The responses and the excitation force being sinusoidal, the maximum value obtained are computed by post-processing the values in MATLAB software.

Table 5.8 Acceleration responses of spot-welded lap joint plate for Case-1

Time (secs)	Acceleration response (g)			Force (N)
	Node-1	Node-2	Node-18	
4.99997625	9.74	-24.1	3.28	-8.73
5.00000676	-13.1	-24.5	-10.8	-8.04
5.00003728	-31.2	-17.2	-21.1	-4.76
5.00006780	-38.9	-5.39	-23.6	0.00274
5.09998235	5.32	-24.8	0.363	-8.81
5.10001287	-17.2	-23.5	-13.4	-7.55

The maximum acceleration responses obtained at all the points on both the plates is divided by the maximum excitation force to obtain the acceleration responses for unit excitation loading of 1N. A few of the values at some nodes are shown in Table 5.9.

Table 5.9 Acceleration responses of spot-welded lap joint plate for Case-1 under unit force.

Acceleration response (g)			Force (N)
Node 1	Node 2	Node 18	Node 5
4.5011	2.8571	2.7098	1

The acceleration responses are divided by the excitation frequency to obtain the velocity responses. The total vibratory energies in the plates have been computed based on Equation (5.4). The power injected at the excitation location is obtained from the cross-spectrum of force and acceleration by Equation (5.1). Finally, the apparent coupling factors have been computed by the power balance equation for two plates as given in Equation (5.3). The apparent coupling factors ( $\eta_{12} = \eta_{21}$ ) for all the

cases of the spot-welded plates obtained from finite element analysis and experiments is listed out in Table 5.10 and Table 5.11 respectively. Similarly, the velocity responses obtained by finite element analysis and experiments for all the cases for the left-hand (LH-plate) and right-hand plate (RH-plate) under consideration have been compared in Figures 5.21 to 5.24. All the points in the plots have been joined by smooth lines. The power inputs for all the cases of the spot-welded plates obtained from finite element analysis and experiments is listed out in Table 5.12 and Table 5.13, respectively.

Table 5.10 Apparent coupling factor obtained experimentally for spot-welded plates

Case No.	Excitation Frequency (Hz)				
	1000	1500	2000	2500	3000
Case-1	0.0016	0.00146	0.00039	0.00149	0.00180
Case-2	0.00034	0.00087	0.00116	0.00146	0.00085
Case-3	0.000318	0.00086	0.00113	0.00156	0.00057
Case-4	0.00159	0.00158	0.00005	0.00027	0.0004

Table 5.11 Apparent coupling factor obtained numerically for spot-welded plates

Case No.	Excitation Frequency (Hz)				
	1000	1500	2000	2500	3000
Case-1	0.0014	0.0096	0.00046	0.0039	0.00098
Case-2	0.0002	0.0099	0.00065	0.0033	0.00051
Case-3	0.0063	0.013	0.00017	0.0098	0.00041
Case-4	-0.0188	0.0049	0.000025	0.0032	0.00010

Table 5.12 Power input (N-m/s) measured experimentally for spot-welded plates

Case No.	Excitation Frequency (Hz)				
	1000	1500	2000	2500	3000
Case-1	0.000133	0.004634	0.001205	0.00023	0.000738
Case-2	0.000197	0.001003	0.000811	0.000395	0.000785
Case-3	0.000194	0.00098	0.000801	0.000426	0.000757
Case-4	0.00004	0.000463	0.00022	0.000119	0.000116

Table 5.13 Power input (N-m/s) obtained numerically for spot-welded plates

Case No.	Excitation Frequency (Hz)				
	1000	1500	2000	2500	3000
Case-1	0.0000360	0.0020856	0.0003005	0.0001142	0.0002411
Case-2	0.0000376	0.0017287	0.0002997	0.0001331	0.0002682
Case-3	0.0000750	0.0031377	0.0002954	0.0001383	0.0002345
Case-4	0.0002811	0.0024555	0.0002916	0.0000964	0.0002089

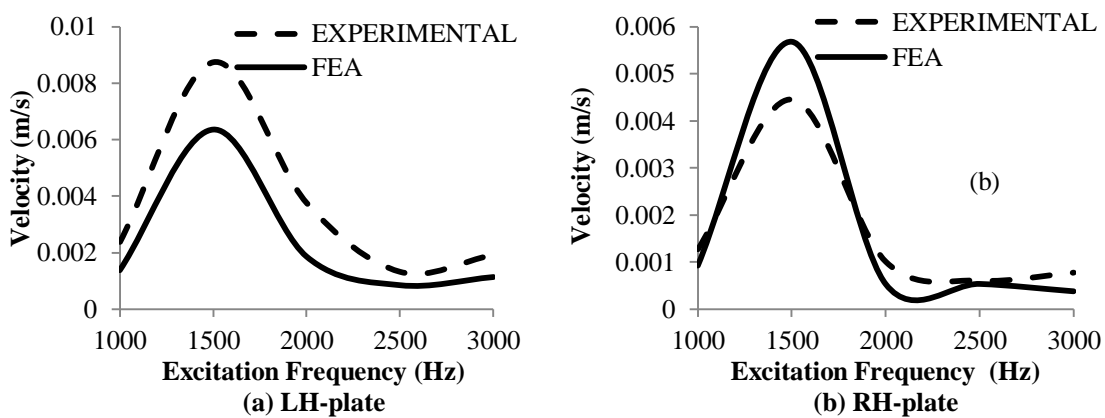


Figure 5.21 Velocity responses of Case -1 for spot-welded plates

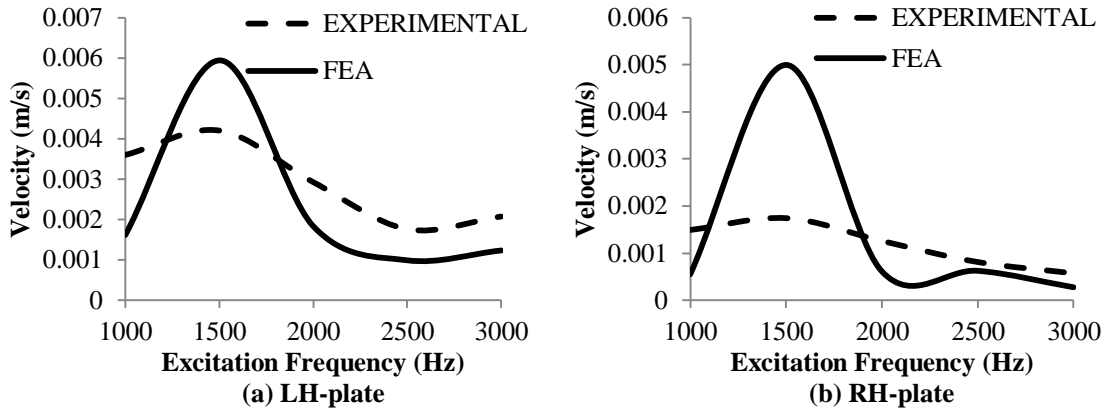


Figure 5.22 Velocity responses of Case -2 for spot-welded plates

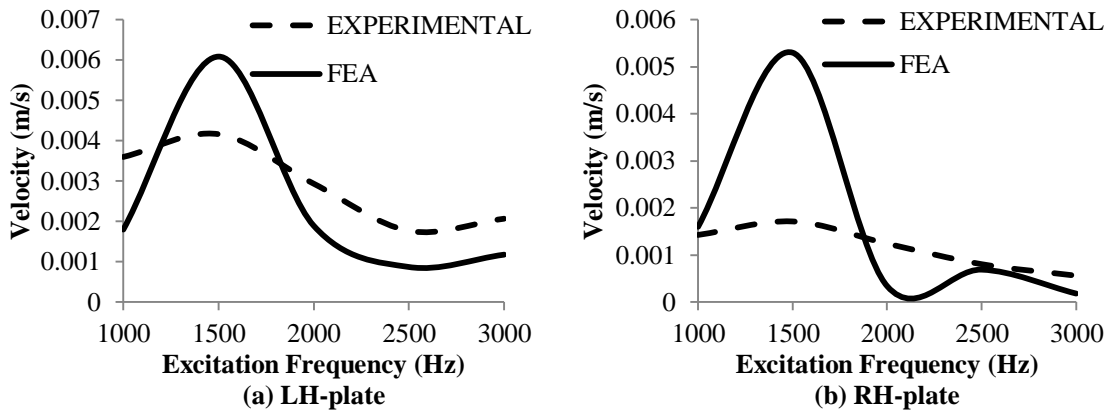


Figure 5.23 Velocity responses of Case -3 for spot-welded plates

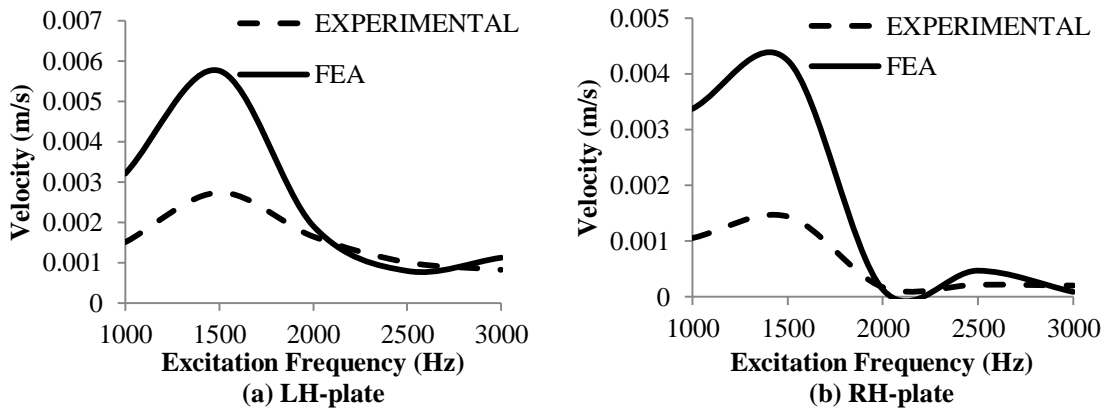


Figure 5.24 Velocity responses of Case -4 for spot-welded plates

In case of coupled plates with fewer spot-welds, noise radiation was observed in the experimental analysis at higher velocity amplitude responses i.e.: at lower excitation frequencies. While carrying out FEA any dissipation effects due to noise radiation is not assumed. Thus, there is a deviation in the FEA and experimental values especially at 2500 Hz. Such noise effects were found to be negligible in case of the acrylic and damped mild steel plates for the bolted joints experimentation, wherein the modal overlap was  $>1$  for all the excitation frequencies. Table 5.14 presents the ratio of velocities obtained in LH-plate and RH-plate at an excitation frequency of 3000 Hz for all the cases of two plates lap joined by spot-welds. It can be observed that as the number of spot welds decreases the total energies and consequently the velocities in the second plate is reduced considerably and therefore the ratio of velocity responses of LH-plate to RH-plate increases. An average percentage difference of 18% has been observed experimentally, for the ratio of velocity responses of LH-plate to RH-plate in comparison to FEA except for case-4 (Table 5.14)

Table 5.14 Ratio of velocity responses obtained for spot welded joints of LH-plate and RH-plate for excitation frequency, 3000 Hz

Case No.	Experimental			FEA		
	LH-plate (m/s)	RH-plate (m/s)	Ratio	LH-plate (m/s)	RH-plate (m/s)	Ratio
Case-1	0.00192	0.000875	2.19	0.001139	0.00041	2.77
Case-2	0.001905	0.000622	3.06	0.001233	0.000320	3.85
Case-3	0.002061	0.000562	3.66	0.001175	0.00028	4.19
Case-4	0.000816	0.000198	4.12	0.001123	0.00014	8.02

It is to be noted that the case of spot weld  $S_1$  being damaged is symmetrical to Case-3. This case of spot weld  $S_1$  being damaged can be detected, as the acceleration values measured by the top row of accelerometers in a case where only the spot weld  $S_1$  is damaged, would be equal to the acceleration values measured in the bottom row of accelerometers for case 3. Similarly, the acceleration values measured by the top row of accelerometers for case 3 would be equal to the acceleration values measured in the bottom row of accelerometers for a case, wherein only spot weld  $S_1$  is damaged. The accelerations measured in the middle row remains unchanged.

### 5.8.1 Joint damage detection

The studies for damage detection consists of three identical plates (namely LH-plate, Middle-plate and RH-plate) coupled in sequence by spot-welded lap joints (Figure 5.27) for all the possible combinations of the cases, discussed in Section 5.2. Table 5.15 presents all possible combinations of three plates with lap joints.

Table 5.15 List of possible combinations for three plates with spot-welded lap joints

<b>Combination</b>	<b>Number of Spot Welds Between LH-plate and Middle-plate</b>	<b>Number of Spot Welds Between Middle-plate and RH-plate</b>
1	Case-1	Case-1
2	Case-1	Case-2
3	Case-1	Case-3
4	Case-1	Case-4
5	Case-2	Case-1
6	Case-2	Case-2
7	Case-2	Case-3
8	Case-2	Case-4
9	Case-3	Case-1
10	Case-3	Case-2
11	Case-3	Case-3
12	Case-3	Case-4
13	Case-4	Case-1
14	Case-4	Case-2
15	Case-4	Case-3
16	Case-4	Case-4

To illustrate the effectiveness of the method used to predict the damage status in the three plates with lap joints, a case of three plates with spot-welded lap joint is presented here. A healthy configuration described as LH-plate, and Middle-plate are

joined using three spot-welds namely  $S_{11}$ ,  $S_{12}$  and  $S_{13}$  as shown in Figure 5.25, and Middle plate and RH-plate are joined using another three spot-welds namely  $S_{21}$ ,  $S_{22}$  and  $S_{23}$ . The damage in the Middle-plate and RH-plate with spot welded lap joints is assumed to be a failure of spot-weld. Figure 5.26 depicts the damage with the absence of spot-weld,  $S_{22}$  and remaining spot-welds are intact. The velocity responses obtained for the RH-plate experimentally, numerically and predicted using SEAL approach for the healthy and damaged configurations are shown in Figures 5.27 and Fig. 5.28. The codes required for carrying out the computations have been developed using MATLAB software.

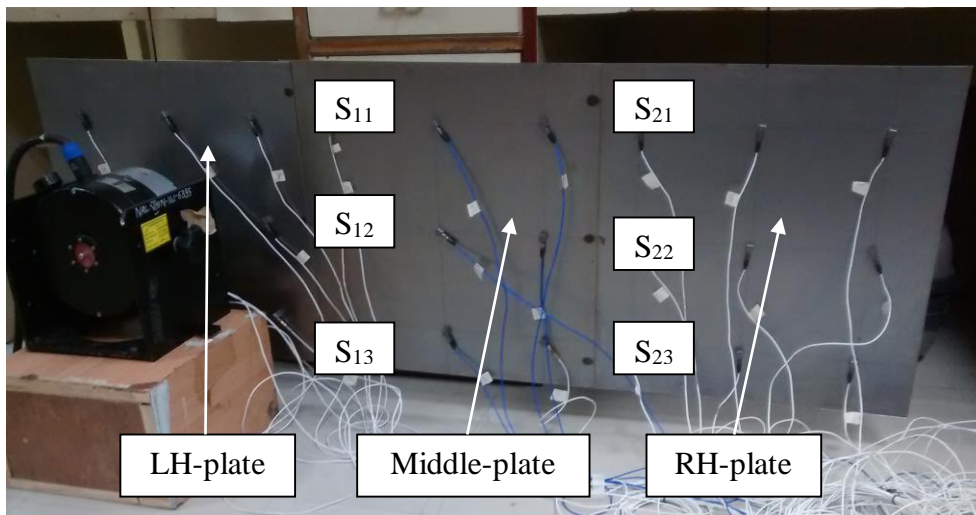


Figure 5.25 Three plates with spot-welded lap joints (healthy configuration: combination -1)

The velocity responses have been predicted by the SEAL approach for the healthy and damaged configuration using the apparent coupling factors listed out in Tables 5.10 and 5.11. These predicted velocity responses for the healthy configuration is compared with the actual experimentation, and finite element analysis obtained responses in Figures 5.27 (a) to 5.27 (c).



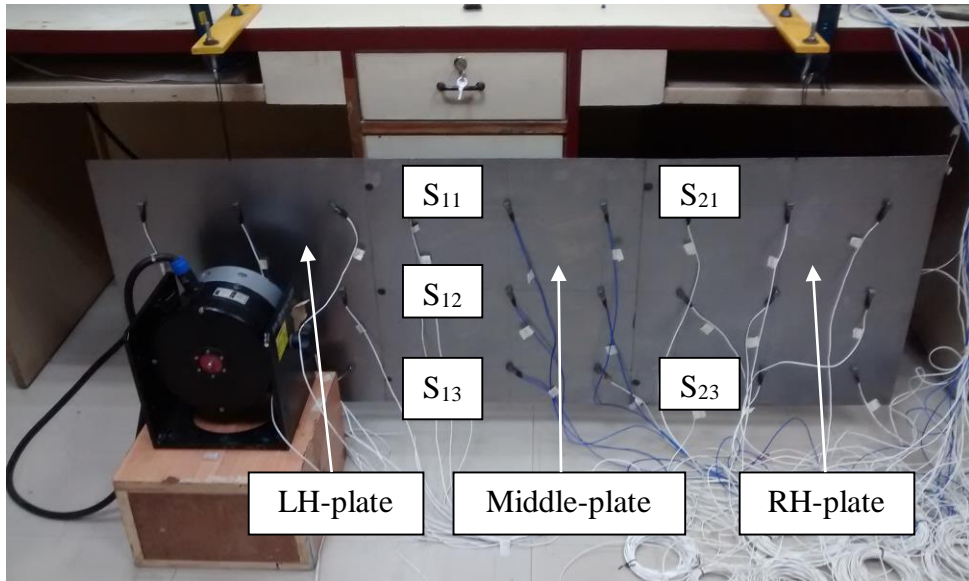


Figure 5.26 Three spot-welded plates with absence of spot-weld S<sub>22</sub> (damaged configuration: combination -2).

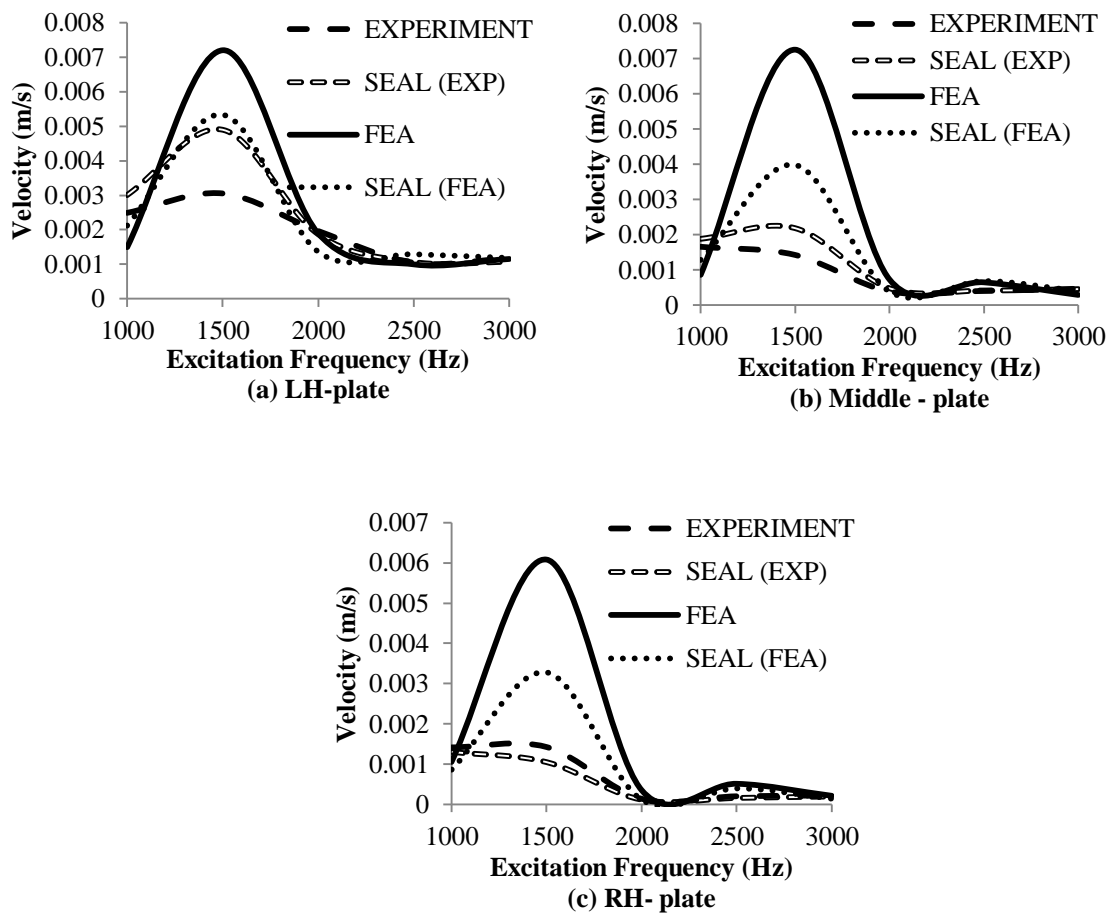


Figure 5.27 Velocity responses for spot-welded lap joints of healthy configuration

The predicted velocity responses for the damaged configuration is compared with the experimentation, and finite element analysis obtained responses in Figures 5.28 (a) to 5.28 (c).

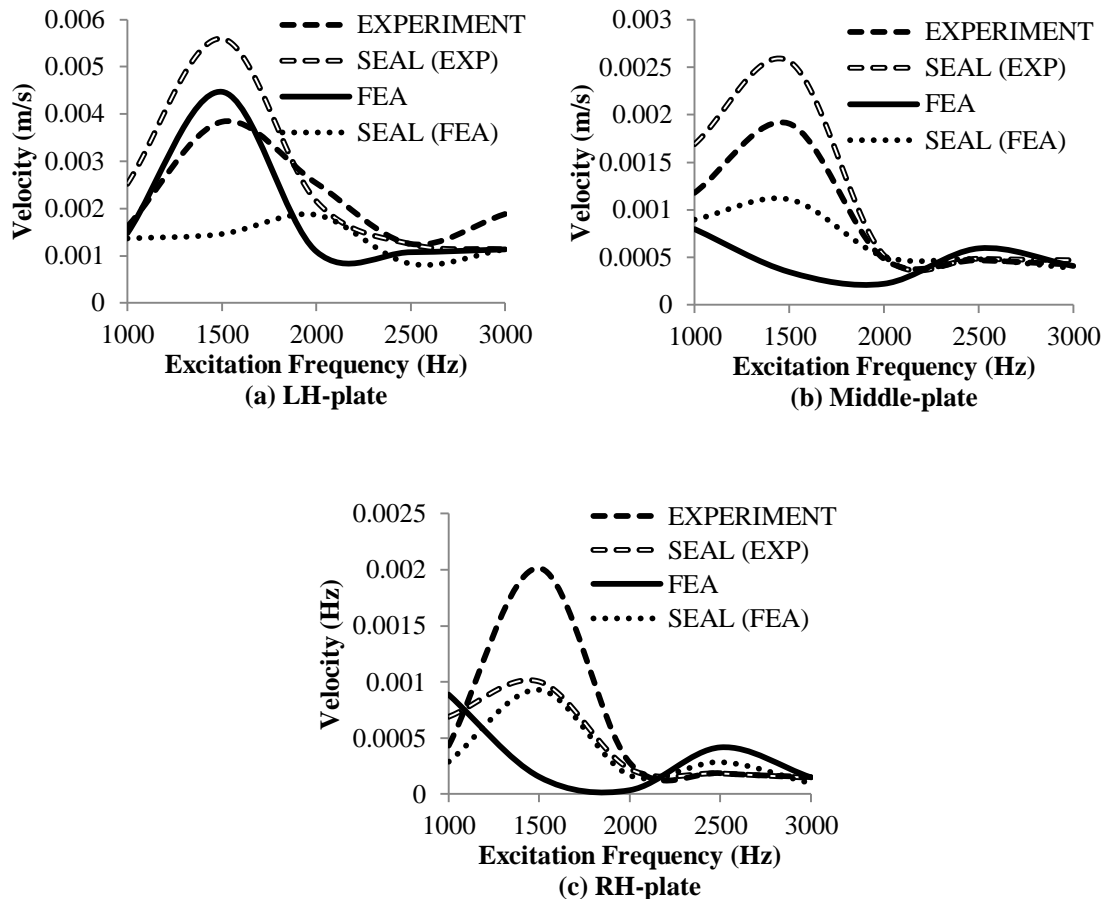


Figure 5.28 Velocity responses for spot-welded lap joints of damaged configuration

The modal density ( $n$ ) per Hz of each plate is 0.0658. The modal overlap factor ( $M=f\eta n$ ) preferred for application of statistical energy analysis principle is greater than one. At 2500 Hz, the modal overlap is 0.97, and at 3000 Hz the modal overlap is 1.42. The effective CLF of two coupled plates with low modal density and low modal overlap fluctuates significantly compared with the ensemble average CLF (Park et.al. 2004). It has been observed in the present case of plates with low material damping, at lower excitation frequencies, the adjoining areas in absence of the spot weld have large amplitudes of vibration in the practical conditions during the experimental test as compared to the FEA simulations.

Variation in the derived coupling factors due to the variation in the excitation force location on the excited plate also reduces with the increase in excitation frequencies. Accordingly, the excitation frequency of 3000 Hz is selected as the deterministic frequency for detection of damage for the combinations listed out in Table.5.15. In practice acceleration responses would be measured. Acceleration response for each plate is computed by multiplying the plate velocity with the frequency of excitation.

Table 5.16 presents the acceleration responses obtained for the plates of healthy (combination-1) and damaged (combination-2) joint at an excitation frequency of 3000 Hz.

Table 5.16 Comparison of acceleration responses for spot-welded joints, excitation frequency of 3000 Hz

PLATE	Name of Methods	Acceleration (m/s <sup>2</sup> )		Percentage Difference
		Healthy	Damaged	
LH-plate	Experimental	22.09	24.12	9.21
	SEAL (Exp)	20.34	21.41	5.25
	FEA	21.73	21.41	-1.47
	SEAL (FEA)	22.44	21.39	-4.70
Middle-plate	Experimental	8.80	8.01	-8.97
	SEAL (Exp)	8.54	8.85	3.58
	FEA	5.54	5.99	8.12
	SEAL (FEA)	7.55	7.37	-2.49
RH-plate	Experimental	4.17	2.83	-32.11
	SEAL (Exp)	3.86	2.74	-29.04
	FEA	4.07	2.80	-31.02
	SEAL (FEA)	2.67	1.90	-28.87

It is observed from Table 5.16 that in case of the damaged joint, the acceleration response in RH-plate is reduced in comparison to the healthy configuration. The percentage reduction in the acceleration response in the RH-plate due to the damaged joint ( $S_{22}$ ) is in the order of 30% in comparison to the healthy plate. The velocity responses predicted using SEAL approach is in close agreement with the actual

experimentation and finite element analysis. A database bank of the expected responses using SEAL approach for the other possible combinations is listed out in Table 5.17. It has been observed in case of plates joined by a single weld (Case-4), the ends of the plates away from the spot weld have large amplitudes of vibration that are limited in the practical conditions during the experimental test as compared to the FEA simulations. Table 5.17 presents the percentage deviation in the acceleration responses on each plate of the remaining combinations in comparison to the healthy configuration (combination 1).

Table 5.17 Percentage deviation of acceleration responses of the other possible combinations in comparison to the healthy configuration (Combination 1), excitation frequency of 3000 Hz

Combination	SEAL – Predicted (Exp) in %			SEAL – Predicted (FEA) in %			FEA in %		
	LH-plate	Middle-plate	RH-plate	LH-plate	Middle-plate	RH-plate	LH-plate	Middle-plate	RH-plate
3	1.1	5.3	-35.1	1.0	3.1	-32.0	1.0	-2.0	-18.7
4	1.1	5.3	-45.7	1.0	5.3	-64.8	1.0	8.7	-51.9
5	4.3	-24.8	-24.8	3.1	-25.4	-25.4	7.5	-17.4	-17.4
6	4.3	-21.9	-43.2	3.1	-23.1	-43.8	5.3	-25.9	-45.7
7	4.3	-20.6	-50.7	3.1	-22.5	-49.2	11.1	-20.6	-62.5
8	4.3	-20.0	-58.8	3.1	-21.3	-73.6	13.6	20.5	-52.2
9	6.5	-35.1	-35.1	4.2	-32.0	-32.0	1.0	-32.0	-39.4
10	6.5	-32.4	-50.7	4.2	-30.1	-49.2	0.0	-22.5	-59.7
11	6.5	-31.5	-57.4	4.2	-30.1	-53.9	1.0	-35.1	-69.2
12	6.5	-30.6	-64.4	4.2	-28.6	-76.1	1.0	-54.5	-84.7
13	7.7	-45.7	-45.7	6.4	-64.8	-64.8	-2.9	-87.7	-82.7
14	7.7	-43.5	-58.8	6.4	-63.9	-73.6	-2.9	-88.2	-81.6
15	7.7	-42.9	-64.4	6.4	-63.6	-76.1	-2.9	-81.4	-84.7
16	7.7	-42.2	-70.2	6.4	-63.0	-87.6	-2.9	-82.7	-93.2

The damage detection approach is based on the extraction of the acceleration response as one of the features that present a unique pattern for each specific damage case. A joint damage-pattern database was developed through simulation of SEAL based joint damage scenarios (Table 5.16 and 5.17). Damaged joint location can be identified simultaneously by best matching the unknown damage feature of acceleration response as an index to that of known ones in the database. A flow chart of the same is shown in figure 29. To find the correct index to the database, advanced pattern classification techniques in combination with other features including noise etc. can be used to locate the damaged joint. This has been included as a part of the future scope of work and has not been dealt in the present studies.

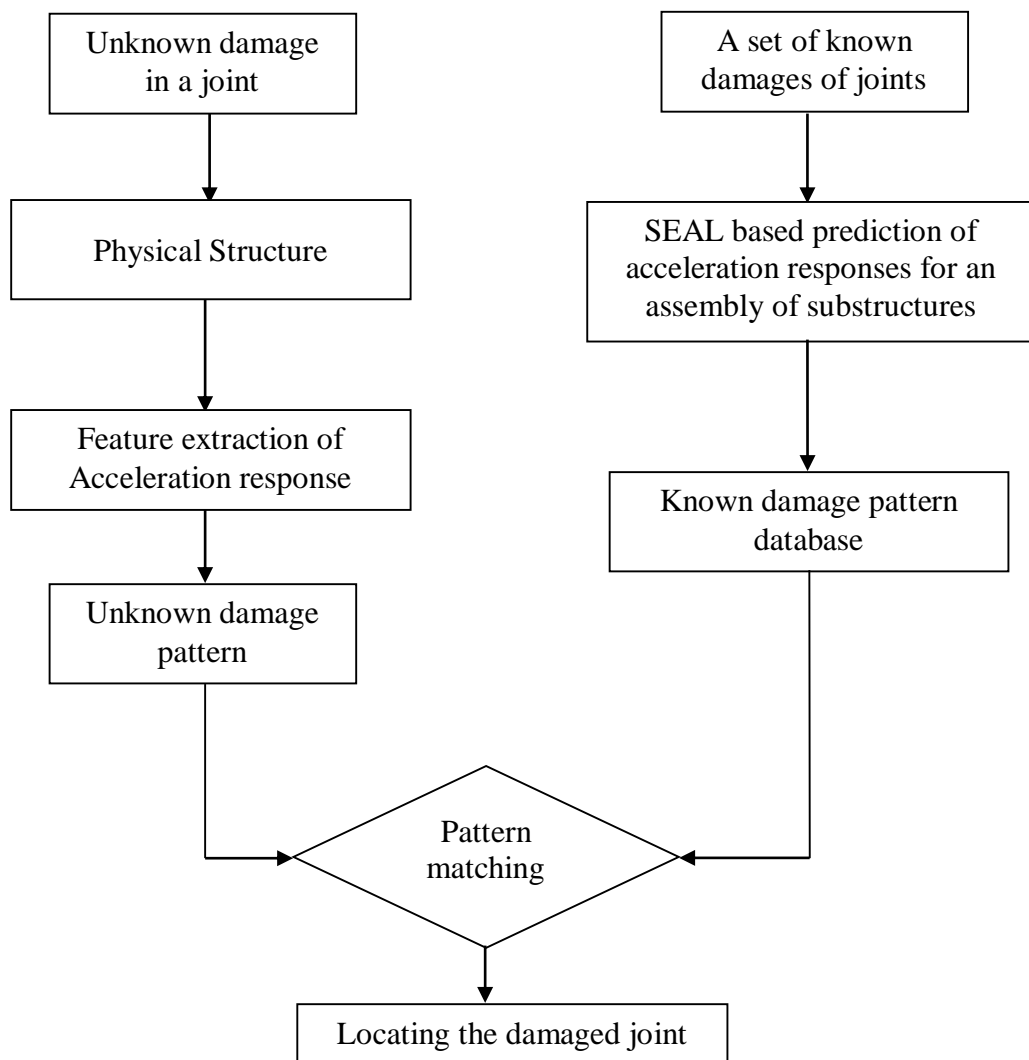


Figure 5.29 Flow chart for possible damage detection in joints

## 5.9 SUMMARY

The finite element model of spot welds is created using the area contact model (ACM2). The response of the sub-structures predicted using apparent coupling factors at low frequencies is not accurate due to the reduction in modal density, modal overlap, and violation of assumptions of uniform energy density in SEA like approach. Excitation frequencies with modal overlap lesser than one are to be avoided as they may generate sudden peak responses (e.g.: at 1500 Hz, Figures 5.21 to 5.24), higher than the average responses in a particular band-width of excitation frequencies.

Coupling strength is reduced due to the failure in any spot-welded joint for a sequentially coupled plate causing the reduction in the acceleration responses of the subsequent plate following the damaged joint (Table 5.14). The maximum percentage reduction of acceleration response in the RH plate, for three spot welded lap joined plates in comparison with the healthy configuration is observed for combination 16, (Table 5.17). The plates are lap joined by a single spot-weld with the least coupling effect and energy transfer from the excited plate in this configuration.

## **CHAPTER 6**

### **DAMAGE DETECTION OF BOLTED PLATES USING STATISTICAL ENERGY ANALYSIS LIKE APPROACH**

#### **6.1 INTRODUCTION**

This chapter discusses the damage studies, extended to bolted joints, wherein, apparent coupling factors have been derived for four cases of bolted mild steel plates and used further to predict the velocity and acceleration responses using SEAL approach for an assembly of three plates lap joined by bolt-assembly. The results obtained have been analyzed and compared by experiments and finite element simulation for healthy and damaged configurations.

#### **6.2 TEST SPECIMENS**

The dimensions of each mild steel plate considered in the studies are length, 500 mm, width, 500 mm and thickness of 1.12 mm. As the mild steel plates have low values of material damping, as observed in the studies for spot-welded plates, the plates were lightly damped by the addition of bitumen based damping sheet to one side of the plate having a full self-adhesive backing as shown in Figure 6.1. The total thickness of the plate along with the backing sheet is 1.21 mm. This gives internal loss factors significantly higher than those of the un-damped plate and a higher modal overlap satisfying SEA assumptions at the excitation frequencies of interest. The internal loss factor dominates all other losses and reduces the reactive component of power flow, and the measurement accuracy of the power is also improved.

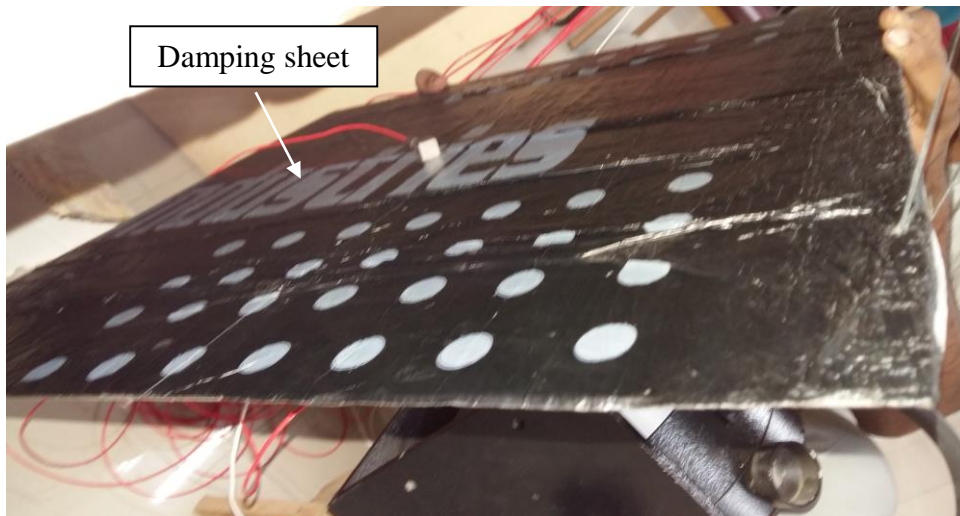


Figure 6.1 Bitumen based damping sheet glued on one side of the mild steel plate

The plates are joined by bolted joints as shown in Figure 6.2 with an overlap length between two sheets of 50 mm. The bolted joints are lined up on the center of the overlap. The diameters of the holes for the bolts of size M8 and 16 mm length is 9 mm. The following cases of two plates joined by bolts have been considered to investigate the apparent coupling factors using the SEAL approach.

**Case-1:** Two plates with lap joint having three bolted joints, B<sub>1</sub>, B<sub>2</sub> and B<sub>3</sub> (Healthy Configuration; Figure 6.2)

**Case-2:** Two plates with lap joint having two bolted joints, B<sub>1</sub> and B<sub>3</sub> (Centre bolt, B<sub>2</sub> assumed to be damaged; Figure 6.3)

**Case-3:** Two plates with lap joint having two bolted joints, B<sub>1</sub> and B<sub>2</sub> (Bottom most bolted joint, B<sub>3</sub> assumed to be damaged; Figure 6.4),

**Case-4:** Two plates with lap joint having one bolted joint, B<sub>2</sub> at the Centre (Two extreme bolted joints, B<sub>1</sub> and B<sub>3</sub> assumed to be damaged; Figure 6.5)



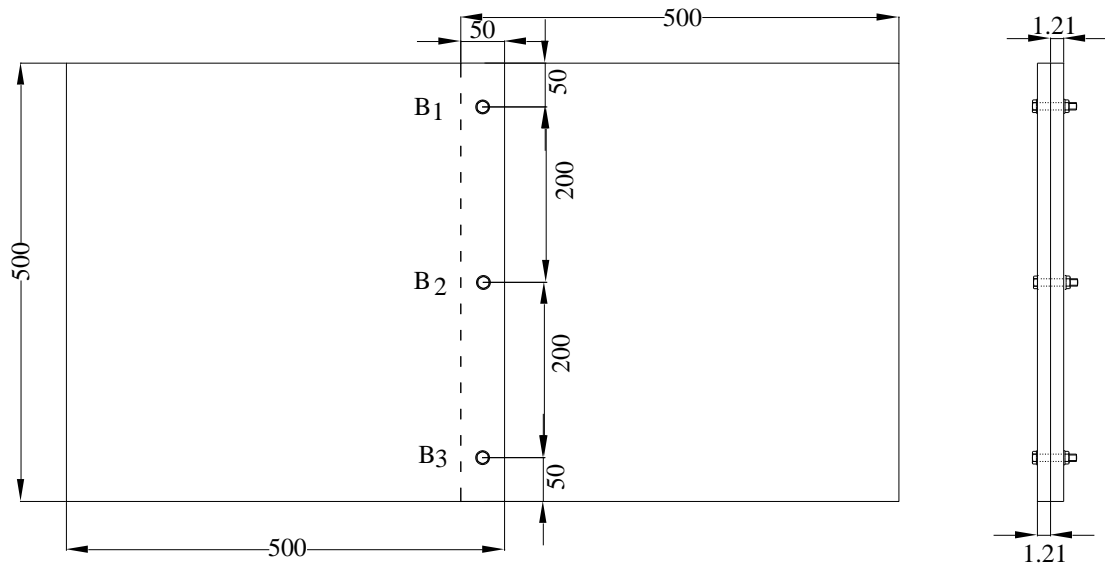


Figure 6.2 Geometric dimensions of plates with bolted lap joint (Case-1)

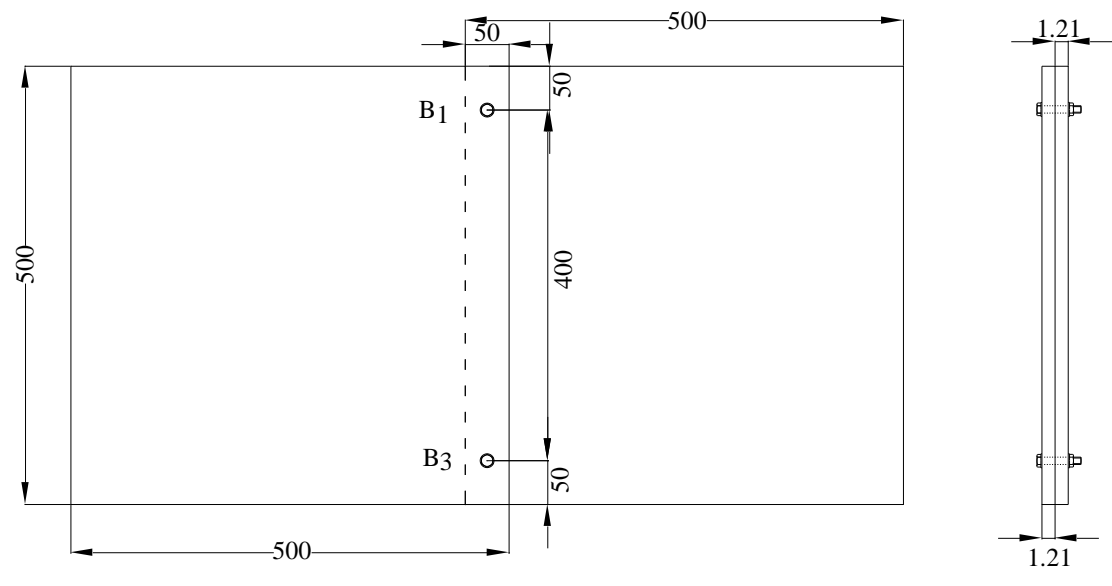


Figure 6.3 Geometric dimensions of plates with bolted lap joint (Case-2)

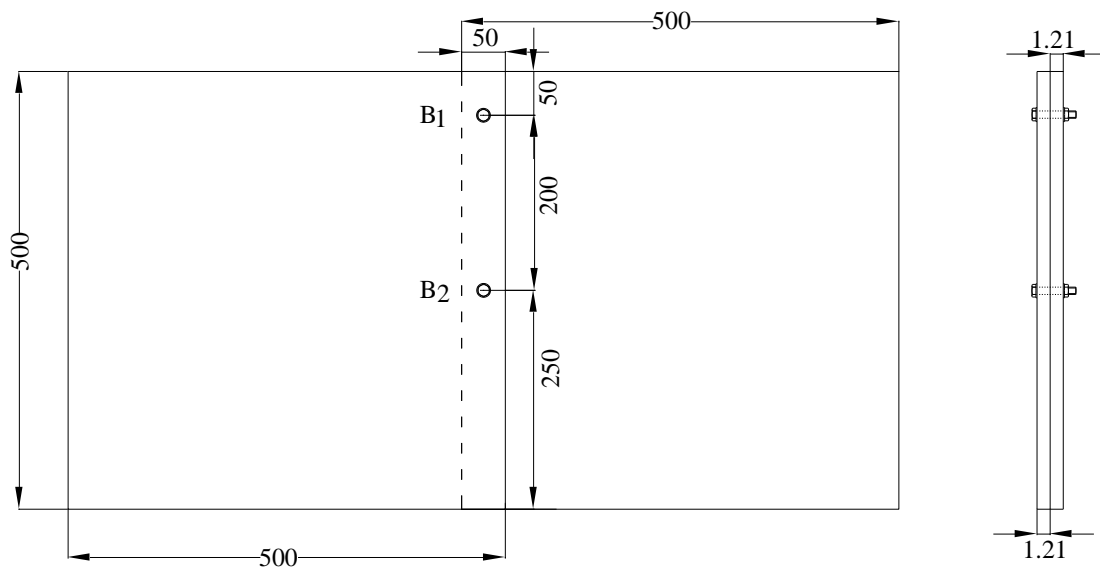


Figure 6.4 Geometric dimensions of plates with bolted lap joint (Case-3)

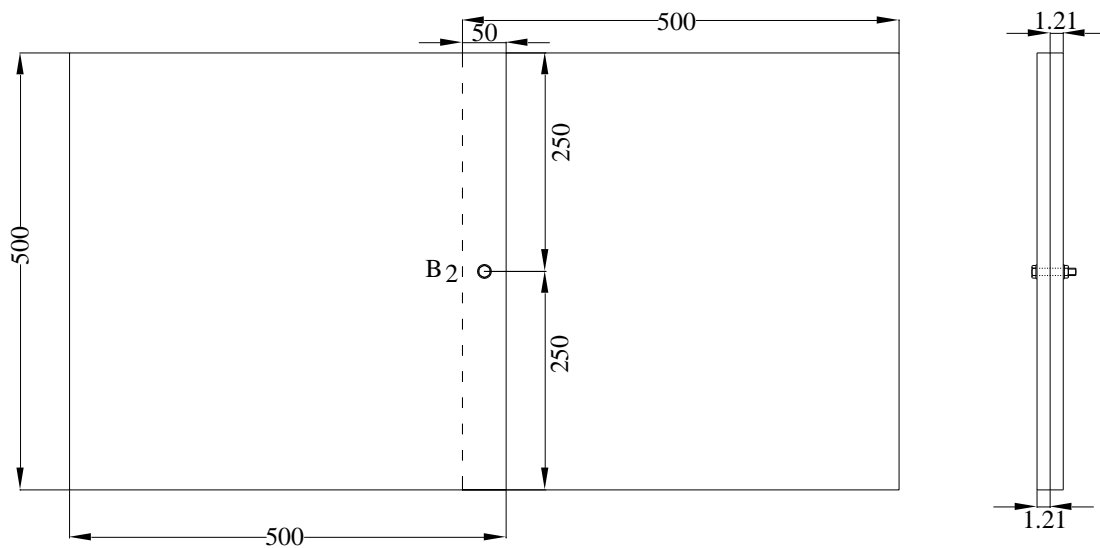


Figure 6.5 Geometric dimensions of plates with bolted lap joint (Case-4)

The damping sheets used are manufactured from bitumen with added mineral fillers and synthetic rubber to form a highly viscoelastic material, designed to minimize acoustic and vibration radiation of sheet metal and is used extensively to reduce vibration in flat, resonant surfaces such as vehicle panels, machine guards, domestic and industrial stainless steel sinks and preparation tables. The substrate is cleaned and dried with an appropriate cleaner like methylated spirit to free it from oil, grease, rust, dust or other particles. The sheet is applied in the horizontal or vertical plane to the underside of a substrate, by turning upside down the substrate with a constant forward

and downward pressure with a hard timber or steel roller on to the surface of the damping sheet to ensure it is securely fixed onto the substrate. For ease of application, bitumen based damping sheets should be applied when the ambient temperature is between 18°C and 25°C. The material becomes brittle and breaks when cold, and should not be handled when the temperature is below 5°C.

### 6.3 EXPERIMENTAL SET - UP

The experimental setup is as shown in Figure 6.6 similar to the earlier case and consists of the bolted plates to be tested, data acquisition hardware, sensors, shakers and computer with modal analysis software.

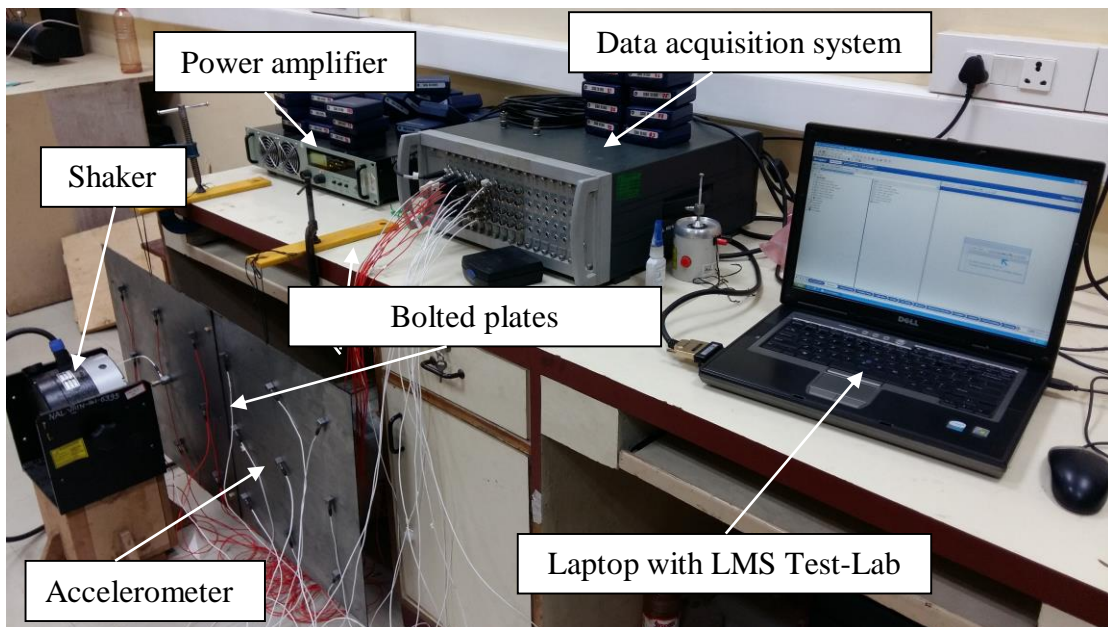


Figure 6.6 Experimental set-up

The bolted plates have been hung by soft strings to simulate a free-free boundary condition. Figure 6.7 shows the accelerometer used for the bolted joint studies and the specifications of the accelerometer is as shown in Table 6.1.



Figure 6.7. Accelerometer for measuring the vibration

Table 6.1 Specification of the accelerometer

Make (PCB piezotronics)	Integrated circuit piezoelectric
Model	356A16
Sensitivity	100 mV/g
Frequency range ( $\pm 5\%$ )	0.5 to 5000 Hz
Resonant frequency	>25 kHz
Measuring range	$\pm 50$ g
Weight	7.5 gms
Temperature range	-54 to 80 <sup>0</sup> C
Size	14 mm x 20.3 mm x 14 mm

The geometry as per the test points, chosen for measurements is created using LMS test lab. Each plate is divided equally into nine regions, and the responses were obtained using nine accelerometers placed centrally for each of the regions. The nodes, i.e., the accelerometer positions and wire frame geometry created for two bolted plates is as shown in the Figure 6.8. The experimental set up for one case (Case-3) for two spot welded plates is shown in Figure 6.9.

To measure the natural frequencies, scope settings with maximum frequency is set to 512 Hz and spectral lines of 2622 Hz, which give a frequency resolution of 0.19 Hz. Uniform windows are chosen for both excitation and response signals. 50% burst

random signal is used for exciting the plate. Same scope settings are imported to test setup and required functions such as time domain data, cross power spectrums, peak spectra, FRF, and auto power spectra, etc. are selected to store into the computer database.

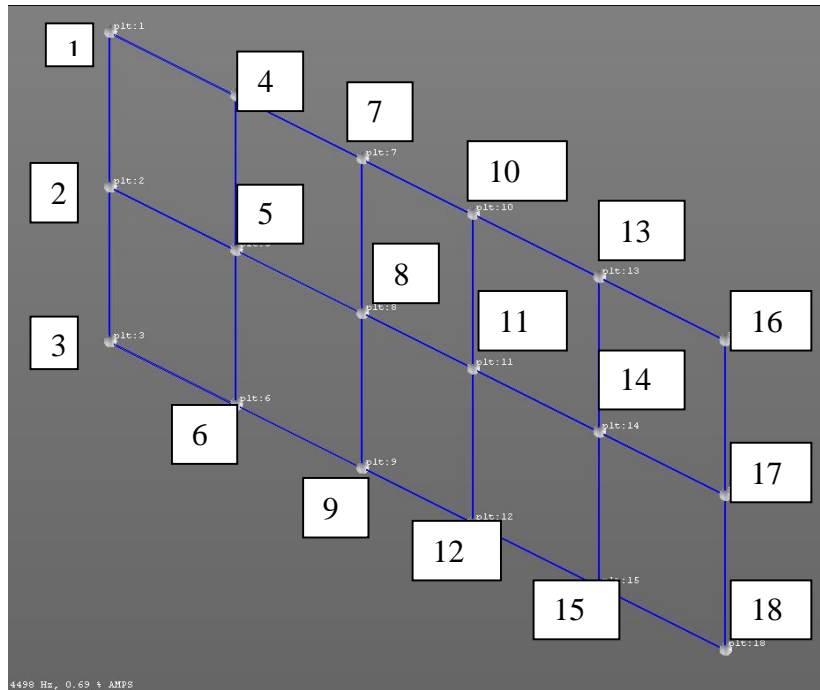


Figure 6.8 Geometry created in Test Lab

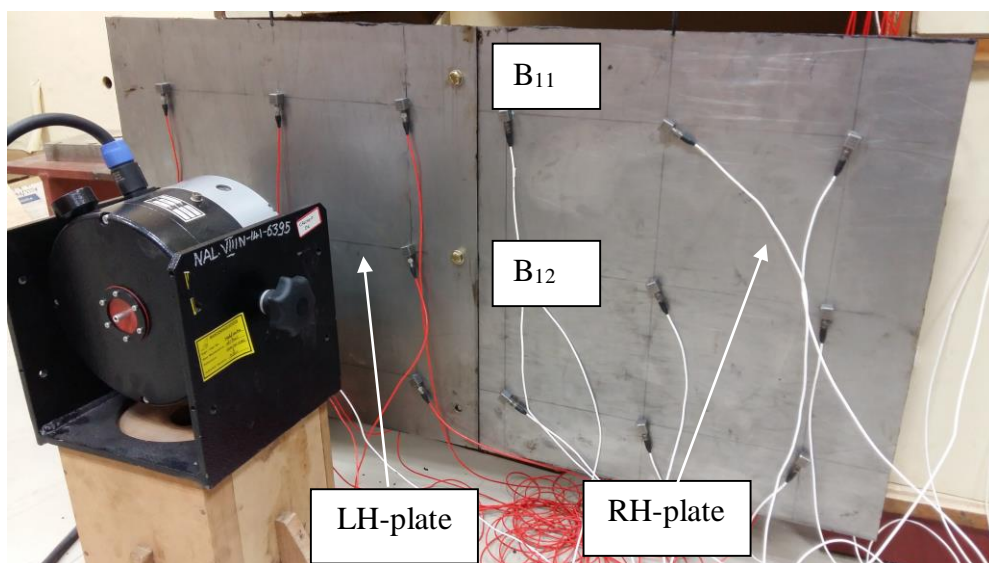


Figure 6.9 Experimental setup for two bolted plates of Case-3

In case of harmonic sinusoidal excitation and acceleration response measurement, 32768 Hz sampling frequency and a maximum bandwidth of 10000 Hz is set. The time-averaged power input into the structural substructure is given by (De Langhe, 1996)

$$P = \frac{1}{\omega} \text{Im} (S_{af}(\omega)) \quad (6.1)$$

In the present case excitation is carried out at discrete frequencies of 500 to 3500 Hz in steps of 500 Hz. The input excitation force is applied to the center (0.25 m, 0.25 m) of one plate (Pt-5, Figure 6.8). The plate is excited for flexural vibratory modes.

In the present case of bolted joints, due to the presence of damping at the joint, non-conservative coupling could be present that may increase the internal losses of the structure (Figure 6.10). To account for these effects, the energy balance equation between two substructures can be expressed as (Sheng. et al. 2004):

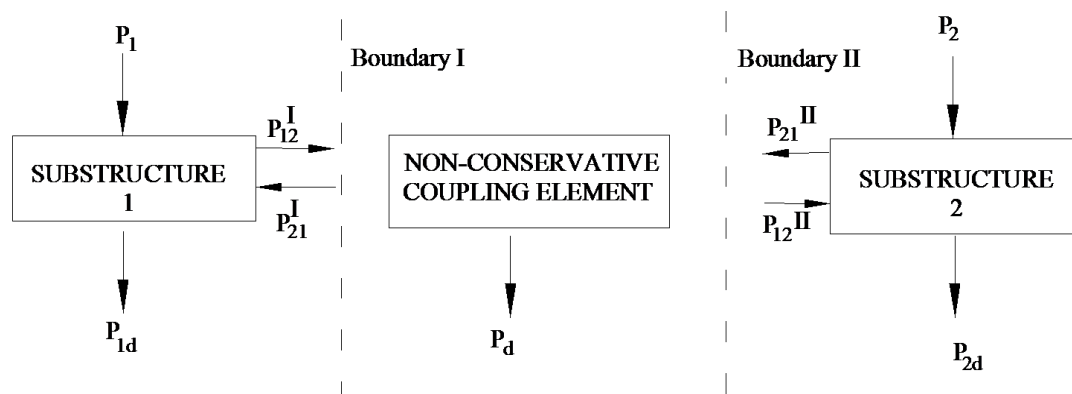


Figure 6.10. Two substructures with a non-conservative coupling joint

$$P_1 = \omega_1(\eta_1 + \eta_{12}^I)E_1 - \omega_2\eta_{21}^I E_2 \quad (6.2)$$

$$P_2 = \omega_2(\eta_2 + \eta_{21}^{II})E_2 - \omega_1\eta_{12}^{II} E_1 \quad (6.3)$$

The coupling loss between substructure  $i$  to  $j$  at boundary I is given by  $\eta_{ij}^I$  and similarly for boundary II. The effective SEA model equations are as follows:

$$P_1 = \omega_1(\eta'_1 + \eta'_{12})E_1 - \omega_2\eta'_{21}E_2 \quad (6.4)$$

$$P_2 = \omega_2(\eta'_2 + \eta'_{21})E_2 - \omega_1\eta'_{12}E_1 \quad (6.5)$$

wherein, the non-conservative coupling and the equivalent internal loss factor for the substructures are given by:

$$\eta'_{12} = \eta_{12}^{\text{II}}, \quad \eta'_1 = \eta_1 + (\eta_{12}^{\text{I}} - \eta_{12}^{\text{II}}) \quad (6.6)$$

$$\eta'_{21} = \eta_{21}^{\text{I}}, \quad \eta'_2 = \eta_2 + (\eta_{21}^{\text{II}} - \eta_{21}^{\text{I}}) \quad (6.7)$$

Assuming that only structure I is excited, the total loss factor  $\eta_{1s}$  of sub-structure I can be expressed as:

$$\eta_{1s} = \eta'_1 + \eta'_{12} - \eta'_{21}E_{21}^{(1)} \quad (6.8)$$

$$0 = \eta'_2 + \eta'_{21} - \eta'_{12}/E_{21}^{(1)}, \quad (6.9)$$

Similar equations can be obtained, if only structure II is excited. Combining these equations the equivalent internal ( $\eta'_1, \eta'_2$ ) and coupling loss factor ( $\eta'_{12}, \eta'_{21}$ ) can be obtained as:

$$\eta'_1 = \frac{\eta_{1s} + \eta_{2s}E_{21}^{(1)}}{1 - E_{21}^{(1)}E_{12}^{(2)}}, \quad \eta'_2 = \frac{\eta_{2s} + \eta_{1s}E_{12}^{(2)}}{1 - E_{21}^{(1)}E_{12}^{(2)}} \quad (6.10)$$

$$\eta'_{12} = \frac{E_{21}^{(1)}}{1 - E_{21}^{(1)}E_{12}^{(2)}}\eta_{2s}, \quad \eta'_{21} = \frac{E_{12}^{(2)}}{1 - E_{21}^{(1)}E_{12}^{(2)}}\eta_{1s}. \quad (6.11)$$

wherein,  $E_{ij}^{(j)}$  represents the energy ratio  $E_i$  to  $E_j$  when the sub-structure  $j$  is excited and  $\eta_{is} = P_i/\omega E_i$ .

## 6.4 FINITE ELEMENT ANALYSIS

An FE model of the structure shown in Figure.6.11 is created using ANSYS V13 software. The plates are modeled using SHELL63 elements with 4.16 mm element size. The minimum finite element size in the relation of a number of elements per wavelength of six is maintained. Shell 63 has both bending and membrane capabilities. Both in-plane and normal loads are permitted. The element has six

degrees of freedom at each node with three translations and three rotations about the nodal  $x$ ,  $y$ , and  $z$ -axes. The FE model for three plates is shown on Figure 6.12.

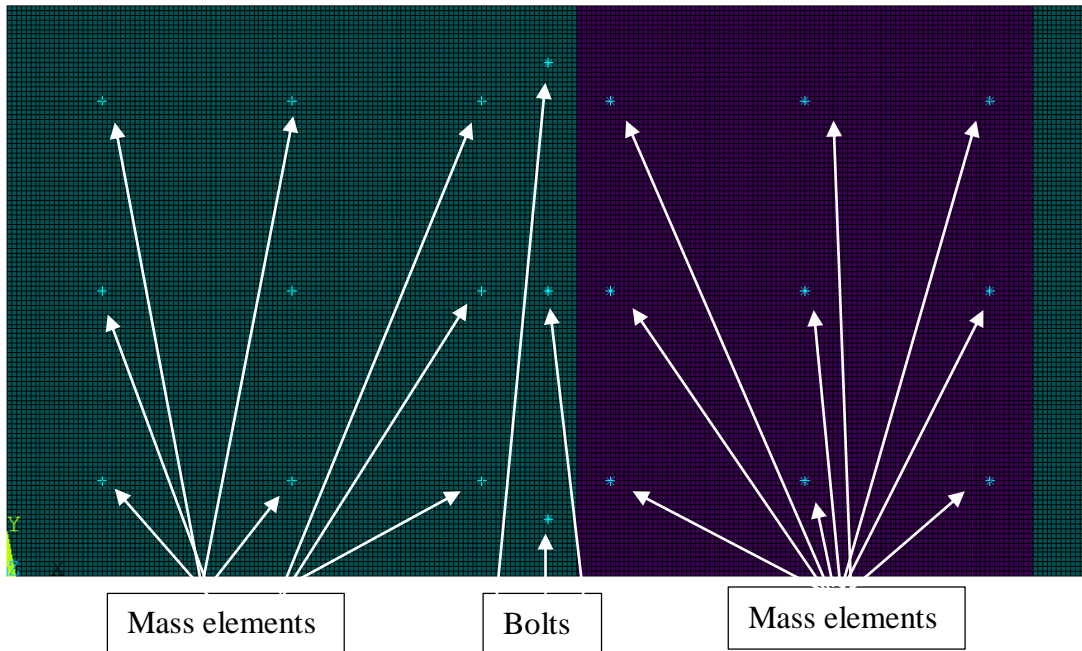


Figure 6.11. Finite element model of two plates

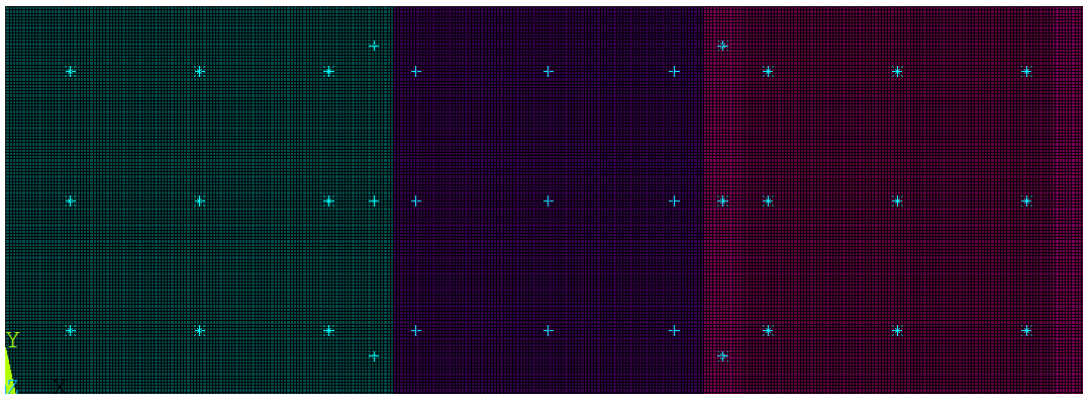


Figure 6.12. Finite element model of three plates

Bolted lap joints have a significant influence on the dynamical behavior of the assembled structures due to creation of strong local flexibility and damping. In modeling the dynamical behavior of assembled structures, the joint interface model must be represented accurately. Therefore, equivalent dynamic models of joints that consist of stiffness and damping elements should be developed, and the joint



parameters should be determined for an accurate vibration analysis. It is a general practice to use experimental measurements to model joints connecting substructures.

A simplistic coupled bolt model approach as shown in Figure 6.13 has been used in the present case. The bolts have been modeled using BEAM188 elements. BEAM188 is suitable for analyzing slender to moderately thick beam structures. The element is based on Timoshenko beam theory which includes shear-deformation effects. BEAM188 has six degrees of freedom at each node. These include three translations and three rotations about  $x$ -,  $y$ -, and  $z$ - directions. This element is well-suited for linear, large rotation, and large strain nonlinear applications. RBE3 element has been used as the constraint equations. It distributes the force or moment applied at the master node to a set of slave nodes, taking into account the geometry of the slave nodes as well as weighting factors.

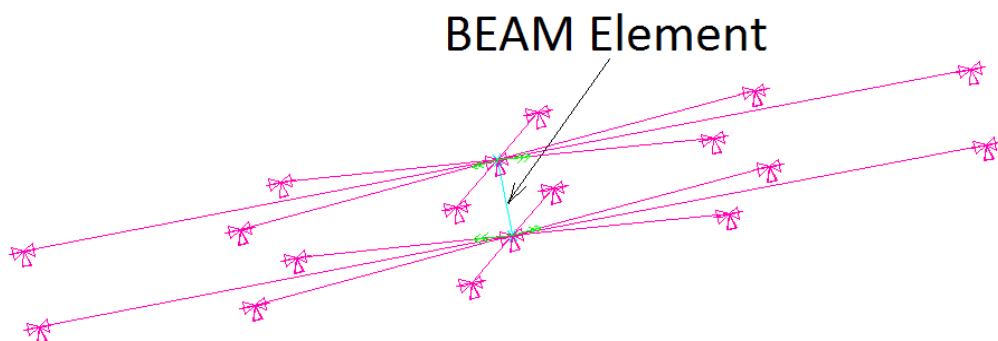


Figure 6.13 Coupled bolt finite element model

The master at which the force or moment to be distributed is applied at the ends of the beam element. This node must be associated with an element for the master node to be included in the DOF solution to the master node degrees of freedom to be used in constraint equations i.e. UX, UY, UZ, ROTX, ROTY and ROTZ. The name of an array parameter that contains a list of slave nodes are the nodes representing the boundary nodes of the hole on the plates. The weighting factor for each slave node defaults to 1.

The force is distributed to the slave nodes proportional to the weighting factors and the moment is distributed as forces to the slaves; these forces are proportional to the

distance from the center of gravity of the slave nodes times the weighting factors. Constraint equations are converted to distributed forces or moments on the slave nodes during solution. RBE3 creates constraint equations such that the motion of the master is the average of the slaves. For the rotations, a least-squares approach is used to define the average rotation at the master from the translations of the slaves.

The density of the mild steel plates is  $7850 \text{ kg/m}^3$ , modulus of elasticity, 210 GPa, with a Poisson's ratio of 0.33. The material and geometric specifications of the bolts used for the studies have been listed in Table.6.2. The bolt, washers and nut is shown in Figure 6.14.



Figure 6.14. Bolt, nut, and washers used for joining the plates

The preload torque of ( $T$ ) 9.5 N-m is achieved by a torque wrench for the M8 bolt of threaded length of 16 mm, 4.6 grade. The preload force  $F_p$  is estimated from Eq.6.12,

$$T = KF_p d \quad (6.12)$$

where  $K$  is the correction or nut factor that depends on the material size, surface friction and threading of the bolt and varies between 0.15 to 0.3. In the present case,  $K$  is assumed to be 0.22 for dry, unlubricated mid-size steel bolts conditions. The initial

strain ( $\epsilon$ ) of  $7.328 \times 10^{-4}$  due to applied preload as given by Eq.6.13 is applied to the FE beam elements representing the bolts,

$$\epsilon = \frac{F_p}{AE} \quad (6.13)$$

where  $A$  is the bolt thread root area as given by Eq.6.14.

$$A = 0.785(d - 0.9382p)^2 \quad (6.14)$$

Table 6.2 Material and Geometrical specifications of the Bolt M8 grade 4.6

<b>Parameter</b>	<b>Values</b>
Diameter ( $d$ )	8 mm
Pitch ( $p$ )	1.25 mm
Proof Stress ( $\sigma$ )	225 MPa
Width ( $w$ )	6 mm
Poisson's ratio( $\nu$ )	0.33
Young's Modulus( $E$ )	205GPa
Preload torque ( $T$ )	9.5 N-m

The natural frequencies and the mode shapes are calculated under the free-free boundary conditions. A harmonic force with unit load intensity is applied in the range of frequencies of 500-3500 Hz at steps of 500 Hz. Unit force of 1 N is applied to the first plate, and the velocity responses on both the plates have been computed. The internal loss factors estimated by the experimental power injection method on a single plate (Figure 6.15) for the excited frequencies as listed out in Table 6.3 has been used for the finite element analysis at the respective frequencies. The values obtained have been found to be consistent with the ones obtained during the experiments for the coupled bolted plates for all the cases.

Table 6.3 Internal loss factor at excited frequencies

Excitation Frequency (Hz)	500	1000	1500	2000	2500	3000	3500
Loss Factor ( $\eta$ )	0.0165	0.0158	0.015	0.0146	0.0145	0.011	0.0109

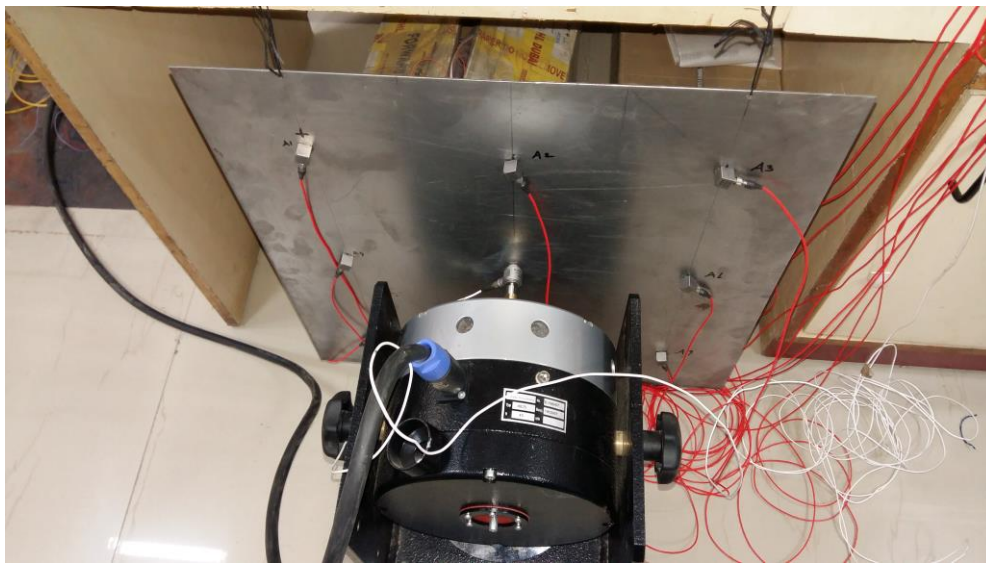


Figure 6.15 Experimental power injection method showing single-plate

The mass of the accelerometers is modeled as a concentrated mass element (mass 21) at the locations wherein the accelerometers have been placed during the experiments. The additional mass of the force transducer has also been included in the concentrated mass element (mass 21) element at the point of excitation force. The mass of the bolt, washer, and nut of 17.4 gms treated to be distributed as two concentrated mass (mass 21) elements at the location of a bolted joint. In the present studies, it has been observed that the excitation at the central location of the plate aids in generation of higher response amplitudes and uniform radial transmission of flexural wave energies across the sub-structures to a larger extent in comparison to the excitation at other locations. Thus, the locations of the excitation are selected at higher response amplitudes.

The velocity responses at the nodes of the plates, wherein responses have been obtained in the experiments, including the power input location. The procedure for computing the total vibrational energy, velocity responses, power inputs remains the same as explained in section 5.6 of chapter 5. The apparent non-conservative coupling factors are computed by Equation (6.11) after computation of power inputs and corresponding energies of each plate.

## 6.5 RESULTS AND DISCUSSION

Table.6.4 presents the comparison of the resonance frequencies obtained from finite element analysis and experiments for the elastic modes of a single plate. Figure 6.16 shows a typical mode shape obtained from the finite element analysis and experiments. It is observed that the maximum error is within an acceptable range of 5%. The resonance frequencies obtained by the inclusion of damping sheet through experiments have been shown in the same table. In case of FEA based simulations, the density of the mild steel plate is tuned to  $8600 \text{ kg/m}^3$  to account for the mass of the damping sheet and match with the experimental frequencies by the inclusion of damping sheet for carrying out further forced response analyses as mentioned in the succeeding sections.

Table 6.4 Comparison of resonance frequencies of a single plate for elastic modes

Mode No.	Without damping Sheet			With damping sheet	
	FEA	Experiment	% Difference	Experiment	% Difference
1	14.90	14.88	0.13	14.23	-4.37
2	21.74	21.77	-0.14	20.77	-4.59
3	27.56	27.39	0.62	26.33	-3.87
4	38.71	38.40	0.81	36.99	-3.67
5	68.82	69.51	-0.99	65.75	-5.31
6	70.96	68.73	3.24	67.80	-1.35
7	77.05	74.65	3.22	73.62	-1.38
8	86.93	85.37	1.83	83.06	-2.71
9	117.8	113.07	4.18	112.55	-0.46
10	131.54	128.51	2.36	125.68	-2.20
11	138.32	141.57	-2.30	132.15	-6.65

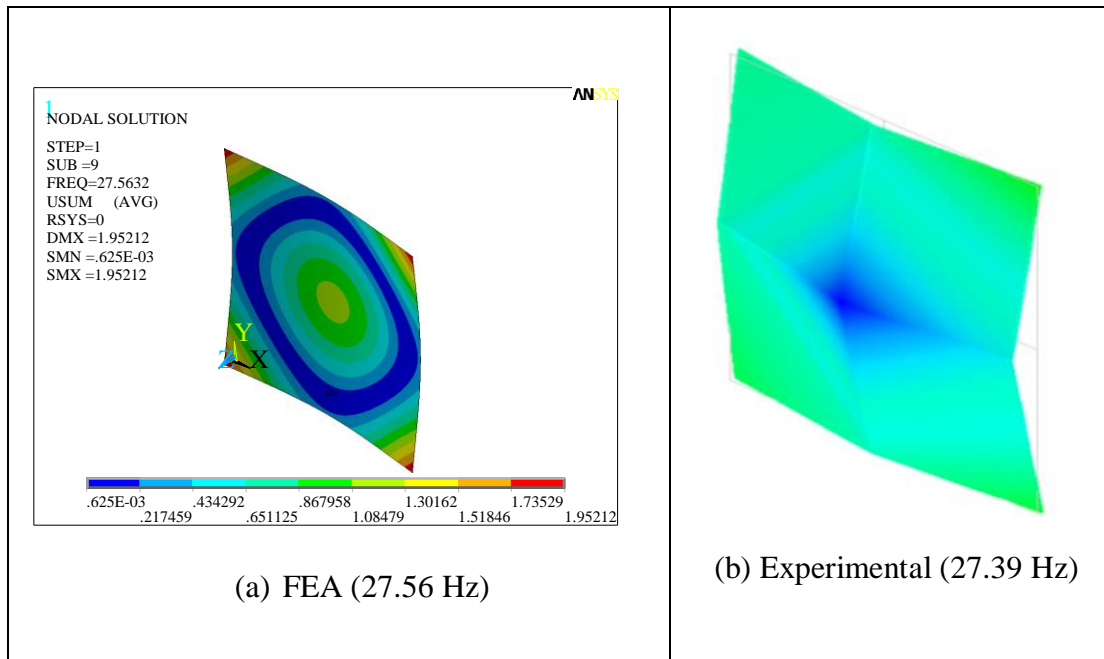


Figure 6.16 Comparison of FEA and experimental mode shape (Mode No-3)

A viscous damping value of 0.1 is maintained on the bolt elements to match with the experimentally obtained results. The FEA obtained results for the effects of pre-load torque (with initial strain) on the resonance frequencies are shown in Table 6.5 for Case 1. Figure 6.17 shows a typical mode shape for bolted joint Case-1 with initial strain obtained from the finite element analysis and experimentation.

Table 6.5 Comparison of resonance frequencies for two and three bolted plates (FEA)

Mode No.	Two – Bolted Plates (Case -1)			Three – Bolted Plates (Case -1)		
	With Initial Strain	Without Initial Strain	% Difference	With Initial Strain	Without Initial Strain	% Difference
1	5.823	5.822	-0.014	3.148	2.727	-13.385
2	7.750	7.555	-2.519	5.529	4.984	-9.852
3	15.671	15.312	-2.291	7.145	7.112	-0.462
4	17.645	17.425	-1.246	10.881	10.415	-4.283
5	25.986	25.950	-0.139	16.236	15.711	-3.234
6	28.523	28.506	-0.060	16.476	15.747	-4.425
7	29.470	29.041	-1.456	24.094	23.818	-1.146
8	32.233	32.227	-0.019	26.588	26.011	-2.170
9	42.830	42.712	-0.276	26.867	26.816	-0.190
10	43.340	43.199	-0.325	28.063	27.985	-0.278

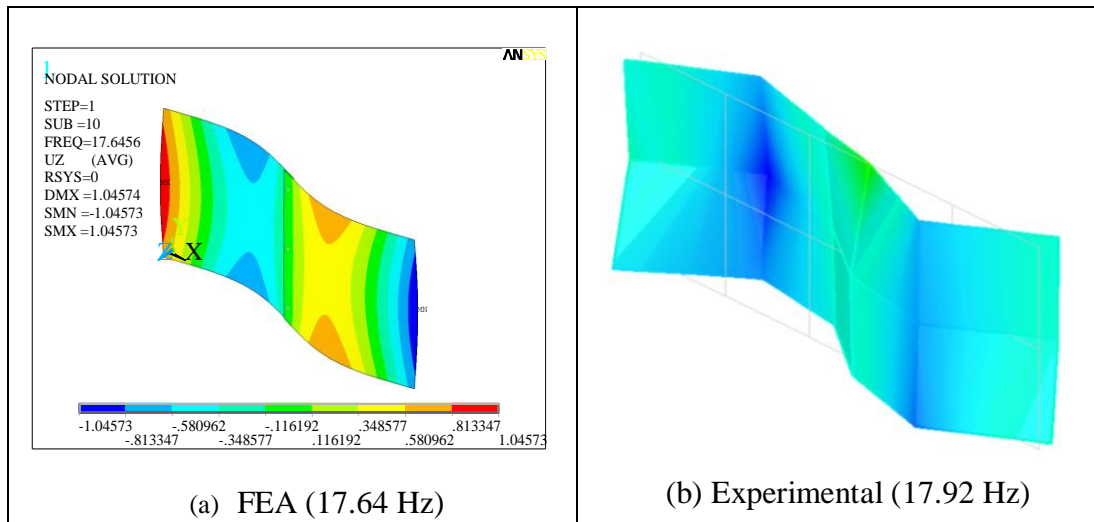


Figure 6.17 Comparison of mode shape of Case-1 with initial strain (Mode No-4)

It is observed that the resonance frequency values decreases with the reduction in pre-load. The percentage variation in the resonance frequency with and without pre-load decreases at higher frequencies.

The procedure of obtaining acceleration responses (Table 6.6) and normalizing it for unit excitation (Table 6.7) is as explained in the section 5.7 of the earlier chapter.

Table 6.6 Acceleration responses of bolted lap joint plate for Case-1

Time (secs)	Acceleration Response (g)			Force (N)
	Node-1	Node-2	Node-18	
0.0000000	0.0557	1.61	0.450	-0.595
0.0000195	0.0045	1.43	0.419	-0.432
0.0000391	-0.0697	1.23	0.416	-0.263
0.0000586	-0.1270	1.01	0.425	-0.089
0.0099800	0.0571	1.77	0.490	-0.748
0.0100000	0.0551	1.61	0.448	-0.593

Table 6.7 Acceleration responses of bolted lap joint plate for Case-1 under unit force

Acceleration Response (g)			Force (N)
Node-1	Node-2	Node-18	Node 5
0.2023	1.6364	0.8333	1

The apparent non-conservative coupling factors have been computed by the Equation (6.13). The apparent coupling factors ( $\eta_{12} = \eta_{21}$ ) for all the cases of the bolted plates, obtained from experiments and numerically have been listed out in Table 6.8 and Table 6.9 respectively. The power inputs have been listed out in tables 6.10 and 6.11 respectively. Table 6.12 compares the resonance frequencies for all the cases of two bolted plates with initial strain. Similarly, the velocity responses obtained by finite element analysis and experiments for all the cases for the left-hand (LH-plate) and right-hand plate (RH-plate) under consideration have been compared in Figures 6.18 to 6.21. All the points in the plots have been joined by smooth lines.

Table 6.8 Apparent coupling factors obtained experimentally for bolted plates

Frequency (Hz)	Coupling factor for plates with bolted joints			
	Case-1	Case-2	Case-3	Case-4
500	-0.41617	0.03391	0.0497	0.03340
1000	0.02306	0.01674	0.01426	0.00820
1500	0.00705	0.00440	0.00400	0.00620
2000	0.00209	0.00542	0.00144	0.00250
2500	0.00134	0.00055	0.00117	0.00203
3000	0.00113	0.00030	0.00099	0.00054
3500	0.00073	0.00017	0.00062	0.00008943

Table 6.9 Apparent coupling factors obtained numerically for bolted plates

Frequency (Hz)	Coupling factor for plates with bolted joints			
	Case-1	Case-2	Case-3	Case-4
500	0.09822	0.00879	0.01001	0.00048
1000	0.00440	0.00033	0.00288	0.00001733
1500	0.01800	0.00027	0.00745	0.00243
2000	0.00226	0.00011	0.00184	0.00487
2500	0.00093	0.0000786	0.00011	0.00016
3000	0.000876	0.00035	0.00087	0.00059
3500	0.00070	0.0000871	0.00026	0.00017



Table 6.10 Power input (N-m/s) measured experimentally for bolted plates

Frequency (Hz)	CASES			
	Case-1	Case-2	Case-3	Case-4
500	0.003267	0.001279	0.002145	0.002535
1000	0.001690	0.007289	0.001274	0.001447
1500	0.000669	0.000922	0.000543	0.000858
2000	0.000262	0.000305	0.000170	0.000252
2500	0.000253	0.000376	0.000184	0.000341
3000	0.000128	0.000144	0.000194	0.000191
3500	0.000165	0.000290	0.000172	0.000102

Table 6.11 Power input (N-m/s) obtained numerically for bolted plates

Frequency (Hz)	Coupling factor for plates with bolted joints			
	Case-1	Case-2	Case-3	Case-4
500	0.002563	0.002453	0.001728	0.000873
1000	0.000742	0.000414	0.000672	0.000243
1500	0.001082	0.001141	0.000741	0.000491
2000	0.000267	0.000273	0.000325	0.000401
2500	0.000217	0.000143	0.000174	0.000160
3000	0.000184	0.000160	0.000185	0.000146
3500	0.000298	0.000260	0.000286	0.000252

Table 6.12 Comparison of resonance frequencies (Hz) for two bolted plates (FEA)

Mode. No.	Resonance frequencies (Hz) (With initial Strain)			
	Case-1	Case-2	Case-3	Case-4
1	5.823	5.1644	5.2108	4.5352
2	7.750	7.7446	6.3054	4.8922
3	15.671	15.485	14.603	13.035
4	17.645	17.400	15.005	14.306
5	25.986	25.872	22.349	17.746
6	28.523	26.546	23.849	22.587
7	29.470	29.430	28.138	26.009
8	32.233	30.067	29.769	27.918
9	42.830	40.466	35.739	30.288
10	43.340	42.627	38.774	36.802

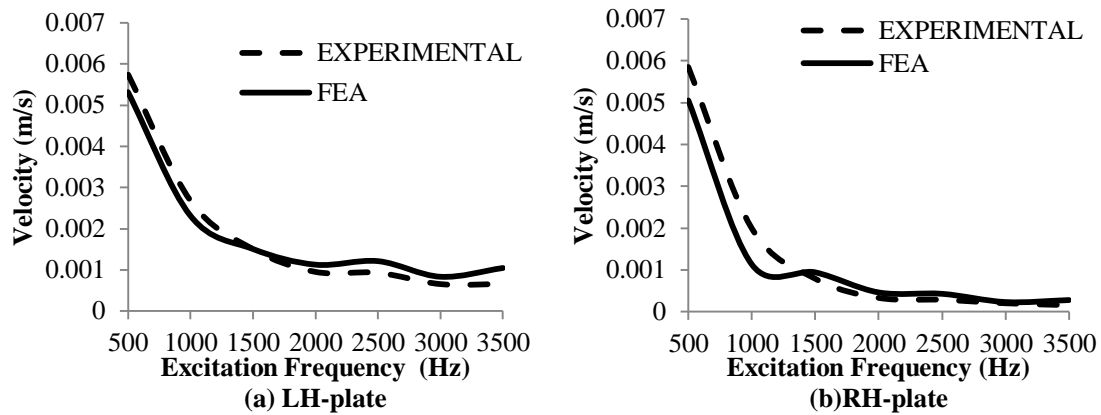


Figure 6.18 Velocity responses of bolted joints for Case -1

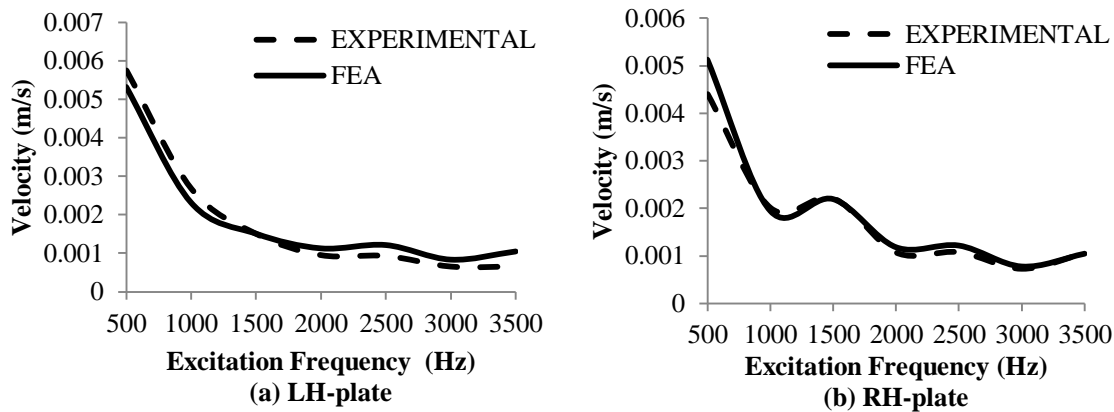


Figure 6.19 Velocity responses of bolted joints for Case -2

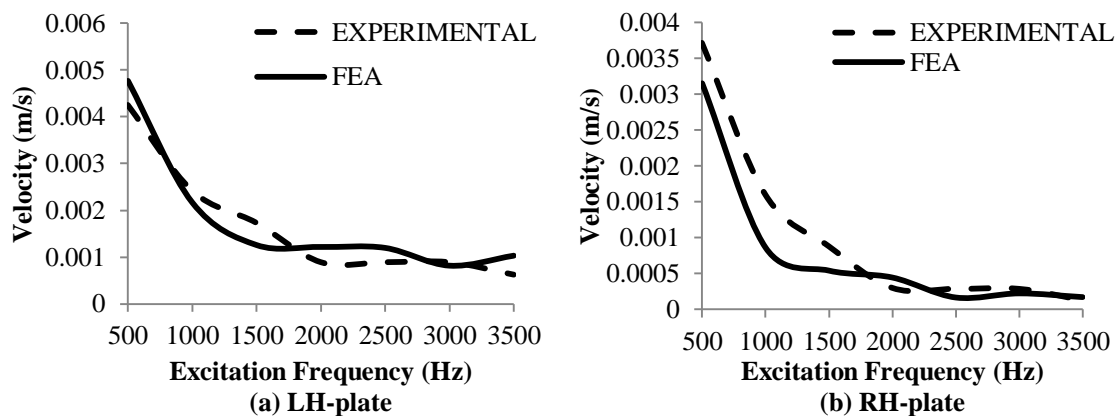


Figure 6.20 Velocity responses of bolted joints for Case -3

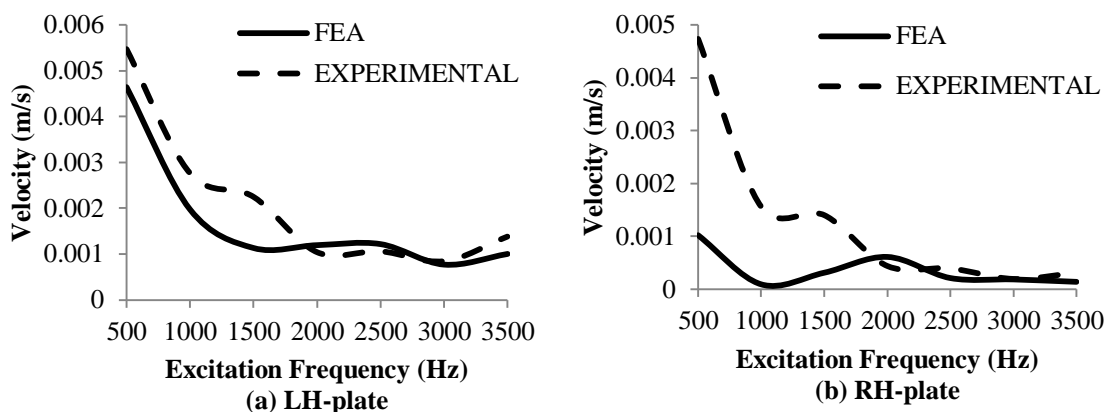


Figure 6.21 Velocity responses of bolted joints for Case-4

Table 6.13 presents the ratio of velocities obtained in LH-plate and RH-plate at an excitation frequency of 3000 Hz for all the cases of two plates joined by bolted joint. It can be observed that as the number of bolts get damaged the total energies and consequently the velocities in the RH-plate is reduced considerably and therefore the ratio of velocity responses of LH-plate to RH-plate increases. It is observed that in Case-2, with the center bolt fully damaged, the ratio of the velocity of LH-plate to RH-plate is higher. It is observed that in connections wherein the overlapping plates are in contact with each other and excited at the central location, the energy propagation through the radius and the central portion of the plates is significant and any absence of the central contact area increases the velocity ratio between two plates, when compared to the absence of the same at the ends. The next chapter explains the effect in detail.

Table 6.13 Ratio of velocity responses obtained for bolted joints of LH-plate and RH-plate for excitation frequency, 3000 Hz.

CASES	Experiment			FEA		
	LH-plate (m/s)	RH-plate (m/s)	Ratio	LH-plate (m/s)	RH-plate (m/s)	Ratio
Case-1	0.00066	0.000203	3.24	0.000834	0.000234	3.55
Case-2	0.000726	0.000122	5.95	0.000778	0.000139	5.58
Case-3	0.000893	0.000269	3.31	0.000816	0.000224	3.62
Case-4	0.000845	0.00019	4.44	0.00077	0.000185	4.14

Forced response finite element analyses at higher frequencies have revealed that there is negligible difference in the velocity responses obtained for the cases with and without pre-load or initial strain in the bolts, provided that the plates remain connected by bolts. Similar results have been observed from the experiments.

### 6.5.1 Joint damage detection

The studies for damage detection consists of three identical plates (namely LH-plate, Middle-plate and RH-plate) coupled in sequence by bolted lap joints (Figure 6.22) for all the possible combinations of the cases as discussed in section 6.2. Table 6.14 presents all possible combinations of three plates with bolted lap joints for predicting the velocity responses using the SEAL approach.

Table 6.14. List of possible combinations for three plates with bolted lap joints.

<b>Combination</b>	<b>Type of Bolted Joint Between LH-plate and Middle-plate</b>	<b>Type of Bolted Joint Between Middle-plate and RH-plate</b>
1	Case-1	Case-1
2	Case-1	Case-2
3	Case-1	Case-3
4	Case-1	Case-4
5	Case-2	Case-1
6	Case-2	Case-2
7	Case-2	Case-3
8	Case-2	Case-4
9	Case-3	Case-1
10	Case-3	Case-2
11	Case-3	Case-3
12	Case-3	Case-4
13	Case-4	Case-1
14	Case-4	Case-2
15	Case-4	Case-3
16	Case-4	Case-4

To illustrate the effectiveness of the method used to predict the damage status in the three plates with lap joints, a case of three plates with bolted lap joint is presented here. A healthy configuration described as LH-plate, and Middle-plate are joined using bolted joints along the coupled junction namely  $B_{11}$ ,  $B_{12}$  and  $B_{13}$  as shown in Figure 6.22, and Middle plate and RH-plate are joined using bolted joints along the coupled junction namely  $B_{21}$ ,  $B_{22}$  and  $B_{23}$ . The damage in the Middle-plate and RH-plate with bolted lap joints is assumed to be a failure of the central bolt,  $B_{22}$  and the remaining bolts are intact. Figure 6.23 depicts the damage with the absence of central bolt,  $B_{22}$  and the remaining bolts are intact. The velocity responses obtained experimentally, numerically and predicted using SEAL approach for the healthy and damaged configurations are shown in Figure 6.24 and Figure 6.25 respectively. The codes required for carrying out the computations have been developed using MATLAB software.

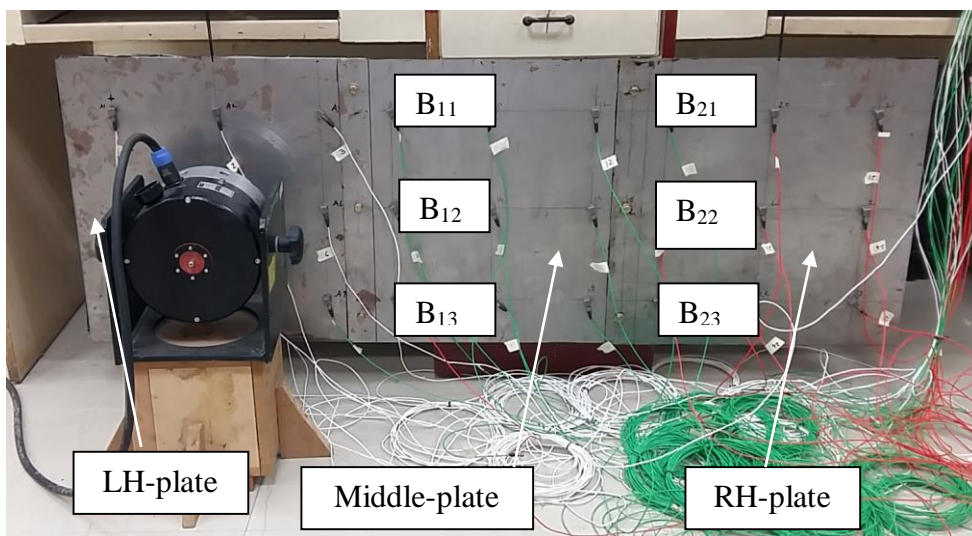


Figure 6.22 Three plates with bolted lap joints (healthy configuration: combination -1)

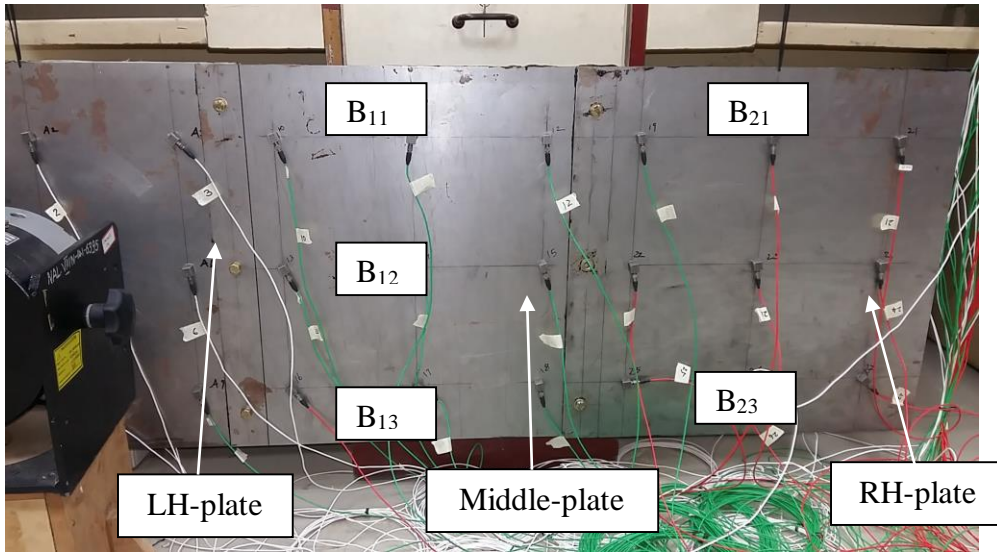
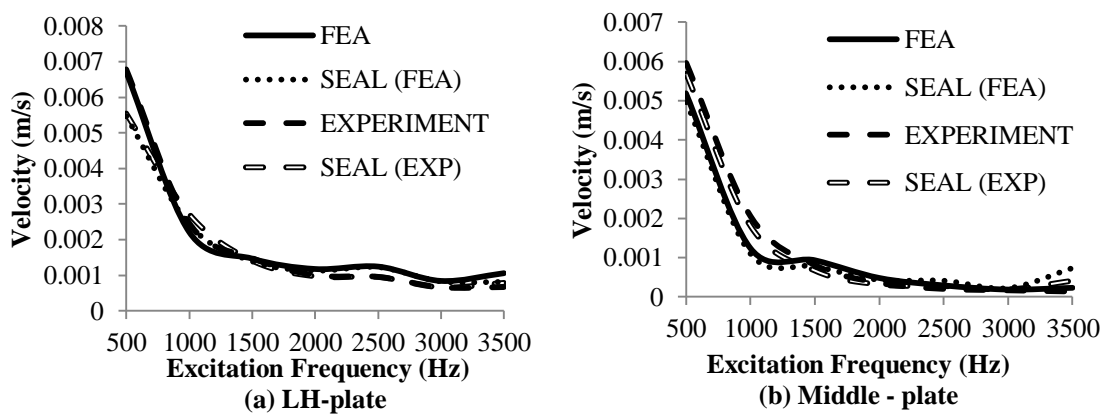


Figure 6.23 Three bolted plates with absence of bolt B<sub>22</sub> (damaged configuration: combination -2)

The velocity responses have been predicted by the SEAL approach for the healthy and damaged configurations using the apparent coupling factors listed out in Tables 6.8 and 6.9. These predicted velocity responses for the healthy configuration are compared with the actual experimentation, and finite element analysis obtained responses in Figures 6.24 (a) to 6.24 (c).



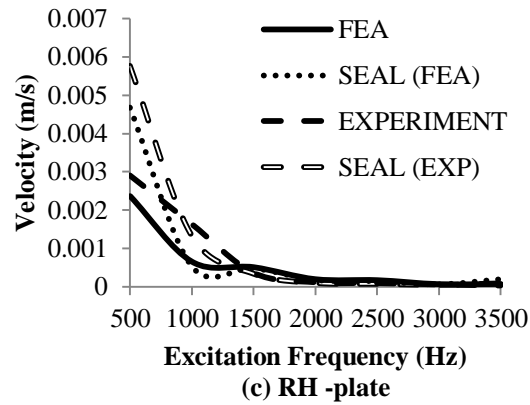


Figure 6.24 Velocity responses for bolted lap joints of healthy configuration

The predicted velocity responses for the damaged configuration are compared with the actual experimentation, and finite element analysis obtained responses in Figures 6.25 (a) to 6.25 (c).

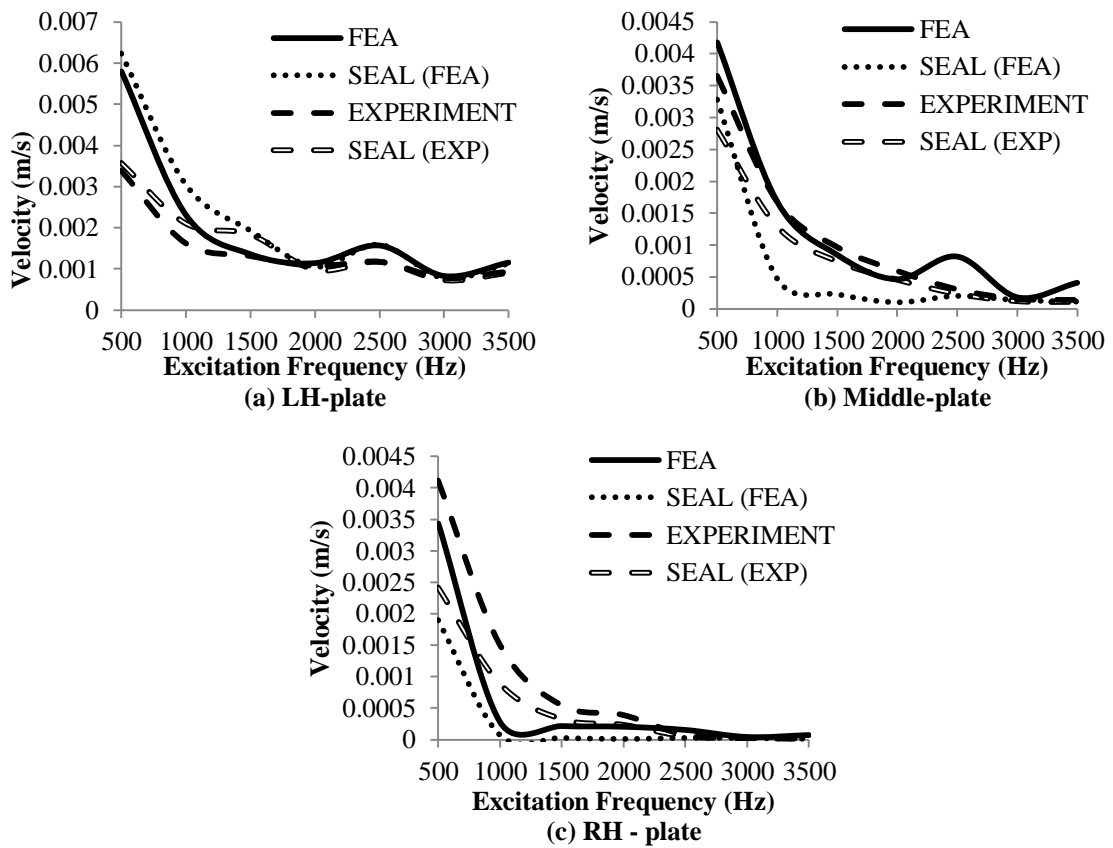


Figure 6.25 Velocity responses for bolted lap joints of damaged configuration

The modal density ( $n$ ) per Hz of each plate is 0.0746. The modal overlap factor ( $M=f\eta n$ ) preferred for application of statistical energy analysis principle is greater than one. In the present case, at all the excitation frequencies equal to or greater than 1000 Hz, due to the application of damping sheet on the side of the plate, the condition is sufficed. At 3000 Hz the modal overlap is 2.46. The variation in the derived coupling factors due to the variation in the excitation force location on the excited plate reduces with the increase in excitation frequencies. The excitation frequency of 3000 Hz is selected as the deterministic frequency for detection of damage for the combinations as listed out in Table.6.14. The acceleration response for each plate, computed by multiplying the plate velocity with the frequency of excitation. Table 6.15 presents the acceleration responses obtained for the plates of healthy (combination-1) and damaged (combination-2) joint at an excitation frequency of 3000 Hz.

Table 6.15. Comparison of acceleration responses for bolted joints, excitation frequency of 3000 Hz.

PLATE	Name of Methods	Acceleration (m/s <sup>2</sup> )		Percentage difference
		Healthy	Damaged	
LH-plate	Experimental	15.608	15.145	-2.97
	SEAL (Exp)	15.302	14.562	-4.84
	FEA	15.832	15.597	-1.48
	SEAL (FEA)	15.400	14.735	-4.31
Middle-plate	Experimental	3.035	2.889	-4.81
	SEAL (Exp)	4.651	4.561	-1.94
	FEA	3.530	3.384	-4.14
	SEAL (FEA)	4.186	4.076	-2.61
RH-plate	Experimental	1.254	0.623	-50.32
	SEAL (Exp)	1.468	0.778	-47.00
	FEA	1.343	0.779	-42.00
	SEAL (FEA)	1.172	0.741	-36.72



It is observed from Table 6.15 that in case of the damaged joint, the acceleration response in RH-plate is reduced in comparison to the healthy configuration. The percentage reduction in the acceleration response in the RH-plate due to the damaged joint (B<sub>22</sub>) is in the order of 45% in comparison with that of the healthy plate. A database bank of the expected responses using SEAL approach for the other possible combinations is listed out in Table 6.16.

Table 6.16. Percentage deviation of acceleration responses of the other possible combinations in comparison to the healthy configuration (Combination 1) at an excitation frequency of 3000 Hz.

Combination	SEAL – Predicted (Exp) in %			SEAL – Predicted (FEM) in %			FEM in %		
	LH-plate	Middle-plate	RH-plate	LH-plate	Middle-plate	RH-plate	LH-plate	Middle-plate	RH-plate
3	1.0	1.0	-19.8	0.7	2.0	-20.4	0.0	8.7	-22.5
4	2.0	4.2	-25.9	1.7	3.9	-36.5	0.0	12.4	-39.4
5	-4.8	-48.5	-48.5	-5.8	-34.5	-34.5	-5.7	-29.4	-36.2
6	-5.7	-47.4	-71.6	-6.8	-34.1	-54.1	-4.8	-18.7	-54.2
7	-3.8	-47.9	-51.0	-5.1	-33.1	-47.9	-5.7	-18.7	-21.3
8	-2.0	-45.7	-61.4	-3.0	-31.0	-53.9	-5.7	-16.7	-32.4
9	2.0	-3.8	-3.8	1.5	-2.5	-2.5	-2.9	-11.5	-12.3
10	1.0	-2.0	-47.1	0.4	-1.8	-31.7	-3.8	7.5	-38.3
11	1.0	-3.8	-9.9	0.5	-2.1	-23.7	-2.9	-12.3	-20.1
12	1.0	-2.0	-30.6	1.3	-0.6	-39.2	-2.0	-20.6	-40.8
13	-7.4	-34.2	-34.2	-9.3	-15.7	-15.7	-7.4	-18.7	-20.6
14	-6.5	-31.5	-62.8	-8.0	-12.9	-39.4	-9.1	-9.9	-52.7
15	-8.3	-34.2	-37.9	-9.6	-14.8	-33.6	-7.4	-16.0	-37.9
16	-8.3	-33.3	-52.6	-9.8	-14.3	-47.7	-8.3	-9.9	-52.4

The energy propagation effects due to the variation in the central excitation towards the left central edge has a marginal effect on the apparent coupling factors computed

by FEA for Case 3 and 4. Accordingly, the apparent coupling factors, 0.00051 and 0.0003 have been used for Case 3 and 4, respectively for sequentially coupled plates after the second or Middle-plate to obtain accurate SEAL based predictions using FEA.

Table 6.16 presents the percentage deviation in the acceleration responses of Case- 3 to Case-16 combinations in comparison to the healthy configuration, Case-1. The percentage deviations have been used as one of the damage indicators. All the possible damage samples considered in the present study for an assembly of bolted plates can be simulated by the SEAL approach to develop a database as one of the features of damage signals.

## **6.6 SUMMARY**

Similar to the observations in the damage of spot-welded joints, the failure in the bolted joints for a sequentially coupled plate causes a reduction in the values of coupling factors, energies, velocity and acceleration response of the subsequent plate following the damaged bolted joint (Table 6.12). The maximum percentage reduction of acceleration response is in the RH plate and for combination 6 for three bolted lap joined plates in comparison to the healthy configuration (Table 6.15). In case of the bolted joints, the overlapping areas of the plate is in close contact with each other. The incorporation of damping and fine-tuning of the stiffness parameters from experiments in the numerical simulations becomes inevitable in case of modelling of the bolted joints and estimation of coupling factors using FEA.

The main aim of pasting the damping materials on the surface of the plates was to acquire accurate CLF by enlarging the internal loss factor and dismissing the possibility of energy backflow from the receiver plate to the excited plate. Thus the added damping was chosen so that internal loss for each plate dominated all other losses, giving a higher modal overlap and smooth frequency response function.

The percentage deviation (Table 6.16) in the acceleration responses on each plate of the remaining combinations in comparison to the healthy configuration (combination 1) has been used as one of the damage indicator.

## CHAPTER 7

### DAMAGE DETECTION OF ADHESIVE BONDED PLATES USING STATISTICAL ENERGY ANALYSIS LIKE APPROACH

#### 7.1 INTRODUCTION

This chapter discusses the damage studies, further extended to adhesive bonded joints, wherein, apparent coupling factors is derived for 4 cases of two adhesive lap bonded plates and used further to predict the velocity and acceleration responses with the SEAL approach for an assembly of three plates lap joined by double-sided adhesive tape. The results obtained have been discussed and compared by experiments and finite element analysis for a healthy and damaged configuration.

#### 7.2 TEST SPECIMENS

The dimensions of each plate, made of acrylic, considered in the studies are length, 300 mm, width, 300 mm and thickness of 1.1 mm. The plates are joined by a double-sided adhesive tape (VHB-3M-4941). The adhesive tape bonds the two plates with an overlap of 12.5 mm. This case of full bonding is classified as the healthy configuration (Case-1). The thickness of the adhesive tape is 1.1 mm and width is 12.5 mm. The following cases of two plates joined by adhesive bonded tape have been considered to obtain the apparent coupling factors using statistical energy analysis like (SEAL) approach.

**Case-1:** Two plates joined with adhesive along the complete lap joint length as shown Figure 7.1. Three segments  $A_1$ ,  $A_2$  and  $A_3$  with each 100 mm lap joint length represents complete healthy plates.

**Case-2:** Two plates joined with adhesive along lap joint total length, 200 mm. i.e., only segments  $A_1$  and  $A_3$  are active joints whereas, in absence of central patch of 100 mm of segment  $A_2$  is assumed to be damaged (Figure 7.2).

**Case-3:** Two plates joined with adhesive along lap joint length, 200 mm of segments  $A_1$  and  $A_2$ , in absence of segment,  $A_3$  is assumed to be damaged ; Figure 7.3)

**Case-4:** Two plates joined with adhesive along lap joint length, 100 mm of segment,  $A_2$  active and remaining two segments,  $A_1$ , and  $A_3$  with total length 200 mm are assumed to be damaged (Figure 7.4)

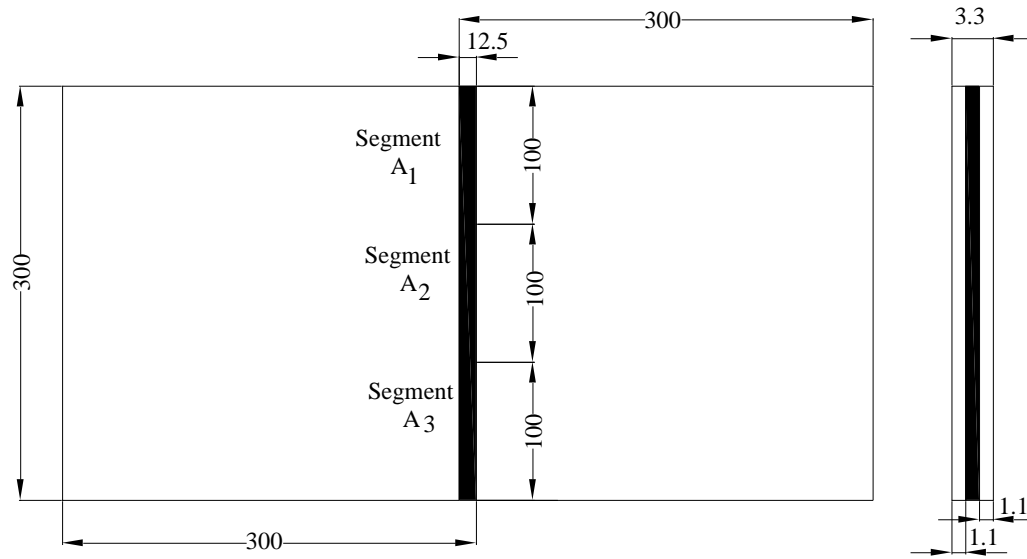


Figure 7.1 Geometric dimensions of plates with an adhesive lap joint (Case-1)

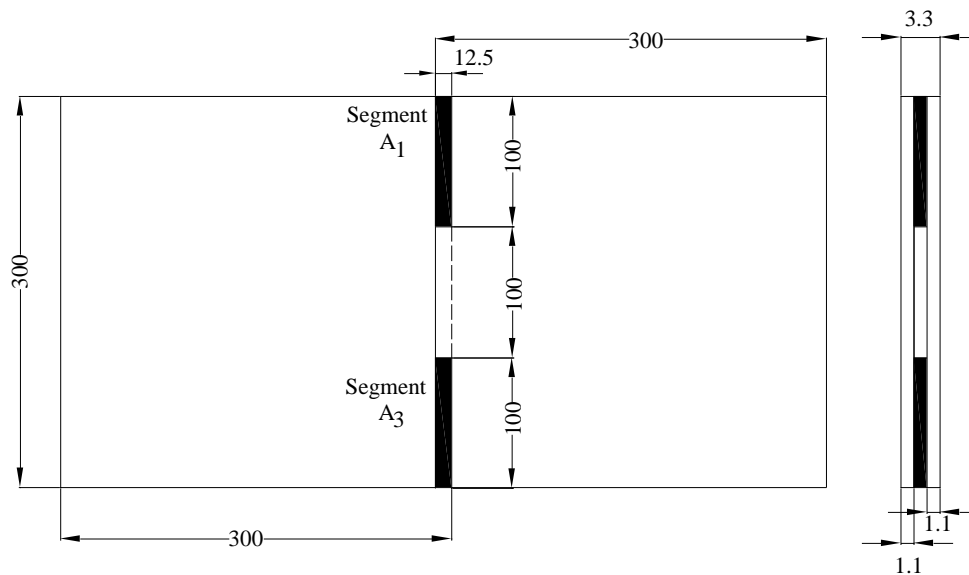


Figure 7.2 Geometric dimensions of plates with an adhesive lap joint (Case-2)

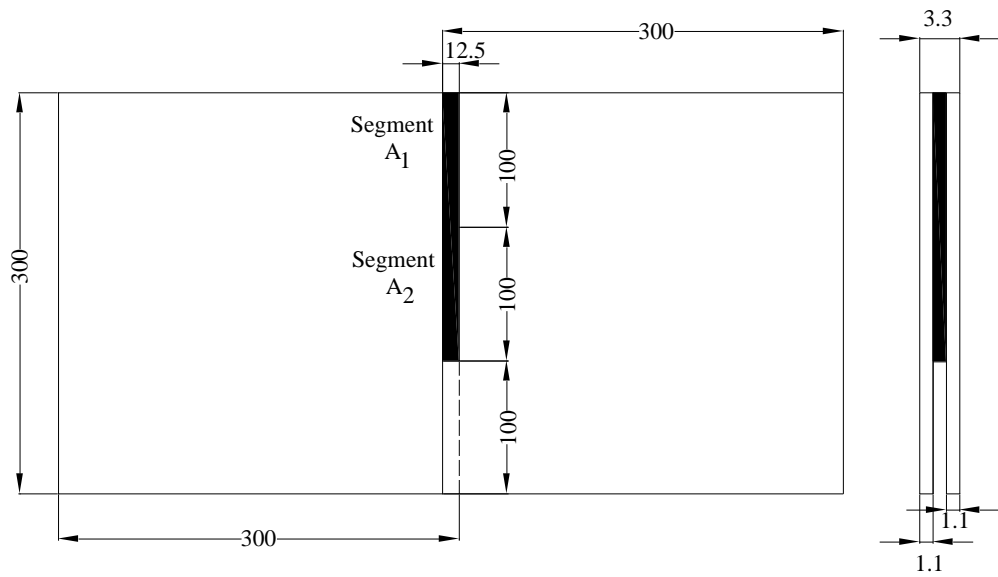


Figure 7.3 Geometric dimensions of plates with an adhesive lap joint (Case-3)

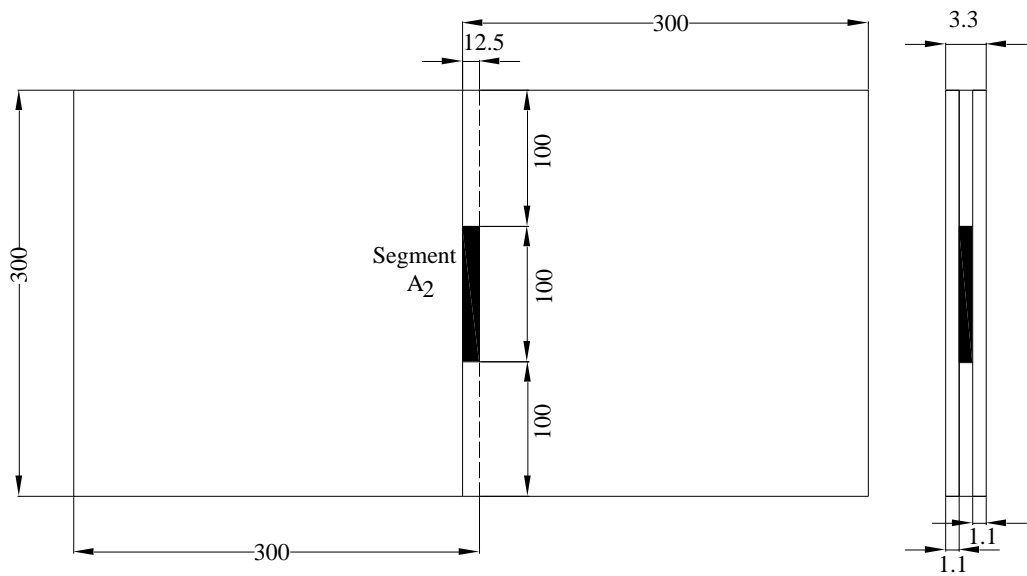


Figure 7.4 Geometric dimensions of plates with an adhesive lap joint (Case-4)

### 7.3 EXPERIMENTAL SET - UP

The experimental setup is similar to the previous cases and consists of adhesive bonded plates to be tested, data acquisition hardware, sensors, shakers and computer with modal analysis software as shown in the Figure 7.5.

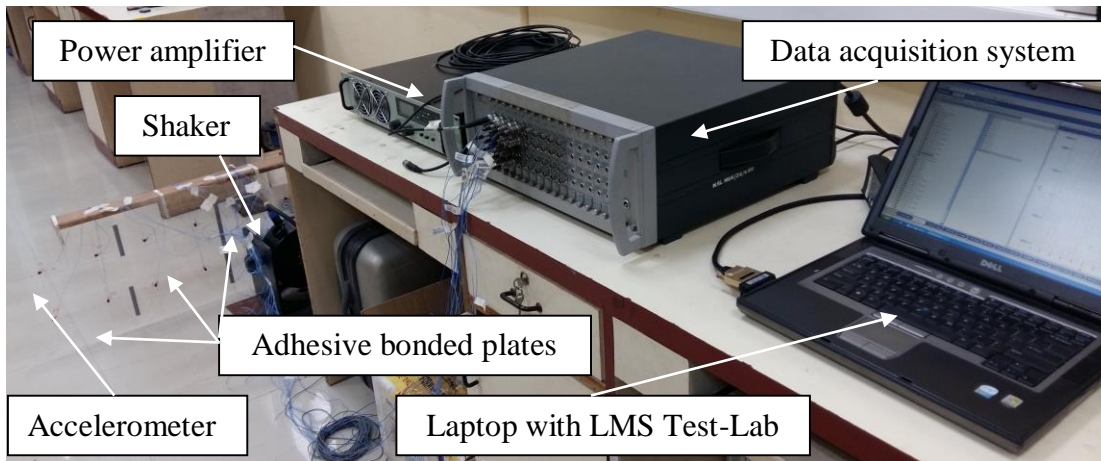


Figure 7.5 Experimental set-up

For acquiring the vibration signals, a uniaxial piezoelectric accelerometer was used. As the density of acrylic is low in the order of  $1140 \text{ kg/m}^3$ , the weight of each plate is  $112.86 \text{ gm}$ . Accordingly, a low weight accelerometer was selected to reduce the mass loading effects. Figure 7.6 shows the uniaxial accelerometer and the specifications of the accelerometer are as shown in Table 7.1.



Figure 7.6 Accelerometer for measuring the vibration

LMS Testlab is used for data acquisition, analysis and extracting the modal parameters. Electrodynamic shakers of Bruel and Kjaer with a force rating of  $200 \text{ N}$  sine (Type 4825) and a compatible power amplifier is used to excite the plate, and the excitation force is measured using force transducer as explained. The shaker had a limitation of excitation frequency beyond  $3500 \text{ Hz}$  and accordingly the maximum excitation frequency for the experiments is limited to  $3500 \text{ Hz}$ . The adhesive bonded plates have been hung by removable lightweight adhesive tapes to simulate a free-free boundary condition.

Table 7.1 Specifications of the accelerometer.

Make (PCB piezotronics)	Integrated circuit piezoelectric
Model	352A24
Sensitivity	100 mV/g
Frequency range ( $\pm 5\%$ )	1.0 to 8000 Hz
Resonant frequency	>30 kHz
Measuring range	$\pm 50$ g
Weight	0.8 gms
Temperature range	-54 to 121 <sup>0</sup> C
Size	4.8 mm x 12.2 mm x 7.1 mm

The geometry as per the test points, chosen for measurements is created using LMS test lab. Each plate is divided equally into four regions, and the responses were obtained using four accelerometers placed centrally for each of the regions. One accelerometer is placed at the central location of excitation of the main plate. The nodes, i.e., the accelerometer positions and wire frame geometry created is as shown in the Figure 7.7. Channels setup is carried out with the setting type of sensor, excitation voltage, units, reference point, measurement point IDs and gain settings.

To measure the natural frequencies, scope settings with maximum frequency is set to 512 Hz and spectral lines of 2622 Hz, which give a frequency resolution of 0.19 Hz. Uniform windows are chosen for both excitation and response signals. 50% burst random signal is used for exciting the plate. Same scope settings are imported to test setup and required functions such as time domain data, Cross Power Spectrums, Peak Spectra, FRF, and Auto Power Spectra, etc. are selected to store into the computer database. In case of harmonic sinusoidal excitation and acceleration response measurement, 32768 Hz sampling frequency and a maximum bandwidth of 10000 Hz is set. The time-averaged power input into the structural substructure is given by (De Langhe, 1996)

$$P = \frac{1}{\omega} \text{Im} (S_{af}(\omega)) \quad (7.1)$$

In the present studies, excitation is carried out at discrete frequencies of 500 to 3500 Hz in steps of 500 Hz.

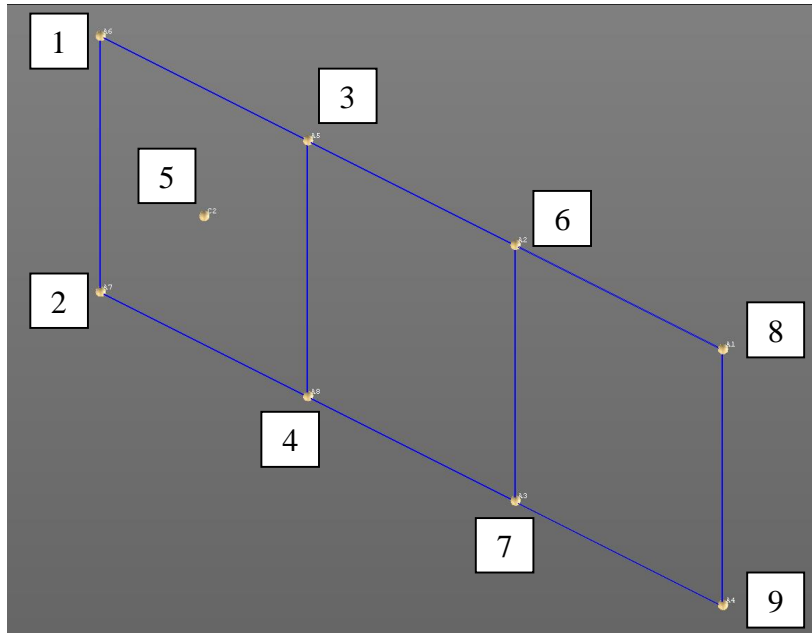


Figure 7.7. Geometry created in Test. Lab.

The input excitation force is applied to the center (0.15 m, 0.15 m) of one plate (Figure 7.7). The plate is excited for flexural vibratory modes. Figure 7.7 shows the geometry created in the test lab for two adhesive bonded plates. The experimental set up for one case (Case-1) for two adhesive bonded plates is shown in Figure 7.8.



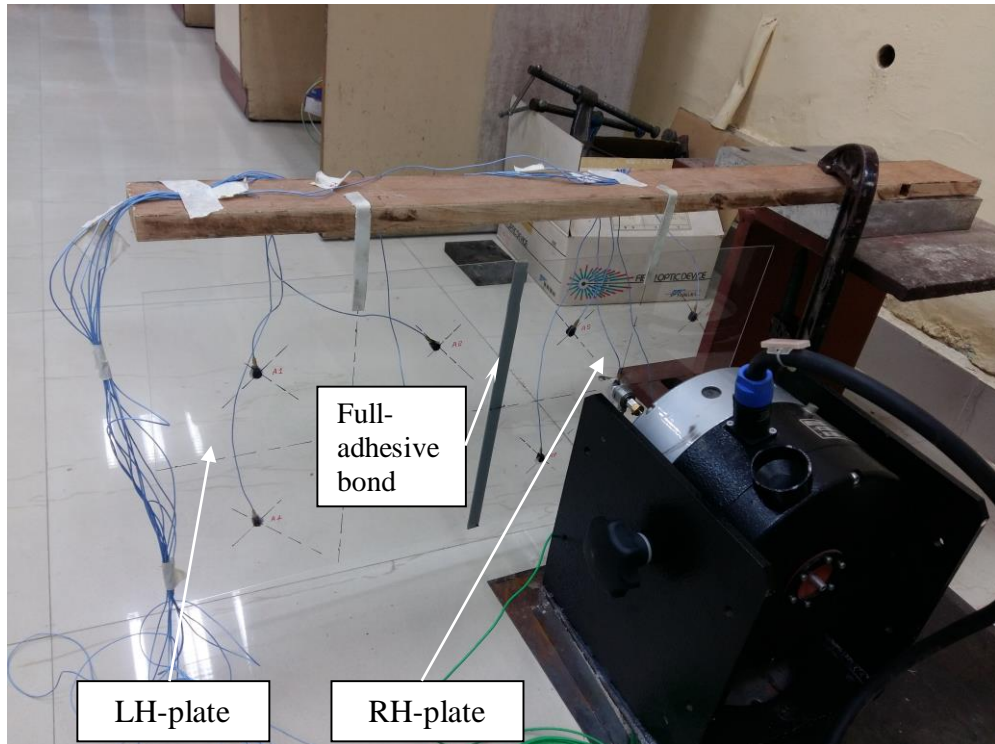
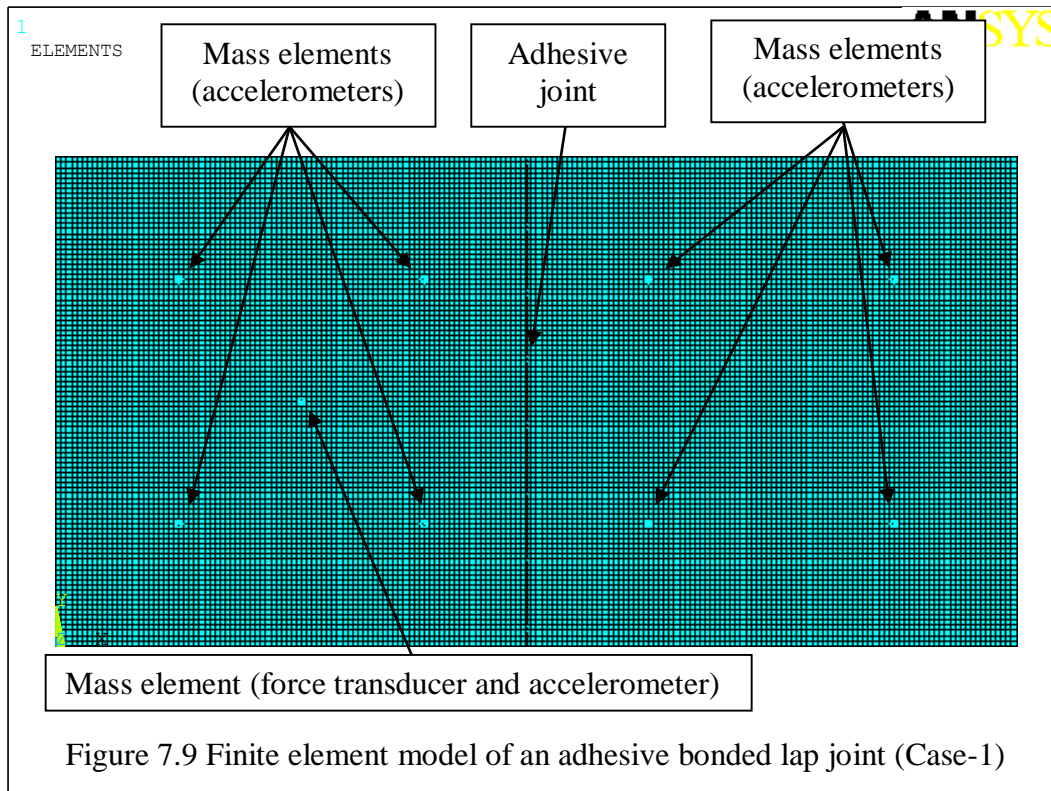


Figure 7.8 Experimentation for two adhesive bonded lap joint plates (Case-1)

In the present case of adhesive bonded joints, due to the presence of damping at the joint, non-conservative apparent coupling could be present that may increase the internal losses of the structure. The equivalent internal loss factors ( $\eta'_1, \eta'_2$ ) and coupling loss factors ( $\eta'_{12}, \eta'_{21}$ ) are computed by using Equations (6.10) and (6.11) as discussed in the Section 6.3.

#### 7.4 FINITE ELEMENT ANALYSIS

Figure.7.9 depicts the FE model of the plates and resonance frequencies are calculated by using ANSYS software. The plates are modeled using SHELL 281 elements.



The adhesive joint is modeled using solid elements (SOLID186 element, 3.125 mm square and 1.1 mm high). The plates have been meshed with a mean mesh size of 3.1 mm and free-free boundary conditions are used for the analyses. The minimum finite element size in the relation of a number of elements per wavelength of six is maintained.

A densitometer (Figure 7.10) based on the buoyancy method was used to measure the density of the acrylic. Similarly, the modulus of elasticity of the acrylic material was obtained from the experimental derivation of the first natural frequency of a cantilever beam of the acrylic material of dimensions width, 30 mm and thickness, 1.1 mm as the material properties were not available in the supplier database.



Figure 7.10 Densitometer for measuring density of acrylic plate

Two beam specimens with lengths of 100 mm and 150 mm have been used for the derivation. The equations for the first natural frequency ( $\omega_n$ ) of a cantilever beam and the derivation for the modulus of elasticity ( $E$ ) is given below:

$$\omega_n = 3.516 \sqrt{\frac{EI}{\rho AL^4}} \quad (7.4)$$

$$\therefore E = \frac{\rho AL^4 \omega_n^2}{(12.36)I} \quad (7.5)$$

where  $\rho$  is the density of acrylic,  $A$  is the cross-sectional area,  $I$  is the area moment of inertia of the cross-section and  $L$  is the length of the cantilever beam. Figure 7.11 shows the experimental setup. Table 7.2 presents the natural frequencies obtained from the experiments and the derived values of modulus of elasticity. The average of the elastic modulus obtained from the above results is 3.18 GPa, which is used in the finite element analysis. Table 7.3 presents the material and geometrical specifications of the acrylic plates used for the studies, that is in line with the values observed in literature. Dynamic analysis of the FE model of the adhesive bonded plates is carried out for a free-free condition and the dynamic frequency spectrum is obtained by

invoking the lanczos method in ANSYS, with unit mass criteria for normalizing mode shapes

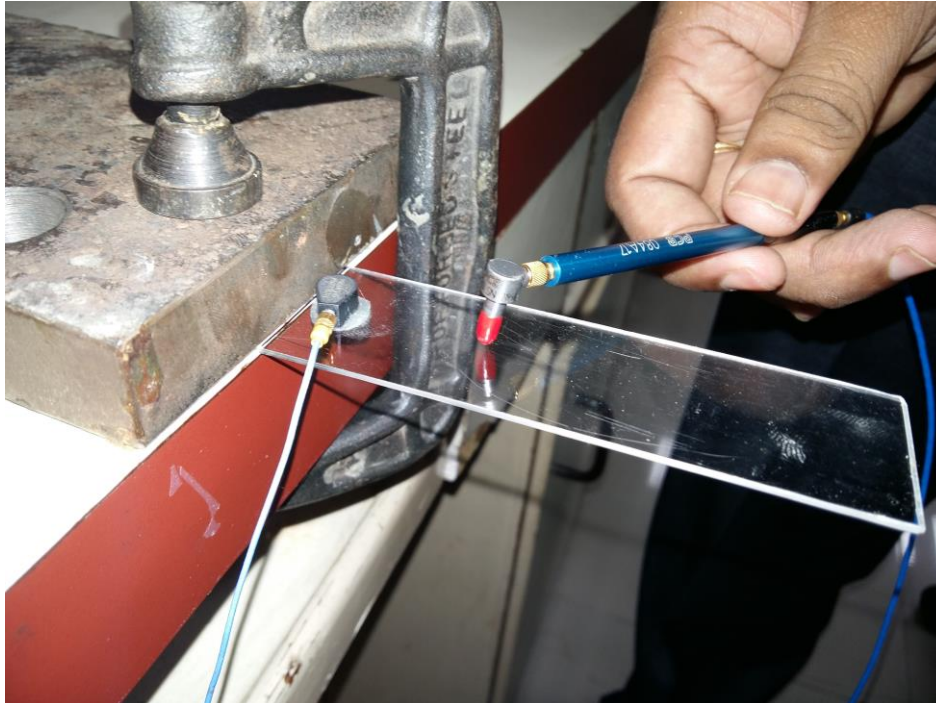


Figure 7.11 Experimental set-up for measuring elastic modulus of acrylic

Table 7.2 Elastic modulus of acrylic obtained from natural frequencies.

Length (mm)	Frequency (Hz)	Youngs modulus (GPa)
100	29.98	3.25
150	13.05	3.11

Table 7.3. Material and Geometrical specifications.

Parameter	Values
Width( $w$ )	0.3 m
Length( $L$ )	0.3 m
Thickness( $t$ )	1.1 mm
Density( $\rho$ )	1140 kg/m <sup>3</sup>
Poisson's ratio( $\mu$ )	0.37
Young's Modulus( $E$ )	3.18 GPa

The adhesive with a density of  $720 \text{ kg/m}^3$ , thickness, 1.1 mm, modulus of elasticity, 0.2 MPa, damping coefficient, 0.08 and Poisson's ratio, 0.49 is used for the analyses.

A harmonic force with unit load intensity is applied in the range of frequencies of 500-3500 Hz at steps of 500 Hz. Unit force of 1 N is applied on the LH-plate, and the velocity responses on both the plates have been computed.

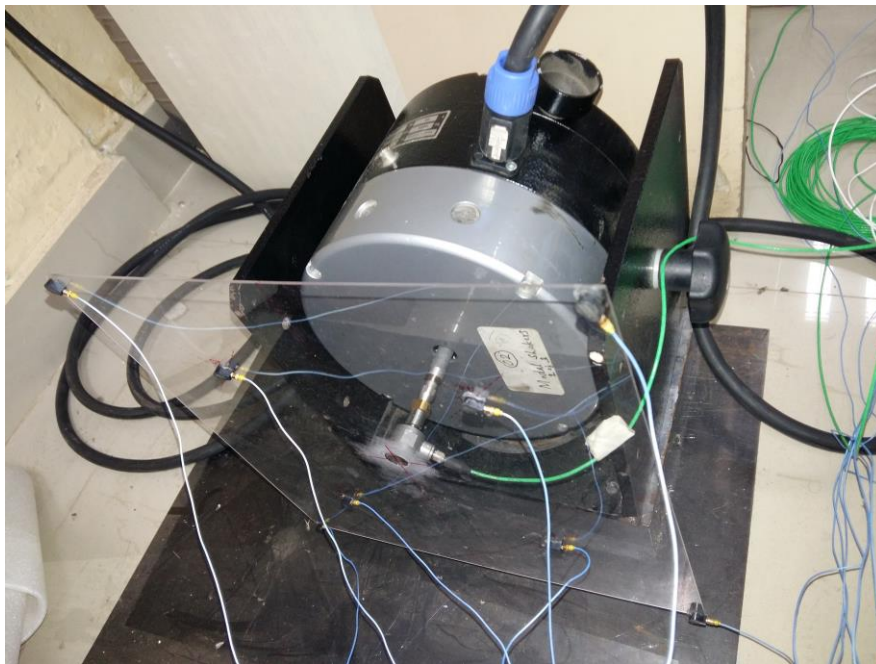


Figure 7.12 Power injection method for a single acrylic plate

The internal loss factors estimated by the experimental power injection method on a single plate (Figure 7.12) for different frequencies as listed out in Table 7.4 is used for the finite element analysis at the respective frequencies. The mass of the accelerometers is modeled as a concentrated mass element (mass 21) at the locations wherein the accelerometers have been placed during the experiments. The additional mass of the force transducer has also been included in the concentrated mass element (mass 21) element at the point of excitation force.

Table 7.4 Internal loss factor at excited frequencies

Excitation Frequency (Hz)	500	1000	1500	2000	2500	3000	3500
Loss Factor ( $\eta$ )	0.09	0.07	0.05	0.034	0.024	0.020	0.021

The total vibrational energy ( $E_i$ ) of each region of the plate is computed using Equation (7.8) after computing the velocity responses and power inputs. Here ( $M_i$ ) is the mass of one of the four regions on each plate and the representative substructure velocity ( $V_i$ ) corresponding to that region.

$$E_i = \frac{M_i V_i^2}{2} \quad (7.8)$$

The total vibrational energy of each plate is computed by the summation of the energies obtained from individual regions of that plate ( $E = E_1 + E_2 \dots E_4$ ). The apparent non-conservative coupling factors are computed by the Equation (6.11) after computation of power inputs and corresponding energies of each plate.

## 7.5 RESULTS AND DISCUSSION

Table.7.5 presents the comparison of the resonance frequencies obtained from finite element analysis and experiments for the elastic modes of a single plate. It is observed that the maximum error of the FEA obtained resonance frequencies, when compared with the experimentally obtained values is within an acceptable range of 5 %. Figures 7.13 and 7.14 shows the mode shapes for two typical modes obtained from the finite element analysis and experiments. Similar trends have been seen for coupled plates, and Table 7.6 and Figures 7.15 and 7.16 shows the mode shapes for two typical modes obtained from the finite element analysis and experiments for Case-1.

Table 7.5 Comparison of resonance frequencies for elastic modes (single-plate)

Mode No.	FEA (Hz)	Experimental (Hz)	% Difference
1	12.92	13.15	-1.75
2	18.96	18.22	4.06
3	24.80	24.54	1.06
4	33.82	34.01	-0.56
5	61.27	60.69	0.96
6	67.31	65.34	3.01
7	77.33	78.56	-1.57
8	103.47	101.21	2.23
9	116.58	118.21	-1.38

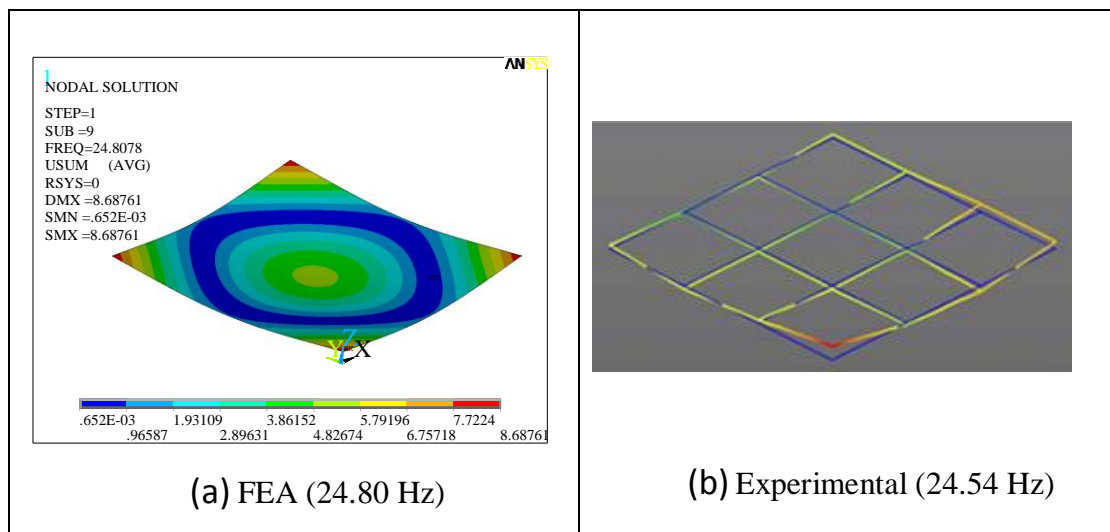


Figure 7.13 Comparison of mode shape (Mode No-3)

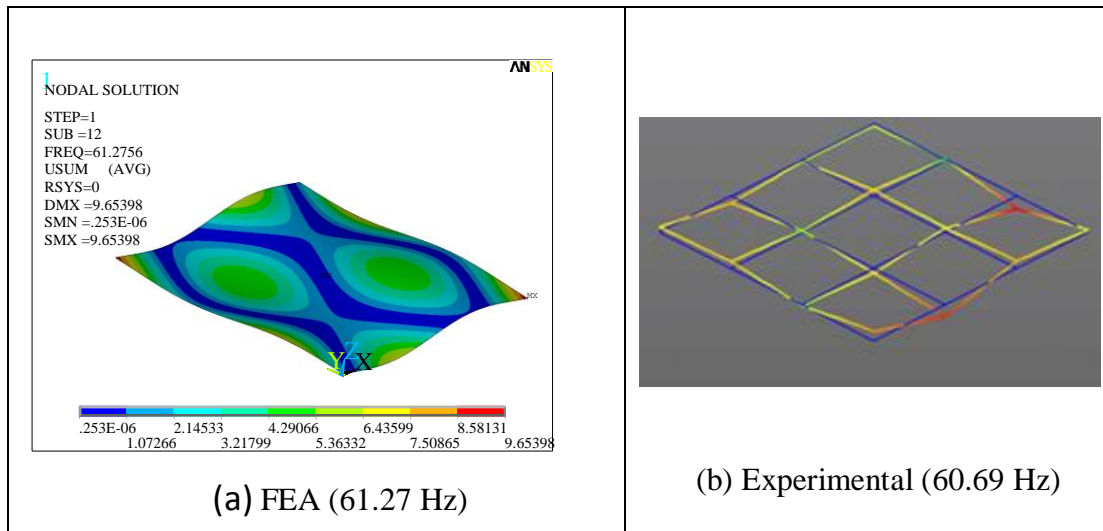


Figure 7.14 Comparison of mode shape (Mode No-5)

Table 7.6 Comparison of resonance frequencies for elastic modes  
(Case -1).

Mode No.	FEM (Hz)	Experimental (Hz)	% Difference
1	5.43	5.22	3.94
2	6.61	6.36	3.91
3	14.09	13.83	1.85
4	15.37	15.51	-0.88
5	22.14	22.35	-0.95
6	25.62	25.95	-1.28
7	26.09	26.65	-2.11
8	29.98	30.37	-1.28



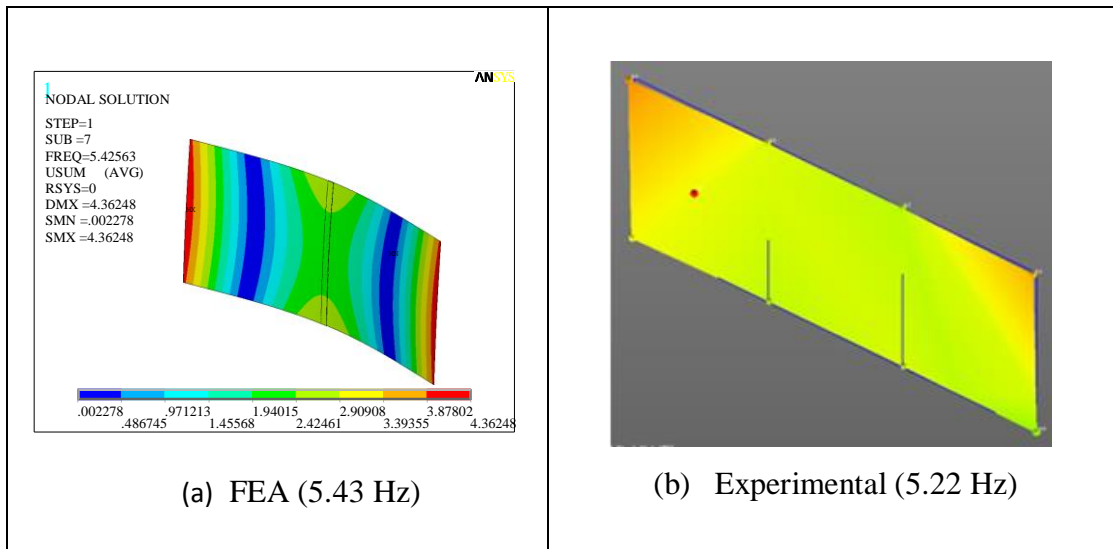


Figure 7.15 Comparison of mode shape for Case-1 (Mode No-1)

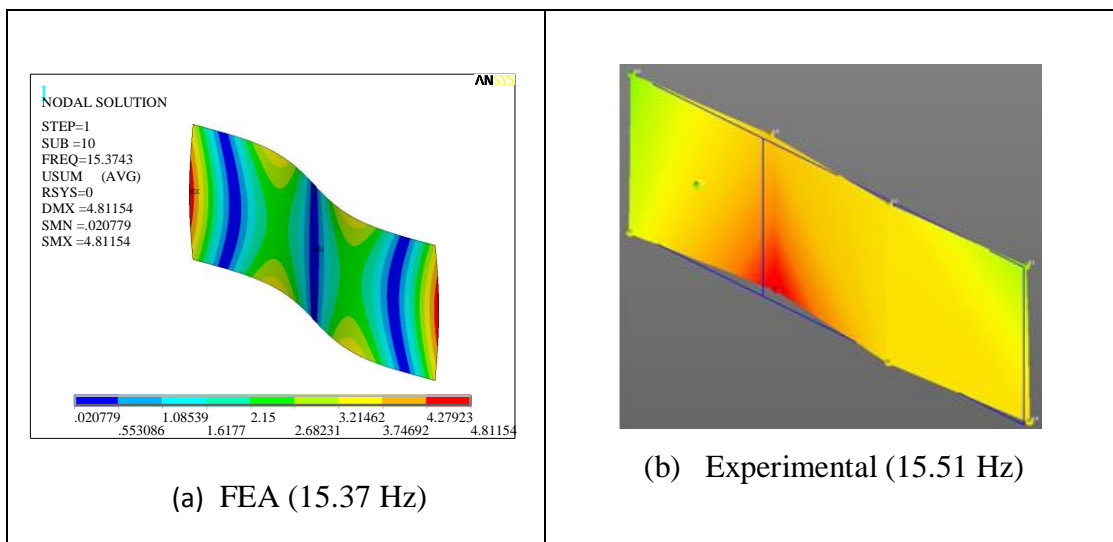


Figure 7.16 Comparison of mode shape for Case-1 (Mode No-4)

The acceleration responses have been obtained from the defined locations by experimentation on the two plates, and some sample values have been shown in Table 7.7. The last column of table 7.7 shows the sinusoidal force excitation at the excitation point on the plate. The responses and the excitation force being sinusoidal, the maximum value obtained are computed by post-processing the values in MATLAB software.

Table 7.7 Acceleration responses of adhesive lap joint plate for Case-1

Time (secs)	Acceleration response (g)			Force (N)
	Node-1	Node-2	Node-9	
1.00000000000	2.05	0.07	0.00	-6.28
1.00001953125	-0.43	0.02	-0.03	-3.45
1.00003906250	-2.89	-0.03	-0.06	-0.01
1.00005859375	-4.93	-0.08	-0.07	3.28
1.04998046875	4.28	0.11	0.02	-8.30
1.05000000000	2.07	0.08	0.00	-6.32

The maximum acceleration responses obtained at all the points on both the plates is divided by the maximum excitation force to obtain the acceleration responses for unit excitation loading of 1N as shown in Table 7.8.

Table 7.8 Acceleration responses of adhesive lap joint plate for Case-1 under unit force excitation

Acceleration Response (g)			Force (N)
Node-1	Node-2	Node-9	Excitation Location
9.1503	0.9248	0.1745	1

The acceleration responses are divided by the excitation frequency to obtain the velocity responses. The total vibratory energies in the plates have been computed based on Eq.7.8. The power injected at the excitation location is obtained from the cross-spectrum of force and acceleration by Equation (7.1). Finally, the non-conservative coupling factors have been computed by Equation (6.11). The apparent coupling factors ( $\eta_{12} = \eta_{21}$ ) for all the cases of the adhesive bonded plates obtained from finite element analysis and experiments have been listed out in Table 7.9 and Table 7.10 respectively. Similarly, the velocity responses obtained by finite element analysis and experiments for all the cases for the left-hand (LH-plate) and right-hand plate (RH-plate) under consideration have been compared in Figures 7.17 to 7.20. All the points in the plots have been joined by smooth lines.

Table 7.9 Apparent coupling factor obtained experimentally for adhesive bonded plates

<b>FREQUENCY (Hz)</b>	<b>CASE</b>			
	<b>CASE-1</b>	<b>CASE-2</b>	<b>CASE-3</b>	<b>CASE-4</b>
500	0.007991	0.008183	0.004039	0.000881
1000	0.001956	0.001779	0.001348	0.001093
1500	0.001061	0.001021	0.001368	0.000487
2000	0.000938	0.000850	0.000538	0.000401
2500	0.002217	0.001250	0.001299	0.000408
3000	0.000350	0.000072	0.0003083	0.000117
3500	0.000218	0.000202	0.000444	0.000454

Table 7.10 Apparent coupling factor obtained numerically for adhesive bonded plates

<b>FREQUENCY (Hz)</b>	<b>CASE</b>			
	<b>CASE-1</b>	<b>CASE-2</b>	<b>CASE-3</b>	<b>CASE-4</b>
500	0.03108	0.01103	0.01721	0.00855
1000	0.00480	0.00188	0.00585	0.00264
1500	0.00110	0.00038	0.00089	0.00020
2000	0.00243	0.00080	0.00214	0.00124
2500	0.00021	0.00004	0.00031	0.00025
3000	0.00046	0.00010	0.00036	0.00016
3500	0.00293	0.00142	0.00172	0.00086

Table 7.11 Power input (N-m/s) measured experimentally for adhesive bonded plates

FREQUENCY (Hz)	CASE			
	CASE-1	CASE-2	CASE-3	CASE-4
500	0.002706	0.002956	0.000695	0.001256
1000	0.000647	0.000603	0.000377	0.000402
1500	0.000305	0.000299	0.000216	0.000279
2000	0.000131	0.000122	0.000194	0.000231
2500	0.000101	0.000060	0.000068	0.000109
3000	0.000081	0.000075	0.000054	0.000122
3500	0.000067	0.000062	0.000053	0.000047

Table 7.12 Power input (N-m/s) obtained numerically for adhesive bonded plates

FREQUENCY (Hz)	CASE			
	CASE-1	CASE-2	CASE-3	CASE-4
500	0.003249	0.003713	0.002958	0.002722
1000	0.000699	0.000665	0.000722	0.000732
1500	0.000359	0.000377	0.000379	0.000404
2000	0.000144	0.000131	0.000138	0.000130
2500	0.000136	0.000079	0.000120	0.000106
3000	0.000110	0.000096	0.000121	0.000127
3500	0.000095	0.000092	0.000109	0.000113

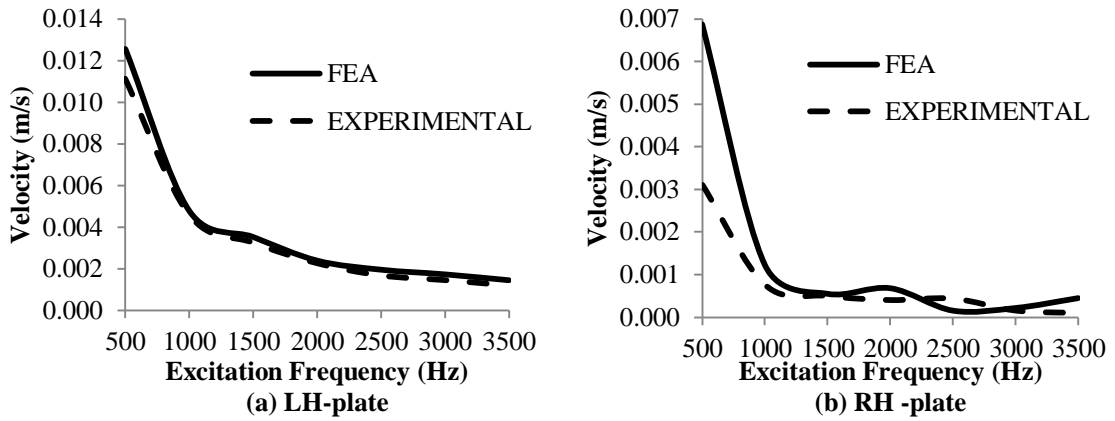


Figure 7.17 Velocity responses of Case-1 for adhesive bonded plates

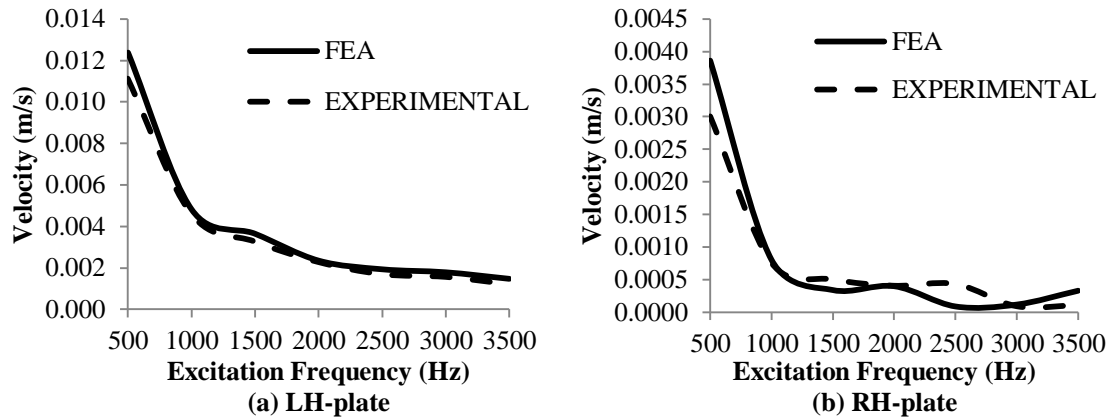


Figure 7.18 Velocity responses of Case-2 for adhesive bonded plates

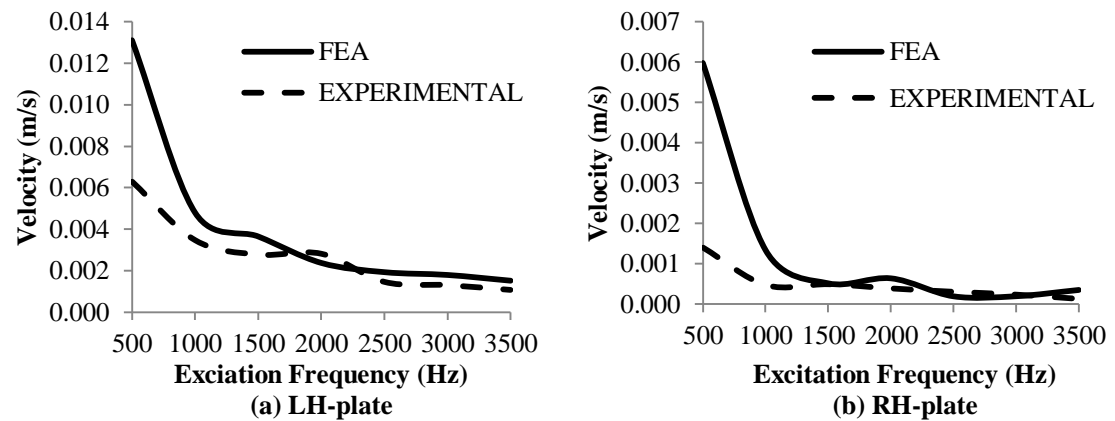


Figure 7.19 Velocity responses of Case-3 for adhesive bonded plates

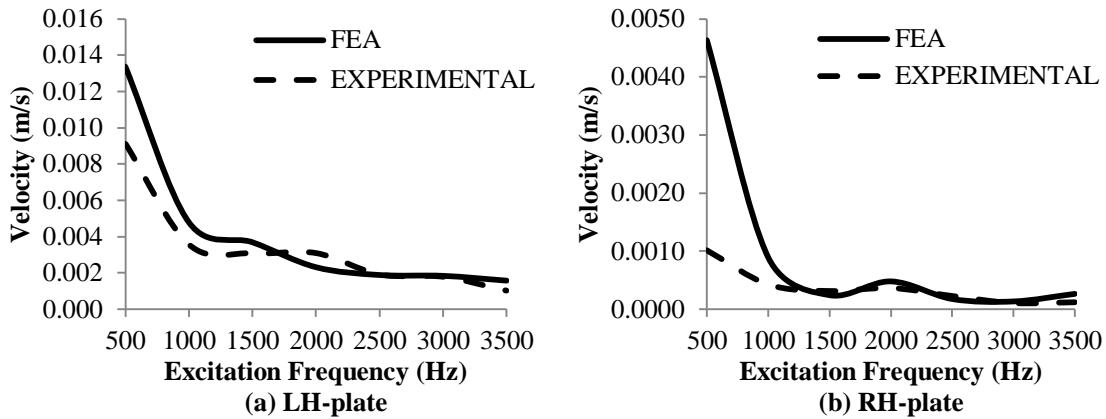


Figure 7.20 Velocity responses of Case-4 for adhesive bonded plates

Table 7.13 presents the ratio of velocities obtained in LH-plate and RH-plate at an excitation frequency of 3000 Hz for all the cases of two plates lap joined by double-sided adhesive tape. It can be observed that as the adhesive joint patch decreases the total energies and consequently the velocities in the second plate is reduced considerably and therefore the ratio of velocity responses of LH-plate to RH-plate increases.

Table 7.13 Ratio of velocity responses obtained for adhesive bonded lap joints of LH-plate and RH-plate for excitation frequency, 3000 Hz

CASES	Experimental			FEM		
	LH-plate (m/s)	RH-plate (m/s)	Ratio	LH-plate (m/s)	RH-plate (m/s)	Ratio
Case-1	0.001471	0.000162	9.09	0.001734	0.000217	7.99
Case-2	0.001517	0.000086	17.68	0.0017891	0.000115	15.56
Case-3	0.001296	0.000113	11.52	0.001793	0.000196	9.15
Case-4	0.001787	0.000113	15.88	0.001841	0.000134	13.74

The acrylic plates are viscoelastic, with reduced density, elastic modulus and areas in comparison to the mild steel plates. The energy propagation effects due to excitation at the left central edge of the excited plate is different from the central excitation. The apparent coupling factor obtained for such an excitation is computed by FEA and

experiments and is as given in the table below. These values have been used for different cases in cases of sequentially coupled plates after the second or Middle-plate to obtain accurate SEAL based predictions

Table 7.14 Coupling factor for edge loading (3000 Hz)

FREQUENCY (Hz)	CASE			
	CASE-1	CASE-2	CASE-3	CASE-4
FEA	0.00456	0.000313	0.007	0.001035
Experimental	0.00358	0.00021	0.0103	0.00106

It is observed that in case-2, with the adhesive mid patch,  $A_2$ , damaged, the ratio of velocity response of LH-plate to RH-plate is higher.

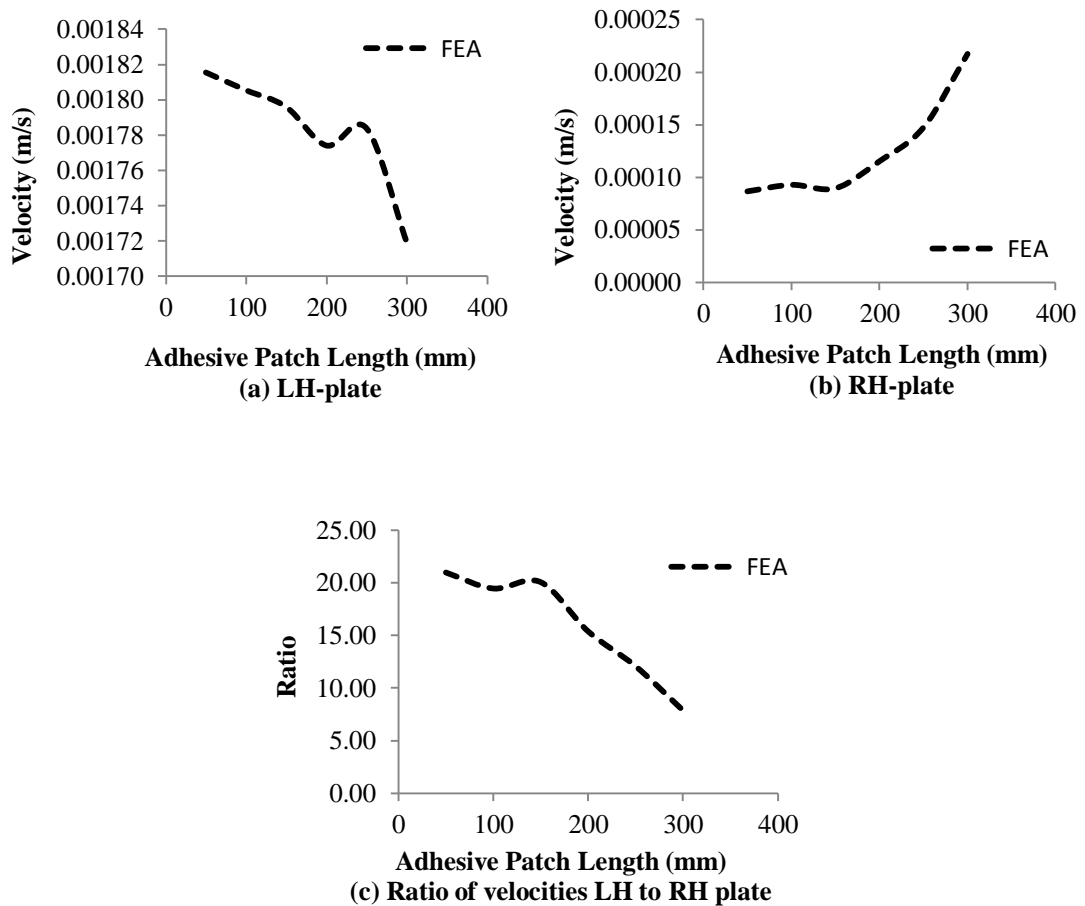


Figure 7.21 Variation of velocity responses with adhesive patch length

To study this variation in velocity ratio, FE based analyses is carried out by gradually increasing the adhesive patch length from the ends till it encompasses the 300 mm length attaining a full healthy state configuration. Figure 7.21 shows that in case, where the LH-plate is excited centrally, the energy propagation though the radius and the central portion of the adhesive patch is significant and any absence of the central adhesive patch increases the velocity ratio between LH and RH plates, in comparison to the absence of the same patch length at the ends. The same effect was observed in bolted joints also.

### 7.5.1 Joint damage detection

The studies for damage detection consists of three identical plates (namely LH-plate, Middle-plate and RH-plate) coupled in sequence by adhesive bonded lap joints (Fig. 7.22) for all the possible combinations of the cases as discussed in section 7.2. Table 7.15 presents all possible combinations of three plates with adhesive lap joints for predicting the velocity responses using the SEAL approach.

Table 7.15 List of Possible Combinations for three adhesive lap bonded plates

<b>Combination</b>	<b>Type of Adhesive Joint Between LH-plate and Middle-plate</b>	<b>Type of Adhesive Joint Between Middle-plate and RH-plate</b>
1	Case-1	Case-1
2	Case-1	Case-2
3	Case-1	Case-3
4	Case-1	Case-4
5	Case-2	Case-1
6	Case-2	Case-2
7	Case-2	Case-3
8	Case-2	Case-4
9	Case-3	Case-1
10	Case-3	Case-2
11	Case-3	Case-3
12	Case-3	Case-4



13	Case-4	Case-1
14	Case-4	Case-2
15	Case-4	Case-3
16	Case-4	Case-4

To illustrate the effectiveness of the method used to predict the damage status in the three plates with lap joints, a case of three plates with adhesive bonded lap joint is presented here. A healthy configuration described as LH-plate and Middle-plate are joined using complete adhesive patch along the coupled junction namely  $A_{11}$ ,  $A_{12}$  and  $A_{13}$  as shown in Figure 7.22, and Middle plate and RH-plate are joined employing another adhesive patch along the coupled junction namely  $A_{21}$ ,  $A_{22}$  and  $A_{23}$ . The damage in the Middle-plate and RH-plate with adhesive bonded lap joints is assumed to be a failure of the central adhesive patch,  $A_{22}$  and the remaining adhesive patches are intact. The velocity responses obtained experimentally, numerically and predicted using SEAL approach for the healthy and damaged configurations are shown in Figure 7.24 and Figure 7.25. The codes required for carrying out the computations have been developed using MATLAB software.

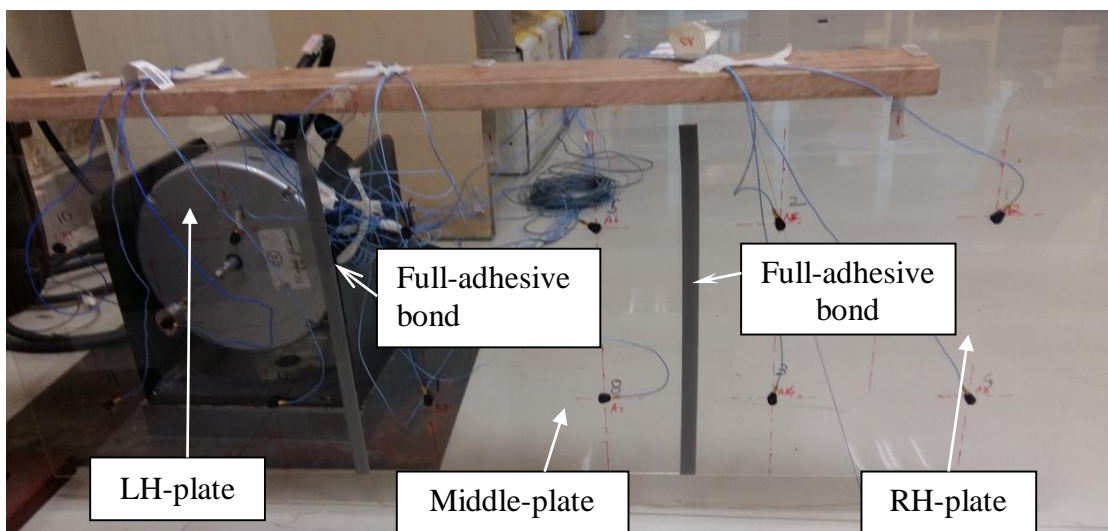


Figure 7.22 Three plates with adhesive bonded lap joints (healthy configuration)

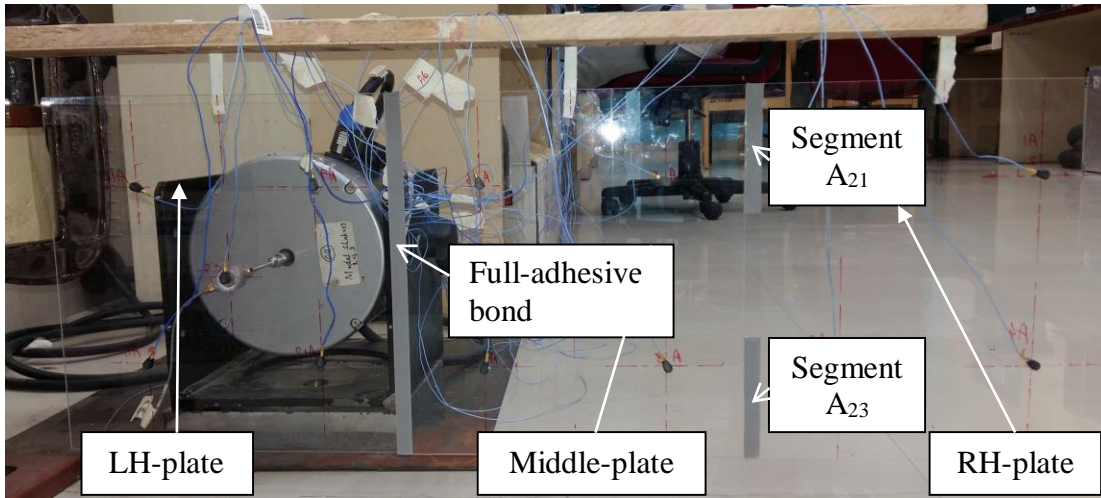


Figure 7.23 Three adhesive bonded lap joined plates with absence of adhesive segment A<sub>22</sub> (damaged configuration)

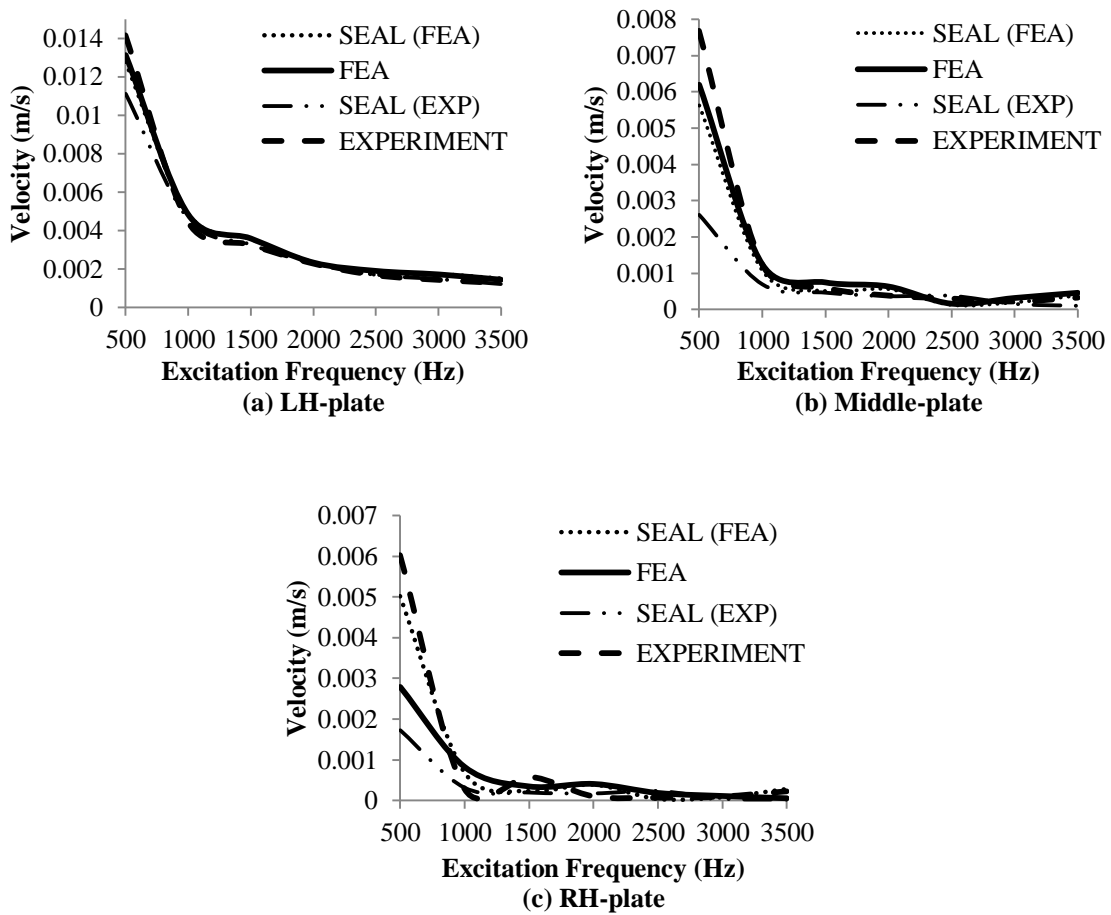


Figure 7.24 Velocity responses for adhesive bonded lap joints of healthy configuration

The predicted velocity responses for the damaged configuration are compared with the actual experimentation, and finite element analysis obtained responses in Figures 7.25 (a) to 7.25 (c).

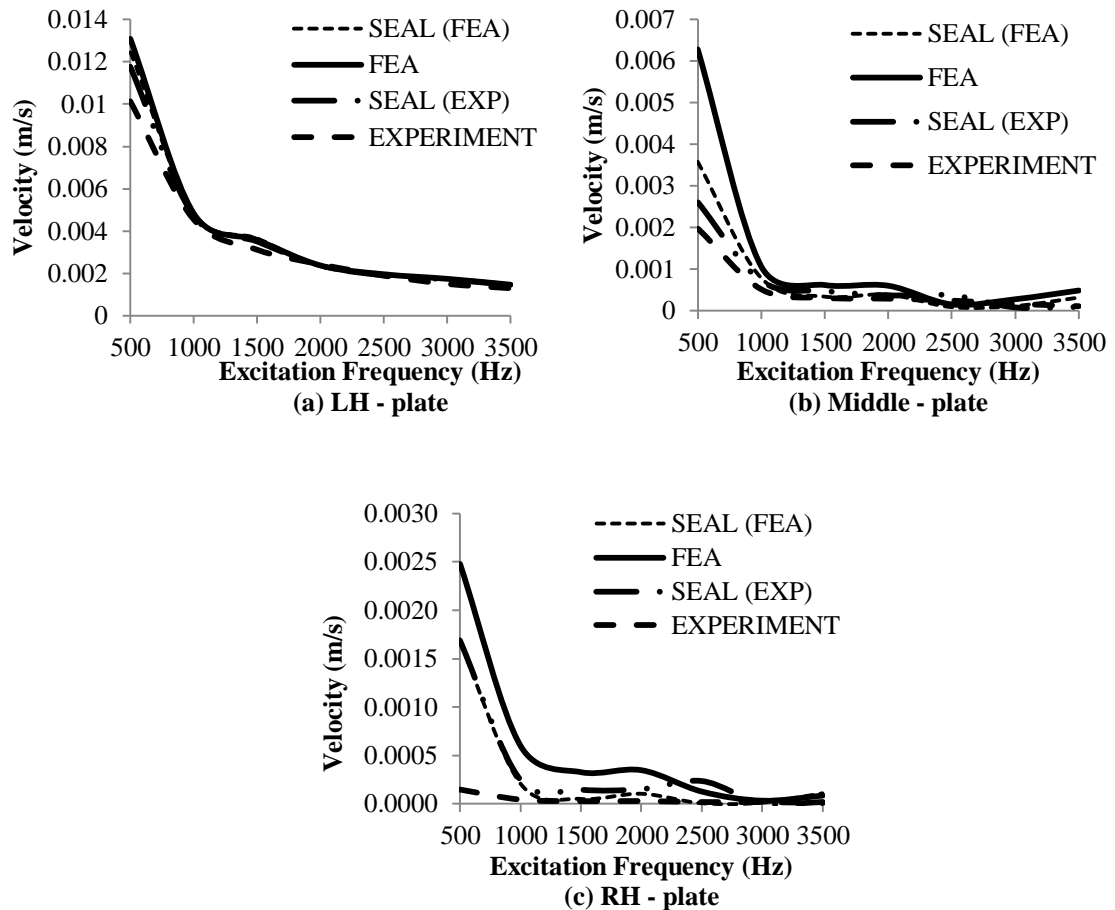


Figure 7.25 Velocity responses for adhesive bonded lap joints of damaged configuration

The modal density ( $n$ ) per Hz of each plate is 0.0788. The modal overlap factor ( $M=f\eta n$ ) preferred for application of statistical energy analysis principle is greater than one at all the excitation frequencies due to higher damping of the acrylic plate. At 3000 Hz the modal overlap is 4.72. The excitation frequency of 3000 Hz is selected as the deterministic frequency for detection of damage for the combinations as listed out in Table.7.15. In practice acceleration responses would be measured. Acceleration response for each plate can be computed by multiplying the plate velocity with the frequency of excitation.

Table 7.16 presents the acceleration responses obtained for the plates of healthy (combination-1) and damaged (combination-2) adhesive bonded joint at an excitation frequency of 3000 Hz.

Table 7.16. Comparison of acceleration responses for adhesive bonded lap joints, excitation frequency of 3000 Hz

PLATE	Name of Methods	Acceleration (m/s <sup>2</sup> )		Percentage difference
		Healthy	Damaged	
LH-plate	Experimental	27.10	27.63	1.98
	SEAL (Exp)	32.22	32.22	0.0005
	FEA	32.47	32.81	1.06
	SEAL (FEA)	33.60	33.60	0.00
Middle-plate	Experimental	4.23	4.51	6.49
	SEAL (Exp)	3.36	3.51	4.59
	FEA	5.93	5.98	0.84
	SEAL (FEA)	4.03	4.26	5.75
RH-plate	Experimental	1.90	0.52	-72.52
	SEAL (Exp)	1.07	0.28	-73.35
	FEA	2.07	0.60	-71.00
	SEAL (FEA)	1.46	0.43	-70.42

It is observed from Table 7.16 that in case of the damaged adhesive joint patch, the acceleration response in RH-plate is reduced in comparison to the healthy configuration. The percentage reduction in the acceleration response in the RH-plate due to the damaged joint ( $A_{22}$ ) is in the order of 70% in comparison with that of the healthy plate. The velocity responses predicted using SEAL approach is in close agreement with the actual experimentation and finite element analysis. A database bank of the predicted responses using SEAL approach for the other possible combinations is listed out in Table 7.17.

Table 7.17 presents the percentage deviation in the acceleration responses on each plate of the remaining combinations in comparison to the healthy configuration (combination 1). This percentage deviation is used as one of the damage indicator.

Table 7.17 Percentage deviation of acceleration responses of the other possible combinations in comparison to the healthy configuration (Combination 1), at an excitation frequency of 3000 Hz

Combination	SEAL – Predicted (Exp) in %			SEAL – Predicted (FEA) in %			FEA in %		
	LH-plate	Middle-plate	RH-plate	LH-plate	Middle-plate	RH-plate	LH-plate	Middle-plate	RH-plate
3	0.02	-5.8	46.3	-1.5	-3.9	15.1	-0.8	-13.0	25.1
4	0.02	3.5	-41.6	-1.5	3.0	-48.2	-1.3	-31.9	-50.5
5	0.46	-54.0	-54.1	-1.0	-50.5	-50.5	3.3	-61.6	-72.8
6	0.46	-51.9	-87.8	-1.0	-47.6	-85.3	2.7	-56.5	-84.5
7	0.46	-56.8	-32.9	-1.0	-51.7	-42.1	2.8	-58.7	-65.6
8	0.46	-52.5	-73.2	-1.0	-48.2	-73.9	2.5	-60.5	-78.6
9	0.09	-5.9	-6.0	-1.3	-16.4	-16.4	1.7	-19.0	3.9
10	0.09	-1.6	-74.9	-1.3	-12.7	-54.2	3.3	-34.4	-30.3
11	0.09	-11.5	37.4	-1.3	-18.4	-2.3	2.4	-23.7	-11.4
12	0.09	-2.8	-45.1	-1.3	-12.6	-56.0	2.3	-32.8	-64.5
13	0.39	-41.7	-41.7	-1.0	-45.4	-45.4	4.5	-39.1	-31.4
14	0.39	-39.0	-84.5	-1.0	-43.0	-70.1	6.0	-53.3	-67.7
15	0.39	-45.1	-14.9	-1.0	-46.7	-36.2	5.0	-47.9	-29.2
16	0.39	-39.7	-66.0	-1.0	-42.9	-71.3	5.2	-58.9	-70.9

## 7.6 SUMMARY

The damping loss factor of acrylic is higher than mild steel plates, which gives a higher modal overlap. The reduction in the adhesive joint patch length for a sequentially coupled plate causes a reduction in the values of coupling factors, total energies, and velocity response of the subsequent plate following the damaged adhesive joint (Table 7.13). The location of the damaged adhesive patch has also been found to have a significant effect on the responses (Table 7.13). The energy propagation through the radius and the central portion of the adhesive patch is significant and any absence of the central adhesive patch increases the velocity ratio between LH and RH plates, in comparison to the absence of the same patch length at the ends (Fig 7.21). The maximum percentage reduction of acceleration response in the RH plate for three adhesive bonded lap joined plates is for combination 6 in comparison to the healthy configuration (Table 7.17).

## CHAPTER 8

### CONCLUSIONS

#### 8.1 SUMMARY

The present research work focused on the numerical and experimental investigations on damage detection in plates with lap joint configurations viz. spot welded, bolted and adhesive bonded using statistical energy analysis like (SEAL) approach. Two materials mild steel and acrylic have been used in the investigations. In the first phase, studies have been carried out to investigate the effects of internal loss factor on the estimation of coupling factors of mild steel plates and the finite element models for spot welds, adhesive bond, and bolted joints. In the second phase, forced harmonic analysis was performed experimentally as well as numerically using commercially available finite element tool to compute velocity responses, total energies and coupling factors of the sub-structures for the healthy and damaged configurations. Further, the velocity and acceleration responses have been predicted for an assembly of three plates with lap joint configurations and compared with experiments and finite element simulation for healthy and damaged configurations. Based on the results, following chapter wise conclusions are drawn.

#### Chapter-3

- Coupling loss factors computed by analytical wave approach are independent of the internal loss factors. The coupling loss factor computed using finite element approach increases linearly as the internal loss factor varies from a zero and converges to the coupling factors obtained by analytical wave approach (Fig. 3.5). The frequency averaged coupling loss factor computed using finite element method is lower by 5.64% as compared to the factor obtain by analytical approach. (Table 3.2). The percentage variation between

the frequency averaged coupling factor obtained by FEA for the beams is 8% lower than the analytically obtained values for beams (Table 3.3)

- At low values of damping, common for most of the materials, the coupling factors computed by the analytical approach would be overestimated. The coupling factor computed by finite element methods or experimental SEA is expected to be more accurate in this region.
- Percentage variation between the velocity responses obtained from FEM varied from 14% at the lowest frequency of 1000 Hz to 0.4% at a higher frequency of 8000 Hz in comparison to the analytically obtained velocity responses for the plates (Fig. 3.10). At higher frequencies, the modal overlap increases and the frequency response is smoothed down, as the statistical energy analysis principles are satisfied. Thus the deviation in the velocity responses computed by both the approaches reduces with increase in the excitation frequencies.

#### Chapter-4

- In the finite element analysis, the spot-welds have been modelled by the area contact model (ACM2). The adhesive patch has been modelled using SOLID 186 elements. A simplified coupled bolt model has been used for modelling the bolted joint.
- Percentage variation between the velocity responses obtained by modelling the spot-welds with three joints in FEM varies from approximately 20% at the lower frequencies to 2% at higher frequencies in comparison to the analytically obtained velocity responses for the excited plate (Fig.4.7). Whereas, for adhesive joint it varies from approximately 12% at the lower frequencies to 3% at higher frequencies (Fig. 4.14). The finite element modelling of joints, discrete joints in particular like the spot welded joints plays an important role in the computation of the coupling factors and its further use statistical energy analysis like approach. The use of analytical wave-based approach or a simplistic FE model assuming a continuous line junction in such models may lead to erroneous prediction of results.



### Chapter-5, 6 and 7

- Average percentage differences of 18%, 14%, and 9 % have been observed for the ratio of velocity responses of LH-plate to RH-plate obtained from experiments for two spot-welded, adhesive bonded and bolted plates, respectively, in comparison with the finite element analysis results for excitation frequency at 3000 Hz. Proper finite element modelling of the joints and incorporation of damping and fine-tuning of the stiffness parameters from experiments in the numerical simulations plays a critical role in the estimation of coupling factors using FEA.
- The response predicted at low frequencies obtained by SEAL approach is not found to be accurate in comparison with finite element approach due to a reduction in modal density, modal overlap and violation of assumptions in the energy balance.
- Failure in any joint for a sequentially coupled plate causes a reduction in the coupling factors, total energies, and velocity and acceleration responses.
- Percentage deviation of acceleration response of the RH plate for three lap joined plates in comparison to the healthy configuration (combination 1) is maximum for combination 16 in case of spot welded plates and combination 6 in case of bolted and adhesive bonded plates. This maximum percentage reduction using SEAL approach from the experimentally derived coupling factors for the spot-welded, bolted and adhesive joints are 70.2, 71.6 and 87.8%, respectively. The maximum percentage reduction using SEAL approach from the FEA derived coupling factors for the spot-welded, bolted and adhesive joints are 87.6, 54.1 and 85.3%, respectively. The maximum percentage reduction using FEA simulations for the spot-welded, bolted and adhesive joints are 93.2, 54.2 and 84.5%, respectively.
- In case of three sequentially coupled plates, for the healthy configuration, the highest acceleration responses for LH-plate at an excitation frequency of 3000 Hz has been observed for the adhesive bonded plates in the range of  $32.4 \text{ m/s}^2$  followed by the spot-welded plates,  $21.73 \text{ m/s}^2$  and bolted plates,  $15.83 \text{ m/s}^2$ .

The acrylic plate has the least mass. In case of the bolted joints, the mild steel plate has the additional weight of the damping sheet.

- SEAL approach has been used to generate velocity responses, and total energies for three lap joined plates with a known damage. An offline joint damage-pattern database was developed through simulation of SEAL based joint damage scenarios. An effort has been made to explore the possibility of localizing a damage by best matching the unknown damage (acceleration responses as one of the features) as an index to that of known ones in the database.

## **8.2 KEY CONTRIBUTIONS**

The main contributions of this study are the following:

1. Coupling factors and velocity responses for two lap joined plates were determined using finite element analysis and experimentation. The obtained responses in FEA has been compared experimentally.
2. Apparent coupling factors derived for the various cases of two lap joined plates have been used further to predict the velocity, and acceleration responses using SEAL approach for three lap joined plates. The results obtained has been compared by experiments and finite element simulation for a healthy and damaged configuration of the same.
3. Statistical energy analysis like (SEAL) approach has been used to generate velocity responses, and total energies for an assembly of three lap joined plates with a known damage. All the possible damage samples considered in the present study for an assembly of bolted plates can be simulated by the SEAL approach to develop a database of the percentage deviation of acceleration response in comparison to the healthy configuration as one of the features of damage signals.

### **8.3 LIMITATIONS**

Response of the sub-structures predicted using coupling factors at low frequencies may not be accurate due to the violation of assumptions in the energy balance equations in SEA like approach. The approach requires prior information regarding the coupling factors of healthy and damaged joint configurations. The need for increased skill in proper FE modeling of different types of joints and incorporation of damping and stiffness parameters from experiments in the numerical simulations plays a critical role in the estimation of coupling factors. In case of highly complex configurations, the cost required would go up as experimental determination of the coupling factors may become inevitable. Further, most of the vibration based damage detection techniques, the requirement of online response measurements and the need to obtain responses in a spatially averaged sense may increase the cost of set-up. Accelerometers are expensive and measure at a single point along a structure. Thus, an array of accelerometers is required to achieve high density of spatial measurements, and as they are attached to the structures, it could affect the overall motion, particularly for light structures.

### **8.4 FUTURE SCOPE**

The implementation of the proposed approach for joints like riveted, soldered joints, etc. can be explored. The approach can also be extended to periodic structures with different shapes other than flat plates and additional excitations.

The use of the data generated and the proposed approach for optimal location of sensors and the use of various pattern recognition methods for joint damage detection in the presence of noise needs to be explored for real-world implementation.

The SEAL approach can be extended to study modal identification in pipes.

## REFERENCES

- Ahmadian, H., Jalali, H., (2007). "Identification of bolted lap joints parameters in assembled structures." *Mechanical Systems and Signal Processing*, 21 (2), 1041–1050.
- Ahmadian, H., Jalali, H., (2007). "Generic element formulation for modeling bolted lap joints." *Mechanical Systems and Signal Processing*, 21 (5), 2318–2334.
- Aragonès, A., Guasch, O. (2015). "Ranking paths in statistical energy analysis models with non-deterministic loss factors." *Mechanical Systems and Signal Processing*, 52–53, 741-753.
- Bies, D.A. and Hamid, S. (1980). "In situ determination of loss and coupling loss factors by the power injection method." *Journal of Sound and Vibration*, 70, 187-204.
- Bloss, B. and Rao, M.D. (2002). "Measurement of damping in structures by the power input method." *Experimental Techniques*, 26, 30-33.
- Capozucca, R. (2014). "Vibration of CFRP cantilever beam with damage." *Composite Structures*, 116, 211-222.
- Carden, E. P., Fanning, P., (2004). "Vibration based condition monitoring: a review," *Structural Health Monitoring*, 3(4), 355–377.
- Castellini, P., Martarelli, M. Tomasini, E, P., (2006). "Laser doppler vibrometry: development of advanced solutions answering to technology's needs," *Mechanical Systems and Signal Processing*, 20(6), 1265–1285.
- Cereceda, C., Jordi, P., Ferran, A. (2015). "Automatic subsystem identification in statistical energy analysis." *Mechanical Systems and Signal Processing*, 54–55, 182-194.
- Chen, X., Chang, F.G., Xiao, H.G. (2013). "Simulation and optimization of vehicle interior noise in mid and high frequency using VA-one", *Applied Mechanics and Materials*, 268-270,851-855.

- Chen, J.G., Wadhwa, N., Cha, Y., Durand, F., Freeman, W.T., Buyukozturk, O.(2015). “Modal identification of simple structures with high-speed video using motion magnification.” *Journal of Sound and Vibration*, 345, 58–71.
- Choi, S. and Stubbs, N. (2004). “Damage identification in structures using the time domain response” *Journal of Sound and Vibration*, 275 (3–5), 577–590.
- Doebbling, S. W., Farrar, C. R., and Prime, M. B. (1998). “A summary review of vibration-based damage identification methods,” *The Shock and Vibration Digest*, 30 (2), 91-105.
- Elie, B., Gautier, F., and David, B. (2013). “Estimation of mechanical properties of panels based on modal density and mean mobility measurements,” *Mechanical Systems and Signal Processing*, 40(2), 628-644.
- Fahy, F. J. (1997). “A technique for the assessment of the strength of coupling between SEA subsystems.” *Journal of Sound and Vibration*, 203(2), 265-282.
- Fredo, C. R. (1997). “SEA-like approach for the derivation of energy flow coefficients with a finite element model.” *Journal of Sound and Vibration*, 199(4), 645-666.
- Gaul, L., Lenz, J., (1997). “Nonlinear dynamics of structures assembled by bolted joints.” *Acta Mech*, 125, 169–81
- Gunes, R., Apalaka, K.M., Yildirim, M., (2007) “The free vibration analysis and optimal design of an adhesively bonded functionally graded single lap joint.” *International Journal of Mechanical Sciences*,49(4), 479–499.
- Goyal, D., and Pabla, B.S., (2016) “The vibration monitoring methods and signal processing techniques for structural health monitoring: A review,” *Archives of Computational Methods in Engineering*, 23(4), 1566-1589.
- Grushtesky, I., Smolnikov, A., (2005). “Determination of coupling factors for two beams using FEM.” *Technical Acoustics*, 24, 1-7.

- Hambric, S.A. (1990). "Power flow and mechanical intensity calculations in structural finite element analysis." *Journal of Vibration and Acoustics*, 112, 542-549.
- Hamey, C.S., Lestari, W., Qiao, P and Song, G. (2004). "Experimental damage identification of carbon/epoxy composite beams using curvature mode shapes." *Structural Health Monitoring*, 3, 333-353.
- Heron, K.H. (1990). "The development of a wave approach to statistical energy analysis." *Proceedings of the Institute of Acoustics*, 3, 551-556.
- Hodges, C.H., Nash, P., and Woodhouse, J. (1987). "Measurement of coupling loss factors by matrix fitting: an investigation of numerical procedures." *Applied Acoustics*, 22, 47-69.
- Hopkins, C. (2002). "Statistical energy analysis of coupled plate systems with low modal density and low modal overlap." *Journal of Sound and Vibration*, 251 (2), 193–214.
- Hwang, S.W., Jeong, W.B., Yoo, W.S., and Kim, K.H. (2004). "Transmission path analysis of noise and vibration in a rotary compressor by statistical energy analysis." *KSME International Journal*, 18 (11), 1909–1915.
- Ibrahim, R.A., Pettit, C.L., (2005). "Uncertainties and dynamic problems of bolted joints and other fasteners." *Journal of Sound and Vibration*, 279, 857–936.
- Iranzad, M., Ahmadian, H., (2012). "Identification of nonlinear bolted lap joint models", *Computers and Structures*, 96-97, 1–8.
- Jalali, H., Ahmadian, H., Mottershead, J.E., (2007). "Identification of nonlinear bolted lap joint parameters by force-state mapping." *International Journal of Solids and Structures*, 44, 8087–8105.
- Kaya, A., Mehmet S., Tekeliog˘lub, Fehim Findik. (2004). "Effects of various parameters on dynamic characteristics in adhesively bonded joints." *Materials Letters* 58, 3451–3456.

- Kim, J., Yoon, J., and Kang, B. (2007). "Finite element analysis and modeling of a structure with bolted joints." *Applied Mathematical Modelling*, 31, 895-911.
- Kuratani, F., Matsubara, K., and Yamauchi, T. (2011). "Finite Element Model for Spot Welds Using Multi-Point Constraints and its Dynamic Characteristics." *SAE Int. J. Passeng. Cars – Mech. Syst*, 4(2), 1311-1319.
- Lakhdar, M., Djermane, M., Boudjemâa, L., Rabiâ, A., Bachir, M. (2013). "Damage detection in a composite structure by vibration analysis." *Energy Procedia*, 36, 888-897.
- Langhe, K.De. and Sas, P. (1996). "Statistical analysis of the power injection method" *J. Acoust. Soc. Am*, 100, 291-303.
- Langley, R S. (1990). "Derivation of the coupling loss factors used in statistical energy analysis." *Journal of Sound and Vibration*, 141(2), 207-219.
- Langley, R.S and Heron, J.H. (1990). "Elastic wave transmission through plate/beam junctions." *Journal of Sound and Vibration*, 143, 241-253.
- Langley, R.S. (1989). "General derivation of the statistical energy analysis equations for coupled dynamic systems." *Journal of Sound and Vibration*, 135(3), 499-508.
- Langley, R.S. (2014). "Efficient parametric uncertainty analysis within the hybrid finite element / statistical energy analysis method." *Journal of Sound and Vibration*, 333(6), 1698-1717.
- López-Díez, J., Torrealba, M., Güemes, A. and Cuerno, C. (2005). "Application of Statistical Energy Analysis for damage detection in spacecraft structures." *Key Engineering Materials*, 293-294, 525-532.
- Lafont, T., Totaro, N. and Bot, A. Le. (2014). "Review of statistical energy analysis hypotheses in vibroacoustics." *Proceedings of the Royal Society*, 470.
- Mace, B. R., and Shorter, P. J., (2000). "Energy flow models from finite element analysis." *Journal of Sound and Vibration*, 233(3), 369-389.

- Mackerle J., (2003). "Review of finite element analysis of fastening and joining: a bibliography (1990–2002)". *Int J Pres. Ves. Pip*, 80, 253–71.
- Maeck, J., Wahab, M., Peeters, B., De Roeck G., De Visscher J, De Wilde W, P (2000) "Damage identification in reinforced concrete structures by dynamic stiffness determination." *Engineering Structures*, 22(10), 1339–1349.
- Madhavan, S., Jain, R., Sujatha, C., Sekhar, A.S. (2014). "Vibration-based damage detection of rotor blades in a gas turbine engine." *Engineering Failure Analysis*, 46, 26-39.
- Mahapatra, D. and Gopalakrishnan, S., (2004). "Spectral finite element analysis of coupled wave propagation in composite beams with multiple delaminations and strip inclusions," *International Journal of Solids and Structures*, 41, 173-1208.
- Manik, D.N. (1998). "A new method for determining coupling loss factors for SEA." *Journal of Sound and Vibration*, 211(3), 521-526.
- Manson, G., Worden, K., and Allman, D. (2003), "Experimental validation of a structural health monitoring methodology: part II. Novelty detection on a gnat aircraft", *Journal of Sound and Vibration*, 259(2), 345-363.
- Marburg S, Schneider S (2003). "Influence of element types on numeric error for acoustic boundary elements." *Journal of Computational Acoustics*, 11, 363–386
- Marwala, T. and Hunt, H.E.M., (1999). "Fault identification using finite element models and neural networks." *Mechanical Systems and Signal Processing*, 13, 475-490.
- Nack, W., Yan, H. and Parrett, A. (2000) "Statistical energy analysis by finite elements for middle frequency vibration." *Finite Elements in Analysis and Design*, 35, 297-304.
- Ni, Y. Q., Zhou, X. T., and Ko, J. M. (2006). "Experimental investigation of seismic damage identification using PCA-compressed frequency response functions and neural networks." *Journal of Sound and Vibration*, 290(1), 242-263.



- Palmonella, M., Friswell, M.I., Mottershead, J.E., Lees, A.W.(2005) “Finite element models of spot welds in structural dynamics: review and updating.” *Computers and Structures*, 83, 648–661.
- Palmonella, M., Friswell, M.I., Mottershead, J.E., Lees, A.W. (2004) “Guidelines for the implementation of the CWELD and ACM2 spot weld models in structural dynamics.” *Finite Elements in Analysis and Design*, 41, 193–210
- Pandurangan, Pradeep. (2006). “Defect Identification in GRID-LOCK Joints.” *Journal of Sound and Vibration*, 199(4), 645-666.
- Pandurangan, P, and Buckner, G.D. (2006). “Vibration Analysis for Damage Detection in Metal-to-Metal Adhesive Joints.” *Experimental Mechanics*, 46, 601–607.
- Park, A, P., Finley, R., and Cater, J. (2017). “Predicting horizontal impact sound transmission for complex floor systems: Using EN 12354-2:2000, finite element method, statistical energy analysis and analytical techniques.” *Building Acoustics*, 24 (1), 55-73.
- Park, W. S., Thompson, D. J. and Ferguson, N. S. (2004). “The influence of modal behavior on the energy transmission between two coupled plates.” *Journal of Sound and Vibration*, 276, 1019-1041.
- Park, W. S., Thompson, D. J. and Ferguson, N. S. (2004). “Variability of the coupling loss factor between coupled plates.” *Journal of Sound and Vibration*, 279, 557-579.
- Park, G., Muntges, D, E., and Inman, D, J., (2001). “Self-monitoring and self-healing jointed structures,” *Key Engineering Materials*, 204, 75–84.
- Reynders, E., Langley, R.S., Dijckmans, A., Gerrit, V. (2014). “A hybrid finite element – statistical energy analysis approach to robust sound transmission modeling.” *Journal of Sound and Vibration*, 333(19), 4621-4636.
- Sampaio, R. P. C., Maia, N.M.M and Silva, J.M.M. (1996). “Damage detection using the frequency-response-function curvature method.” *Journal of Sound and Vibration* 226, 1029-1042.

Santos, R.O., Pereira, V.S., Arruda, J.R.F. and Dos Santos, J.M.C. (2008). "Structural damage detection using energy flow models," *Shock and Vibration*, 15, 217–230.

Sierra, A., (2001). "Evolution of Fisher discriminants," *IEEE Journal*, 3(1), 747-752.

Shankar K. and Keane A. J. (1997). "Vibrational energy flow analyses using a substructure approach: the application of receptance theory to FEA and SEA." *Journal of Sound and Vibration*, 201, 491-513.

Sheng, M.P., Wang, M.Q., Sun, J.C. and Qian B. (2004). "Statistical energy analysis for a complicated coupled system and its application in engineering." *Journal of Sound and Vibration*, 274(2004), 877-891.

Simmons, C. (1991). "Structure-borne sound transmission through plate junctions and estimates of SEA coupling loss factors using the FE method." *Journal of Sound and Vibration*, 144, 215-227.

Sohn, H., Farrar, R.C., Hunter, N.F, and Worden, K. (2001). "Structural health monitoring using statistical pattern recognition techniques." *ASME Journal of Dynamic Systems, Measurement, and Control: Special Issue on Identification of Mechanical Systems*, 123(4), 706-712.

Stubbs, N., and Kim, J. (1996). "Damage localization in structures without baseline modal parameters," *AIAA Journal*, 34(8), 1644-1649.

Tan, K., Guo, N., Wong, B., and Tui, C. (1995). "Experimental evaluation of delaminations in composite plates by the use of Lamb waves," *Composite Science and Technology*, 53, 77-84.

Thite, A.N. and Mace, B. R. (2007). "Robust estimation of coupling factors from finite element analysis," *Journal of Sound and Vibration*, 303, 814-831.

Tol, S., Ozguven, N, H., (2015). "Dynamic characterization of bolted joints using FRF decoupling and optimization." *Mechanical Systems and Signal Processing*, 54-55, 124–138.

- Trendafilova, I. and Heylen, W. (2003), "Categorization and pattern recognition methods for Damage Localization from Vibration Measurements," *Mechanical Systems and Signal Processing*, 17 (4), 825-836.
- Trendafilova, I., and Imbabi, M. (2004). "Novel health monitoring procedure for reinforced concrete slabs." *Applied Mechanics and Materials*, 1, 65-70.
- Troclet, B. (2009). "FEM/SEA Hybrid method for predicting mid and high-frequency structure-borne transmission", *The Open Acoustics Journal*, 2, 45-60.
- Vaziri, A., Hamidzadeh, H.R., and Nayeb-Hashemi (2001). "Dynamic response of adhesively bonded single-lap joints with a void subjected to harmonic peeling loads." *Journal of Multi-body Dynamics*, 215, 199.
- Vaziri., H. Nayeb-Hashemi. (2002). "Dynamic response of tubular joints with an annular void subjected to a harmonic axial load." *International Journal of Adhesion & Adhesives*, 22, 367–373.
- Vaziri, A., Nayeb-Hashemi. (2004). "Experimental and Analytical Investigations of the Dynamic Response of Adhesively Bonded Single Lap Joints." *Journal of Vibration and Acoustics*, 126, 85.
- Wahab, A.M., and De Roeck, G., (1999). "Damage detection in bridges using modal curvatures: application to a real damage scenario." *Journal of Sound and Vibration*, 226(2), 217–235.
- Wang, J. and Sas, P. (1990). "Method for identifying parameters of mechanical joints." *Journal of Applied Mechanics, transactions of the ASME*, 25, 337-342.
- Wang, H., Hung, C., and Chang, F., (1996). "Bearing failure of bolted composite joints," *Journal of Composite Materials*, 30 (12), 128-1313.
- Wen, J.L., Xiao, Y.L., Song, L.L., Lin, Y.L. (2012). "The characteristic analysis of vibration for a high-speed train-ballastless track-bridge system based on a hybrid FE-SEA method" *Applied Mechanics and Materials*, 226-228, 387-391.

White, C.A., Henry, C.H., Whittingham, B., Herszberg, I.C., Mouritz, P.A., (2008). "Damage detection in repairs using frequency response techniques." *Composite Structures*, 87, 175–181.

Whittingham, B., Herszberg, C., and Chiu, W.K. (2006). "Disbond detection in adhesively bonded composite structures using vibration signatures." *Journal of Composite Structures*, 75, 351–363.

Xiaocong He. (2011). "A review of finite element analysis of adhesively bonded joints." *International Journal of Adhesion & Adhesives*, 31, 248–264.

Xu, S. and Deng, X. (2004) "An evaluation of simplified finite element models for spot-welded joints" *Finite Elements in Analysis and Design*, 40, 1175–1194.

Yap, F. F., Woodhouse, J. (1996). "Investigation of damping effects on statistical energy analysis of coupled structures." *Journal of Sound and Vibration*, 197, 3, 351-371.

Yang, X., Xiao, Y., Shi, Y. (2013). "Statistical energy analysis of wind noise in high-speed train cab" *Applied Mechanics and Materials*. " 249-250, 307-313.

Yoshimura, M. and Okushima, K. (1977). "Measurement of dynamic rigidity and damping property for simplified joint models and simulation by computer." *Annals of the CIRP*, 25, 193-198.

Yuan, J., and Liu, X. (2013). "Semi-supervised learning and condition fusion for fault diagnosis." *Mechanical Systems and Signal Processing*, 38, 615-62.

Zang, C. and Imregun, M. (2001), "Structural damage detection using artificial neural networks and measured FRF data reduced via principal component projection," *Journal of Sound and Vibration*, 242(5), 813-827.

Zhang, G., Yan, Y. (2013). "Applications of statistical energy analysis in influencing factors analysis of aircraft Vibro-acoustic response characteristics." *Applied Mechanics and Materials*, 300-301 (2013), 810-813.

Conference proceedings:

Borgaonkar, A.V., and Mandale, M.B., (2014). “Estimation of modal density by theoretical, experimental and FEM method of idealized subsystems.” in *Proceedings of the 3<sup>rd</sup> International Conference on Recent Trends in Engineering and Technology*, Elsevier, 1-7.

Doebling, S., Farrar, C., and Goodman, R., (1997). “Effects of measurement statistics on the detection of damage in the Alamosa Canyon Bridge.” in *Proceedings on the 15<sup>th</sup> International Modal Analysis Conference*, 3089(1), 919-929.

Farrar, C, Doebling, S., Straser, E., and Cornwall, P., (1997). “Variability of modal parameters measured on the Alamosa Canyon Bridge.” *Proceedings on the 15<sup>th</sup> International Modal Analysis Conference*, 3089(1), 257-263.

Ho, Y.K. and Ewins, D.J. (2000). “On the structural damage identification with mode shapes.” *Proceedings of the European COST F3 Conference on System Identification and Structural Health Monitoring*, Madrid, Spain, 677-686.

Ma, R., and Fu, H., (2004). “Smart, active sensing technique using wavelet analysis method on damage detection of a composite plate.” *Proceedings of the 2004 IEEE International Conference on Networking, Sensing and Control*, 773-77.

Ma, Y. C., Bolton, J.S., Jeong, H., Ahn, B. and Shin, C. (2002). “Experimental statistical energy analysis applied to a rolling piston-type rotary compressor.” *International Compressor Engineering Conference*, paper 1571.

Stubbs, N., Kim, J.T., and Farrar, C.R., (1995). “Field Verification of a Non-destructive Damage Localization and Severity Estimation Algorithm,” in *Proc. 13<sup>th</sup> International Modal Analysis Conference*, 210–218.

Xiaocong He, Shanfeng Gao, Wenbin Zhang. (2010). “Torsional Free Vibration Characteristics of Hybrid Clinched Joints.” *International Conference on Measuring Technology and Mechatronics Automation*.

Yen, G., and K. Lin. (1999). “Conditional health monitoring using vibration signatures,” *Proceedings of the 38<sup>th</sup> Conference on Decision and Control*, 4493-4498.

### Books and Reports:

Fritzen, C.P., Balageas, D., Guemes, A., (2006). *Structural health monitoring*, vol 493. ISTE, London.

Hopkins, C. (2007). *Sound insulation*, Butterworth-Heinemann, Elsevier, Oxford.

Jolliffe, I.T. (2002). *Principal component analysis*, Springer-Verlag, New York.

Lalor, N. (1990). *Considerations for the measurement of internal and coupling loss factors of complex structures*, ISVR Technical Report No.182

Lyon, R. H. (1975). *Statistical Energy Analysis of Vibrating Systems*. Cambridge, MA: MIT Press

Nortons, M. P. (1989). *Fundamental of Noise and Vibration Analysis for Engineers*, Cambridge University Press, New York, Port Chester Melbourne Sydney.

Purekar, A. (2006). *Piezoelectric Phased Array Acoustic-Ultrasonic Interrogation of Damage in Thin Plates*, Doctoral dissertation, University of Maryland, Department of Aerospace Engineering.

Rytter, A. (1993). *Vibration-Based Inspection of Civil Engineering Structures*, Doctoral dissertation, Aalborg University, Department of Building Technology and Structural Engineering.

Swanson, A. (2013). *ANSYS 13.0 user's manual*, ANSYS Inc.

Scheffer, C., Girdhar, P., (2004). *Practical machinery vibration analysis and predictive maintenance*, Elsevier, Amsterdam.

Tou., J.T and Gonzales R.C. (1974), *Pattern recognition principles*, Addison-Wesley Publication.

**List of Publications based on Ph.D. Research Work**

<b>Sl. No.</b>	<b>Title of the Paper</b>	<b>Authors ( In the same order as in the paper, underline the Research Scholar's name)</b>	<b>Name of the Journal / Conference / Symposium, Vol., No., Pages</b>	<b>Month &amp; Year of Publication</b>	<b>Category *</b>
1	A comparison of different methods for determination of coupling factor and velocity response of coupled plates	Achuthan C. Pankaj, Sridhar Sastry, S. M. Murigendrappa	Journal of Vibro-engineering, 15(4), 1885-1897.(SCI and Scopus Indexed )	Dec, 2013	1
2	Detection of damage in spot welded joints using statistical energy analysis like approach	Achuthan C. Pankaj, M.V. Shivaprasad, S. M. Murigendrappa	International Journal of Acoustics and Vibration, 22(2) (SCI and Scopus Indexed)	June 2017	1
3	Determination of coupling factors for Adhesive bonded plates	Achuthan C. Pankaj and S. M. Murigendrappa	ARNP Journal of Engineering and Applied Sciences, 11(12), 7968-7972. (Scopus Indexed)	June 2016	1
4	Determination of coupling factors for spot welded plates	Achuthan C. Pankaj and S. M. Murigendrappa	International Conference on Theoretical, Applied, Computational and Experimental Mechanics, IIT-Kharagpur.	Dec 2014	3

5	Determination of coupling factors for Adhesive bonded plates	Achuthan C. Pankaj and S. M. Murigendrappa	International Conference on Design, Advanced Manufacturing, and Simulation, Saveetha University, Chennai.	April 2016	3
6	Determination of coupling factors for bolted plates using finite element analysis	Achuthan C. Pankaj and S. M. Murigendrappa	International Conference on Theoretical, Applied, Computational and Experimental Mechanics, IIT-Kharagpur.	Dec 2017	3
7	Determination of apparent coupling factors for adhesive bonded acrylic plates using SEAL approach.	Achuthan. C. Pankaj, M.V. Shivaprasad, S. M. Murigendrappa	AIP Conference Proceedings <b>1943</b> , 020024 (2018)	April 2018	3

\*

Category: 1 : Journal paper, full paper reviewed  
2 : Journal paper, Abstract reviewed  
3 : Conference/Symposium paper, full paper reviewed  
4 : Conference/Symposium paper, abstract reviewed  
5 : others (including papers in Workshops, NITK Research Bulletins, Short notes etc.)  
(If the paper has been accepted for publication but yet to be published, the supporting documents must be attached.)

**Research Scholar**

Achuthan.C.Pankaj

**Research Guide**

Dr. S. M. Murigendrappa





### **BIO-DATA**

1. **Name** : Achuthan.C.Pankaj  
2. **Father's Name** : A.Pankaj  
3. **Date of Birth** : 03/01/1976  
4. **Nationality** : Indian  
5. **Marital Status** : Married  
6. **Address** :

#### **Permanent Address**

Flat No: 202, Sreevari Enclave  
3<sup>rd</sup> Main, Vinayakanagara  
Kodihalli,  
Bangalore.  
Pin-560017, Karnataka, India

7. **Mobile Number** : +91-9008090109  
8. **E-mail id.** : acpankaj@nal.res.in  
9. **Educational Qualification** :

<b>Qualification</b>	<b>College/school</b>	<b>University/Board</b>	<b>Year of Passing</b>	<b>Performance</b>
Ph.D. in Mechanical Engineering	National Institute of Technology Karnataka	National Institute of Technology Karnataka	Pursuing	-----
M.Tech in CAD/CAM	National Institute of Technology, Allahabad, Uttar Pradesh.	University of Allahabad, Uttar Pradesh.	2000	81%
B.E in Mechanical Engineering	Maharashtra Institute of Technology, Pune, Maharashtra.	University of Pune, Maharashtra.	1997	66%

I declare that above information is true and correct to best of my knowledge and belief.

*(Achuthan.C.Pankaj)*